TECHNICAL REPORT

STEWS-RE-I-70-2

EXPLORATORY DEVELOPMENT OF THE WSMR CINETHEODOLITE

FINAL REPORT

BY

LOWELL D. YATES

JUNE 1970

INSTRUMENTATION DEVELOPMENT DIRECTORATE
NATIONAL RANGE ENGINEERING
WHITE SANDS MISSILE RANGE
NEW MEXICO

TECHNICAL REPORT

STEWS-PE-I-70-2

EXPLORATORY DEVELOPMENT OF THE WSMR CINETHEODOLITE

FINAL REPORT

BY

LOWELL D. YATES

JUNE 1970

DA PROJECT 1S265302D240 04 02

INSTRUMENTATION DEVELOPMENT DIRECTORATE
NATIONAL RANGE ENGINEERING
WHITE SANDS MISSILE RANGE
NEW MEXICO

Destroy this report when no longer needed. Do not return it to the originator.

Disclaimer

The findings in this report are not to be construed as an official Department of the Army position unless so designated by other authorized documents.

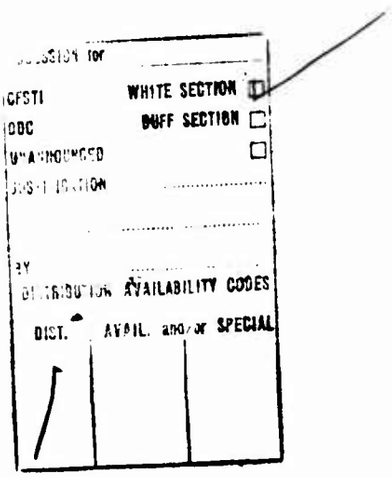

ABSTRACT

A breadboard instrument was developed for the purpose of establishing the feasibility of a novel and unique type of theodolite with far greater dynamic pointing accuracy than is possible with conventional theodolites. This report documents the results of the test and evaluation and the measurement techniques employed. The report discusses design deficiencies of the breadboard instrument along with recommended improvements for future development of an operational instrument.

ACKNOWLEDGMENT

The author gratefully acknowledges the technical assistance given in the preparation of this report by William E. Mimmack, Staff Physicist, and by the members of the WSMR Cinetheodolite Task Team: John Dart, Ray Kaufman, and Richard Sandoval.

TABLE OF CONTENTS

TABLE OF CONTENTS (Cont'd)

TABLE OF CONTENTS (Cont'd)

LIST OF ILLUSTRATIONS

LIST OF ILLUSTRATIONS (Cont'd)

LIST OF ILLUSTRATIONS (Cont'd)

LIST OF TABLES

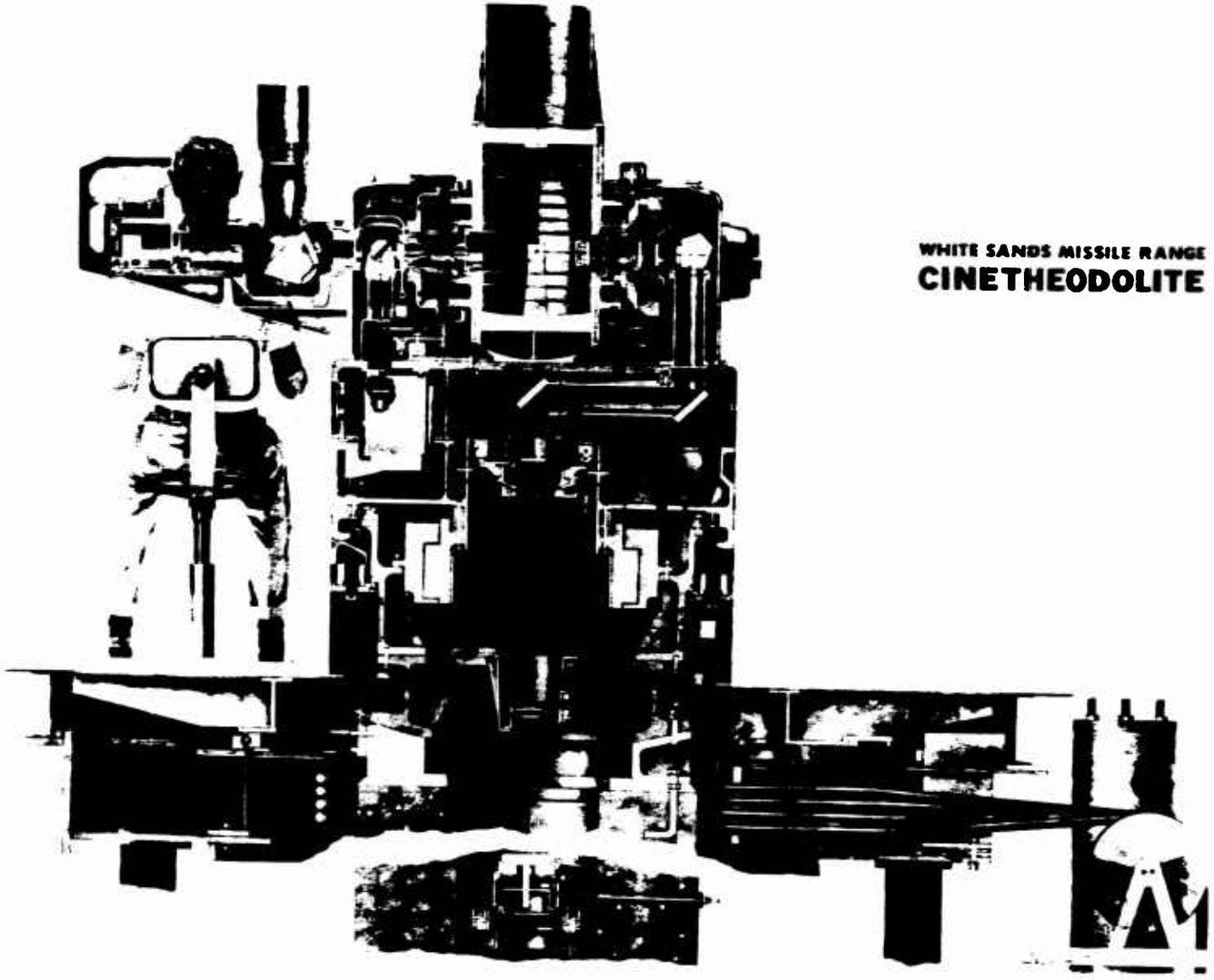

WHITE SANDS MISSILE RANGE
CINETHEODOLITE

FRONTISPIECE

INTRODUCTION

BACKGROUND

Requirement analyses performed over the last decade at WSMR have continued to indicate a growing need for a very high-accuracy space position measuring system. Conventional or "mechanical" theodolites cannot provide the required dynamic accuracy, and it has been established that current "state-of-the-art" manufacturing techniques and materials cannot adequately support the development of a mechanical theodolite that will limit or compensate for its own mechanical dynamic errors to ±2 arc-seconds without employment of a high-performance error monitoring and recording system. Much has been written (see Table I) about the "principle of optical compensation" and the prototype cinetheodolite design which meets the high dynamic accuracy requirements by means of this concept.

The WSMR Cinetheodolite system design goal was "to provide a capability for passive determination of vehicle position with a precision of ±1.0 to 1.5 feet at altitudes of 100,000 to 150,000 feet at selected sampling rates up to 50 per second." This objective in terms of range support from a trajectory measurement system, when translated into instrumental pointing accuracy, indicates the development of a theodolite with a static pointing accuracy of 2 to 5 seconds of arc and a dynamic accuracy of 3 to 6 seconds of arc. It is the latter objective, the dynamic accuracy, that required a radical change in theodolite design concept. It has been the experience of most cinetheodolite users that a 5 to 15 arc-second static instrumental accuracy in a dynamic situation is degraded to 20 to 45 arc-seconds because of bending and other mechanical distortions of the instrument resulting from high tracking rates and other aspects of the operational environment.

There have been recent claims by instrument manufacturers of static pointing accuracies equivalent to that of the WSMR Cinetheodolite. However, the claims are based on structural analyses performed by the manufacturer and not on comprehensive tests. Even if such accuracies were established under initial laboratory conditions, it is highly unlikely that the mechanical theodolite with its dependence upon ultra-precise preloaded bearings could maintain this accuracy long without serious degradation due to "wear" under normal field conditions. If by some miracle this static accuracy could be maintained in the field with a mechnical theodolite, the most stringent performance requirement remains: dynamic pointing accuracy. No manufacturer of a mechanical theodolite has ever publicly quoted (as of December 1969) a figure for the dynamic accuracy of their instrument at moderate or high tracking rates. This is because, in all the approaches proposed, the dynamic accuracy is exceedingly difficult to achieve, and such a claim would be difficult to substantiate, as this report indicates in the section titled "Accuracy Evaluation," without the development of a sophisticated test complex.

TABLE I. LIST OF REFERENCED DOCUMENTS

1. "Requirements and Preliminary Design Study for the WSMR Cinetheodolite," IRM Interim Report, Phase I, March 1961.

2. "Analysis of the Data Optical System, WSMR Cinetheodolite," RID-O Technical Memorandum 62-3.

3. "A Briefing on the WSMR Cinetheodolite Development," Optics Division Technical Memorandum 64-1.

4. "Accuracy Evaluation Plan, WSMR Cinetheodolite," Optics Division Technical Memorandum 64-2.

5. "Problems of the Fiducial Image Motions, WSMR Cinetheodolite," Optics Division Technical Memorandum 64-8.

6. "The WSMR Cinetheodolite Graduated Circle Recording System," Optics Division Technical Memorandum 66-14.

7. "Accuracy Evaluation of the WSMR Cinetheodolite," Optics Division Technical Memorandum 69-4.

8. "Prototype and R&D Test Facility for the WSMR Cinetheodolite," Data Collection Directorate, September 1964.

9. Purchase Description, "Optical Data Train Redesign, WSMR Cinetheodolite," WSMR NR-RE-PD-1047-68.

10. "A Design Study of the WSMR Cinetheodolite Optical System," Final Report, prepared by Keuffel and Esser Company under Contract No. DAAD07-69-C-0119.

The WSMR Cinethedolite is able to achieve its dynamic accuracy through a fundamentally different approach to the cinetheodolite design problem. Almost all angle-measuring systems rely completely upon mechanical rigidity, precision of bearings, tube stiffness (or stiffness of a radar dish) and other mechanical constraints for the basic instrumental accuracy. (One possible exception to this generalization may be the phased-array radar. However, it should be noted that the static pointing accuracy of a modern radar does not exceed the dynamic pointing accuracy of the conventional 20-year-old cinetheodolites still in use on national test ranges.) In the use of such instruments, it is further assumed that the instrument does not tilt on the azimuth bearing, that the antenna or the optical system does not wobble about the elevation bearing, that no flexure occurs while the instrument is moving, and that the precision that is built into the instrument is maintained under both static and dynamic conditions. These assumptions are simply not true, and, within the constraints of the strength of available materials, it does not appear to be feasible to build an instrument that will maintain stability in the low arc-second region when subjected even to moderate tracking dynamics. The WSMR Cinetheodolite, on the other hand, utilizes a principle that takes into account the fact that there will be deformations of the theodolite frame and that there will be errors introduced by mislevel, azimuth bearing runout, elevation bearing wobble, bending due to acceleration and gravitational effects, and many other sources. The instrument design also assumes that the nonrotating base of the instrument is not stable, i.e., that the structure upon which the theodolite rests is moving with respect to the earth and, indeed, that the earth is tilting. No instrument, planned or proposed, other than the WSMR Cinetheodolite, has any hope of compensating for all of these sources of errors.

THE WSMR CINETHEODOLITE CONCEPT

The WSMR Cinetheodolite compensates for these errors by means of an internal optical orientation system that operates as described in the following paragraphs.

Referring to Figure 1, the first critical element of this system is the Gravity Reference Mirror (GRM) system (4). This device consists of a damped spherical pendulum supported by an air bearing, with an optical flat normal to the longitudinal axis of the pendulum. The GRM system has a demonstrated capability to define the local gravity vector within 0.2 arc-seconds, and to eliminate variations in this vector, if the frequency of the forces causing these variations does not exceed the natural frequency of the pendulum. (The breadboard GRM has a natural frequency of approximately 1 hertz.) The GRM establishes a plane normal to the gravity vector immediately beneath the WSMR Cinetheodolite. Earth tremors, motions of the supporting pier, and other perturbations, as long as their amplitude and frequency are within the permissible excursions of the GRM, will not affect the orientation of this plane.

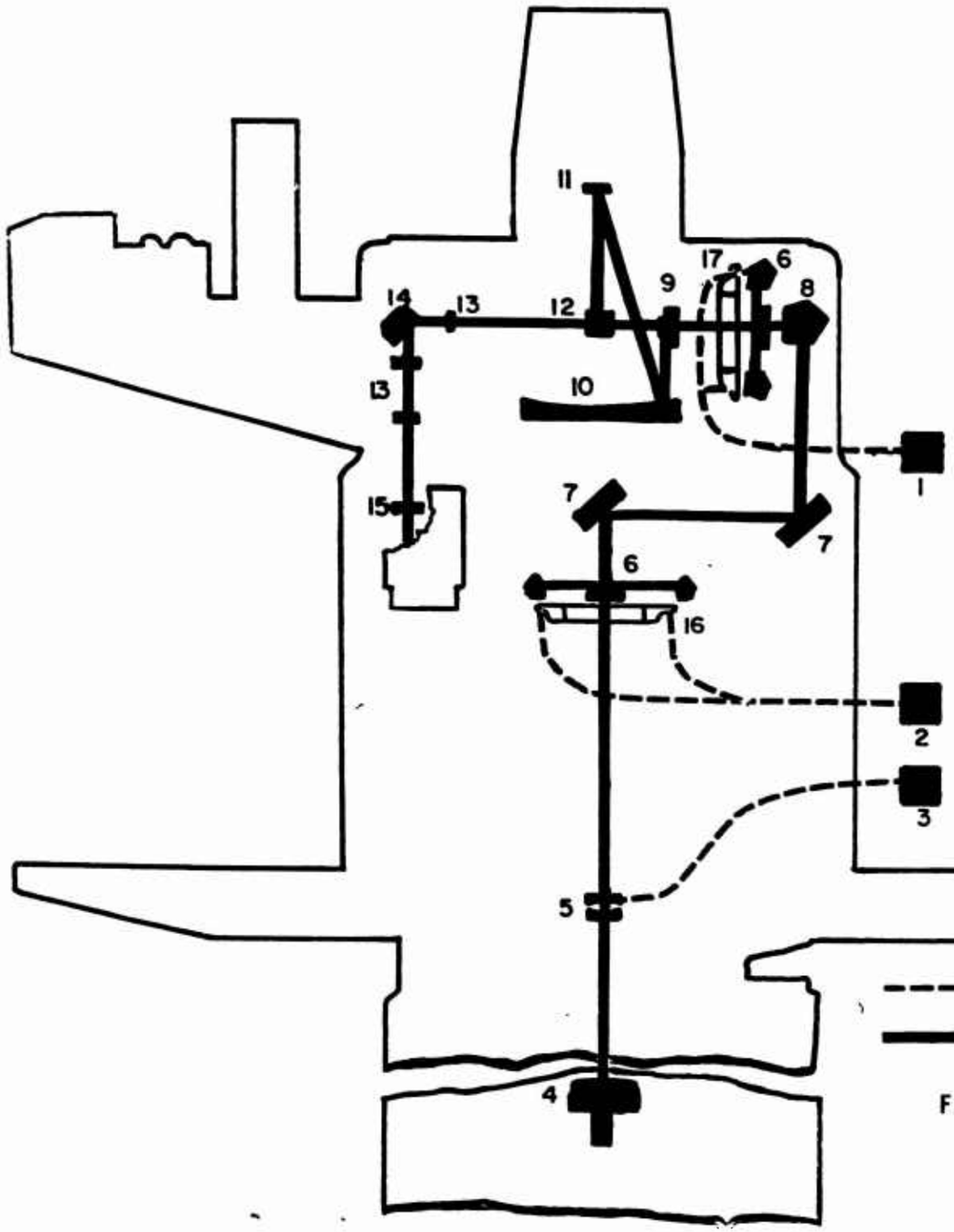

FLASHTUBES AND FIBER OPTICS

1. ELEVATION DIAL
2. AZIMUTH DIAL
3. FIDUCIAL

OPTICAL ELEMENTS

4. GRAVITY REFERENCE MIRROR
5. MISLEVEL OBJECTIVE
6. SCALE-READING OPTICS
7. RHOMBOID DEVIATOR
8. PENTA PRISM
9. ROTATING PENTA ASSEMBLY
10. MAIN OBJECTIVE
11. SECONDARY MIRROR
12. COMBINING PRISM
13. ERECTING LENS
14. 90° DEVIATOR
15. FOCUSING WEDGE

DIALS

16. AZIMUTH DIAL
17. ELEVATION DIAL

FLASHTUBES AND FIBER OPTICS

OPTICAL PATH

FIGURE 1 DATA OPTICAL TRAIN SCHEMATIC

The basic cinetheodolite design utilizes this precise reference in the following way: a target is engraved on the rear surface of the "mislevel objective" lens (5) located in the nonrotating base of the cinetheodolite. This surface also corresponds to the rear nodal point of the lens, which is located one-half focal length from the front surface of the GRM. The target is illuminated by a high-intensity flashlamp (3). The optical effect of this arrangement is that a collimated beam of light emerges from the "mislevel objective." The direction of this beam is insensitive to tilting of the "mislevel objective" and forms the basic reference for the WSMR Cinetheodolite.

This column of light (called the fiducial image beam), after emerging from the mislevel objective, monitors azimuth bearing runout and other azimuth-derived sources of error. This beam of light is then displaced by a periscope assembly (7) in the horizontal plane, while maintaining verticality, in order to pass through a dual penta-prism system (8), splitting the fiducial beam into two to monitor perturbations of the elevation axis. Misalignment, bearing wobble and runout, and other sources of error produced at this point yield a displacement in the ultimate position of the fiducial image, thus providing a means by which the errors may be eliminated.

After monitoring elevation-axis errors each of the fiducial image beams passes through a pair of beam-splitting devices (9), each of which is also a dual penta-prism assembly. These devices are designed so that, if angular motion occurs, the centroid of the two resulting images is constant. Inasmuch as there are two of these assemblies, four images result from the single beam with which we started. These four beams are directed to the primary mirror (10), to the secondary mirror (11), the combining prism (12), erecting lens (13), 90° deviator (14), and on to the film at the focal plane of the camera. In this way, the single fiducial target on the "mislevel objective" produces four fiducial images at the focal plane. These four images form the fiducial reference against which the position of the missile image is measured. Since the missile image and the fiducial beams are all acted upon in the same manner by the main optical system (by tube bending or gravitational effects on the primary mirror cell), the relative position of the missile image, with respect to the fiducials, will be essentially independent of primary effects.

A similar situation exists for the azimuth and elevation graduated circles. These scales are optical flats precisely engraved with 0.2-arc-second graduation accuracy. The scales (16 and 17) are illuminated at two points on a diameter by flashlamps (1 and 2). The resulting images are directed by means of penta-prisms and plane mirrors into the main data train. To remove eccentricity errors, the angular indices are derived at two points on the diameter, in the same manner as the numerical data, and are processed through the data train in an identical fashion, except that the beams do not pass through the main optics.

The data presented to the focal plane of the WSMR Cinetheodolite thus consists of the missile image, four fiducial images, and four scale readings. The other design features of the WSMR Cinetheodolite are more or less conventional, although completely modern and representative of the current state of the art. The operator's guide scope incorporates significant human engineering improvements in that the operator faces forward, views with binocular vision through a single objective, and is not required to move his head during the tracking process. The annular platform is a separate unit, isolated from the instrument in order to further reduce mechanical motions introduced into the theodolite by the operator and control equipment. The camera and camera control system provide a 50-sample-per-second capability which operates in synchronism and phase with range time.

This discussion of the basic principle of operation of the WSMR Cinetheodolite is a simplified version of the actual means by which the instrument is rendered insensitive to mechanical deformation, and serves only to illustrate the manner in which this is accomplished. More detailed descriptions of the design concept, the principle of optical compensation and the techniques utilized to implement the principle, are to be found in WSMR documents indicated in Table I.

TESTING

The primary function of this report is to present data which have determined the degree to which the breadboard instrument meets the design objective, to present the evaluation of the WSMR Cinetheodolite breadboard instrument in terms of the design objectives, and to discuss the data analyses which form the basis of the evaluation. This is done by discussing subsystem performance with a strong accent on subsystem deficiencies. This type of format may seem a somewhat negative way of describing the performance of a new and unique instrument, but it must be remembered that the breadboard instrument installed and tested at WSMR was not expected to perform as a completely developed fieldworthy instrument. The primary intent of the instrument was to determine the feasibility of the concept and indicate the problem areas needing special attention for further development. As this report indicates, the design concept is thoroughly validated, and minor as well as major problem areas are delineated. The rationale for this type of approach was to make the report as useful as possible to personnel involved in future development of the instrument rather than to justify the development per se.

Since the delivery and installation of the breadboard instrument at WSMR, July 1967, considerably more time has been devoted to the development of precise measurement techniques than has been given to the test and evaluation of the instrument itself. This is not surprising when considering that in the 30 or more years of theodolite history it is only recently that the Test Ranges have become interested in making measurements of dynamic instrumental

pointing accuracy. This new requirement also coincides with a new requirement for making measurements in the field with accuracies previously achieved only in the laboratory. The impact of the dual requirement, at first, produced some confusion and many abortive attempts by the task team to formulate meaningful test procedures and provide adequate instrumentation to implement the tests. Much of the difficulty stemmed from the fact that the manufacturers of optical laboratory instrumentation have never been particularly concerned about the dynamic response of their instrumentation; e.g., the Hilger-Watts Autocollimator, long used as a standard for high-precision measurements at WSMR, was thought, prior to the WSMR Cinetheodolite evaluation tests, to have a flat response up to approximately 10 hertz. It was late in the test program before it was discovered that the usable bandpass of that autocollimator, as well as other available autocollimators, did not exceed one hertz. It is easy to see how misconceptions such as the example given can have disastrous effects on a test program.

It is unfortunate that this report cannot treat extensively the measurement techniques developed by the WSMR Cinetheodolite test program because this information would probably be of much interest to people involved in the test and development of theodolites. The reason for not including this information is simply that the evolution of an optimum or reasonably efficient test program is still in process here at WSMR and will probably continue for a year or more or until a production prototype is delivered. It is expected that a separate report on cinetheodolite testing methods and the WSMR Cinetheodolite test complex will then be published.

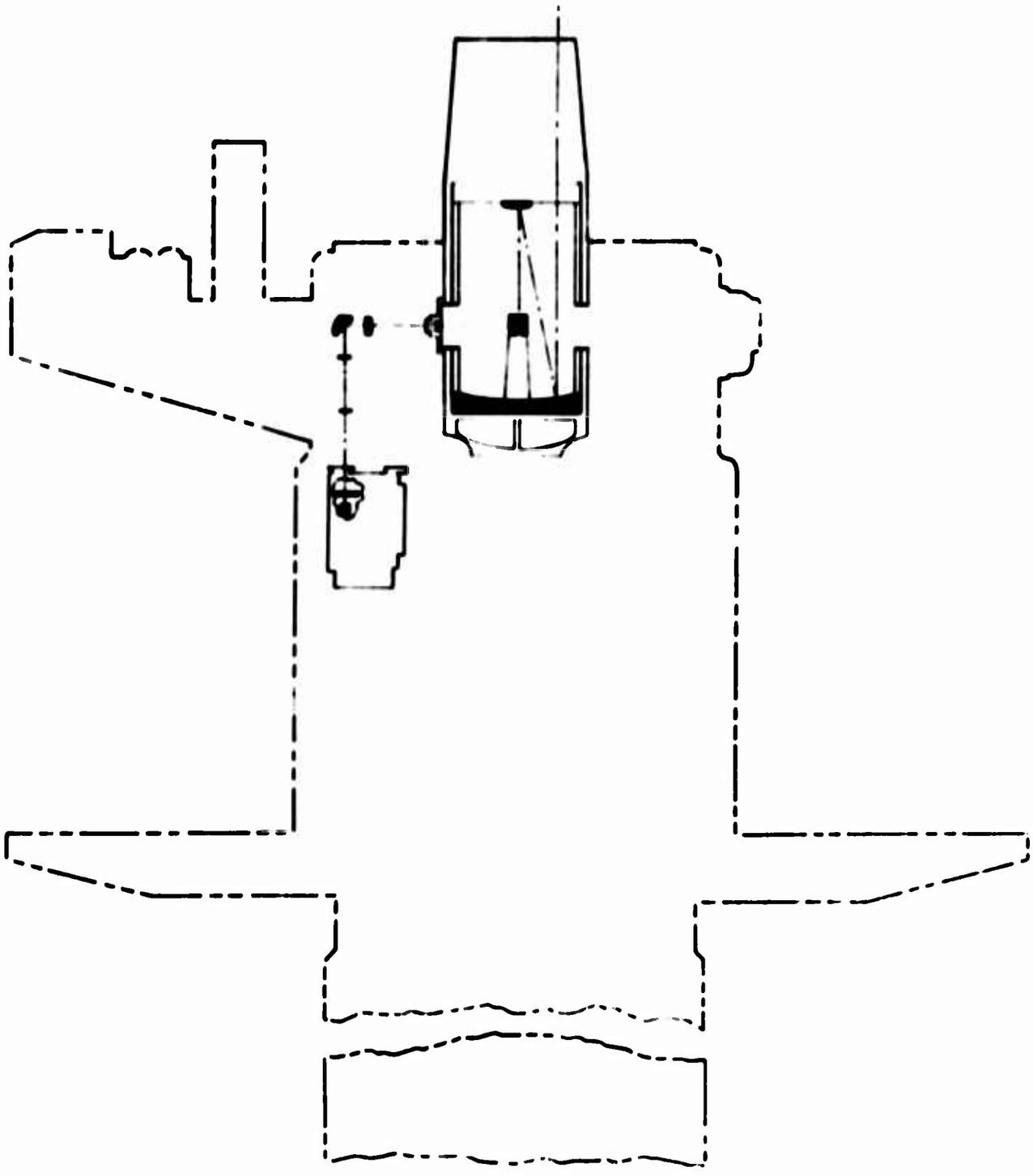

MAIN OPTICAL SYSTEM

MAIN OPTICS

CONFIGURATION

The main optical system, i.e., the optics which image the missile in the film plane, consists of a Cassegrain telescope, a field lens, erecting lenses, and focusing plates. The telescope (illustrated in Figure 2) is a 76-inch focal length, f/6.5 (f/8.2 with the primary mirror obscuration caused by the secondary mirror) system consisting of a 26-inch focal-length, paraboloidal primary mirror made of fused quartz and a 9.6-inch focal-length, hyperboloidal secondary mirror. The secondary is held in place by a thick flat plate of optical glass, rather than a metal structure, in order to eliminate one source of diffraction effects. A flat mirror set at a 45-degree angle reflects the light from the secondary to the telescope's prime focus point at the side of the telescope tube. At this point there is a field lens. This is also the point at which the light from the optical data train for the graduated circles is focused and joins the light from the missile. The light continues from the field lens to an erector lens shown in Figure 3, which collimates so that light can pass through the next glass plates and wedges properly. The first such plate has a wedge cemented to it that deviates the fiducial beams by the proper amount but leaves the rest of the light undeviated. A prism then turns the entire beam by ninety degrees, and the light passes through another glass plate holding a wedge whose function is to split off the graduated circle beams. The light is then refocused by the second erector lens, whose eventual focus point is at the film plane. Between this lens and the film plane, however, there is a filter disk and a set of focusing plates. The filter disk contains six different optical filters, any one of which may be placed in the light beam. The focusing plates allow the system to be focused on objects as close as 2000 yards from the instrument, while not affecting the focus of the fiducial and index images or the graduated circles.

The image-forming capability of the main optical system, at least in the theoretical model, is fairly close to being limited by diffraction for objects near the optical axis. There is a small amount of axial chromatic aberration. Off axis, there is some curvature of field, distortion, and lateral color. Other aberrations seem to be virtually absent. The performance of the actual as-built cinetheodolite, however, must inevitably fall somewhat short of the theoretical due to tolerance build-ups incurred in manufacturing and assembly. Because of this, after the cinetheodolite was fabricated and assembled, the main optics were tested at the contractor's plant.

TESTS

Conventional Tests

The image distortion was determined by photographing a square test pattern through the optical system and measuring the deviation of the lines. Distortion is a critical aberration as it pertains directly to the instrument's

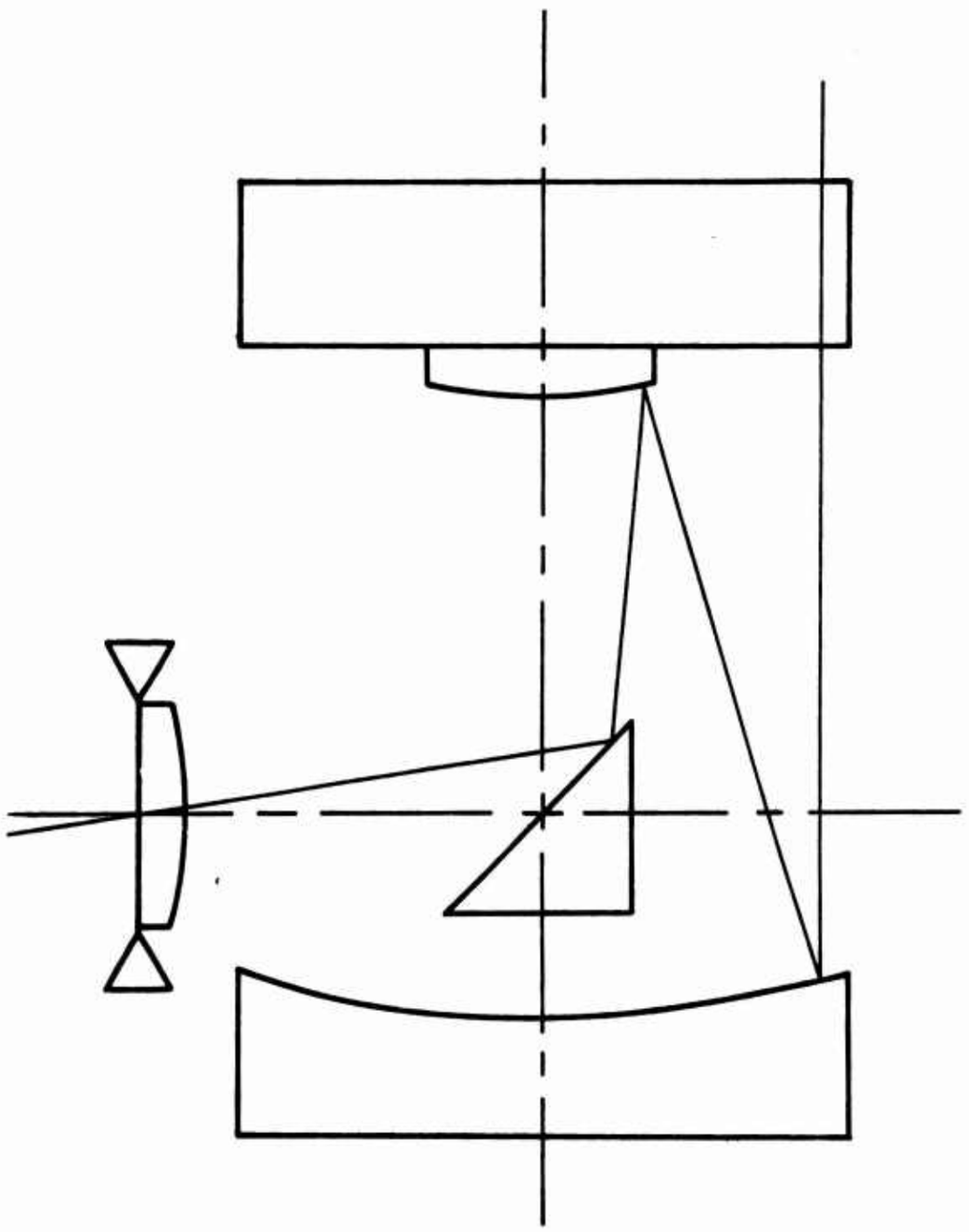

FIGURE 2 MAIN TELESCOPE

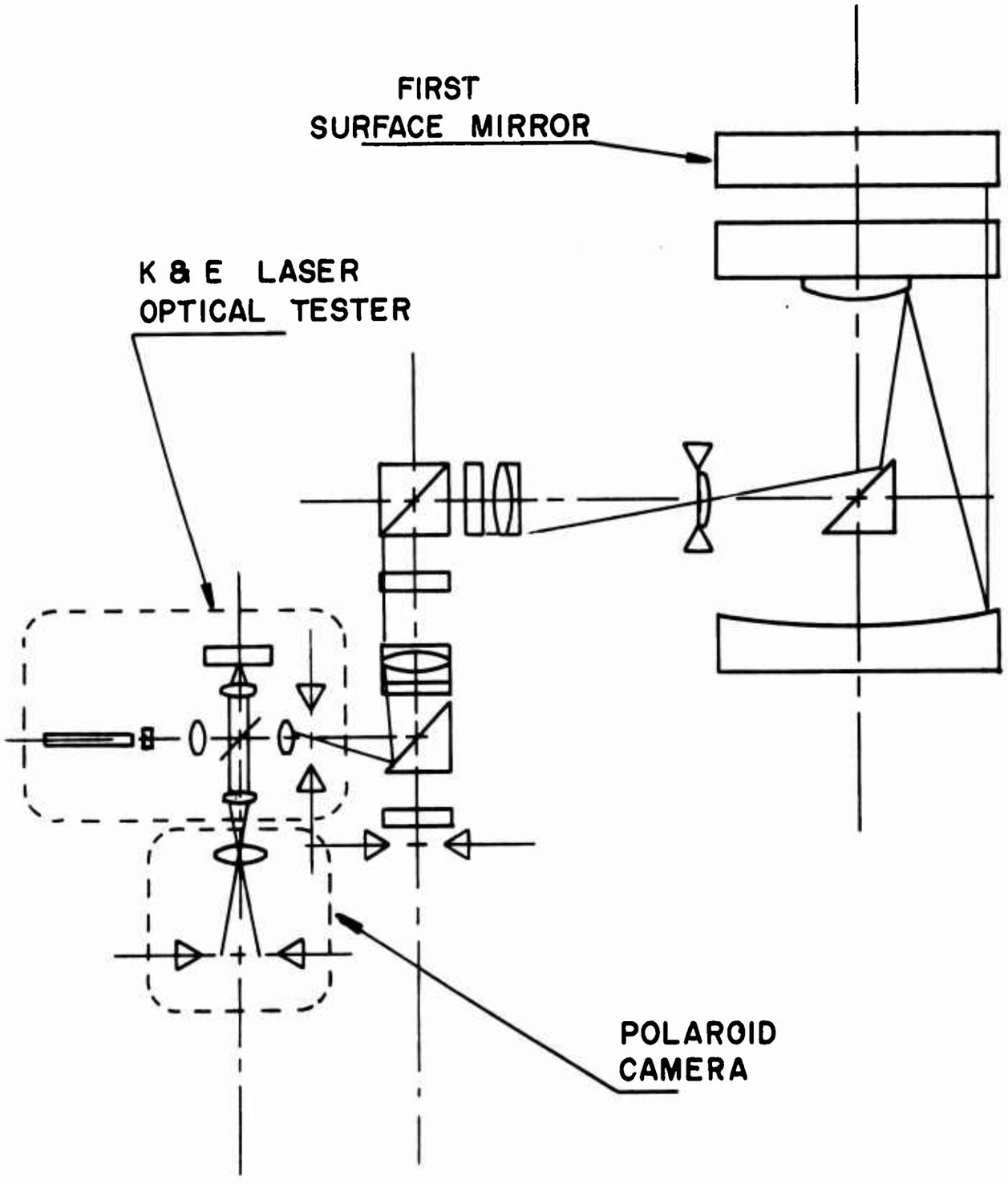

FIGURE 3 TEST SCHEMATIC MAIN OBJECTIVE WSMR CINETHEODOLITE

scale factor and, hence, its accuracy. It amounted to a maximum of 0.8 arc-seconds of barrel-type distortion. Curvature of field was determined by making visual and photographic observations of the same test pattern and of resolution charts, and noting the variation of the "best focus." The maximum field curvature found by this method was about 0.008 inches, which was considered completely acceptable.

Resolution and contrast testing was then conducted by photographing a high-contrast and a low-contrast target. The target patterns were the standard square three-bar arrangement, providing a series of resolution steps from about one second up, in ratios of 1.12 to 1. Twenty steps of resolution patterns were available, with each step oriented in two orthogonal directions. The pictures were made on Kodak high-resolution plates, which prohibited testing with the red filters in the optical system because of the spectral sensitivity of the emulsion. Therefore, only the clear and yellow filters were used. In order to eliminate loss of resolution due to vibration and air turbulence, a powerful electronic strobe light was used to illuminate the resolution targets. Exposure times on the order of one millisecond were then made possible.

Testing was carried out in three areas of the field of view of the optical system: in the center, in the "zonal" intermediate areas, and near the edge. The developed plates were then examined under high-power microscopes, and the smallest clearly discernible target patterns were identified (separately for horizontal and vertical patterns). Since the optical system focal length was known, it was a simple matter to convert the measured resolution in microns to seconds of arc. The tabulated data from four photographs, with all four possible combinations of two filters and two contrast ratios, are given in Table II.

The following comments summarize the information that can be gleaned from the data in Table II.

1. Area Comparison - From the grand average line and the area comparison line just below it, it is seen that resolution is about the same over the entire field, although at the bottom (1.8 seconds), and at the left (1.7 seconds), it is slightly inferior to the remainder of the field (1.3 to 1.5 seconds).

2. High Versus Low Contrast - Both kinds of readings are averaged on two lines and at the far right are the grand averages, which are 1.59 seconds for high contrast and 1.55 seconds for low contrast. The difference is not significant. This is an indication that the optical signal-to-noise ratio is quite good.

3. Clear Versus Light Yellow Filters - On the next two lines of Table II are averaged the respective readings through these filters. To the right of these two lines are the grand averages, 1.60 arc-seconds for the clear

TABLE II. RESOLUTION PICTURE ANALYSIS

Contrast	Filter	Top V	Top H	Right V	Right H	Center V	Center H	Bottom V	Bottom H	Left V	Left H	Grand Average
High	Clear	1.3	2.6	1.3	1.3	1.3	1.7	1.3	1.3	1.7	1.3	
High	L. Yel.	1.3	1.3	1.3	1.3	1.3	2.2	1.3	2.2	1.3	2.9	
Low	Clear	1.3	1.3	1.3	1.3	1.3	1.3	2.6	2.2	1.3	2.6	
Low	L. Yel.	1.3	1.3	1.3	1.3	1.3	1.3	1.3	2.6	1.3	1.3	
Grand Average (Area Comparison)		1.3	1.6	1.3	1.3	1.3	1.6	1.6	2.1	1.4	2.0	
		1.5		1.3		1.5		1.8		1.7		1.56
High Contrast		1.3	2.0	1.3	1.3	1.3	2.0	1.3	1.8	1.5	2.1	1.59
Low Contrast		1.3	1.3	1.3	1.3	1.3	1.3	2.0	2.4	1.3	2.0	1.55
Clear Filter		1.3	2.0	1.3	1.3	1.3	1.5	2.0	1.8	1.5	2.0	1.60
Light Yellow		1.3	1.3	1.3	1.3	1.3	1.8	1.3	2.4	1.3	2.1	1.64

Grand Average of Vertical Lines = 1.38 seconds

Grand Average of Horizontal Lines = 1.73 seconds

Astigmatic Information

Zonal				1.3	1.3			1.6	2.1			1.58
Axial						1.3	1.6					1.46
Rim		1.3	1.6							1.4	2.0	1.59

Spherical and Coma Information

All tabular values represent finest lines clearly resolved and are expressed in seconds of arc.

filter and 1.54 for the yellow filter. Again the difference is insignificant and indicates that the telescope optical system does not have excessive chromatic aberration.

4. Astigmatism - The grand average of the vertical target patterns showed 1.38 seconds resolution and that of the horizontal lines, 1.73 seconds. The difference, 0.35, represents a small and tolerable amount of astigmatism.

INTERFEROGRAMS

A final test of the overall optical system performance was conducted by making interferograms through the system and then analyzing them. It had been planned earlier to make a series of pictures of an "artificial star" and analyze the resulting diffraction patterns, but because of vibration and other problems, it was found to be impossible to obtain usable pictures in the manufacturer's facilities.

Figure 3 shows a schematic diagram of the setup used to make the interferograms. The "laser optical tester" is a tiny interferometer that can be attached to the end of a gas laser and placed at the eyepiece or in the film plane of an optical instrument. A rugged steel weldment with fine-adjustment provisions was bolted to the side of the cinetheodolite, and on it was mounted a gas laser to which was attached the compact interferometer. As the focal plane of the cinetheodolite is relatively inaccessible, a flat prismatic deviator was mounted just over the film plane to bring the image plane outside the instrument. A large optical flat was used to reflect the light emerging from the front of the telescope back through the system and, thus, "double pass" the system with the laser light. Testing was done with the telescope tube oriented both horizontally and vertically. The interferogram pictures were made with a Polaroid camera.

These pictures were subsequently analyzed with the aid of a computer program written for that purpose. The picture is a compound of the wavefront deformities caused by the instrument being tested, the deformities caused by the test equipment, and the arbitrary orientation of the interferometer. The computer program must mathematically remove the latter two factors before the interferogram can meaningfully relate to the instrument being tested. This is done by determining the fringe count at a uniformly distributed scatter of points across the photograph and inputting this information with the X and Y coordinates of each point. The computer then prints a "map" of the actual wavefront, with symbols representing increments of fringes, and the actual separation between consecutive symbols printed out at the top of the page.

Figure 4 is a representation of this map on which contour lines have been drawn. The average reference plane is denoted by a 0 symbol. The numbers (1, 2, 3 and so on) indicate that at those points the wavefront is

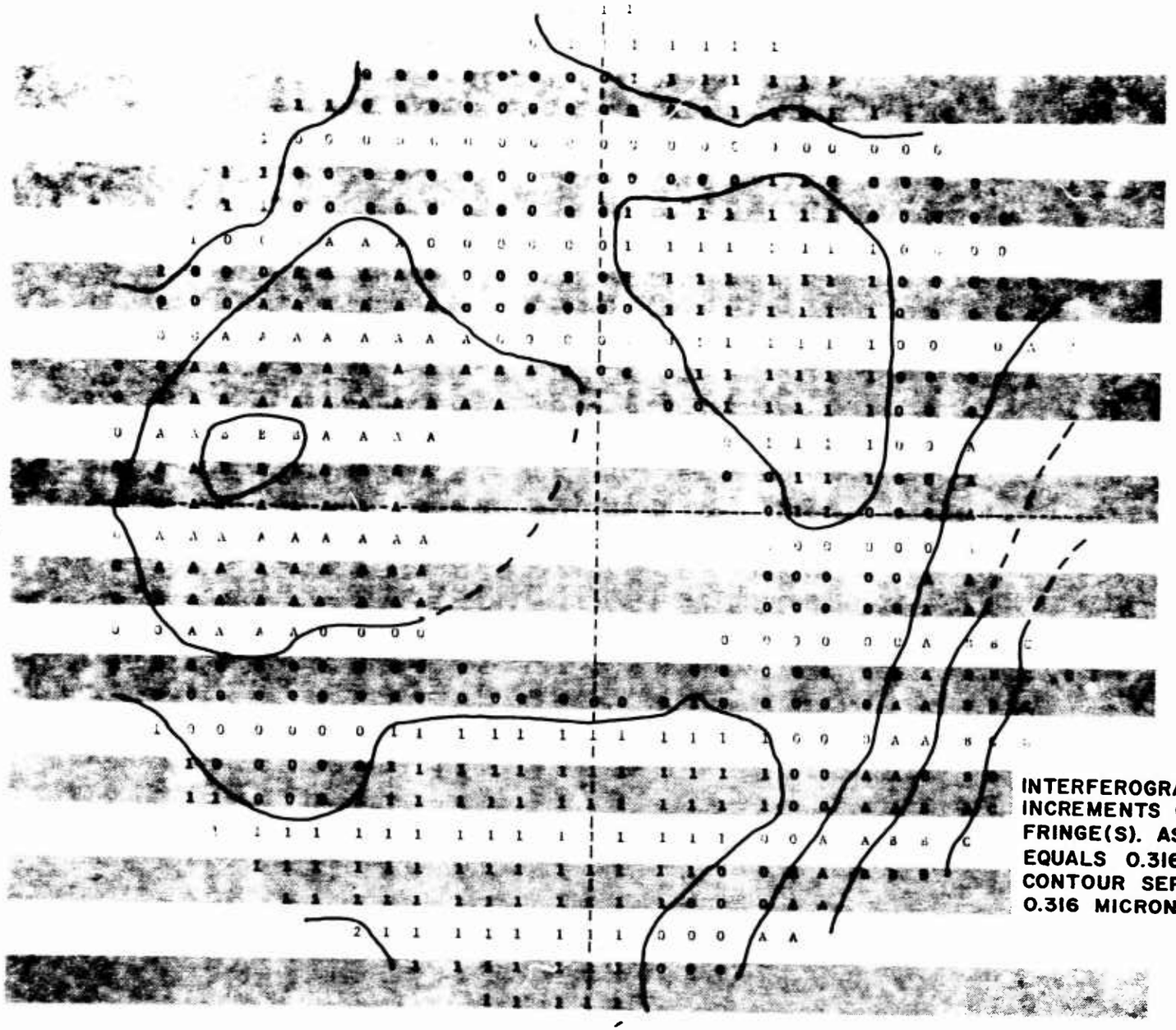

INTERFEROGRAM, BY INCREMENTS OF 1.000 FRINGE(S). AS ONE FRINGE EQUALS 0.316 MICRON, CONTOUR SEPARATION IS 0.316 MICRON.

FIGURE 4

"advanced" that number of fringes ahead of the average plane. The letters (A, B, C and so on) mean that the wavefront is retarded 1, 2, or 3, or more fringes, respectively, behind the average wavefront. In actuality, the worst error is the edge near "4 o'clock" which is retarded 3 fringes (as shown by the letter "C"). There is a lesser depression of two fringes on the left, just above the centerline. On the other hand, there are four "plateaus" showing a rise of one fringe (from number "1") and just one spot that shows a "mountain peak" of two fringes. The vacant area in the center of the interferogram corresponds to the occluded Cassegrain spot on the objective, and the vacant area on the right rim at "3 o'clock" corresponds to the occlusion caused by the mask sheltering the four small penta-prisms that deviate light from the cinetheodolite mislevel objective.

Figure 5 shows a hand-drawn cross-section of the interferogram map down the vertical centerline. The sectional view brings out the dips and rises in the wavefront that are depicted by contour lines on the map of Figure 4. Having a section of the wavefront, one may draw a line tangent to it at any point, with due allowance for arbitrary scale factors. Likewise, the normal to the wavefront at the same point represents the direction of a ray of light at that point, and the collimation in seconds of arc can be directly determined from measurements of this wavefront. The computer was programmed to do this over the entire map rather than at just one selected cross-section, and the result is shown in Figure 6, a representation of the computer-printed "Decollimation Graph," in increments of integral arc-seconds. In this figure, the number 2, for example, means that at that point of the wavefront that particular ray is decollimated by two seconds.

Since the direction of every ray at every spot, and the focal length of the system are known, the data can be converted to a spot diagram (Figure 7). Unlike the other printouts, which were in a sense pictorial representations of what was taking place at the entrance pupil, it is a representation of what takes place at the film plane. If a single ray lands on some spot, there is a number "1." If seven of the original 600 rays hit the same spot, a "7" shows on the printout. Ideally, all the rays should pile up on dead center, but even the slightest deformation of the wavefront will cause decollimation in that area. This program automatically scales the spot diagram and prints the scale on the first line (13 microns to the inch). Knowing the wavelength and the focal length, one can also draw in the scale for seconds of arc. On this diagram, one second equals 0.877 inch.

Examination of the spot diagram shows a scattering of spots off to the left at about a 15-degree angle. This follows directly from the wavefront interferogram (Figure 4) where the narrow contour lines of greatest change of the wavefront per unit distance are also at about a 15-degree angle to the vertical. This somewhat oval blur indicates a small amount of astigmatism in the system.

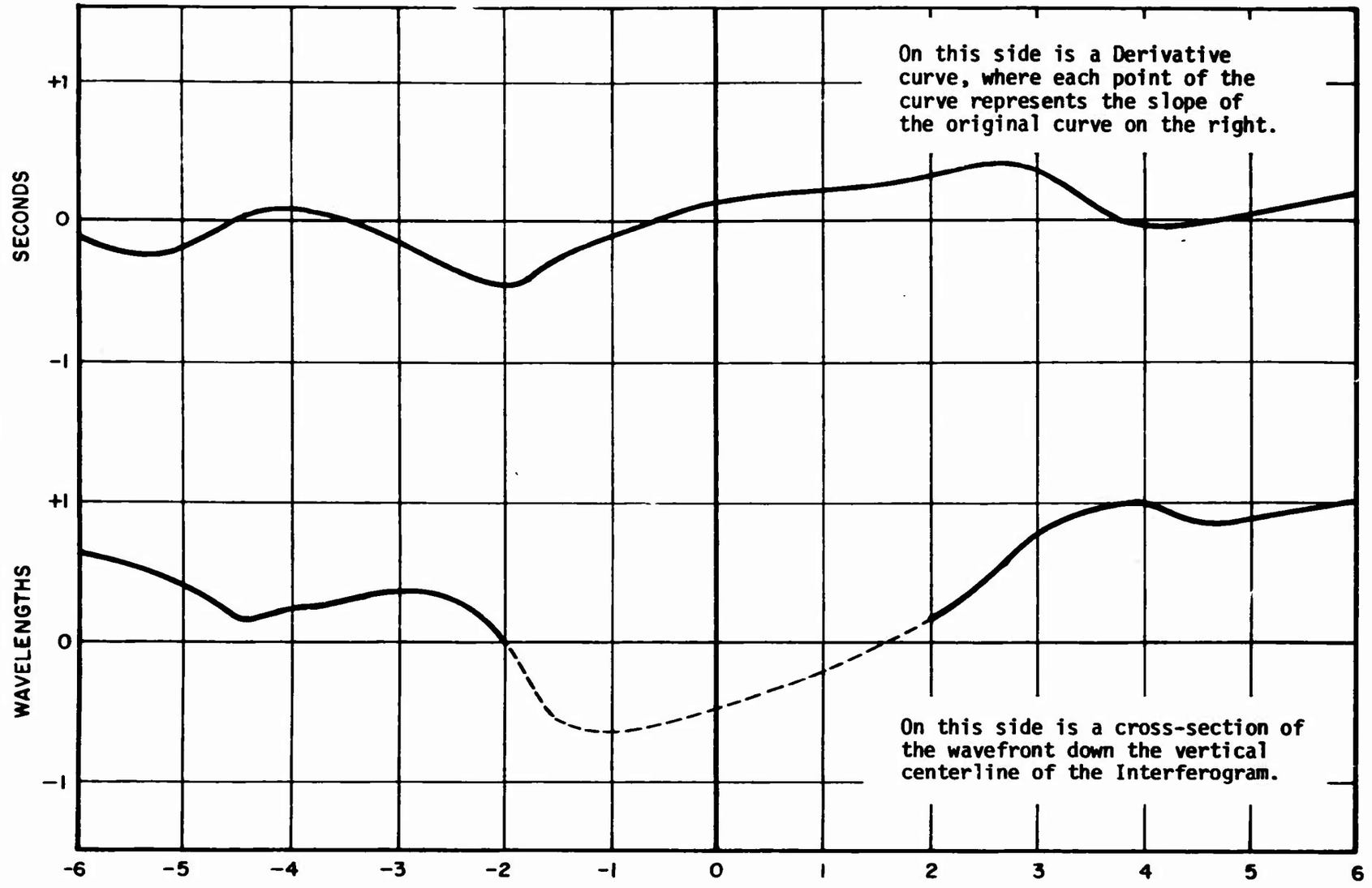

FIGURE 5 CROSS-SECTION OF WAVEFRONT

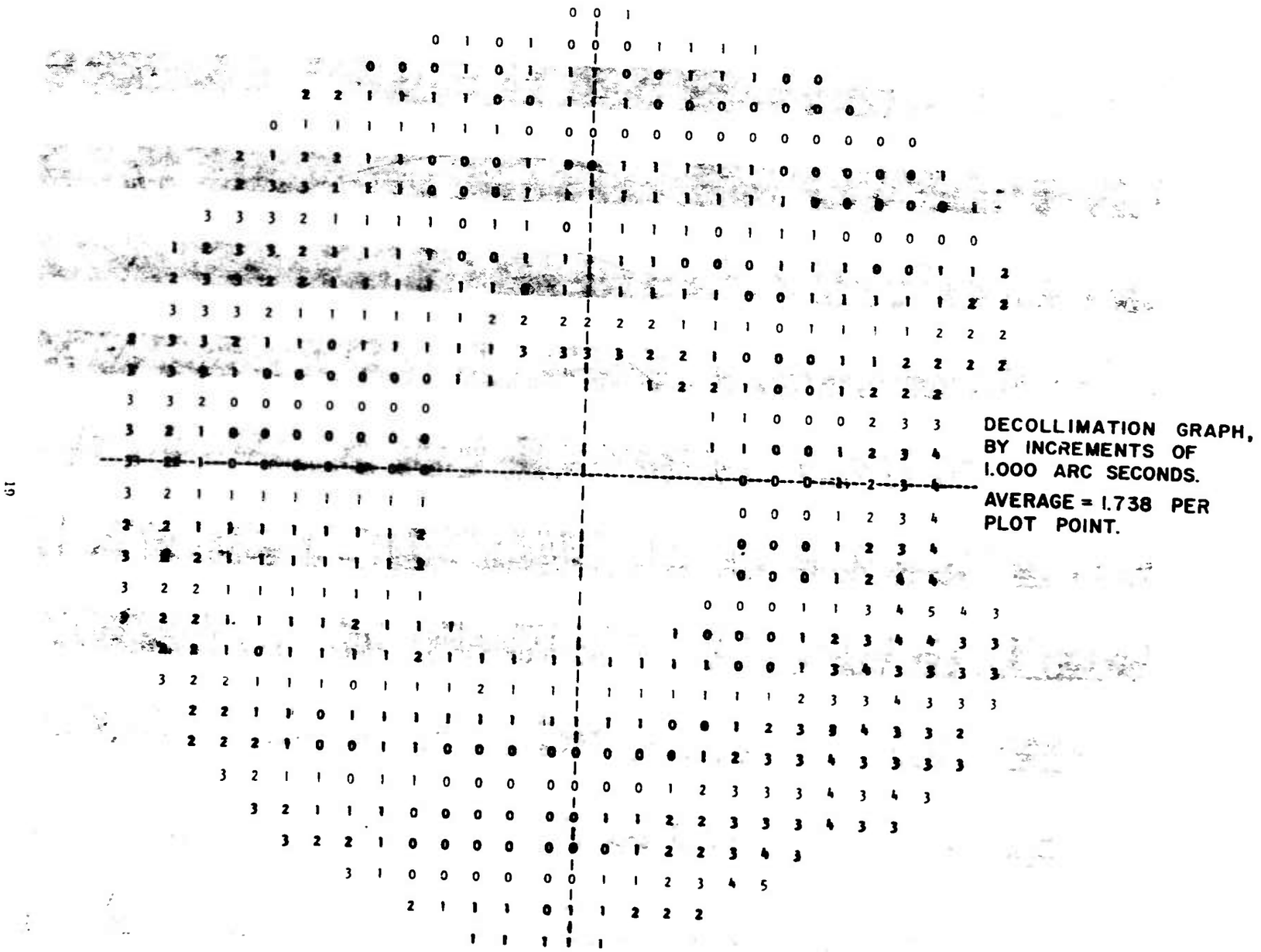
DECOLLIMATION GRAPH,
BY INCREMENTS OF
1.000 ARC SECONDS.
AVERAGE = 1.738 PER
PLOT POINT.

FIGURE 6

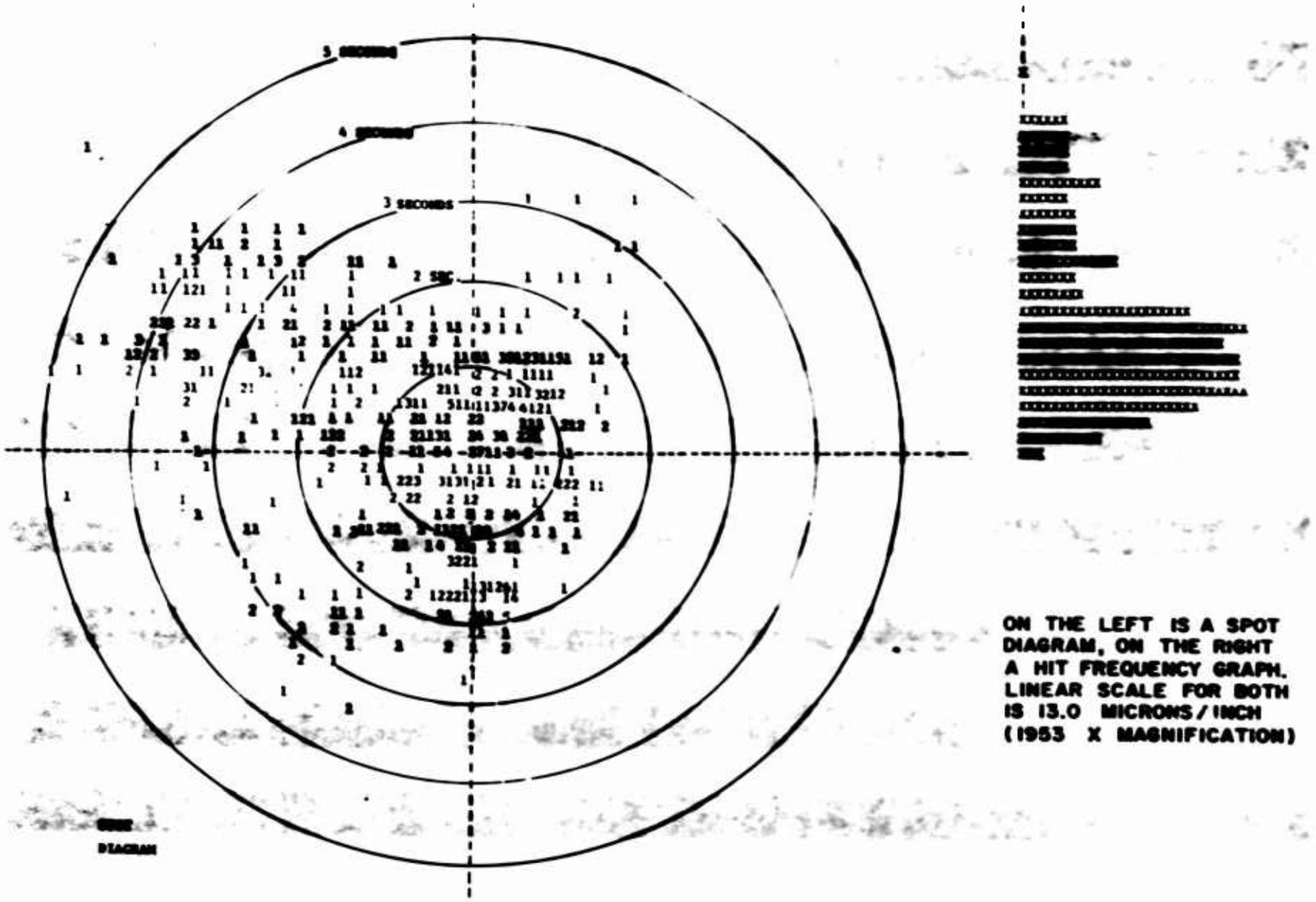

ON THE LEFT IS A SPOT DIAGRAM, ON THE RIGHT A HIT FREQUENCY GRAPH. LINEAR SCALE FOR BOTH IS 13.0 MICRONS / INCH (1953 X MAGNIFICATION)

FIGURE 7 SPOT DIAGRAM AND HIT FREQUENCY

The computer was also made to determine the radius to each hit and total the number of hits in each ring bounded by radial increments. This is printed as a graph to the right of the spot diagram, using the same vertical scale of 13 microns to the inch. A curve of hits per unit area is plotted on the final computer printout shown in Figure 8. The vertical scale was carried over from the preceding plots, and the horizontal scale was arbitrarily chosen. A vertical scale of seconds of arc is superimposed on this graph.

This last luminosity graph permits one to predict the resolution of the optical system. If a criterion similar to the Rayleigh criterion is used (namely that the radius of the Airy disk equals the resolution), then one could similarly say that the line which included half the area under the luminosity curve could be used to denote resolution. On this basis, one would expect about 0.7-second resolution, but the diffraction losses are not yet taken into account.

All the work described so far was based on geometric optics. In the more realistic world of physical optics, results may vary from ray diagrams because wave motions can strengthen each other to form energy peaks or interfere to cancel out altogether. An optically perfect 12-inch aperture telescope would still have a limiting resolution of 0.52 second according to the Rayleigh criterion. This is based on the well-known formula

$$R = \frac{1.22\lambda}{A}$$

where R is the resolution in radian measure, lambda the wavelength of the light being used (0.6328 micron), and A is the aperture or objective diameter. Expressing all in the same unit (microns) and converting radians to seconds,

$$R = \frac{1.22 \times 0.6328}{305{,}000 \times 0.00000485} = 0.52 \text{ second} .$$

Adding diffraction error, 0.5 second, to interferogram-measured aberration losses, 0.7 second, a resolution of 1.2 seconds should be expected. As already seen, resolution measured by analyses of target patterns varied between 1.3 and 2.6 seconds, averaging 1.56 seconds. This shows good agreement with the theory. The small discrepancy could be accounted for by residual chromatic aberration and internal flare (neither measurable by the interferogram), or simply by subjective variation in evaluation of resolution target patterns.

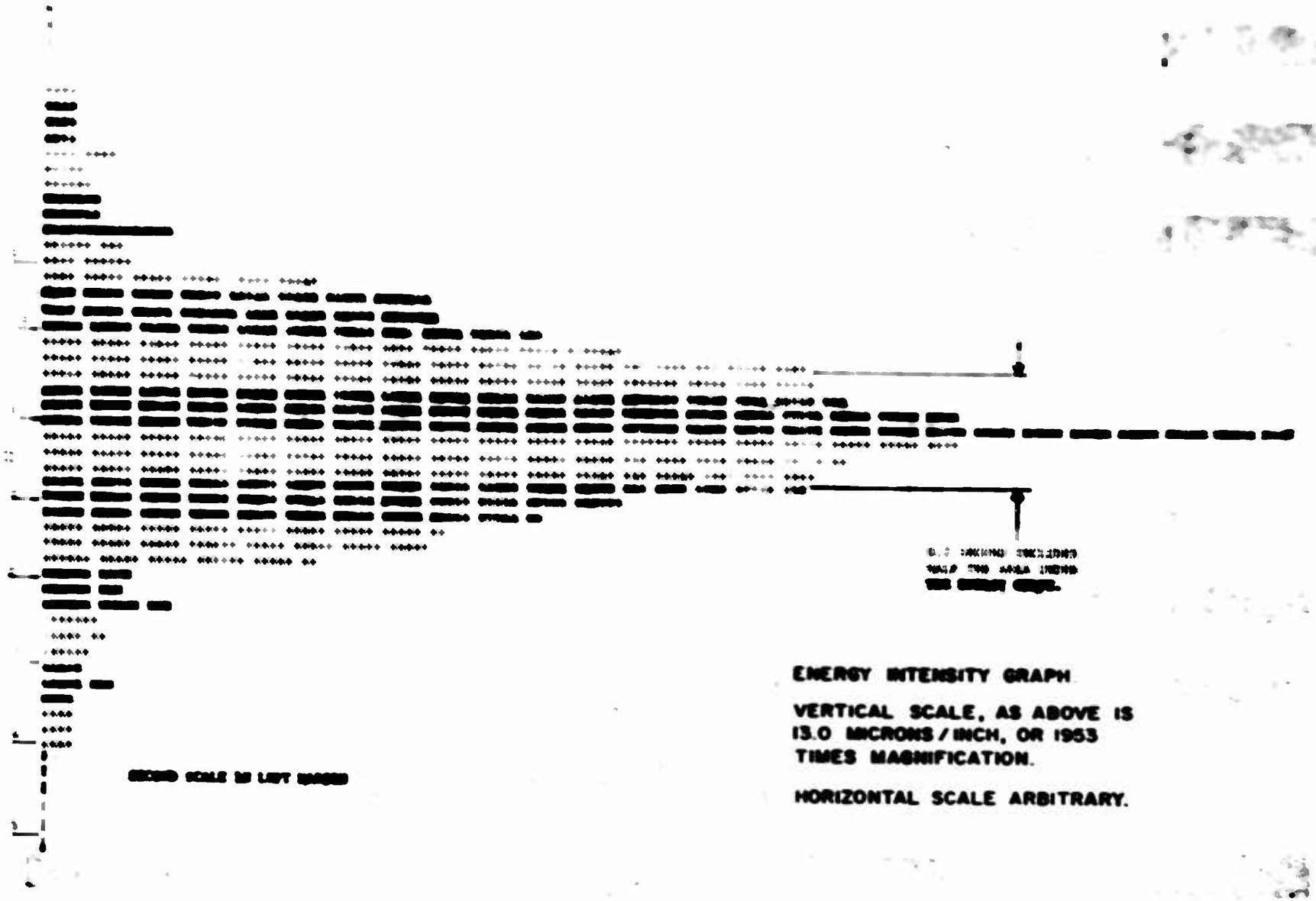

ENERGY INTENSITY GRAPH

VERTICAL SCALE, AS ABOVE IS 13.0 MICRONS / INCH, OR 1953 TIMES MAGNIFICATION.

HORIZONTAL SCALE ARBITRARY.

FIGURE 8

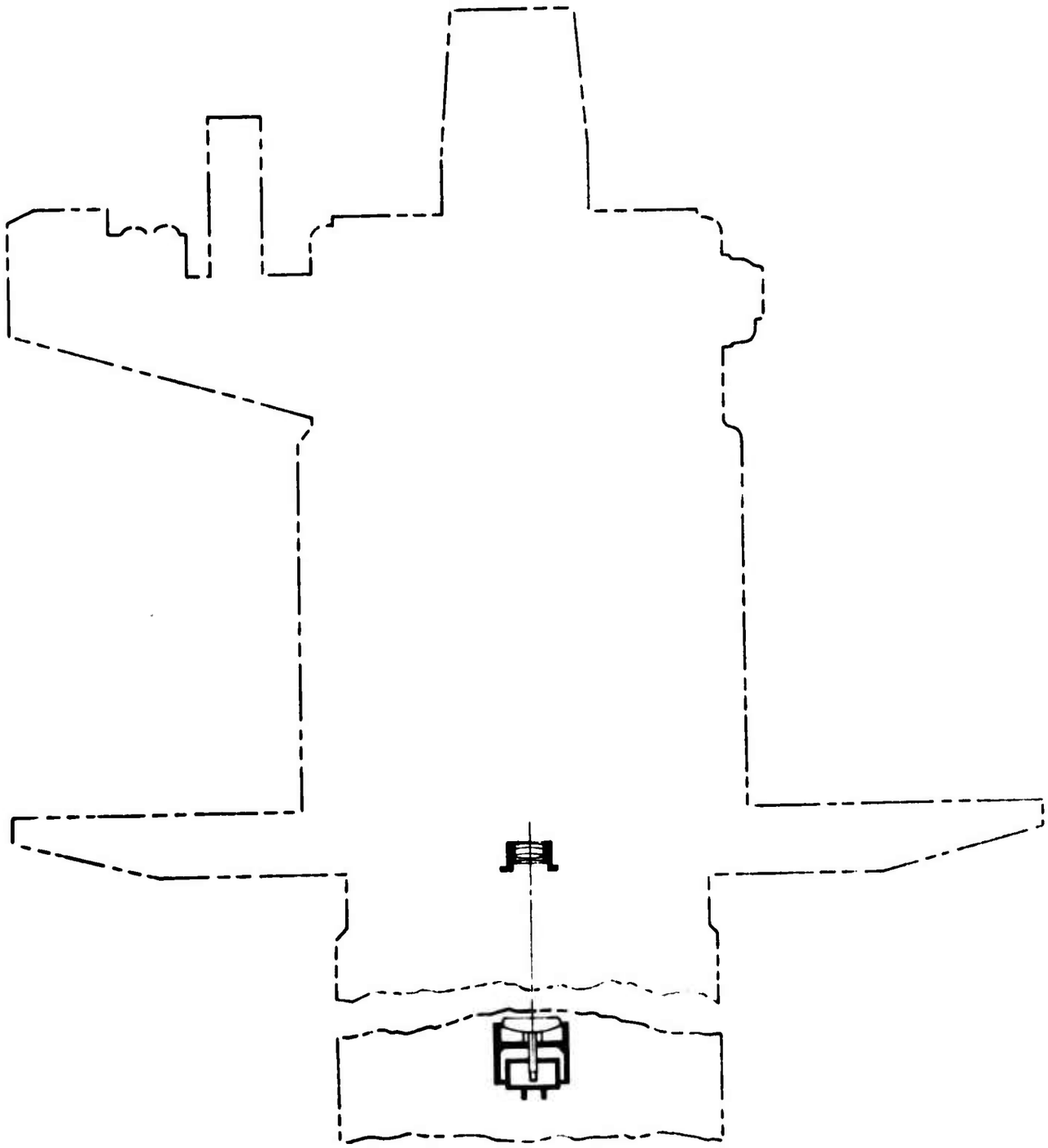

GRAVITY REFERENCE MIRROR SYSTEM

THE GRAVITY REFERENCE MIRROR SYSTEM

CONFIGURATION

The heart of the WSMR Cinetheodolite instrument is the Gravity Reference Mirror (GRM) system whose function is to maintain a vertical collimated light beam from which the reference fiducial images are formed. Because of surface irregularities and unequal distribution of mass in the earth's crust, the gravity vector at different geographical points does not represent a "true vertical" to the accuracy required by the WSMR Cinetheodolite System. The relationship between the "true vertical" and local gravity, however, has been determined at Bill Site and is stable enough to permit utilization as a reliable reference system. At WSMR, simple mercury pools have been used to establish and maintain a vertical reference and are still used in some applications. The primary reason that a mercury pool was not used in the WSMR Cinetheodolite was the low reflectivity which would have added to the problems of the "light-starved" optical data train. The reflectivity of pure mercury is 76 percent, but this value decreases rapidly with even a slight amount of surface oxidation.

The GRM, a pendulum whose upper surface is a highly reflective flat mirror, is supported on a gas bearing as shown in Figure 9. The critical components are two glass pads separated by the bearing fluid which supports the upper pad. The lower surface of the upper pad and the upper surface of the lower pad have been worked so that these surfaces are spherical and conform very accurately. A pendulous stem is attached to the upper pad and extends downward through a hole in the center of the lower pad and into a receptacle containing damping fluid. Other components include the housing, leveling legs and air inlet fittings. The assembly behaves like a simple damped pendulum of length equal to the radius of curvature of the spherical surfaces. The device is made into a vertical reference element by rotating the upper pad about a vertical axis and adjusting the balance of the upper pad until no deviation of the normal to the mirrored flat surface is noticed with this rotation. When balanced, it remains level within about 0.1 arc-second over a base tilt range of several arc-minutes. The damping fluid is used to prevent flutter of the pendulous mass that might be caused by minute air flow irregularities and to absorb any energy imparted to the pendulous mass by geoseismic or other perturbations, especially those occurring near the natural resonant frequency of approximately 1 hertz. The GRM is shown in Figures 10 through 12.

Supporting equipment for the gas bearing of the GRM consists of a dry air supply assembly, which includes a Bell & Gosset oil-less air compressor, Model SYC 010-IAD; a small Air Draulics Company storage tank; a Hanna Company oil and water trap and regulator; a King filter, Model 1/2 20 RG; a King-Visi-Guard dryer, Model 1716-1; the final pressure regulator; a

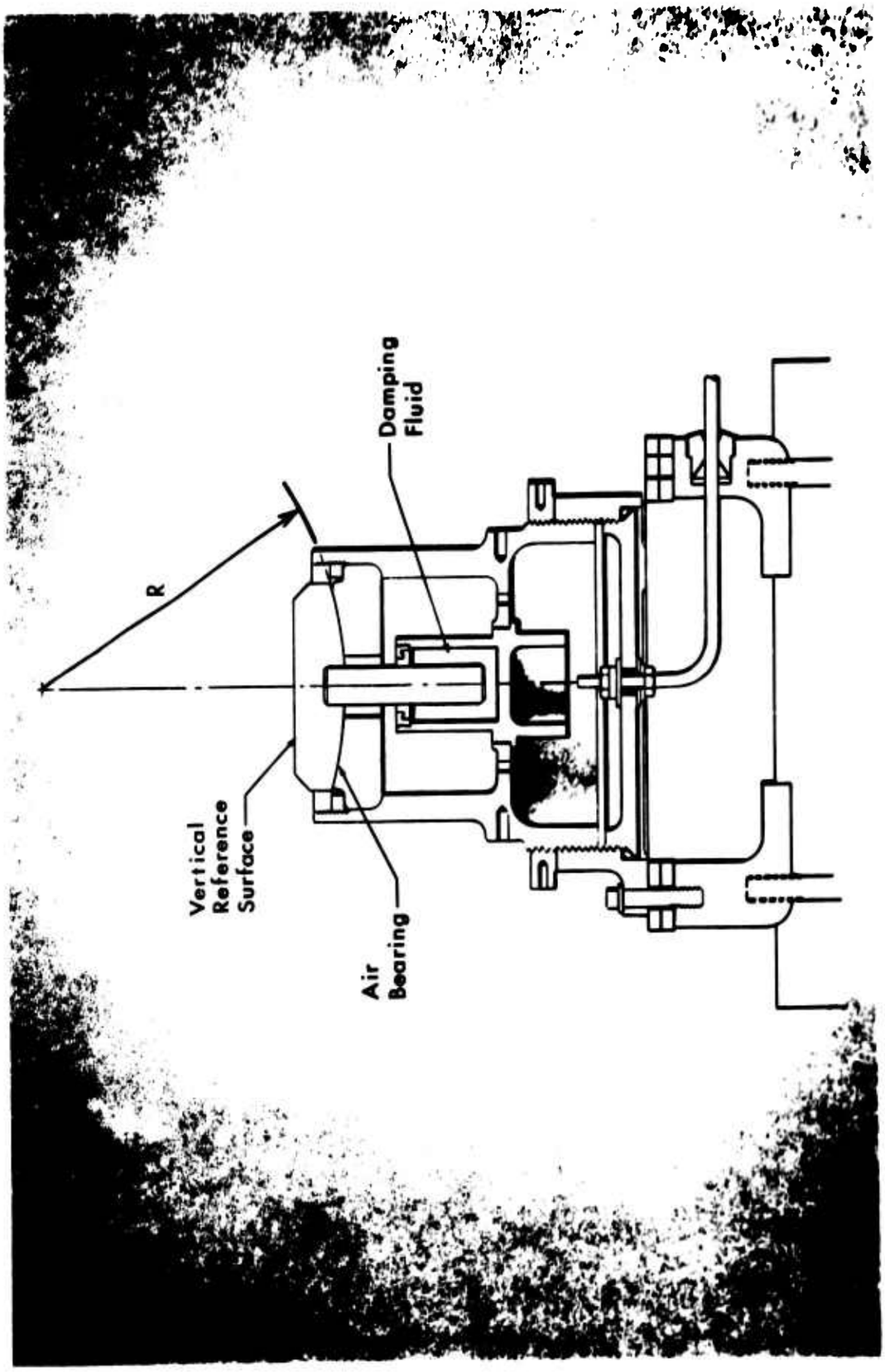

FIGURE 9 GRAVITY REFERENCE MIRROR

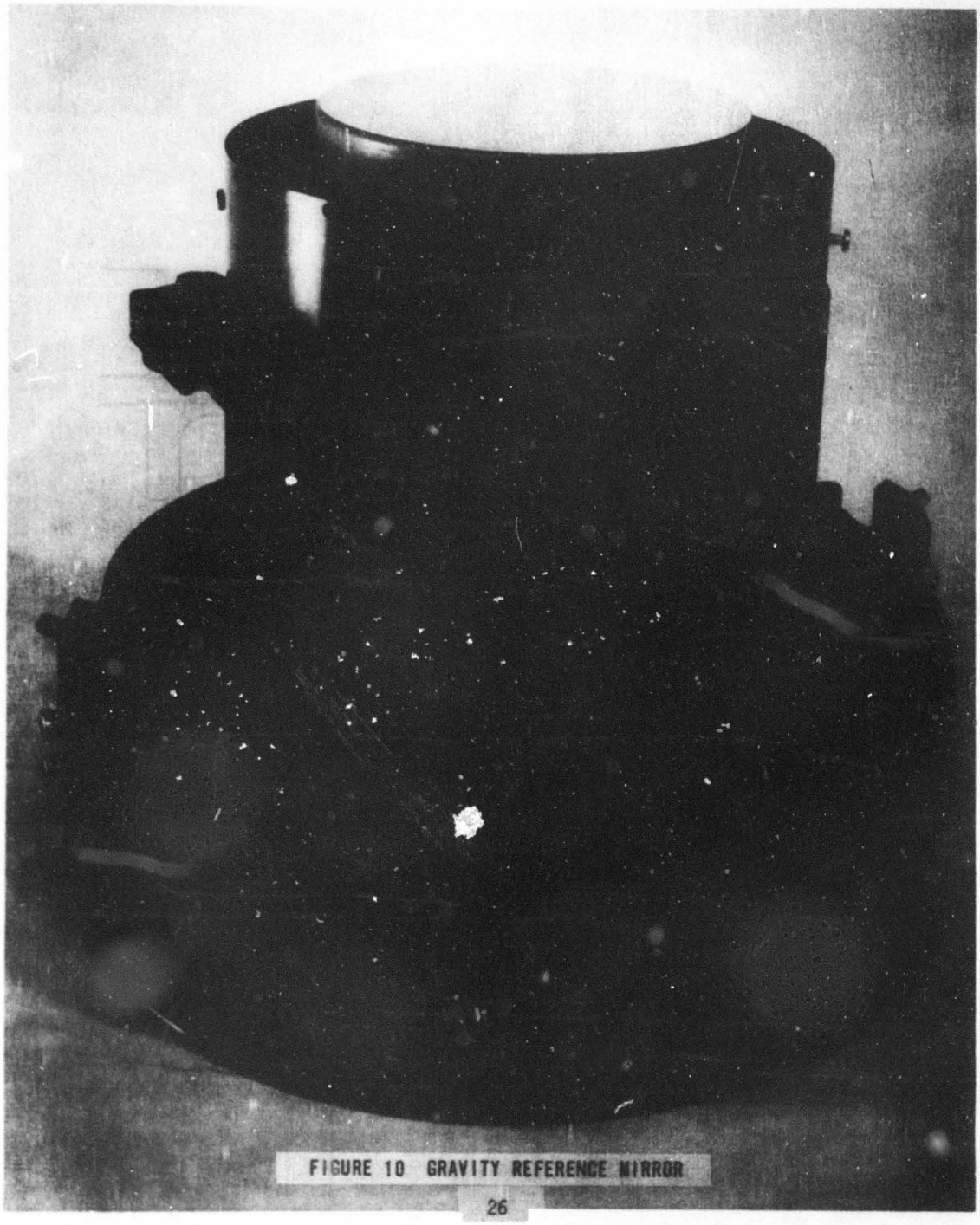

FIGURE 10 GRAVITY REFERENCE MIRROR

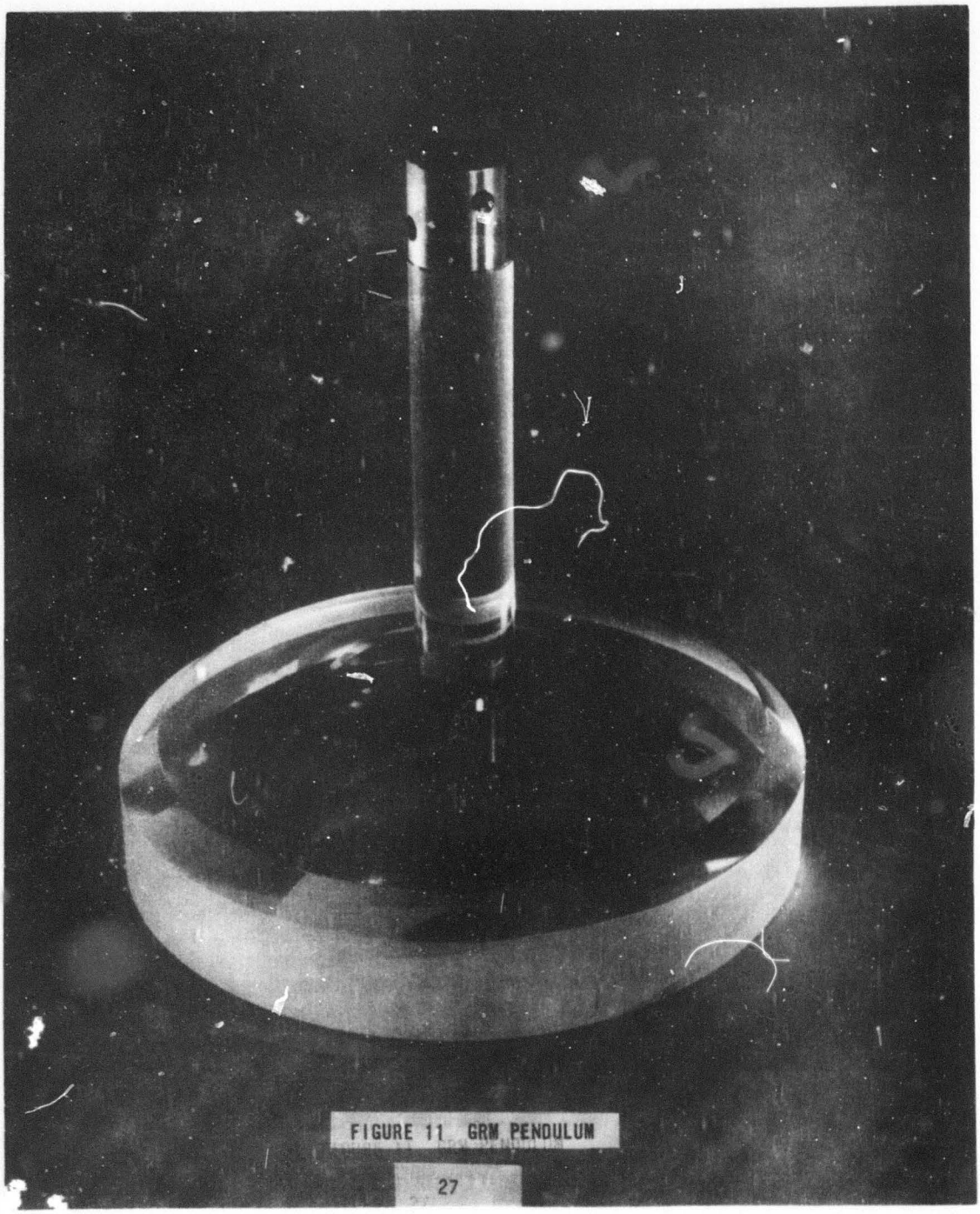

FIGURE 11 GRM PENDULUM

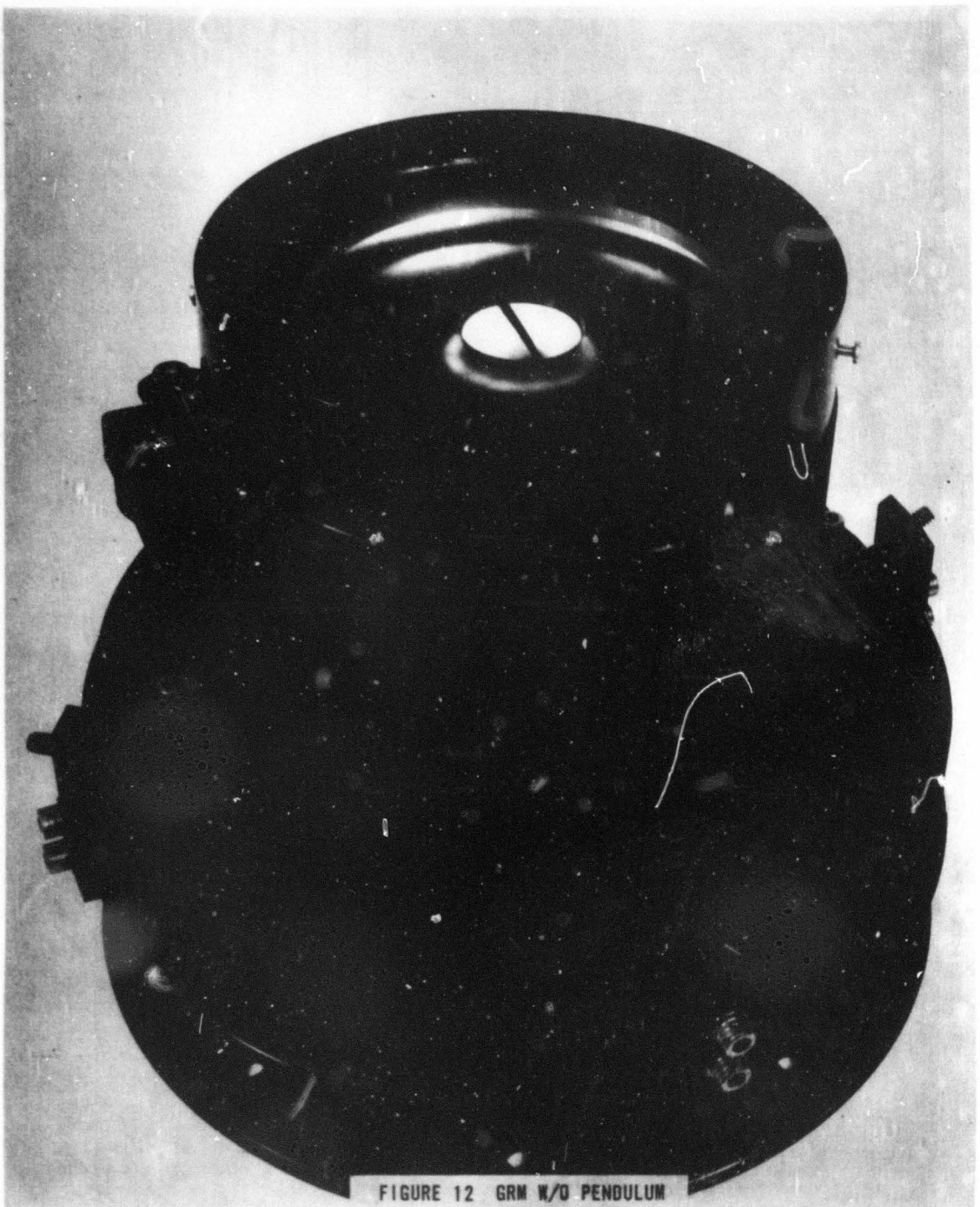

FIGURE 12 GRM W/O PENDULUM

Hasting Mass Flow Meter, Model 4LF-5K; and the required hoses, fittings and pressure indicators. The air flow rate is not critical. However, smoothness of air flow is critical since perturbations in air flow are coupled to the pendulous mass. Air flow rates from 3000 to 5000 cc per minute are acceptable, but performance at the rate of 3500 cc per minute is optimum. The compressor is located outside the building, and the other components are installed below the cinetheodolite near its main concrete mounting pedestal. The compressor supplies air at 160 PSIG to 175 PSIG to the small storage tank which helps to remove pressure fluctuations and removes some moisture during humid weather. The air then passes through the filter and trap which removes any oil and more moisture, the preregulator which decreases pressure and further decreases fluctuations, the renewable desiccant to remove remaining moisture, and the final regulator which removes any pressure fluctuations remaining and controls the air flow rate to the GRM. This air flow rate is monitored by the flow meter.

GRM TESTS

Static Tests

Two GRM's were delivered to WSMR by the contractor. The static tests were performed on GRM #1 in order to determine its long-term stability. The test site first selected was a remote telescope site, T-5, thought to be well isolated from the effects of vehicular traffic and other seismic disturbances associated with range work areas. The apparatus was set up at T-5 site as shown in Figure 13 Outputs of the tilt meter, the dual-axis autocollimator, the pressure transducer and the thermistors were recorded on the six-channel ink oscillograph. Time and air flow were manually recorded on the oscillograph at half-hour intervals. Readings from the two Hilger-Watts autocollimators were recorded. The long-term stability test ran approximately 175 continuous hours. Near the end of this time, the GRM was rotated several times, in 120-degree increments, to test orientation with respect to the local gravity vertical. Following the long-term stability test, the GRM was replaced by an optical flat, attached rigidly to the pier floor, to calibrate motion of the pier. Tests indicated the T-5 site pier supporting the instrumentation was in a constant whip-lash type of motion with a magnitude of 0.75 to 1.50 seconds of arc. Less overall motion occurred with the GRM than when an optical flat replaced it, indicating the GRM was reducing the vibrations of the pier floor. The physical configuration of the pier suggested that floor motion was less than instrumentation motion, which implied a maximum GRM motion of several tenths of an arc-second. Because the tests at T-5 could not give the absolute position of the GRM as a function of time, its position with respect to gravity vertical was determined within one-tenth of a second of arc by means of a series of azimuth rotations of the GRM.

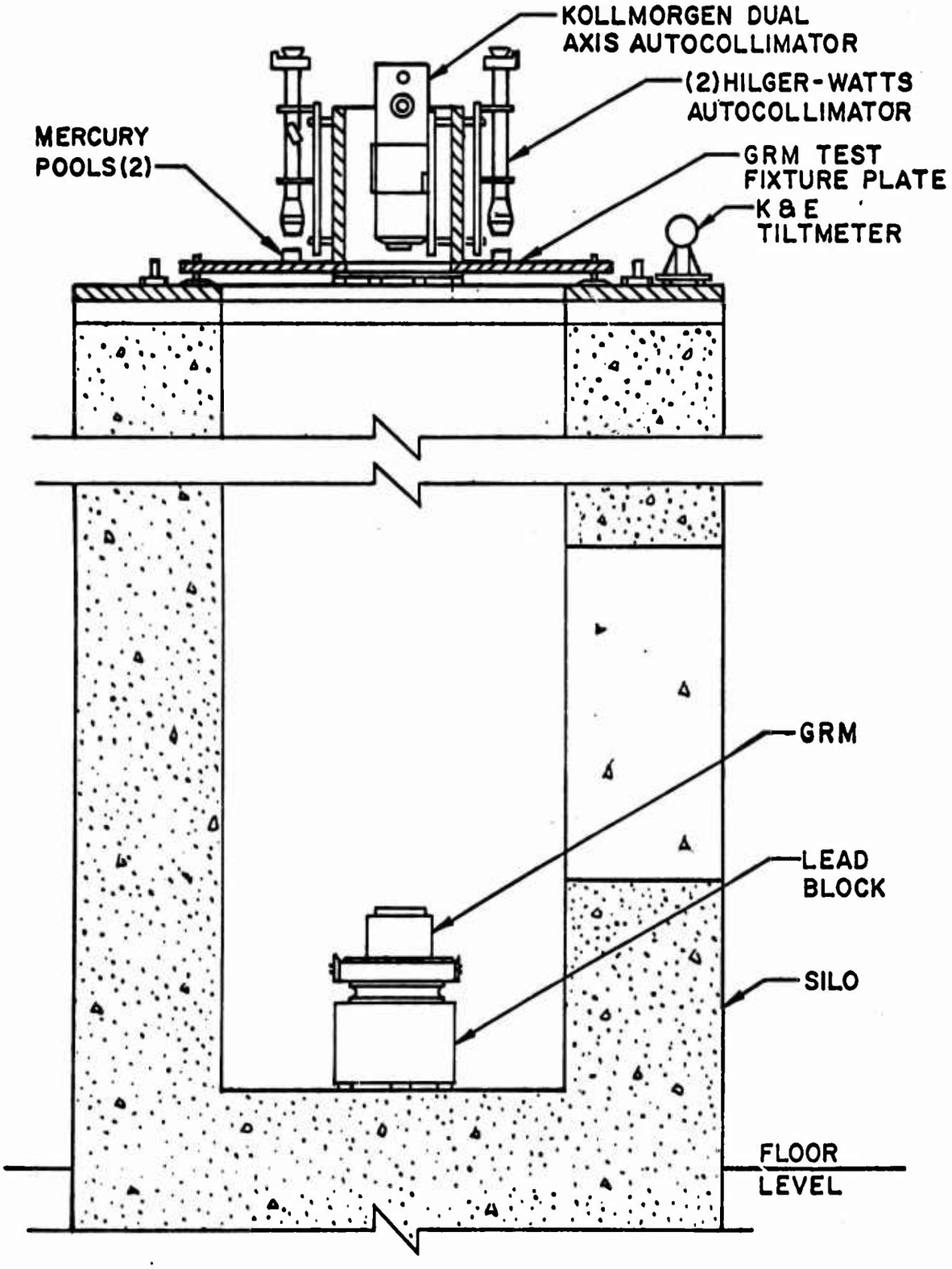

FIGURE 13 TEST APPARATUS AT T-5 SITE

In an attempt to obtain an instrument pier without the whiplash problems of T-5, the cinetheodolite pier at Bill Site was tried next. Despite the rigid construction of the Bill Site pier, whiplash of two arc-seconds between the GRM top and the pier bottom occurred. The test was conducted in the same manner as at T-5 site. A Hilger-Watts autocollimator fixed to the pier top monitored the motion of an optical flat fixed to the pier floor. The tests at Bill Site indicated that an isolated pier of minimal height must be found to reduce pier motion. A sunken, isolated pier in the optical tunnel in Building 1554 met all criteria and was utilized. With the test setup shown in Figure 14, the Hilger-Watts autocollimator was rigidly mounted 15 inches above the pier floor. Motion between the collimator and floor was approximately one-tenth of a second of arc or less, except for short-term motions of several tenths of an arc-second, possibly due to road traffic. The results obtained at Building 1554 indicated that with the GRM mounted on a stable platform relatively free of seismic motion the long-term stability of the GRM is approximately $\pm$0.1 arc-second for periods in excess of 200 hours.

Dynamic Tests

The static tests, although providing a measure of long-term stability required prior to the star tests, provided no information as to how the GRM would respond to specific inputs. The star tests or the static tests of the instrumental pointing accuracy were performed under ideal quiescent conditions without operators moving about and with complete absence of theodolite motion while the stars were being photographed. These data were of little use for evaluating the GRM's capability to compensate for shock-excited pedestal motion when the theodolite is used as a tracking instrument.

In order to determine the response of the GRM to small inputs approximate in magnitude to actual shock excitation levels observed during the high-acceleration dynamic tests, it was necessary to design and develop special instrumentation. It was necessary to tilt the GRM base dynamically by two arc-seconds over a range of frequencies considerably greater than that of the GRM bandpass. This was accomplished by first fabricating a special table and a magnetostrictive driver to provide a controlled dynamic tilt to the table, illustrated in Figure 15. It was thought that a table supporting the GRM, a suitable driver, a Hilger-Watts autocollimator to monitor the table motion, and another autocollimator to monitor the corresponding motion of the GRM were all that would be required to derive the small signal transfer function of the GRM. This was not the case. When the autocollimator was set up, as in Figure 16, to monitor the dynamic tilt table position, the first measurements indicated that the test system had a bandpass of less than one hertz. As the electronics and the driver response for the magnetostrictive driven tilt table were estimated to exceed 60 hertz, the autocollimator response was highly suspect.

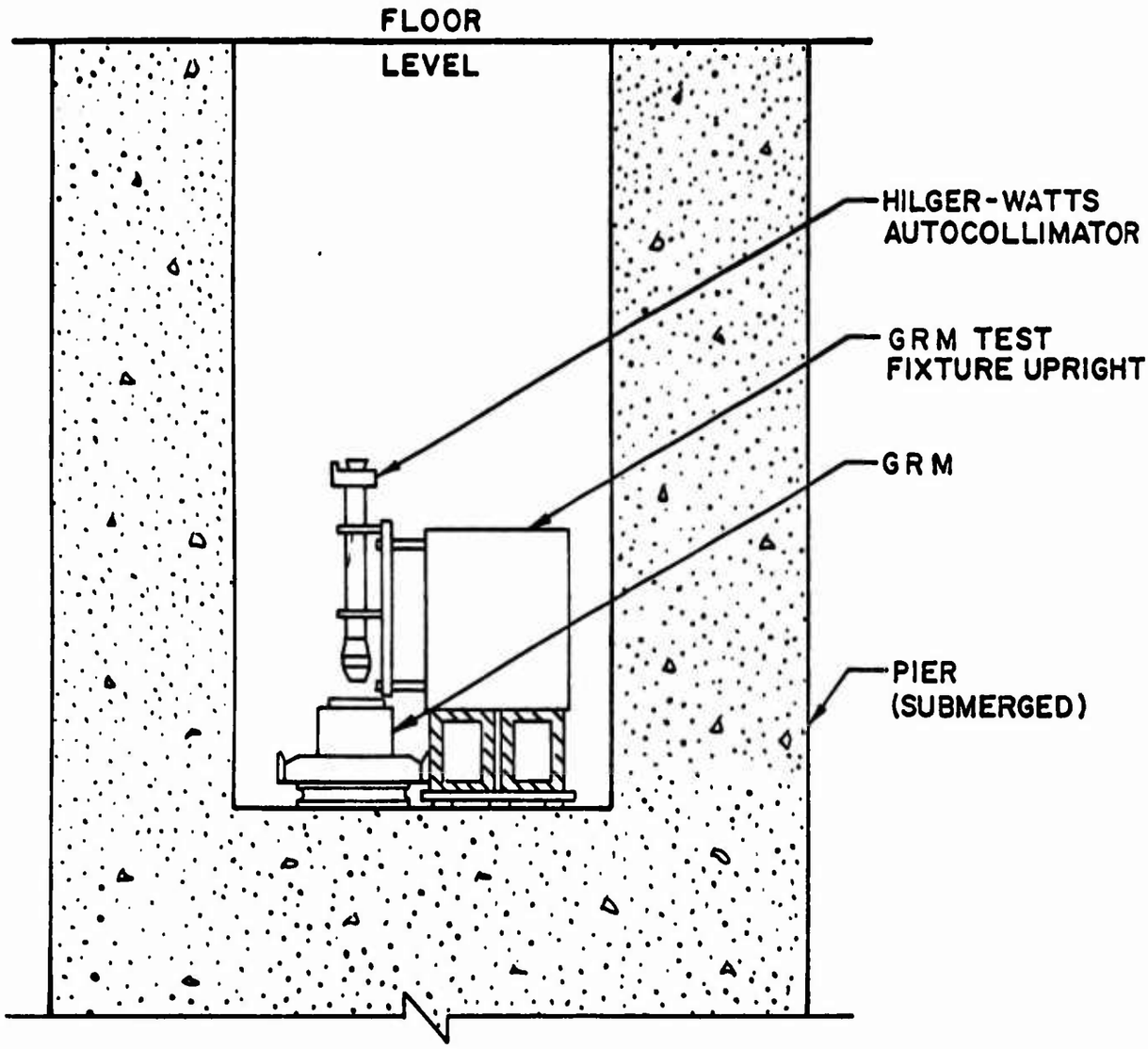

FIGURE 14 TEST APPARATUS BLDG 1554

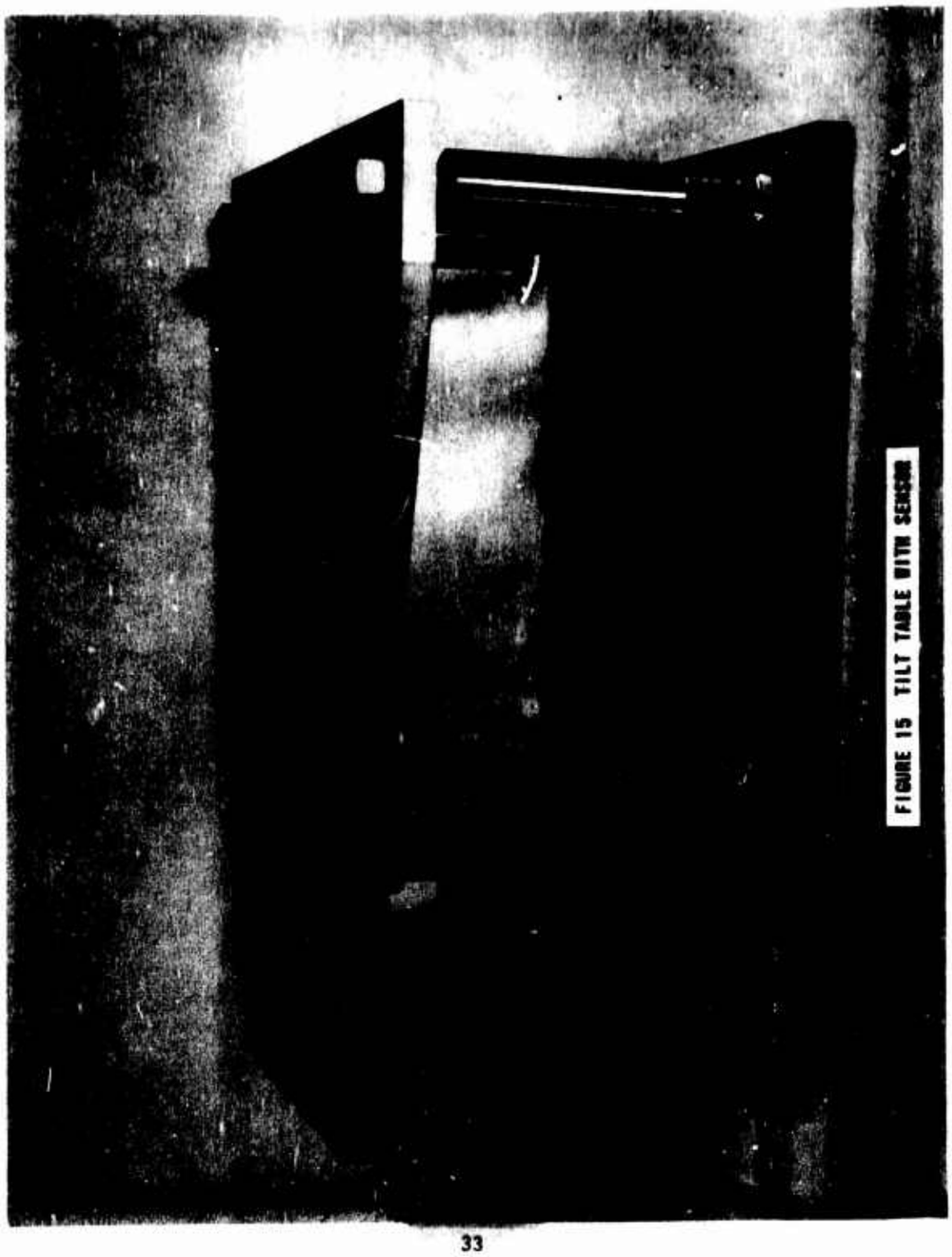

FIGURE 15 TILT TABLE WITH SENSOR

To accurately determine dynamic position of the tilt table for a broad range of frequencies, the table was equipped with differential capacitive sensors and the autocollimator response was measured. The bandpass of the Hilger-Watts autocollimator, as shown in Figure 17, was less than one hertz. At first this would seem to nullify or render questionable much of the previous GRM test data, if it were not for the fact that only average position is required for long-term stability determination, and amplitude measurements at the higher frequencies would not alter the results of the static tests. Where the theodolite is used as a tracking instrument at high accelerations and operating personnel are moving about, shock waves with high-frequency components will be coupled into the GRM base to some degree. Also when the theodolite is being used to track missiles, each photograph represents a unique point in the trajectory and average position of the GRM is of little use. Instantaneous and exact amplitude and phase angle error of the GRM are required. With the autocollimator discredited because of its limited bandpass, it could not now be used except to record initial conditions and to statically calibrate the electronic sensor instrumentation. Instead, a special capacitive sensor system was fabricated to monitor the instantaneous angular position of the GRM relative to its base. It is shown installed on the GRM in Figure 18. The complete test setup used is shown in Figures 19 through 21.

For the input signals, the sensor was in the form of a differential capacitor, with one isolated plate above and the second isolated plate below the table top. For the output signals, the sensor was also a differential capacitor, which consisted of a pair of isolated plates, the mirrored surface of the pendulum, and a pair of grounded plates. It was mounted on top of the GRM. The individual differential capacitors were connected to separate bridges, so that their two sections became separate arms of their respective bridges. Thus, any unbalance of either bridge produced an output proportional to the direction and magnitude of the tilt angle. Conventional amplifiers were used to amplify the outputs of the bridges. With a capability of measuring input and output amplitude and phase over a bandwidth greatly exceeding that of the GRM response, tests were conducted with the results shown in Figures 22 and 23. To determine the optimum damping, an empirical course of action was followed, and the effect of each change was determined by plotting a frequency response curve. This procedure determined the proper viscosity of the silicone oil along with the most suitable depth of the oil in the dashpot (Figure 24).

It is obvious from shock excitation observed at the GRM base during moments of high acceleration that either a GRM more independent of base tilt should be developed or that means for isolating the GRM from shock frequencies higher than one hertz should be employed. An in-house effort to solve this problem is continuing. To more accurately identify the problem, a transfer function was derived for the manufacturer's recommended conditions, i.e., with the GRM pendulum stem extending 5/8 inch into 100 centistoke oil.

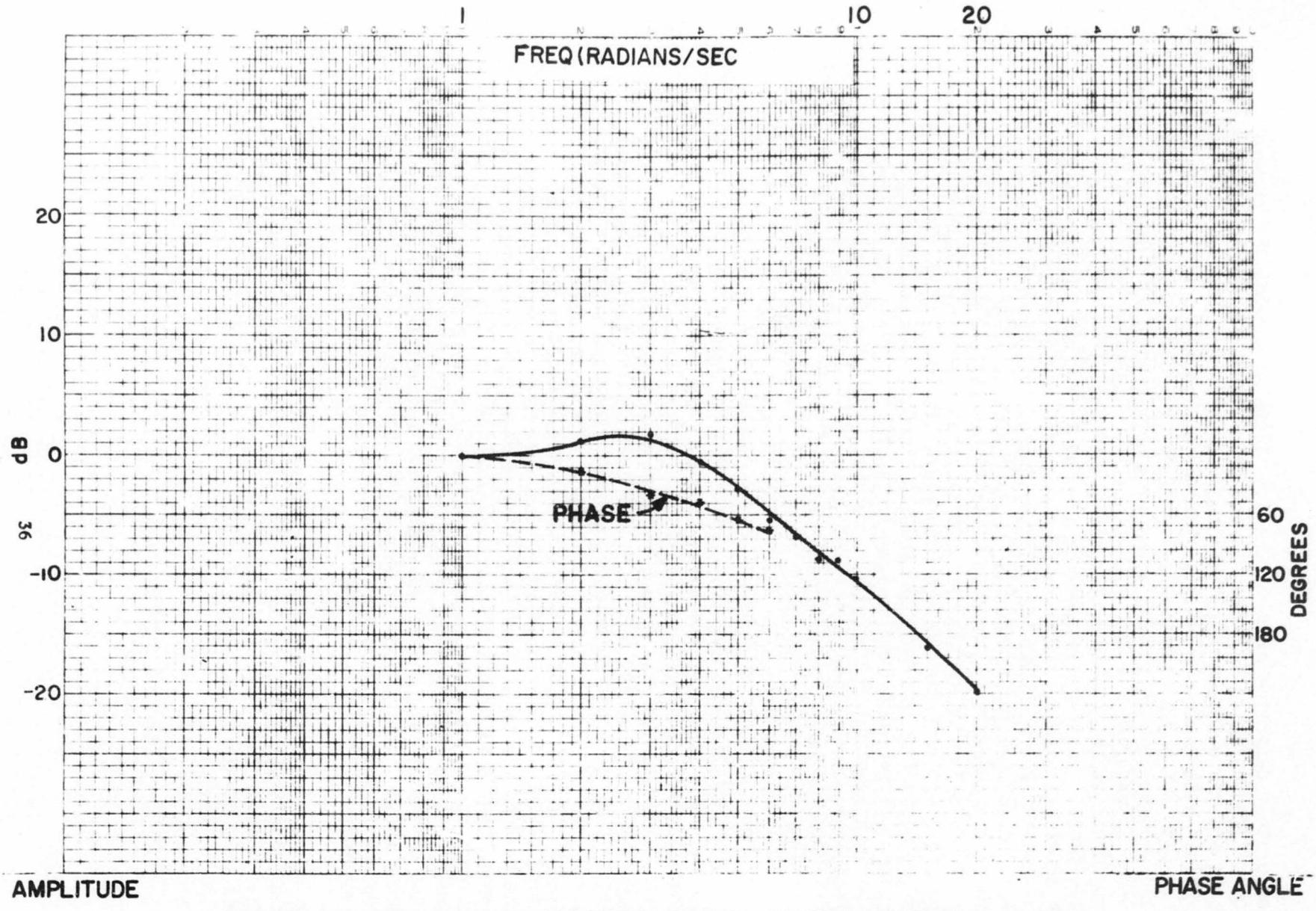

FIGURE 17 FREQUENCY RESPONSE HILGER WATTS AUTOCOLLIMATOR

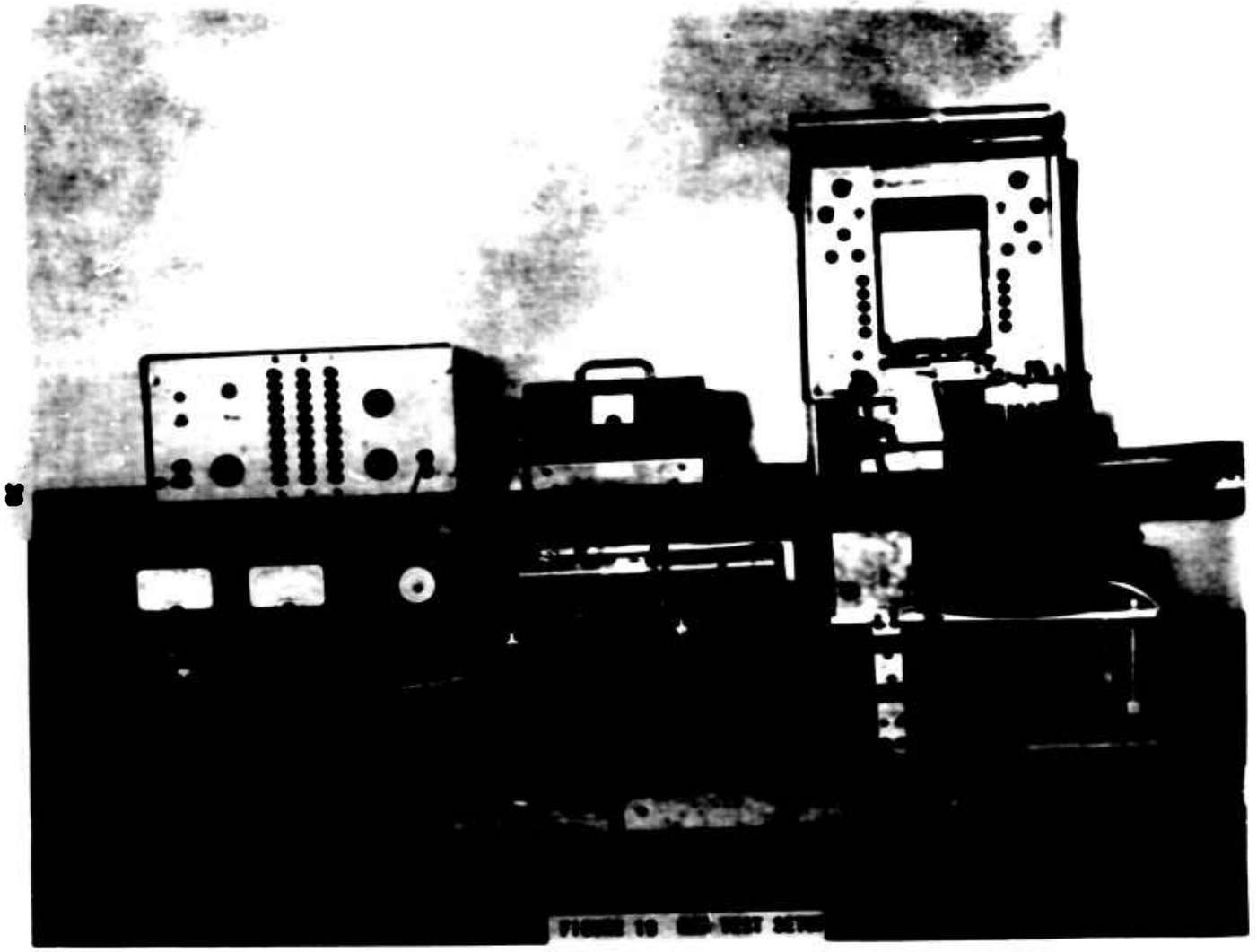

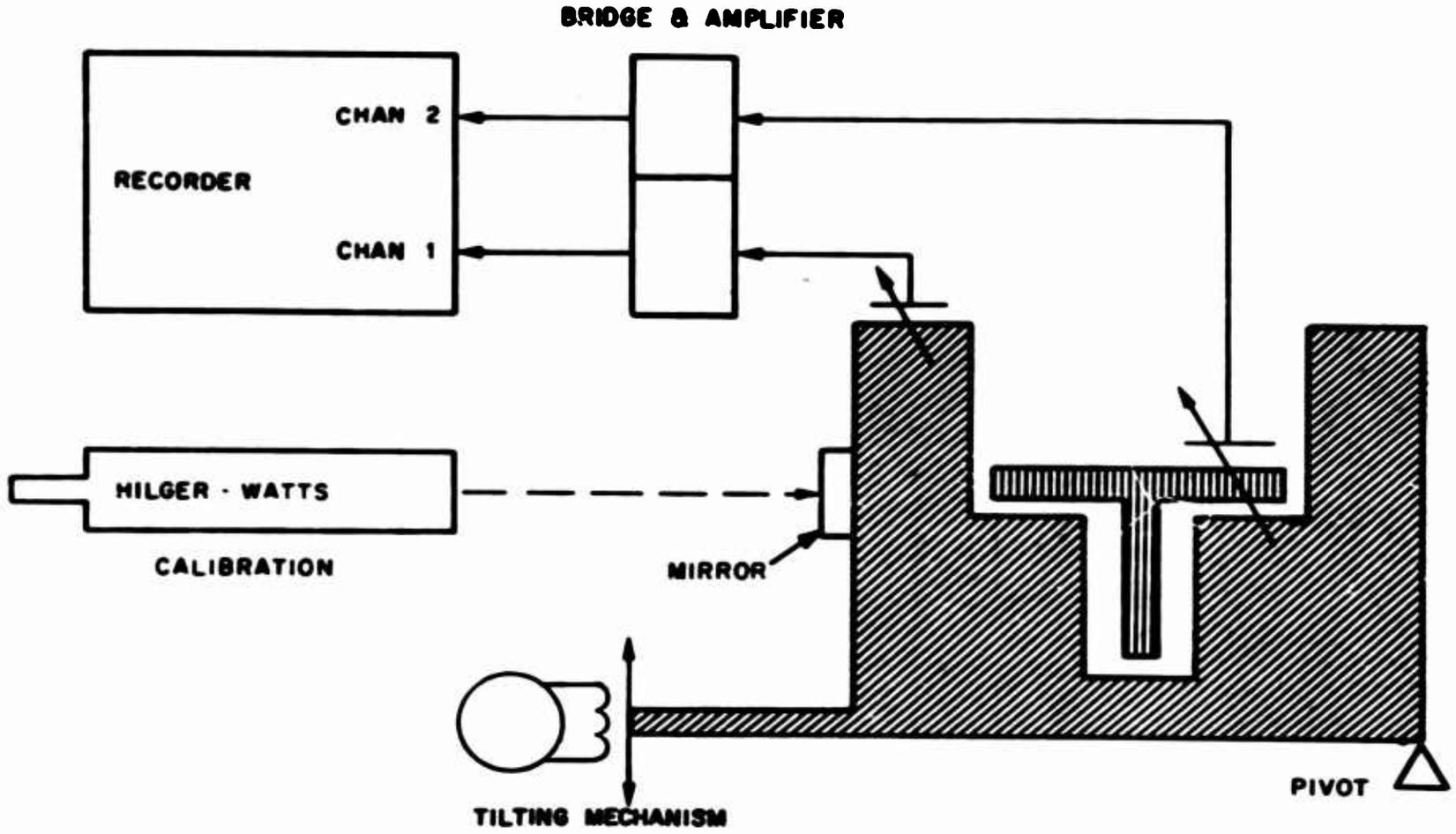

FIGURE 20 GRM FREQUENCY RESPONSE TEST

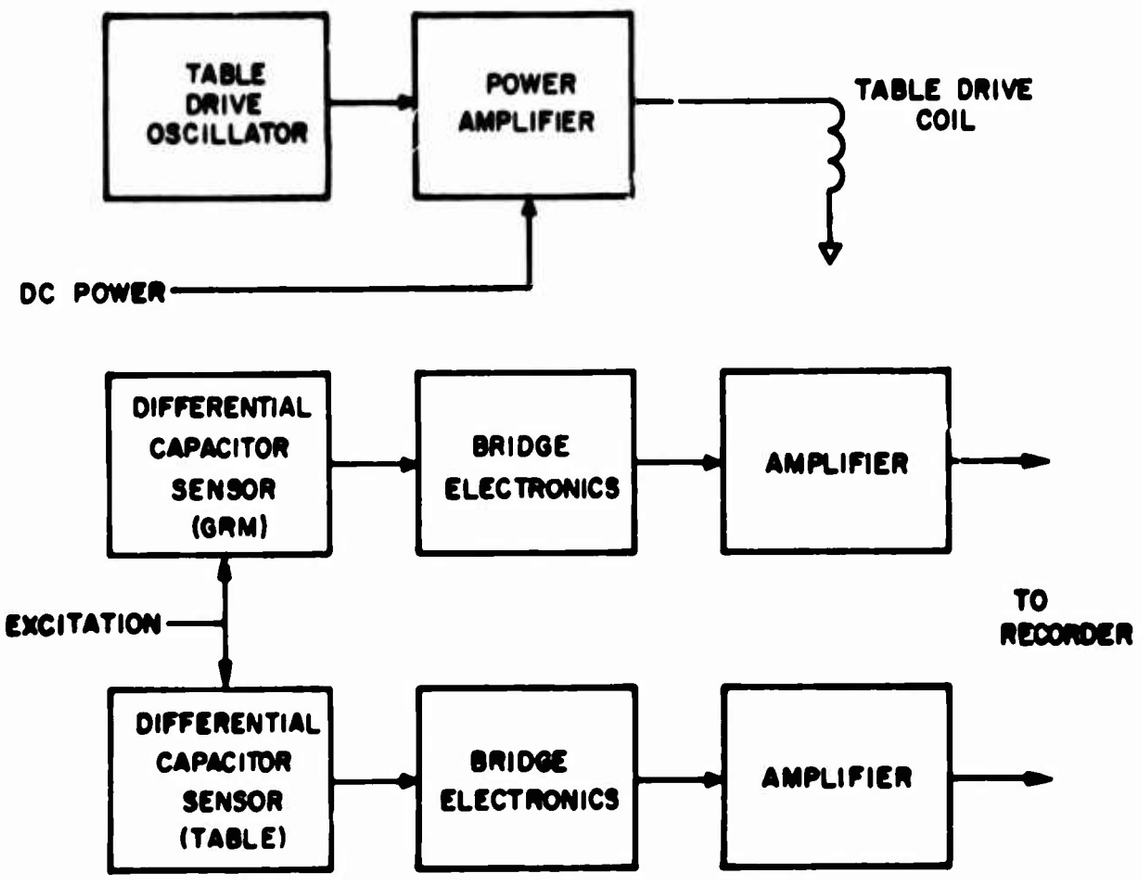

FIGURE 21 FREQUENCY RESPONSE MEASUREMENT SYSTEM

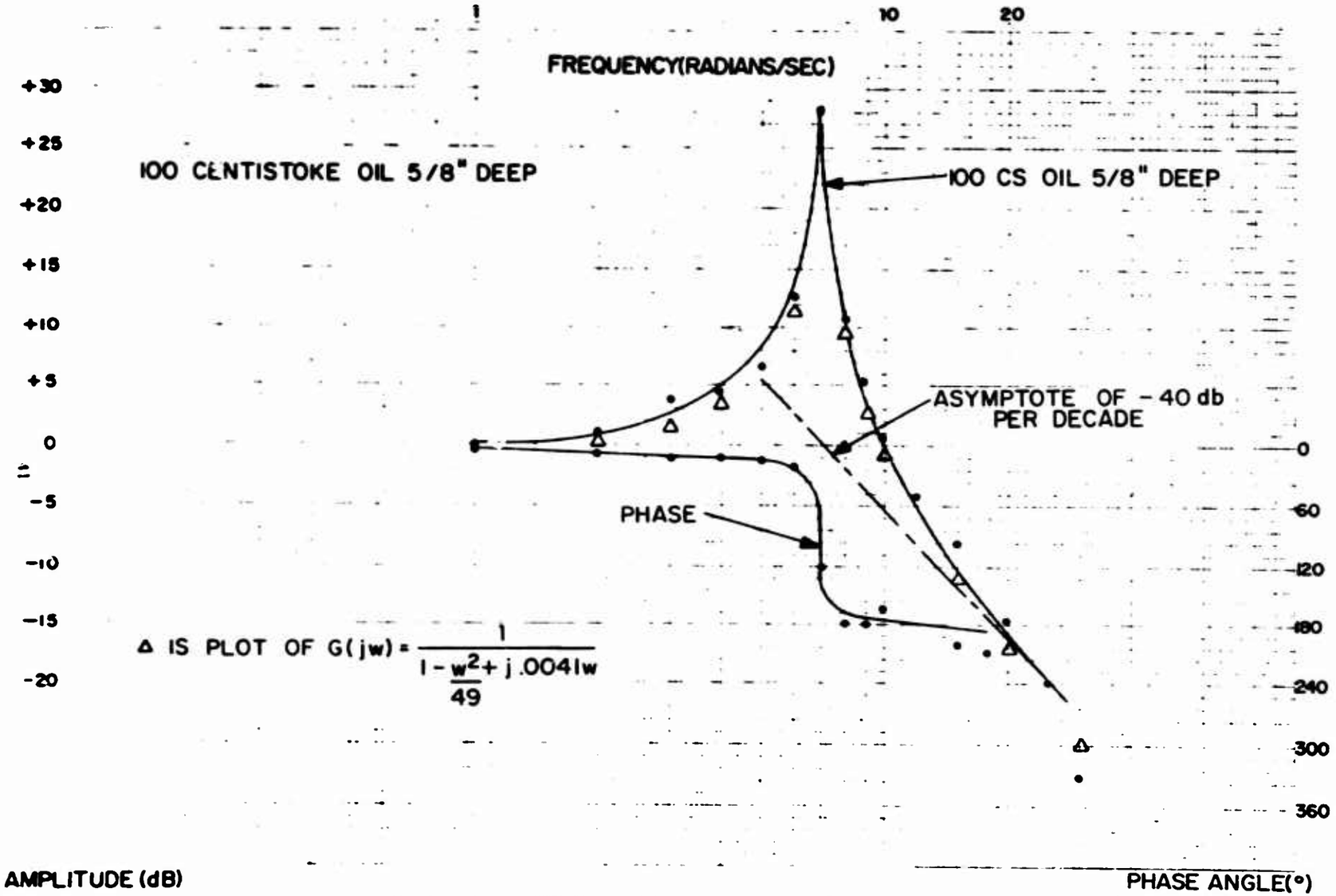

FIGURE 22 FREQUENCY RESPONSE OF GRM #1

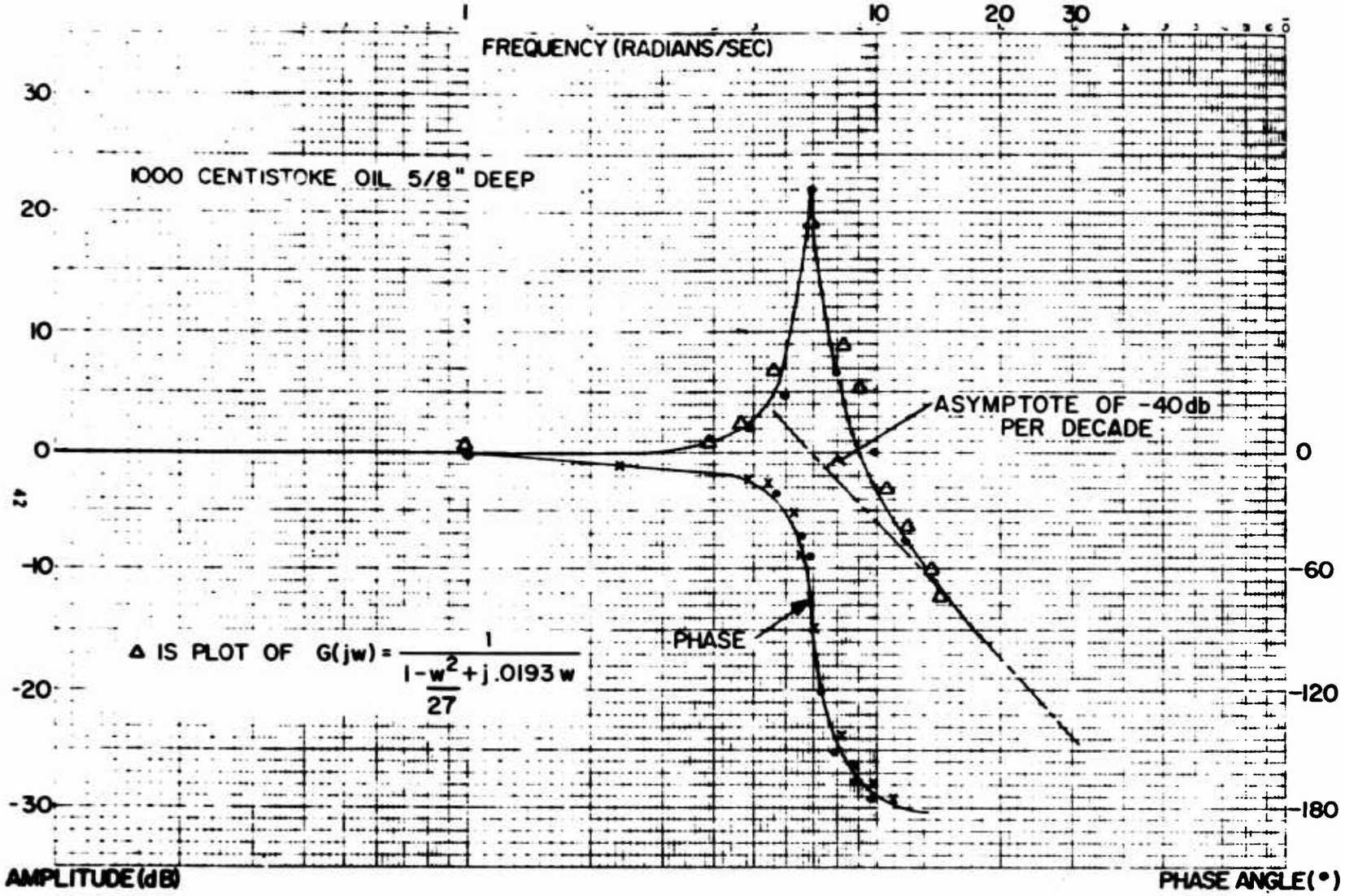

FIGURE 23 FREQUENCY RESPONSE OF GRM #2

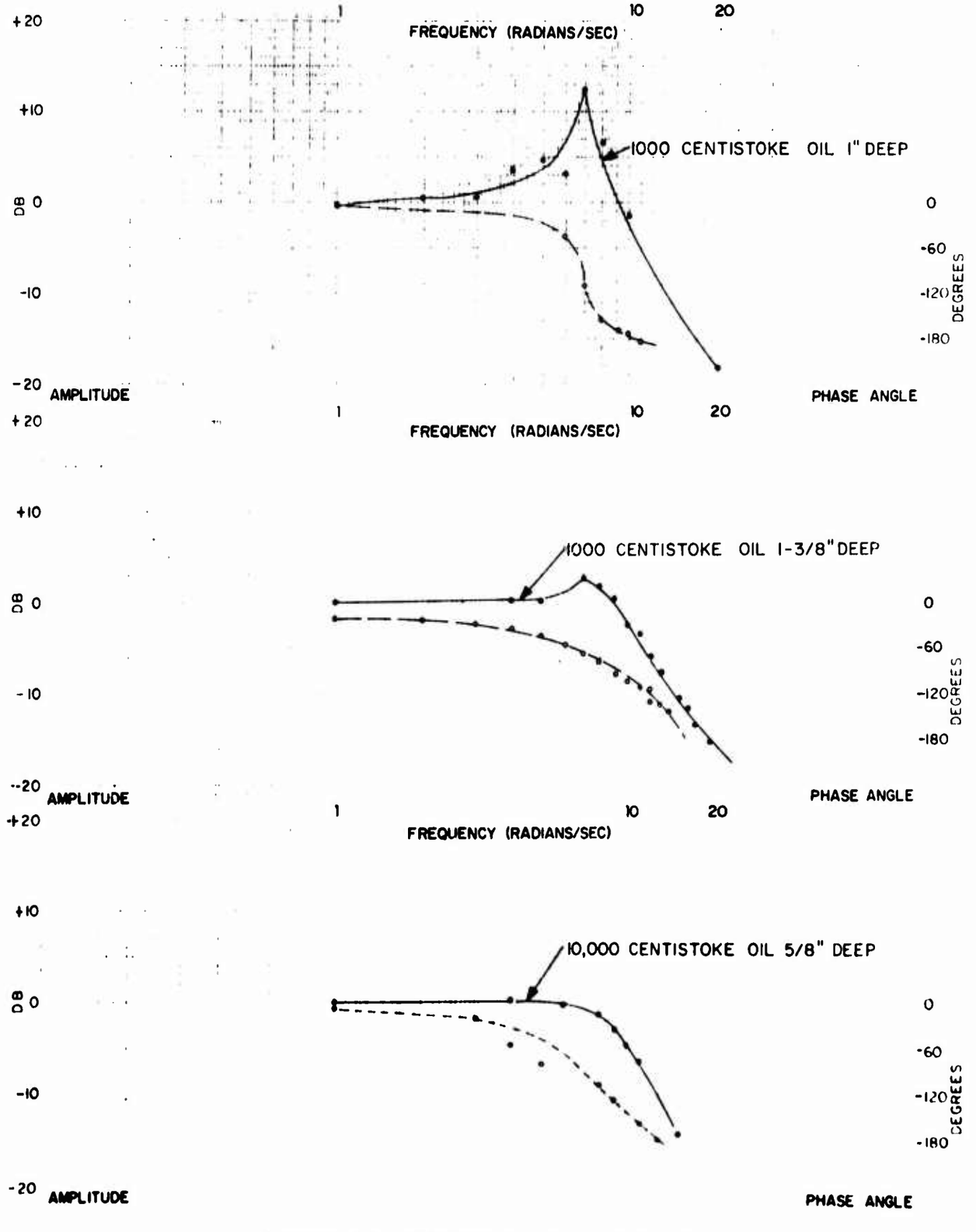

FIGURE 24 FREQUENCY RESPONSE OF GRM #1

The transfer function was obtained from the frequency response curve by approximating the plot with straight lines having slopes that were multiples of 20 dB per decade. In conjunction with the straight lines, a plot of the phase shift was also used. It was of value in analyzing and determining the probable number and general character of any break points in the plot. For the GRM's under test, the straight line approximation was a second-order curve with a slope of -40 dB per decade. This gave the general form of the transfer function as

$$G(S) = \frac{K(\omega_m)^2}{S^2 + 2\xi\omega_m S + \omega_m^2}$$

where ω_m was the break frequency or the undamped natural frequency. The term Xi(ξ) was the damping ratio. Changing the general equation by substituting $S = j\omega$, the transfer function becomes

$$G(j\omega) = \frac{K}{(\frac{j\omega}{\omega_m})^2 + \frac{2\xi}{\omega_m}\omega_m(j\omega) + 1} .$$

The value of K was found by determining the dc gain when $j\omega = 0$. Then

$$G(j\omega) = \frac{1}{1 - (\frac{\omega}{\omega_m})^2 + \frac{2\xi}{\omega_m}(j\omega)} .$$

In this equation, the damping ratio ξ was the only quantity not known and its value was obtained by use of the curves of damped oscillatory movements which are shown in Figures 25, 26 and 27. These curves were generated by the GRM's after they were shocked into oscillation and allowed to come to rest. From them we obtained delta (δ) by the relationship of

$$\delta = \log \frac{x1}{x2} .$$

Then this value of δ was used to obtain ξ by

$$\xi = \frac{\delta}{\delta^2 + 4\pi^2} .$$

If the constants are collected for GRM #1, they can be substituted to obtain a specific solution to the equation. Using Figure 14 to find ω_m and Figure 25 to obtain ξ the equation is as follows:

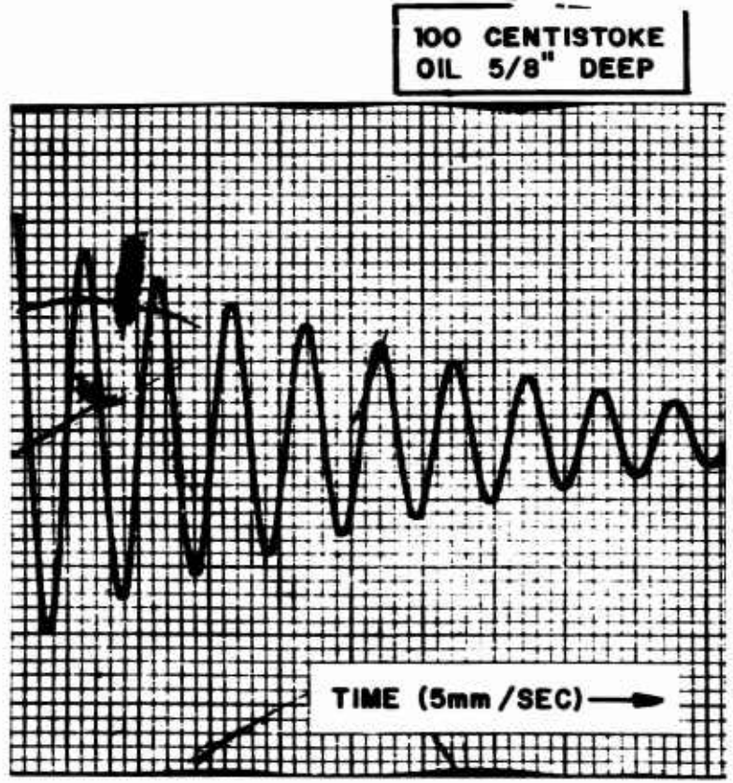

FIGURE 25 SHOCK EXCITED GRM #1

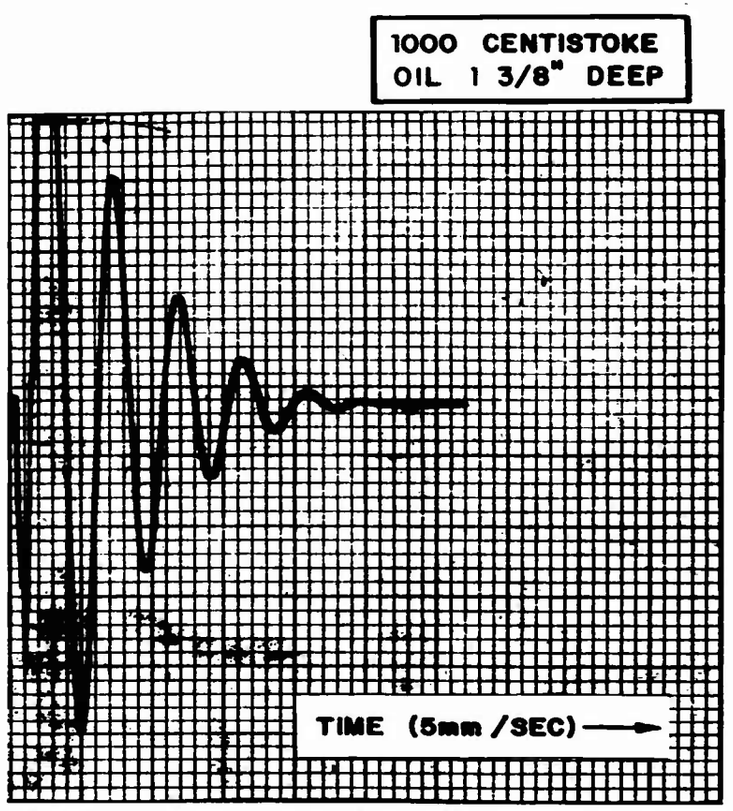

FIGURE 26 SHOCK EXCITED GRM #1

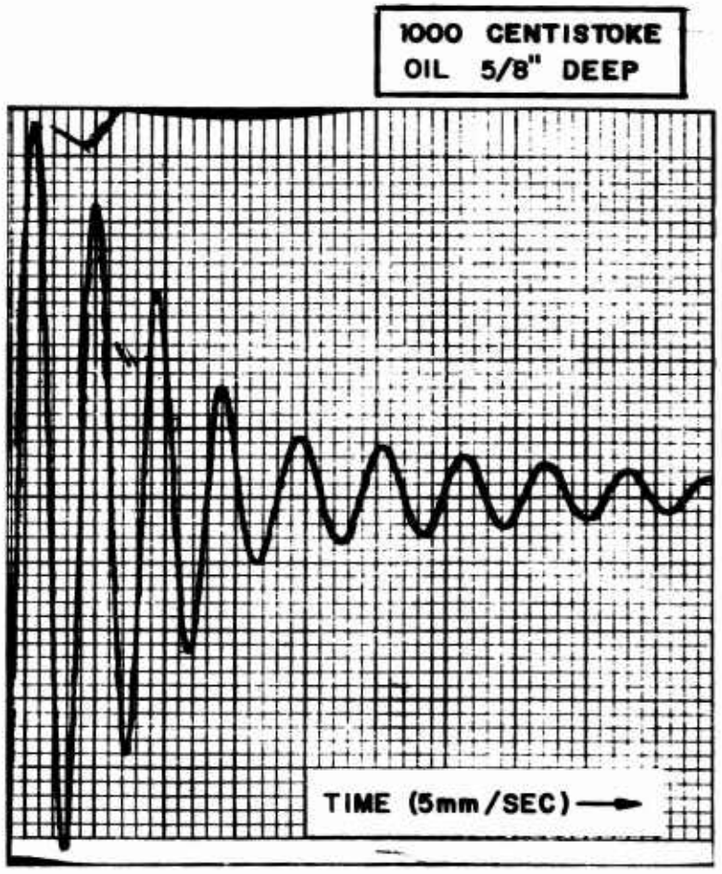

FIGURE 27 SHOCK EXCITED GRM #2

$$G(j\omega) = \frac{1}{1 - 0.0204\omega^2 + j(0.0041\omega)} .$$

From the frequency response tests, the following characteristics were also derived.

1. Bandpass - The bandpass includes all frequencies from zero to a point 3 dB down. Using this criteria, the bandpass was taken as 1.6 hertz.

2. Resonant Frequency - The resonant frequency of both GRM's was 1.16 hertz.

3. Damping Factor - From the curves of Figure 25 and Figure 27, the damping factor for GRM #2 was 0.035 and for GRM #1 was 0.014. Such low damping factors provided for greater freedom of movement, but they also permitted the GRM to oscillate for 14 or 15 seconds after it had been shocked into oscillation. From the curves of Figure 26, the use of 1000-centistoke silicone oil at a depth of 1-3/8 inches on the stem of the pendulum was recommended. More severe damping was tried, but it increased the phase lag of the pendulum which resulted in a greater delay before the GRM responded to external disturbances. Therefore, less damping along with a smaller phase lag was considered optimum for the GRM. The transfer function for this degree of damping ($\xi = 0.35$) is

$$G(j\omega) = \frac{1}{1 - \frac{\omega^2}{49} + 0.1\, j\omega} .$$

GRM SYSTEM DEFICIENCIES

1. Poor Frequency Response - Refer to section titled "Main Optics."

2. Inadequate Isolation of GRM - Cinetheodolite azimuth accelerations were coupled to the GRM in varying degrees. The maximum peak-to-peak shock-excited GRM oscillation did not normally exceed 0.8 arc-second. Occasionally, however, such oscillations reached approximately 2.0 arc-seconds peak-to-peak.

3. Defective Air Compressor - The air supply compressor required two overhauls. A better air compressor is required or a more efficient final flow rate regulator must be obtained or both. The present regulator controls flow by dumping the excess, thus wasting appreciable amounts of dry, pressurized air.

4. Defective Flow Meter - The Hastings Model LF-5K mass flow meter failed and was replaced with a Brooks Rotameter Type 2-1110-7901.

5. Desiccant Unit - The desiccant required changing approximately every third day. An automatic desiccant regenerating system is desired.

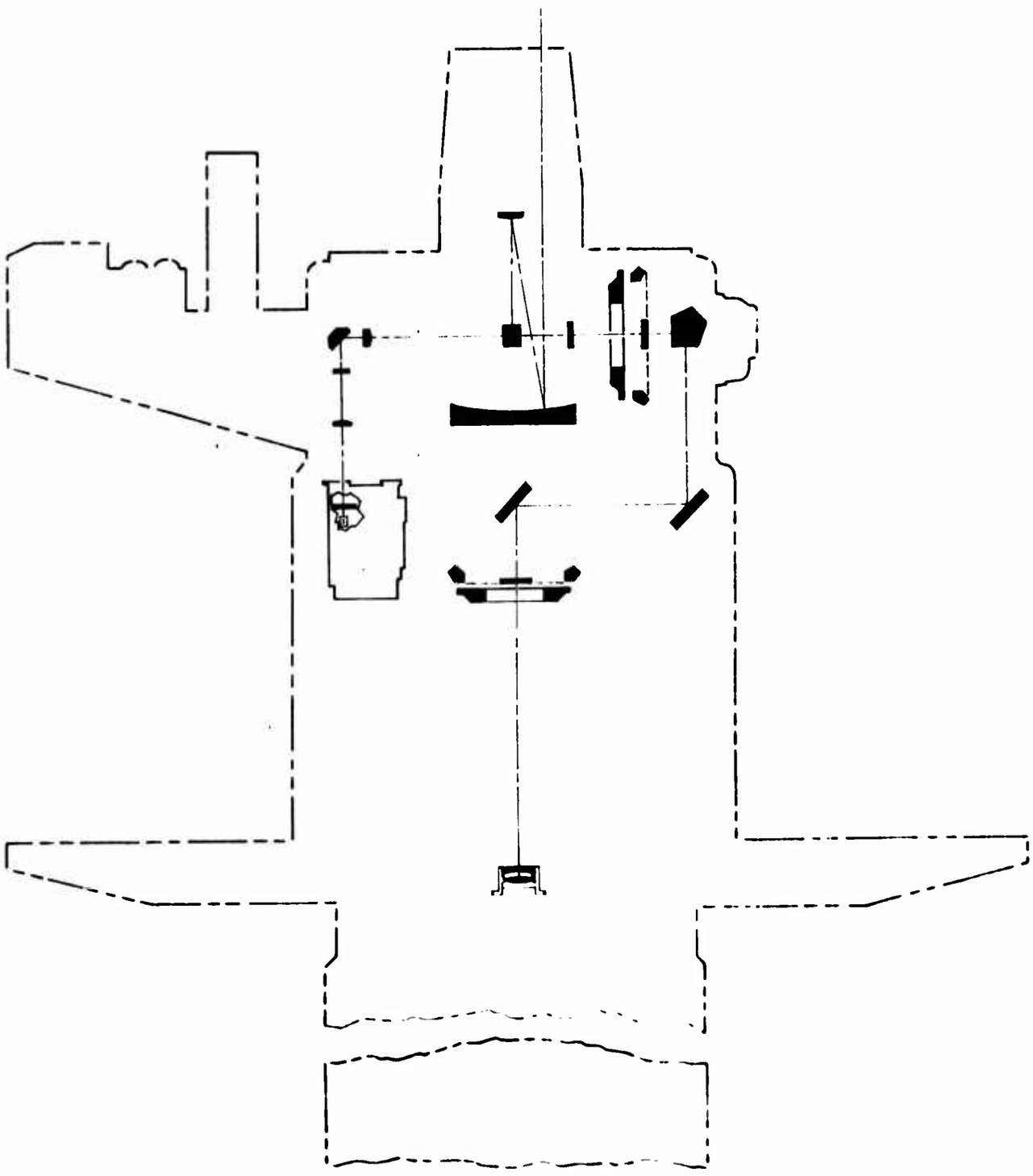

DATA TRAIN

OPTICAL DATA TRAIN

CONFIGURATION AND THEORY OF OPERATION

Theodolite error theory has been discussed in detail by several authors[2,3,4]. The equations that have been developed from theodolite error theory for the correction and calibration of azimuth and elevation angle errors assume perfect mechanical rigidity in the theodolite. Since this is a somewhat unrealistic assumption, a conventional cinetheodolite will have a certain amount of inaccuracy caused by mechanical distortions, especially in a dynamic situation.

The WSMR Cinetheodolite, unlike other cinetheodolites, does not depend solely on the mechanical integrity of the instrument for its accuracy. It does take all the advantages of a well-designed mechanical instrument, but also incorporates an optical compensation system. In addition to compensating for static bending and earth movement, this system compensates for errors introduced into the system by the dynamics of tracking. These errors are listed below and are noted in Figure 28.

1. Collimation error due to lens whip.

2. Elevation error due to lens sag.

3. Standards error due to unequal trunnion standards height, thermal effects, and bearing errors.

4. Azimuth index error due to elevation bearing errors and trunnion standards twist.

5. Mislevel, azimuth bearing error, and overturning moments on the azimuth bearing due to elevation acceleration.

6. Relative motion between the earth and the instrument base.

This optical error compensation system or optical data train is shown in Figure 29 and its operation is as follows.

The first element in the train is the GRM discussed in the section titled "The Gravity Reference Mirror System."

The next element in the train is the gravity reference collimator. The lens is designed so that the rear nodal point is at the outer surface of the rear element. An illuminated target is located at the nodal point. The reflecting surface of the GRM is placed one-half the focal length of

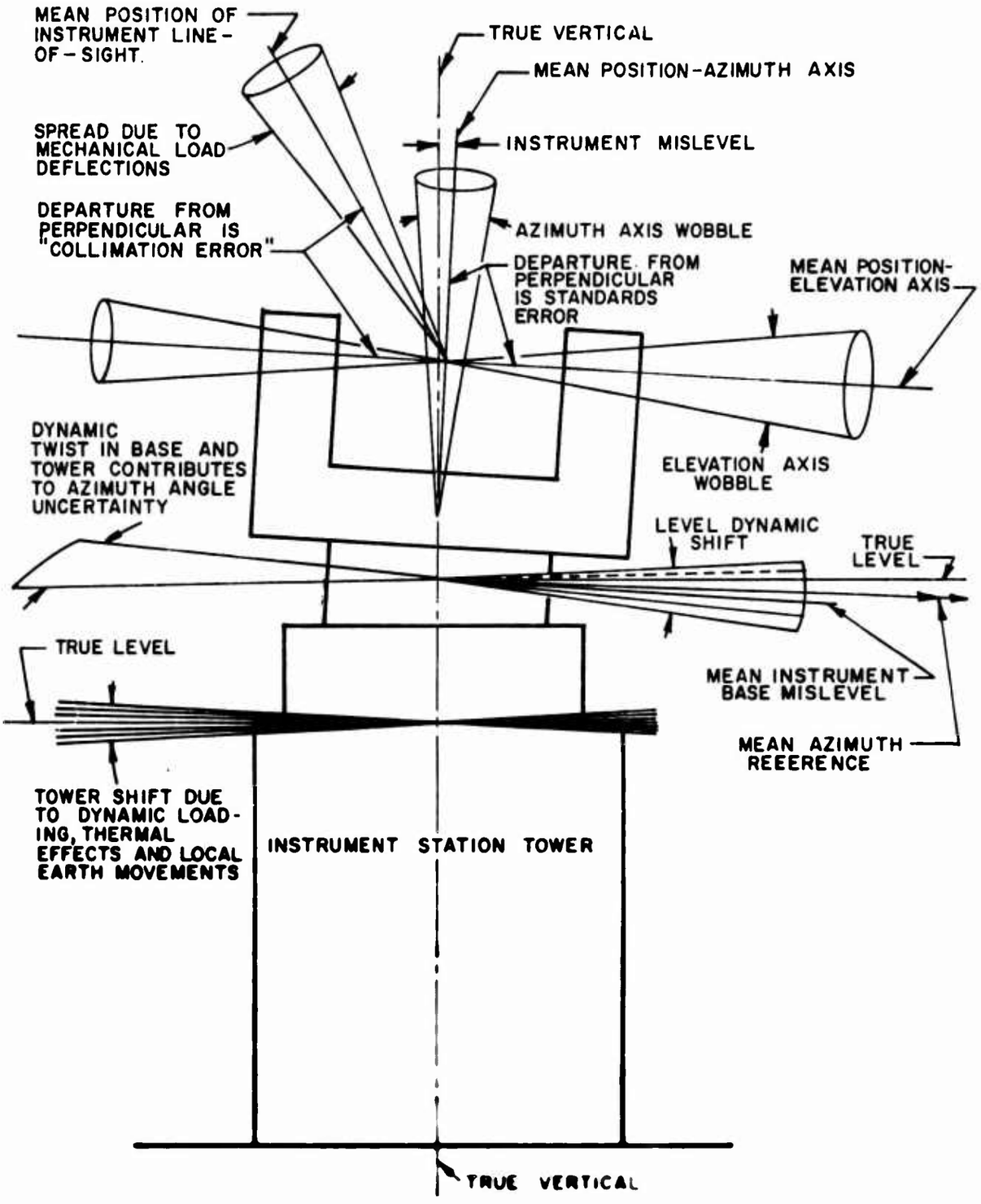

FIGURE 28 BASIC THEODOLITE ERRORS

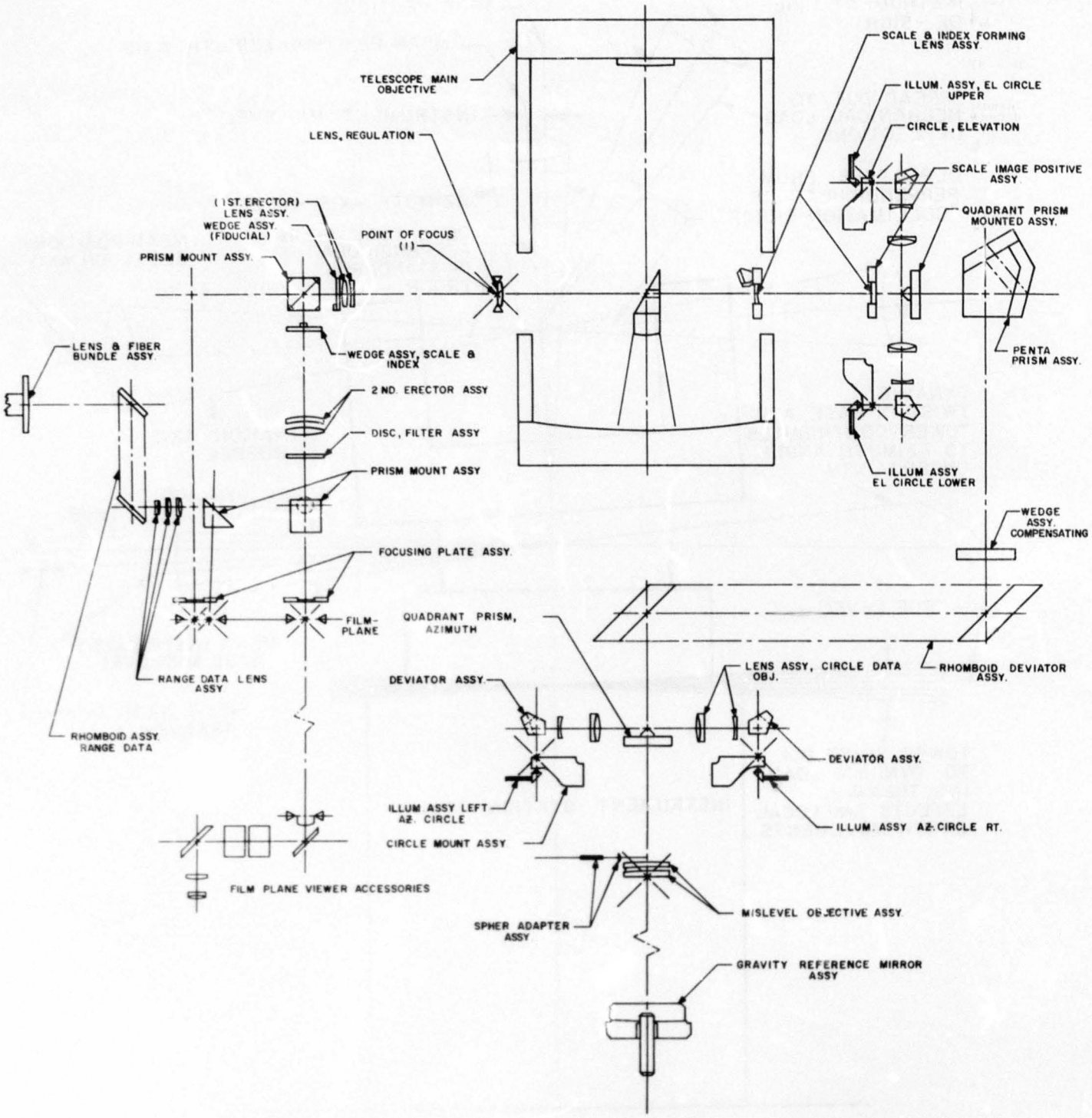

FIGURE 29. OPTICAL TRAIN DATA

the mislevel objective away from the target. This allows the image of the target to be formed by the GRM at the focal point of the lens. Thus, light from the target forms a collimated beam after passage through the lens.

Two properties of this system are important. The first is that the direction of a line from the focal point of the lens to the rear nodal point is always perpendicular to the surface of the GRM. The second is that, since the direction of this line defines the direction of the collimated beam, the beam remains vertically oriented regardless of any tilt of the collimator lens. Emerging from the vertical reference collimator is a beam of collimated light which is very accurately normal to the local level surface, and remains so regardless of pedestal tilt within the limits of ±2 arc-minutes.

The azimuth graduated circle recording system is mounted above the mislevel objective. Figure 29 shows how both sides of the circle are illuminated and how the output light beams are deviated 90 degrees toward the center of the instrument. One of the 90-degree deviators that intercepts the light passing through the circle is a plain penta-prism and the other is a roof penta-prism. The result of having a roof penta-prism on one side of the circle and a plain penta-prism on the opposite side is shown in Figure 30. If there is any circle eccentricity, the effect noted at the film plane will be that the information from one side of the dial will move in a direction opposite to that of the information from the other side of the dial. To compensate for eccentricity, the mean position of the two graduated circle marks on the film is measured. After leaving the 90-degree deviator, the light beams carrying the dial information are collimated These beams strike the surface of the quadrant prism assembly and are directed toward the rhomboid deviator. From this point on, the light beams from the azimuth circle and the vertical reference target follow an identical path.

The collimated beams then pass through the rhomboid deviation assembly. This assembly serves merely to offset the optical path. An optical offset is required because of the mechanical configuration of the instrument This is the most critical element in the instrument because it represents a compromise in the design and it does depend on mechanical constraint for its stability. As long as the two flats of this deviation assembly remain accurately parallel, the beam emerging from it will remain vertical no matter how the deviator is tilted.

The next optical element through which the collimated light beams pass is a 90-degree deviator assembly. This assembly is shown in Figure 31 It is made up of two penta-prisms mounted side by side, one of which is a normal penta-prism and the other a roof penta-prism. The penta-prisms have the well-known property that they are constant deviating systems with

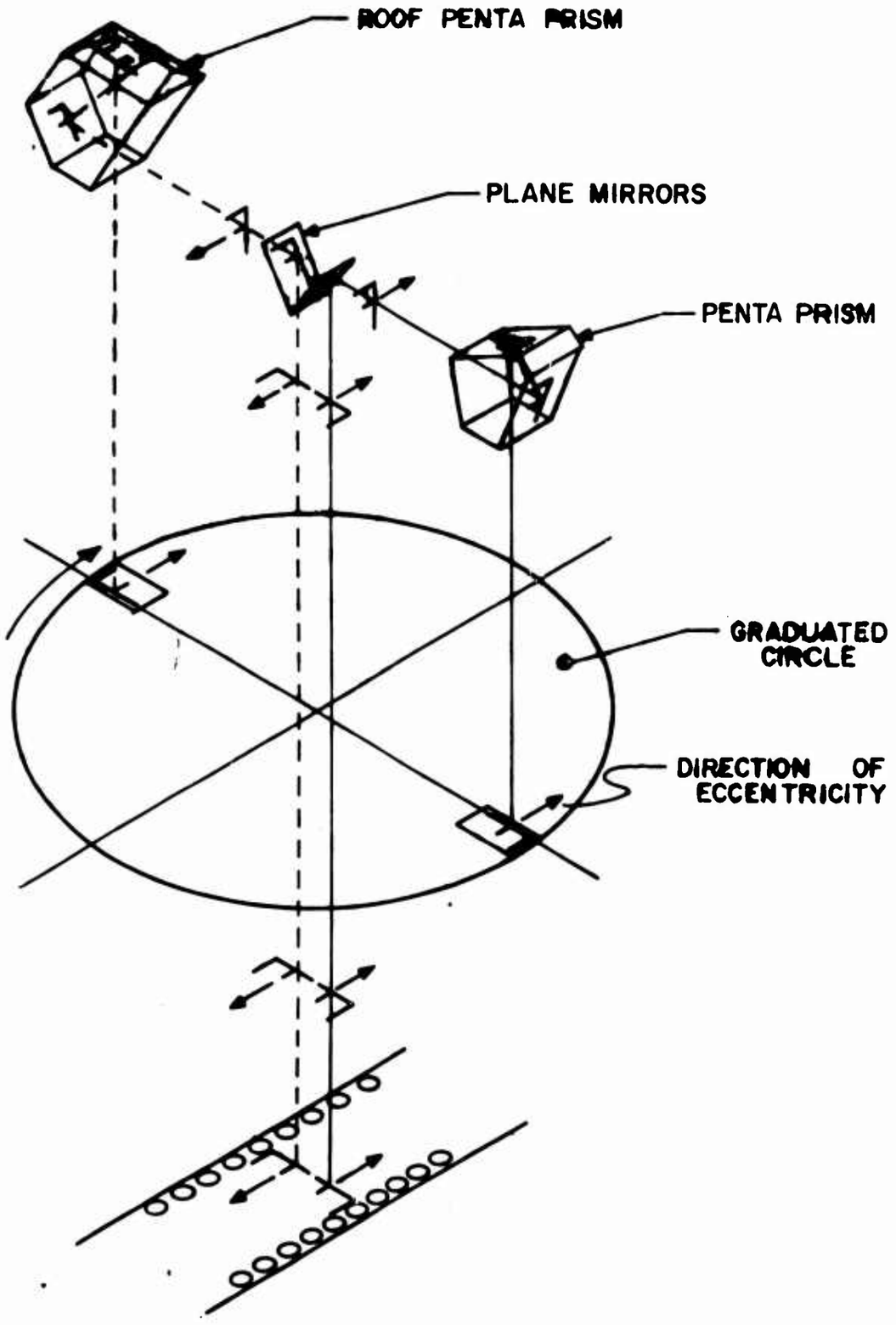

FIGURE 30 EFFECT OF AZIMUTH DIAL ECCENTRICITY

respect to rotation about the z-axis as shown in Figure 31. The behavior of the 90-degree deviator with respect to rotations about the x-axis is shown in Figure 32. The direction of the average of these two beams is that which defines the direction of the horizontal axis of the theodolite. This direction is insensitive to all tilts of the instrument.

The next assembly in the optical data path is the elevation circle recording system. Compensation of elevation circle eccentricity is identical to that for the azimuth graduated circle. Light beams from the elevation graduated circle and the vertical reference target enable forward mislevel error compensation. A forward mislevel of the instrument causes every component in the elevation circle data system, shown in Figure 33, to rotate in the direction of the forward mislevel. This motion does not, however, have any effect on the direction of the rays in the space beyond the two plane mirrors. Therefore, if one fixes the components of the elevation circle to a coordinate system, a forward mislevel will not cause any motion of the graduated circle images. The index marker, however, is fixed in space and is not dependent on the elevation circle data system for its position. The forward mislevel then does cause a deviation between the images formed by the elevation circles and the elevation index image formed by the vertical reference target. This deviation is equal to the mislevel experienced by the instrument; hence, we get the proper compensation of the graduated circle reading. The proper direction of the index deviation also had to be selected. The beam coming out of the plain penta side of the penta-prism assembly gives the proper direction, and was selected to form the elevation index image.

After the elevation graduated circle data enters the optical path, the rays that will form images of the azimuth dial, elevation dial, azimuth index, and elevation index pass through an image-forming lens and are focused at the point of focus shown in Figure 29.

Referring again to the 90-degree deviation assembly, part of the light coming out of the roof penta and part of the remainder of the light coming out of the plain penta is intercepted by two smaller 90-degree deviators. These two deviators direct the beam toward the primary mirror of the Cassegrain objective. The pointing axis of the instrument is defined by these 90-degree deviators in a manner analogous to the way the horizontal axis is defined by the first 90-degree deviators. The second set of deviators rotates about the elevation axis, thus always directing the beam toward the primary mirror of the Cassegrain objective. The original two beams of light from the first 90-degree deviator are split into four beams by the second set of 90-degree deviators. The pointing axis is defined as the average direction of these four beams. This direction is insensitive to any mechanical errors or deflections of the instrument whatever

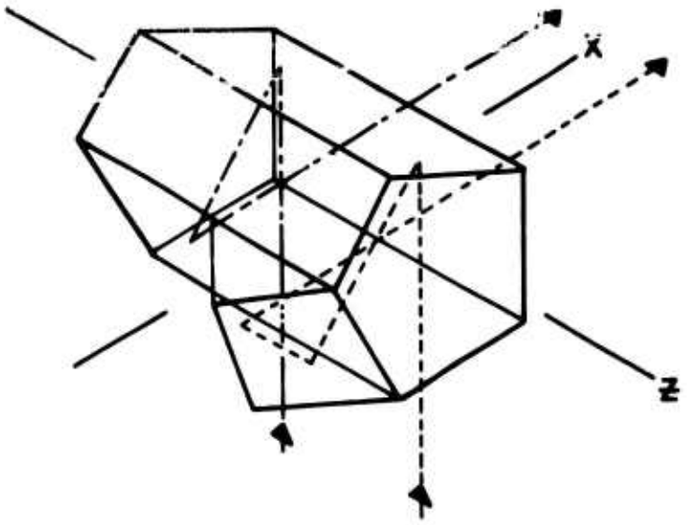

FIGURE 31 90° DEVIATION ASSEMBLY – Z AXIS ROTATION

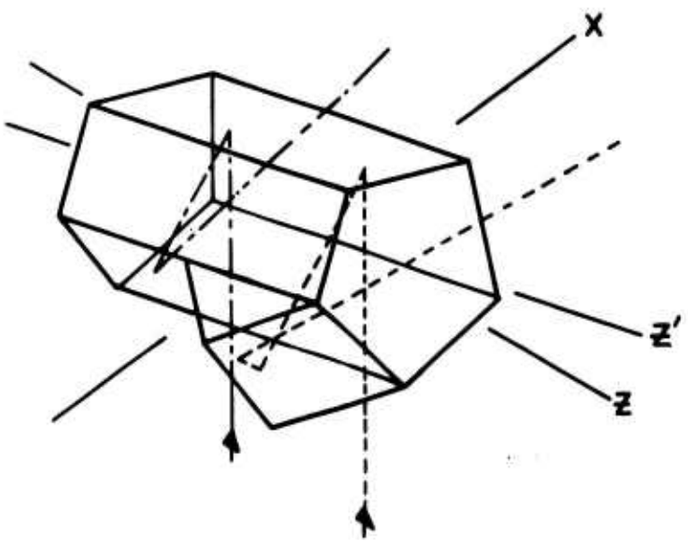

FIGURE 32 90° DEVIATION ASSEMBLY – X AXIS ROTATION

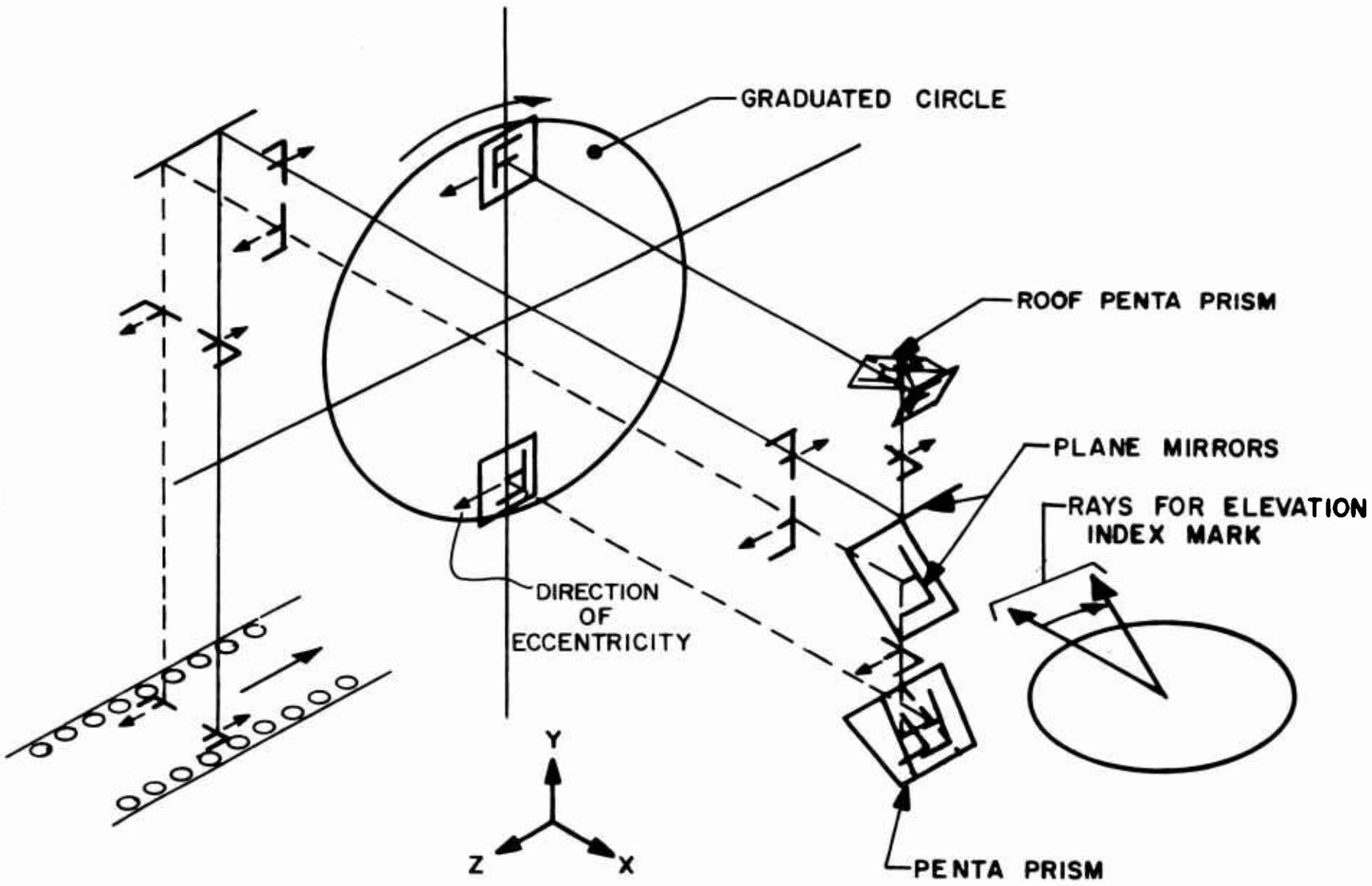

FIGURE 33 EFFECT OF ELEVATION DIAL ECCENTRICITY AND FORWARD MISLEVEL

The four beams of light from the second 90-degree deviators fall upon the primary mirror of the objective, which forms in the focal plane four images of the vertical reference target. The light entering the main optical system follows the same path to the focal plane as these four beams. Consequently, any motion of the lens system affects the positions of the four reference images and the main image in the same way, and no error is introduced by these motions. All images formed by the circle recording systems, the vertical reference target, and the main optical system are brought to the point of focus shown in Figure 29. From that point on, the remainder of the optical system serves to focus and position the images.

TESTS

No specific optical data train tests were conducted at WSMR. In essence, the optical data train was tested in its entirety throughout the accuracy evaluation detailed in the section titled "Accuracy Evaluation." In addition, comprehensive testing of the main optics was conducted at the manufacturer's plant as detailed in the section titled "Main Optics."

DEFICIENCIES

The performance of the optical data train was adequate to accomplish the accuracy evaluation of the WSMR Cinetheodolite, but there are some data train deficiencies that need to be corrected in the production pilot model and follow-on units. These are as follows.

Fiducial Images

1. The images are 700 microns in diameter, at least an order of magnitude larger than the optimum size.

2. Because of the high T-number (low light transmission) of the optical data train, the contrast of the images to the background is low.

3. Some of the images are asymmetric.

Dial and Bar Images

1. The bar images are not accurately parallel.

2. Because of the high T-number of data train, the density of the bar images is not uniform and there is insufficient contrast.

3. Some of the bar images are very asymmetric.

These deficiencies are such that the attainable measurement accuracies are not compatible with the accuracy goals of this system.

Field of View

The field of view of the data train is too narrow and causes obscuration of the dial bars to the extent shown in Figure 34. This causes a certain percentage of the frames of data to be unusable.

DATA TRAIN REDESIGN

A contract was awarded to Keuffel and Esser Company to redesign the optical data train to eliminate these problems. As a result, the following improvements will be made.

1. The size and shape of the small triangular apertures will be changed. This will result in improved contrast, resolution, and symmetry of the images.

2. The fiducials and the dial data will be imaged at a higher magnification. This will result in improved precision of measurement.

3. The fiducial images will be reduced in size from 700 microns to 200 microns diameter. This also will result in improved precision of measurement.

4. Chromatic aberration resulting from wedges and lenses will be greatly reduced since no wedges will be used in the new system.

5. The method of presenting the dial data will be changed to allow more precise measurements with fewer readings.

6. The fiber optics used in the fiducial and circle illumination system will be eliminated and a new improved light source will be used. This will result in improved image quality.

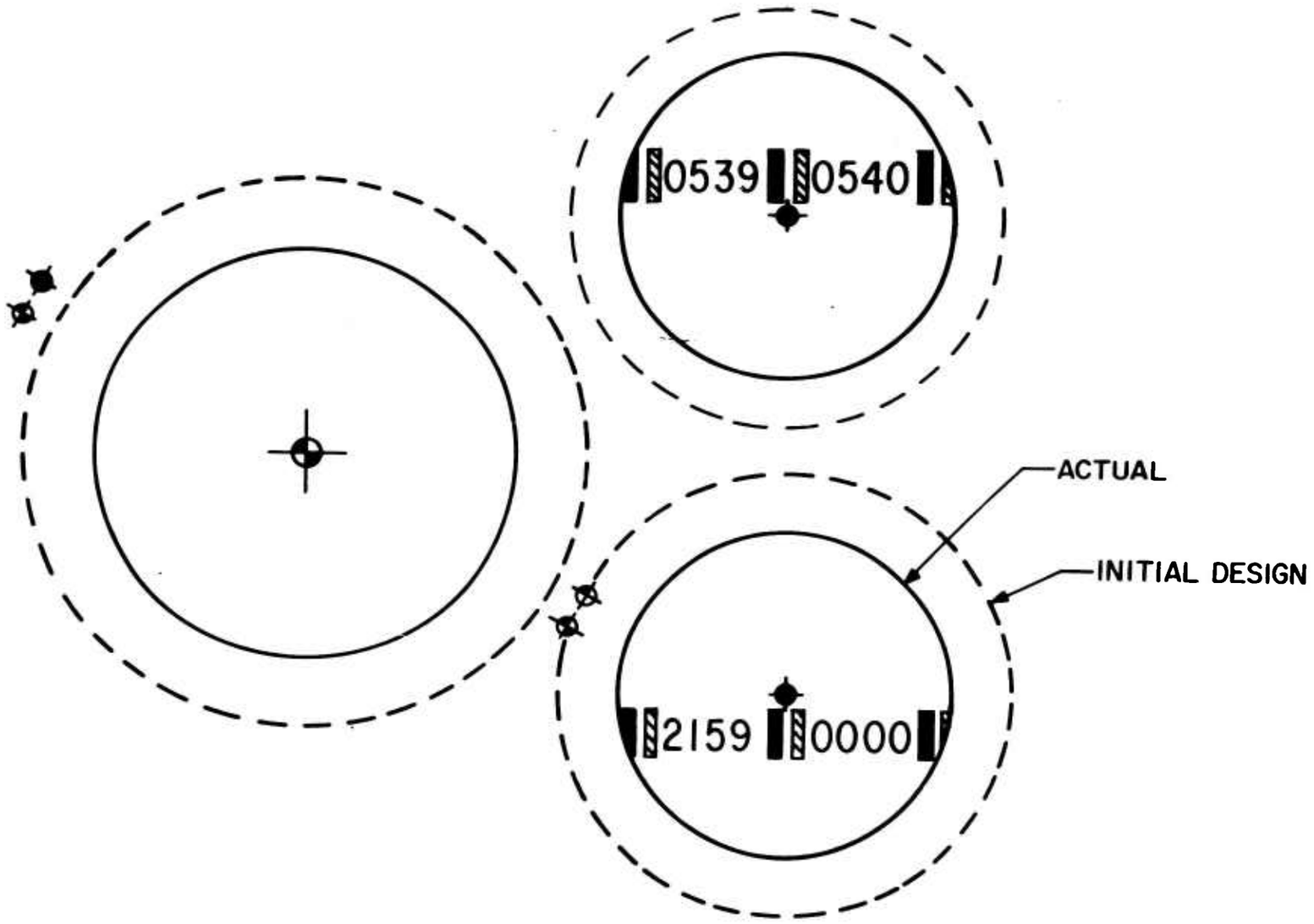

FIGURE 34 SYSTEM FIELD OF VIEW

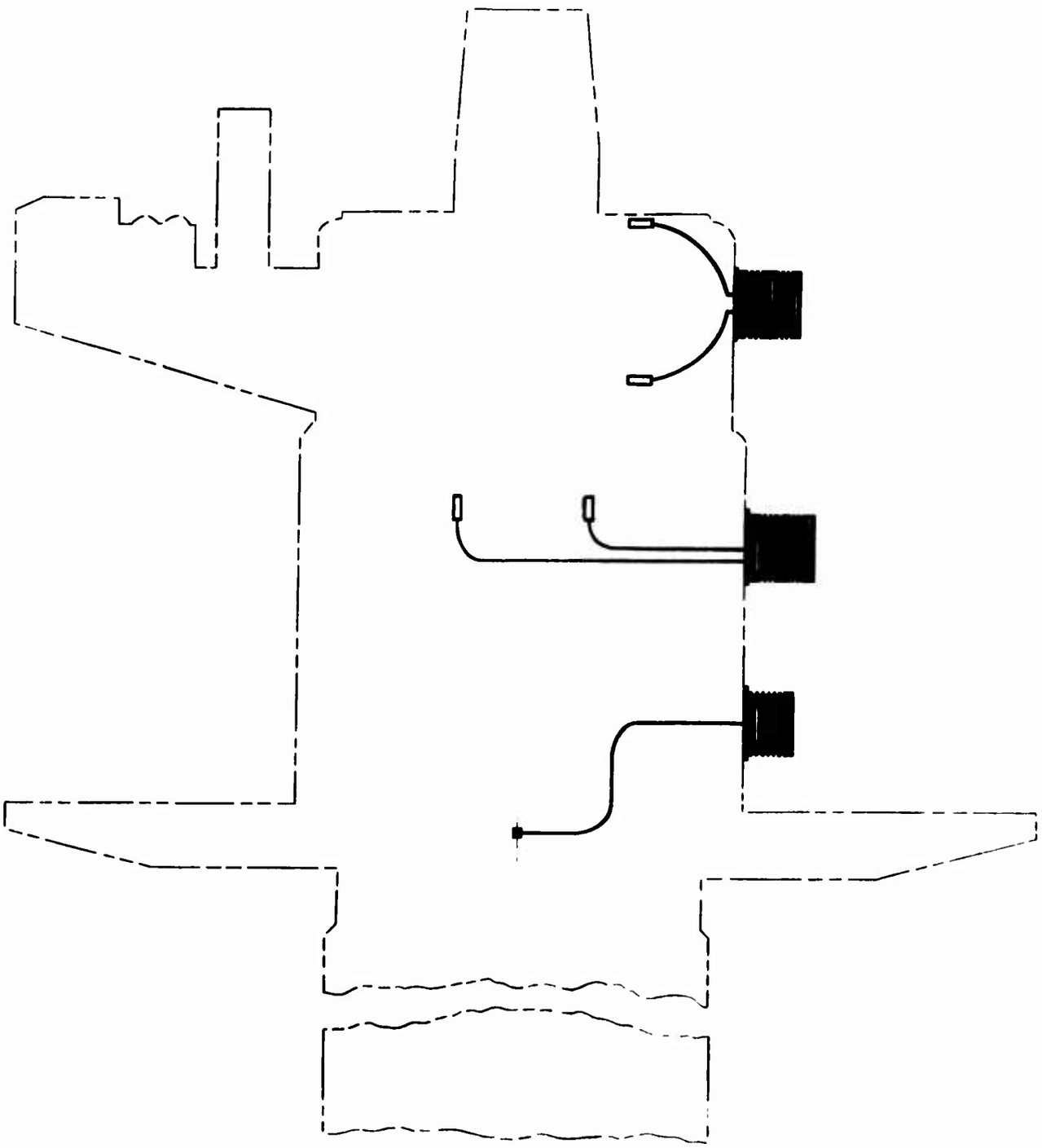

ILLUMINATING SYSTEM

DIAL AND FIDUCIAL ILLUMINATION SYSTEM

BACKGROUND

The primary requirement of the WSMR Cinetheodolite photographic recording system is that it must image fiducial marks and dial data on the film with sufficient density and sharpness to permit accurate and reliable data reduction from the film. In order to "freeze" the motion of the dial and prevent blurring of the dial image at moderate azimuth and elevation velocities, the dial image exposure must take place in 100 microseconds or less. For the fiducial images, the lower image velocities even at high tracking rates permit exposures of up to 1 millisecond. As long as the exposure time does not exceed 20 percent of these maximum values, the symmetry of the intensity curve about the midpoint in time of the exposure does not have to be considered; this was the case with the breadboard instrument. As the light that forms the images must travel through the very high f-number optical data train photographic system, a high-intensity flashlamp was indicated. Three flash heads, a fiducial flash head assembly, an elevation dial flash head assembly and an azimuth dial flash head assembly with appropriate high-voltage power supplies, comprise the illumination system of the breadboard WSMR Cinetheodolite. In attempting to meet the 50-frame/second flash rate requirement for readable dial and fiducial images, the contractor encountered many problems. He only succeeded in flashing the lamps at five frames per second, and this was accomplished only for a brief period. The following is a summary of some of the problems experienced by the contractor.

1. The initial design called for the EG&G FX-31 strobe lamp as a source of illumination for the optical data train system. Preliminary tests disclosed that the illumination level was far below that needed to record the elevation dial data on Eastman Kodak Linagraph Shellburst (LSB) film.

2. Testing was resumed with an FX-76 20-watt lamp which is approximately five times brighter than the FX-31 lamp. Input energy was increased to three joules per flash to obtain enough density on the LSB film. A condenser system was also designed especially for the FX-76 lamp, but a new Bausch and Lomb glass fiber bundle gave better results than the improved condenser system. These tests were also conducted on the elevation dial data train. With the lamp rated at 20 watts, a maximum pulse rate of only seven flashes per second was possible, while a pulse rate of 50 flashes per second is required. A marginal density was obtained through the No. 29 red filter, by operating at 6.7 joules per flash, and the lamp could only be operated at three flashes per second. It was suggested using multiple lamps fired sequentially, but that would have required 17 lamps at three flashes per second to obtain 50 flashes per second.

3. Tests were started using the FX-24 lamp which has flat ends, the idea being to place the fiber optic bundle against the flat end for better light concentration. The FX-24 lamp proved to be brighter than the FX-76, requiring a six-joule input to obtain a satisfactory film density with one flash. This required the FX-24 to operate at a 300-watt rating and the lamp overheated badly. The flashlamp supplier suggested a water-cooled lamp such as the FX-74B-1.5; however, tests with this lamp proved that it was inferior to the FX-24. Its arc was not positionally stable and seemed to separate. The FX-74B-1.5 flashtube proved to be wholly unsatisfactory.

Testing was resumed with the FX-24 lamp in distilled water coolant. When photographing through a clear filter, three joules per flash were required. At 50 flashes per second this would amount to a 140-watt output, and in ten minutes operating time it would raise the heat of one quart of water 37°F. Tests were also run on the time duration of the flash and are listed in Table III.

TABLE III. ENERGY/TIME REQUIREMENTS

Joules	Volts	Microfarads	Time Duration
6.3	1,900	3.5	9 microseconds
6.0	1,500	5.5	13 microseconds
6.0	900	15.0	20 microseconds

From earlier tests it was discovered that five times more light was needed to illuminate the fiducial than the elevation dial. Consequently, it was felt that 16.5 joules with a 5.5-microfarad capacitor at 2,430 volts would suffice for the worse case (red filter) of the fiducial images.

Actual tests were next run to determine the quality of the four fiducial images in a single flash. Nine joules were required for a satisfactory image using the clear filter, and 13 joules using the light yellow filter.

4. Table IV lists the calculations for effective f-numbers.

TABLE IV. F-NUMBER CALCULATIONS

	f-No.	Refract. Surfaces	Reflect Surfaces	Effective f-No.	T.L.N.	Stops	Energy Needed
Index	201	34	7	388	1(base)	0(base)	
Fiducial Pp	210	34	11	566	2.13	1.09	
Fiducial Pr	210	34	12	585	2.27	1.44	
Fiducial Rp	210	34	12	585	2.27	1.44	9 joules/ flash
Fiducial Rr	210	34	13	646	2.78	1.48	
Elevation Data	200	28	4	322	0.68	-0.55	
Elevation Bars	200	28	5	342	0.77	-0.37	2.9 joules/ flash
Azimuth Data	200	34	8	433	1.25	0.32	
Azimuth Bars	200	34	9	462	1.42	0.51	5.3 joules/ flash

In Table IV, Column 1 is based strictly on entrance pupil area and equivalent focal lengths, to get the familiar reciprocal relative aperture, or f-number.

Column 2 totals the number of refracting surfaces in each particular optical path, for which we assume 1.5 percent loss of light at each glass-to-air surface.

Column 3 totals the number of external reflecting surfaces for which we assume 12.0 percent loss of light per surface.

Column 4, the "effective f-number," is calculated from the three preceding columns.

Column 5, T.L.N. (Times Light Needed), with index images as an arbitrary base 1.

Column 6, "Stops," are photographic stops from the same base. One stop means doubling or halving of the light. This film (LSB) appears to have a latitude of slightly over plus or minus one stop from "best" exposure.

Column 7 lists recommendations based on tests to date. The nine joules would suffice for all fiducials. The index images, on the same lamp, might be a little overexposed, but could be filtered down.

The 2.9 joules would suffice in the clear for the evaluation data and bars (both on one lamp). As a better alternative, the lamp could be run at 4.4 joules and utilize a 1.5 filter-factor light yellow filter to reduce lateral color.

The 5.3 joules suffices in the clear for both azimuth requirements (one lamp); or, use 8.0 joules with the same light yellow filter for the same reason.

At 5.8 joules with an 8-microfarad capacitor, the pulse width was approximately 10 microseconds. Higher voltages and lower capacity give shorter pulse widths, but spontaneous flashing of the lamp occurs when operating above 1,700 volts.

5. Tests were continued with the FX-24 lamp operating under high-power conditions.

The first tests were made with distilled water. One of the results of the tests showed that the metal electrodes of the lamp could not be immersed in water.

In the first test, the lamp was operated at 50 watts for seven minutes. The temperature of the water, which was not recirculated, rose to 160°F.

In the second test, a pump was added, circulating the water at one pint per minute. The lamp was operated at 50 watts for seven minutes and the temperature of the water rose to 100°F. In both tests, the lamp showed no deterioration.

In the third test, the power was increased to 174 watts. The lamp operated for 4-1/2 minutes and then stopped flashing. Investigation showed that the solder used to seal the glass to the metal electrode melted, and the xenon gas escaped. The section of the lamp which was in the water showed no deterioration.

A liquid freon compound was obtained and test showed that the entire lamp could be immersed with satisfactory operation.

Tests were run with the lamp operated at the 174-watt level. The lamp withstood three tests of five minutes each without failure. The temperature of the freon rose approximately 10°F. Localized boiling was noted around the quartz tube rather than at the electrodes.

A larger power supply was not available for higher power tests.

Several new FX-24 lamps were purchased which had larger electrodes and could stand more heat. Transistor heat fins were also procured which fit over the tube and provided a larger cooling area.

The foregoing tests established that the 50-per-second capability could not be realized in the short time remaining in the breadboard development phase and liquid-cooled flashlamp system with reduced performance requirements was purchased. The contract specified a rate of 10 flashes per second and a life of 10,000 flashes with a design goal of 100,000 flashes. Although the flashlamp did not satisfy even the reduced requirements, the system's performance established feasibility of the basic WSMR Cinetheodolite concept.

CONFIGURATION

The flashlamp system consists of three flash heads and two power supplies as follows.

1. Fiducial Flash Head Assembly.
2. Fiducial Lamp Power Supply (PS-190).
3. Elevation Flash Head Assembly.
4. Azimuth Flash Head Assembly.
5. Elevation/Azimuth Lamp Power Supply (PS-191).

The flash heads are installed on the cinetheodolite (see Figure 1). The PS-191 is mounted on the annular platform and PS-190 is installed in an electronics cabinet at the ground level.

THEORY OF OPERATION

Flash Head Assembly

All three flash heads are electrically identical to the one illustrated in Figure 35. Each assembly consists of an energy storage capacitor of 20.1-microfarad capacity, an FX-51 xenon flashlamp, and a trigger circuit.

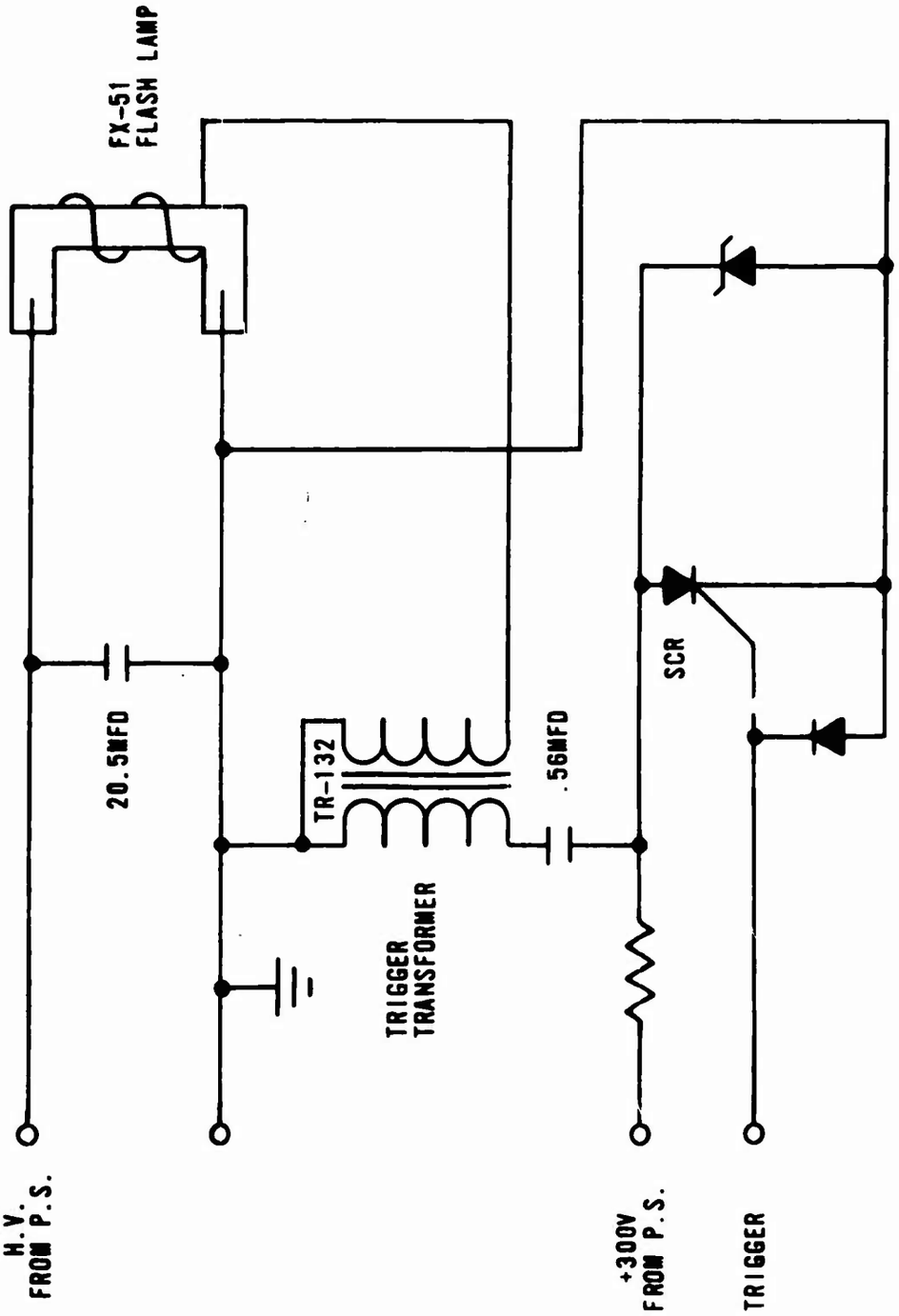

FIGURE 35 FLASH HEAD SCHEMATIC

Figure 36 is a photograph of the FX-51 flashlamp. Figure 37 shows both types of flash heads. The mechanical features of each flash head are a sealed chamber filled with a fluorocarbon coolant and an expansion chamber, separated by a neoprene diaphragm. The expansion chamber is dimensioned to permit a rise of internal bulk temperature to 165°F. The base plate of the flash head is fitted with sealed glass windows for light transmission. The fiducial flash head has one window, and azimuth and elevation flash heads have two each.

Internally, the fiducial flashtube (Type A) is mounted in such a fashion that its end abuts the light exit window. The dial flashtubes (Type B) are mounted between two sealed periscopes so that the two light beams emitted from the tube ends enter their respective periscopes and are deflected 90° to exit the chamber in parallel beams.

The high-intensity light flashes are directed from the windows through fiber optic conduits to their respective targets in the optical data train.

The flash heads operate as follows.

Energy from the power supplies is conducted to the flash heads shown in Figure 35 through the connecting cable and charges the 20.1-microfarad capacitor to 1,350 volts.

At the same time a small capacitor is charged to 300 volts dc. This capacitor is connected in series with a trigger transformer and a silicon controlled rectifier (SCR). When the SCR is turned on, the capacitor is discharged. The discharge current in the primary winding of the trigger transformer induces 15 kilovolts in the secondary winding, which is connected to the trigger wire of the flashtube. At the flashtube, this voltage ionizes the xenon gas in the tube envelope rendering it conductive. The energy stored in the 20.1-microfarad capacitor can now discharge through the flashtube. This discharge converts the energy into heat and light. The heat is distributed by the coolant, permitting three minutes of continuous operation at a flash rate of five flashes per second, and after one minute of cooling, a second run of three minutes. The system, under these operating conditions, has a large margin of safety with regard to temperature.

Power Supply and Trigger Amplifier

The two power supplies are identical electrically, except that the PS-190 has a single output and the PS-191 has a dual output. The power supply and regulation circuitry are shown in the block diagram of Figure 38. The power supply proper consists of a power transformer, a high-voltage rectifier bridge and a current-limiting resistor. Line voltage from the input

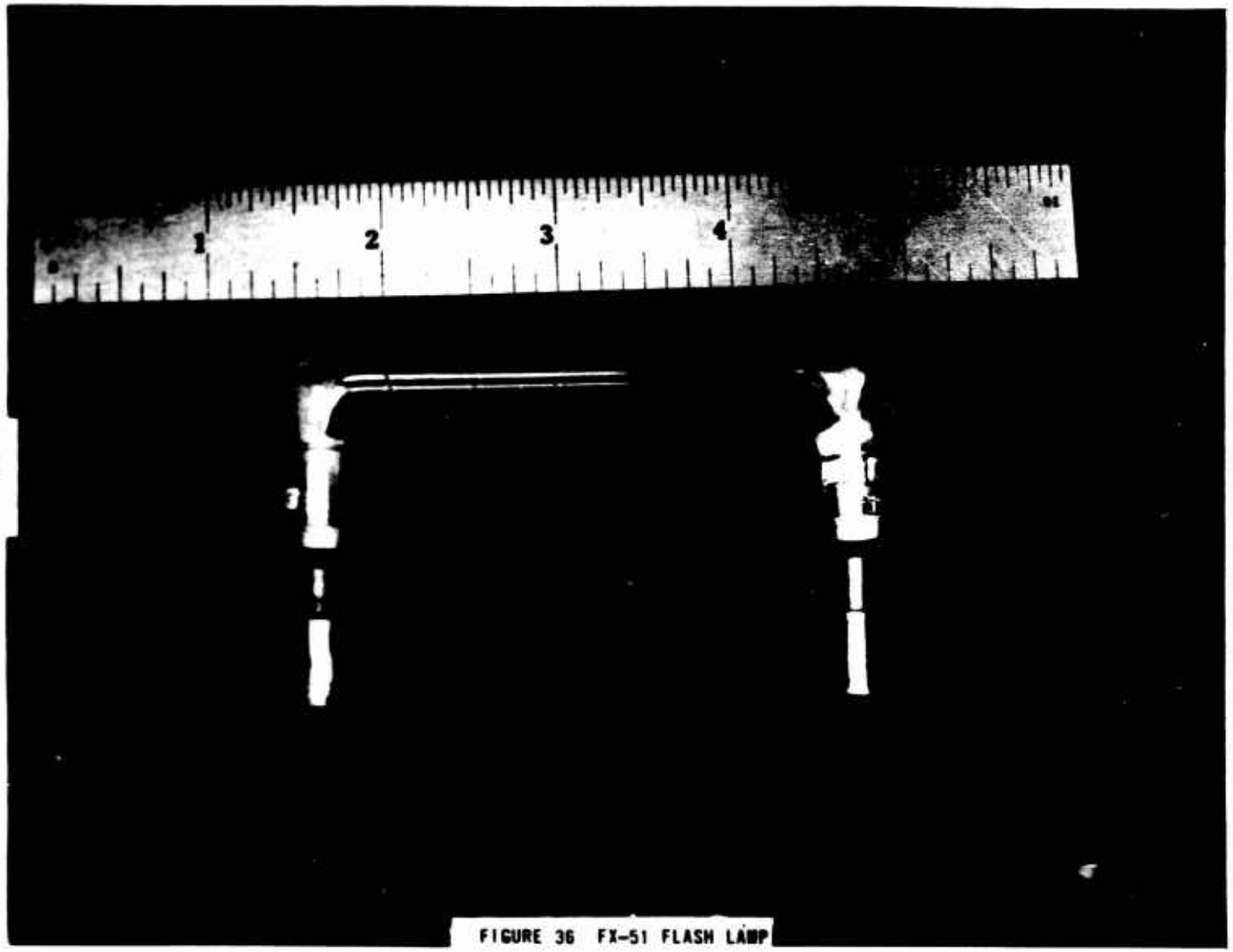

FIGURE 36 FX-51 FLASH LAMP

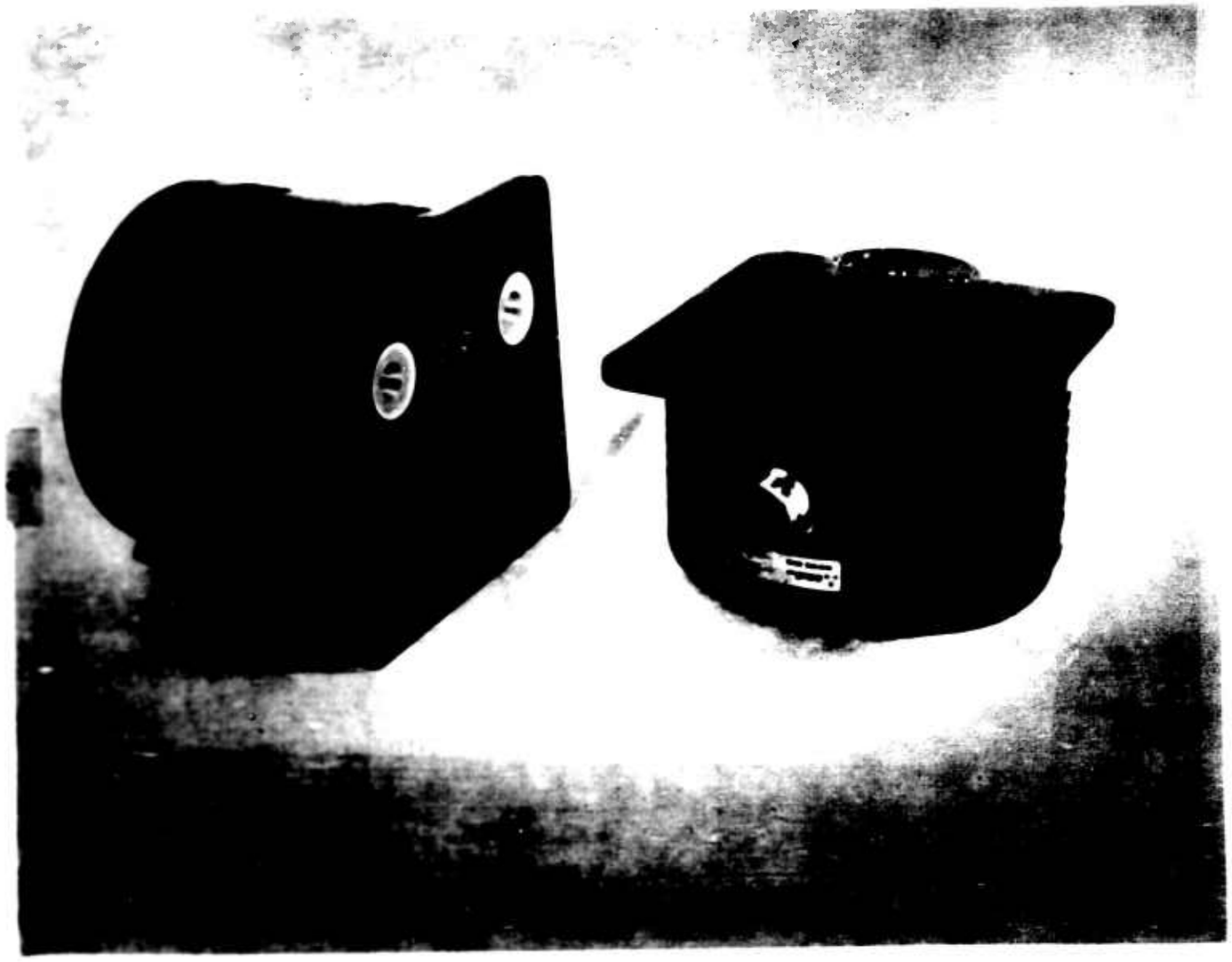

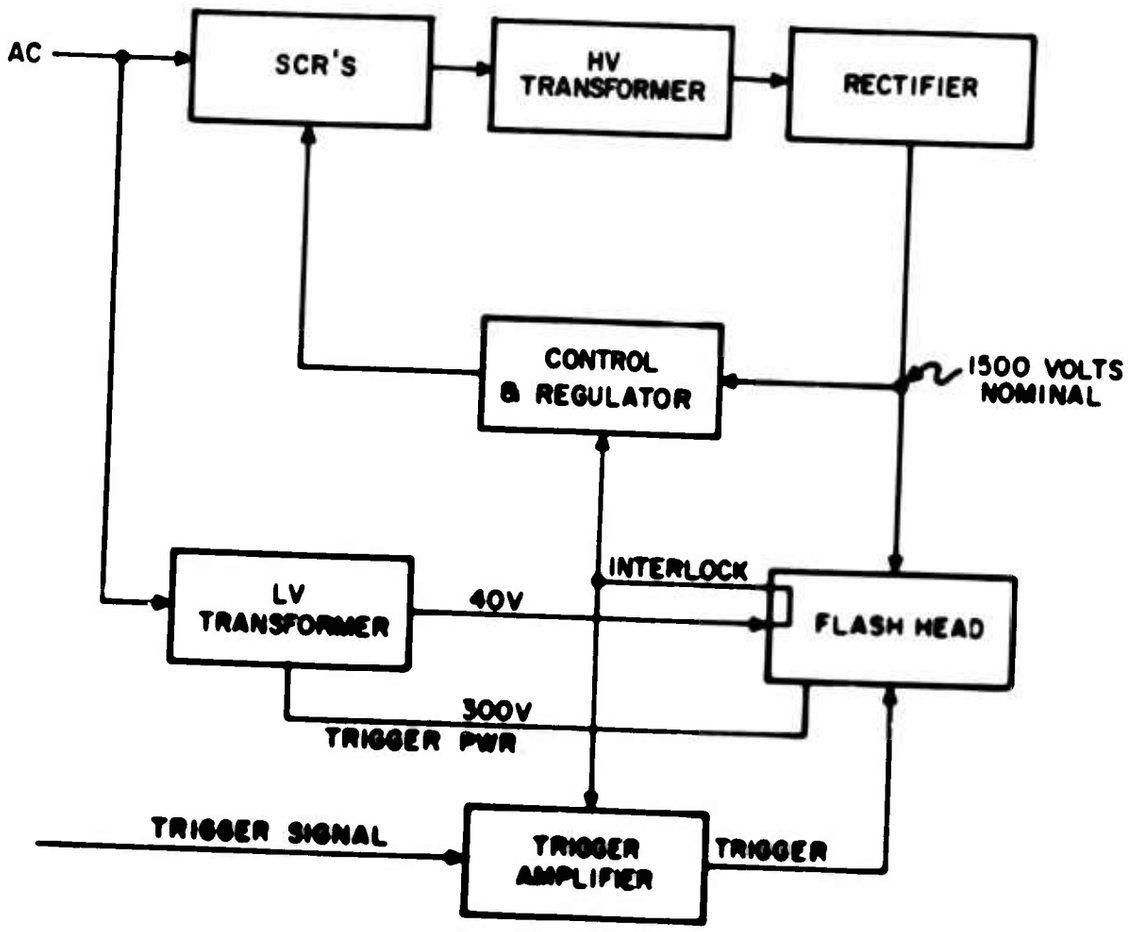

FIGURE 38 FIDUCIAL ILLUMINATION SYSTEM

power connector is fed to the primary winding of the power transformer through the two SCR's which are gated by the control and regulation circuits. The resultant ac voltage in the transformer secondary is converted in the diode bridge rectifier to 1,350 volts dc and fed through the output connector to the energy storage capacitor in the flash heads. The voltage across the energy storage capacitor is sampled through a 10-megohm resistor to serve as an error signal for the regulation circuit. The rate at which the storage capacitor is charged is controlled by a unijunction transistor timing circuit. This circuit operates as follows. A full-wave rectified but unfiltered voltage is fed through a constant current amplifier to the timing capacitor connected to the emitter of the unijunction transistor. The capacity and current source are so chosen that the unijunction transistor fires on every half cycle at a phase angle sufficient to charge the storage capacitor to the desired voltage within 90 milliseconds. The feedback current from the 10-megohm resistor turns a transistor off when the desired voltage (1,350 volts) is reached at the capacitor bank. This prevents the unijunction transistor from reaching the firing voltage.

Whenever the unijunction transistor fires, a gate pulse is coupled into the two control SCR's, turning on the one in phase with the supply voltage. This permits current to flow in the primary of the high-voltage transformer. The power for this circuit and the trigger amplifier is derived from a low-voltage transformer and is regulated to 20 volts dc with adequate filtering. This voltage is interlocked through the flash heads, in order to prevent unloaded operation of the power supply. The trigger amplifier inverts the trigger signal and amplifies it to sufficient power to gate on the SCR in the flash head trigger circuit.

TEST RESULTS

During the static and dynamic pointing accuracy tests, the three flash heads were fired a total of 51,348 times (17,116 x 3). Twelve flash head failures occurred. Their useful life is indicated in Table V. Eight were repaired at WSMR and four were returned to EG&G for repair. Three of the eight flash heads repaired at WSMR had fractured xenon flashtube envelopes and the other five had miscellaneous trigger circuit failures. New flash heads failed to fire approximately 10 percent of the time and misfire percentage increased with lamp deterioration. Although the flash heads were rated at ten flashes per second maximum, they were operated at the much lower rates required for the static and dynamic pointing accuracy tests. No optical filters were used during the tests and slight underexposure was noted on the test plates. More light is desirable if no filters are used, and mandatory if filters are used. Lamp power supply failures involved two SCR's in the main section and two rectifier diodes in the logic section of one supply.

TABLE V. FLASHLAMP LIFE

Failure Date	Head Type	Cause	Approximate Flash Life
February 68	FY-007 B	*	3500
February 68	007 B	*	3
March 68	006 A	FX-51 fractured	4500
April 68	007 B	Trigger transformer	500
June 68	007 B	Trigger transformer	6500
June 68	007 B	Trigger SCR & Zener	5500
September 68	007 B	*	7500
September 68	006 A	*	12000
February 69	006 A	FX-51 fractured	5000
February 69	007 B	FX-51 fractured	3500
February 69	007 B	Trigger arc over to cylinder	1500
September 69	006 A	Trigger SCR	1500

*Unknown; repaired at EG&G.

DEFICIENCIES

1. All flashlamps misfired approximately 10 percent of the time.

2. The minimum lamp life requirement is 500,000 flashes. The average flash head life has been 5,000 flashes, with individual lives varying from three to over 12,000 flashes.

3. The required maximum repetition rate is 50 flashes per second; the flash head system is only capable of five flashes per second.

4. Maximum duty cycle of three minutes on, one minute off, three minutes on, thirty minutes off falls short of range requirements.

5. The light output is insufficient for routine film processing.

FUTURE DEVELOPMENT OF THE DIAL AND FIDUCIAL ILLUMINATION SYSTEM

Soon after installation of the breadboard instrument at WSMR, it became apparent that the most serious design deficiency of the WSMR Cinetheodolite instrument was the dial and fiducial illumination system. Contract DAAD07-69-C-0119 was let to K&E on 7 March 1969 to correct this as well as other less critical design deficiencies. Two current design changes are contributing to a solution of the problem. The apertures within the data train optics are being increased substantially, increasing the speed from an effective f/400 to an f/100 system, thus, reducing the flashtube radiance requirement. The second design change in process relates directly to the flashtube configuration and the efficiency of light utilization by the data train, reducing the flashtube power required by a factor of 4 to 5. The ideal light source to form collimated beams would be point sources or at least relatively small sources. In Figure 39, it can be seen that most of the energy radiated by the 30-mm long plasma is wasted; less than 5 percent of the light emitted by the flash is utilized by the data train optics. The 1.5-mm plasma from an improved lamp is utilized better and requires one-sixth of the power. It is most unfortunate that preoccupation with high power output from flashtubes occurred in the exploratory development phase because it was the use of high power outputs rather than high radiance that produced the problems of low life expectancy and low flash rates. Data from the current contract indicates that flash rates of 50 to 60 per second present no problem; that 1 joule or less is an adequate power input; that a life expectancy for the flashtubes of 10^7 flashes will be a realistic goal for a fieldworthy production instrument; and finally, that a liquid cooling system will not be required.

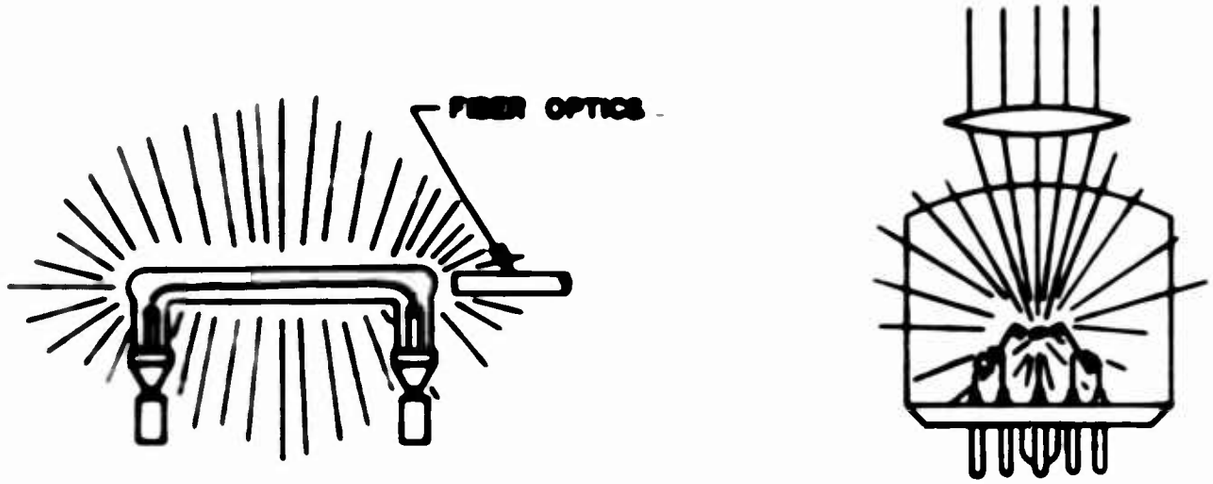

FIGURE 38 FLASH SOURCE UTILIZATION

DATA LAMP SYSTEM

CONFIGURATION

General

In contrast to the dial and fiducial images previously discussed, requiring highly precise measurement, the data matrix images are merely binary bits whose presence or absence is their only significant aspect. No optical data train is required, and consequently, the design problems associated with this system were relatively minor.

The data lamp system contains all equipment necessary to insure photographic recording of the entire data block required for the cinetheodolite, exclusive of the optics which are installed in the cinetheodolite instrument.

The data block of 84 characters in 12 columns and 7 rows includes orientation, mission, station, target, day of year, time of day in seconds and milliseconds, tracking mode, vertical reference alarm, camera synchronization, 12 parity lights and several spare positions (reference Figure 40).

The data lamp system consists of two basic units: the data lamp control and the data lamp module unit.

Data Lamp Control

The data lamp control was produced by General Applied Science Laboratories under subcontract from K&E. It is housed in an electronics cabinet located at ground level adjacent to the K&E cabinet. The control includes the following.

1. An adjustable high-voltage supply for the data lamps, with manual control and voltmeter.

2. All required low-voltage supplies complete with test meter and meter selector switch.

3. Six thumbwheel switches for insertion of mission, target and station data.

4. All electronics required to sequentially test the data lamps, including a Nixie tube display to indicate the number of any defective lamp or lamp circuit.

5. All electronics required for vertical parity check of the matrix signals.

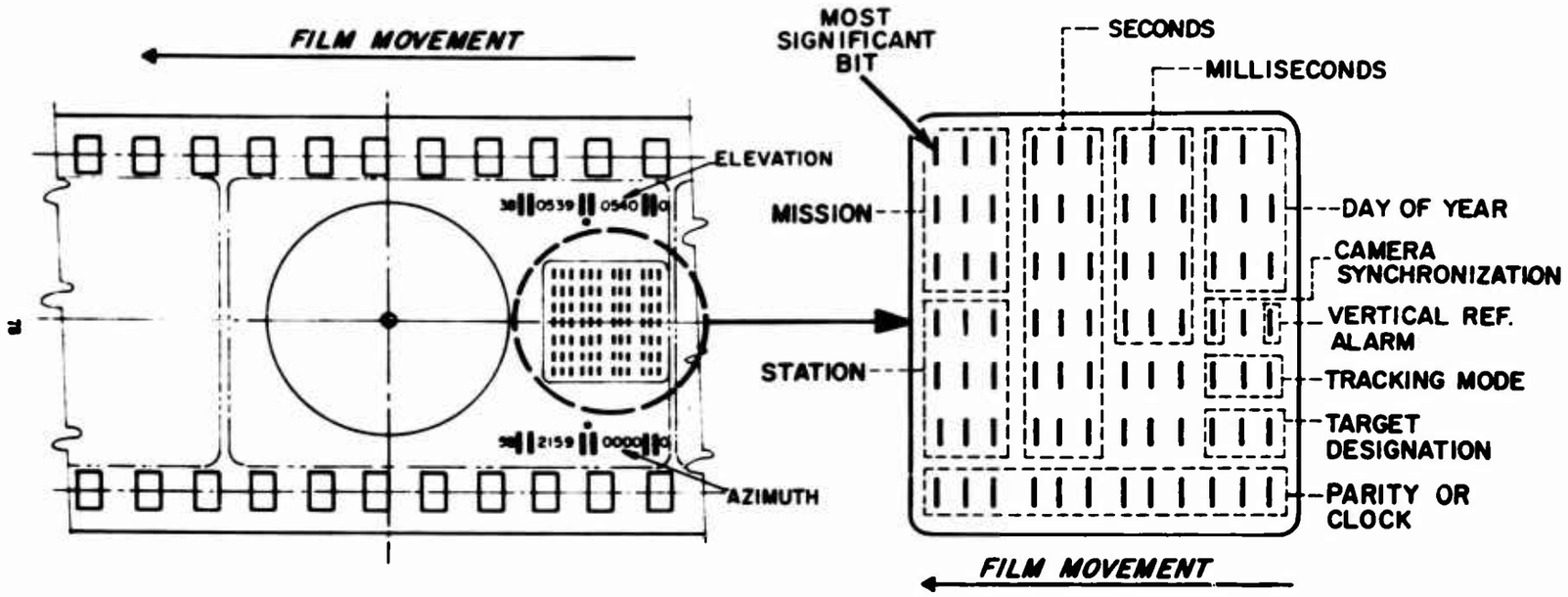

FIGURE 40 TIMING AND STATUS FORMAT

6. All electronics required to interface input signals with corresponding circuits in the data lamp modules unit. Figure 41 is a photograph of the data lamp control panel.

The Data Lamp Modules Unit

This unit is located on a bracket extending from the cinetheodolite. The light output of the data lamps is conducted into the cinetheodolite by a large fiber optic bundle which is terminated in an 84-character mask. A lens and mirror assembly in the cinetheodolite completes the light path to the camera compartment. The data lamp modules unit houses 12 modules, each of which includes seven FX-31 flashlamps, seven photodiodes, and seven sets of the required electronics for control and sequential tests of the flashlamps. Figure 42 is a photograph of the data lamp assembly including the fiber optic bundle.

THEORY OF OPERATION

Normal Mode

An input trigger signal produces a 5-microsecond data transfer signal. This signal loads the WSMR time input register illustrated in Figure 43 and starts a 15-microsecond delay multivibrator. The delayed output triggers a pulse generator which produces the second gate signal. This signal strobes the output gates of all the data lamps. If data is present at an output gate the data lamp is strobed.

Test Mode

Pressing the test switch initiates the test mode. The trigger signal line is inhibited and will remain inhibited until test sequence completion. The Nixie tube counter is reset to 00. After a short delay, the counter is preset to 01. The counter output now strobes Data Lamp 1. If it flashes, its photodiode signal starts a 25-microsecond delay. Completion of the delay sends a count pulse to the counter, which advances one count (02) and strobes Data Lamp 2. This sequence continues until all 84 lamps have been strobed. At the count of 85, the test sequence is completed by resetting the counter to 00 and after a delay, releasing the inhibit that had been placed on the trigger signal line. Thus, the system is again ready for normal operation.

Parity Generation

The data present at the six bits of each column is compared to see if an even number are true. If they are, an output is produced for the parity lamp of that column. Thus, the total number of bits per column of the matrix, including parity, should always be odd. If an even number occurs, it indicates that the recorded data is in error and should not be used.

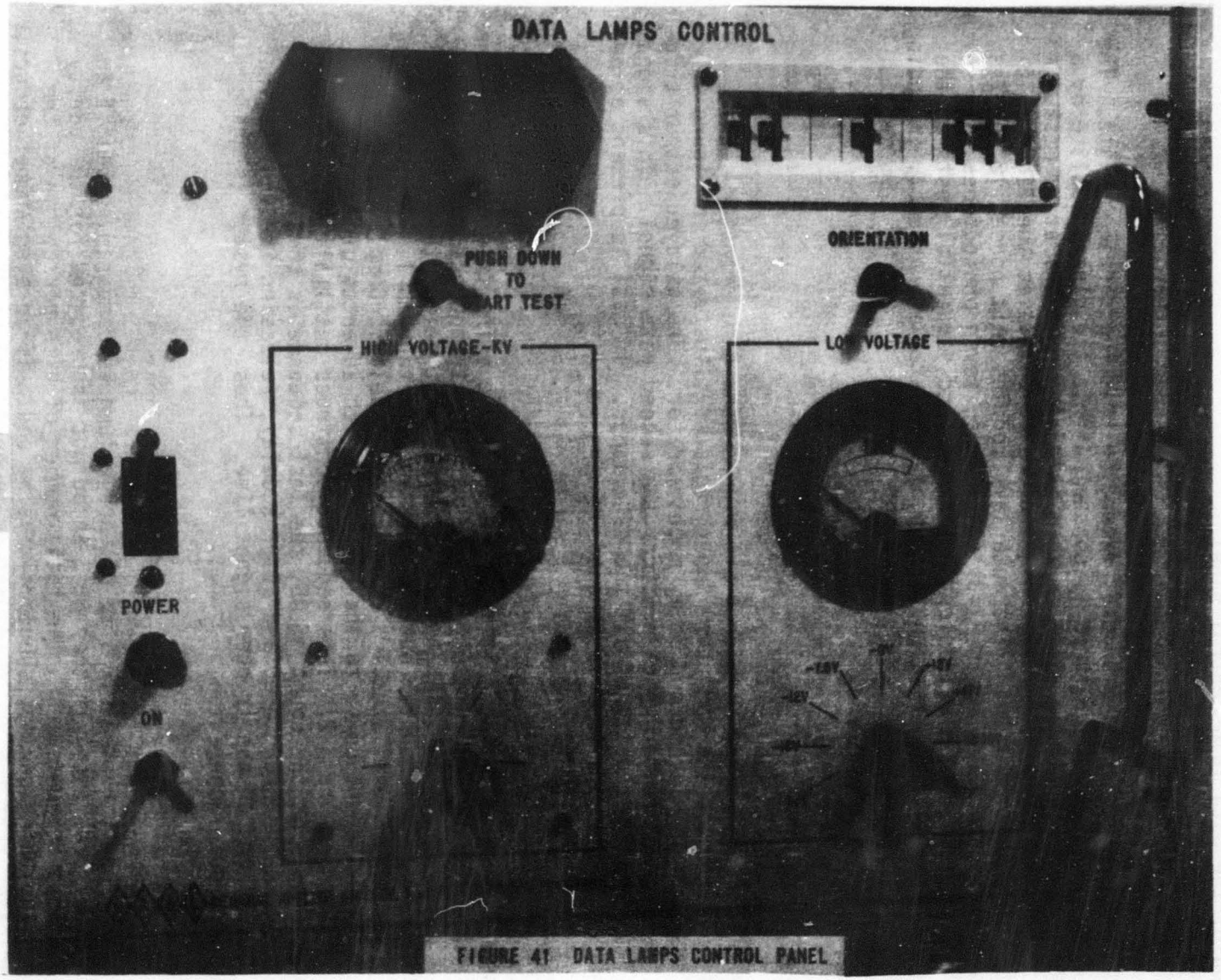

FIGURE 41 DATA LAMPS CONTROL PANEL

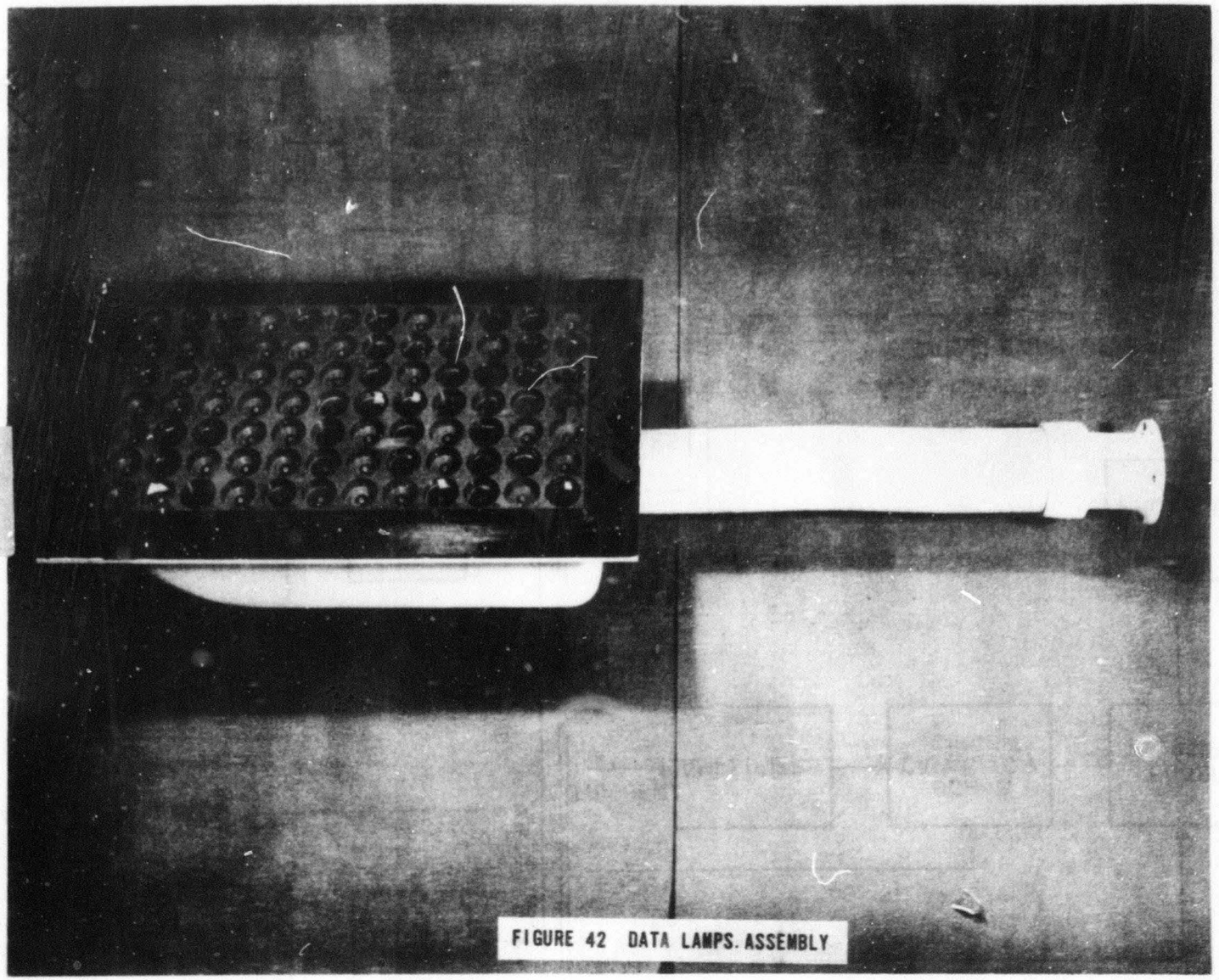

FIGURE 42 DATA LAMPS. ASSEMBLY

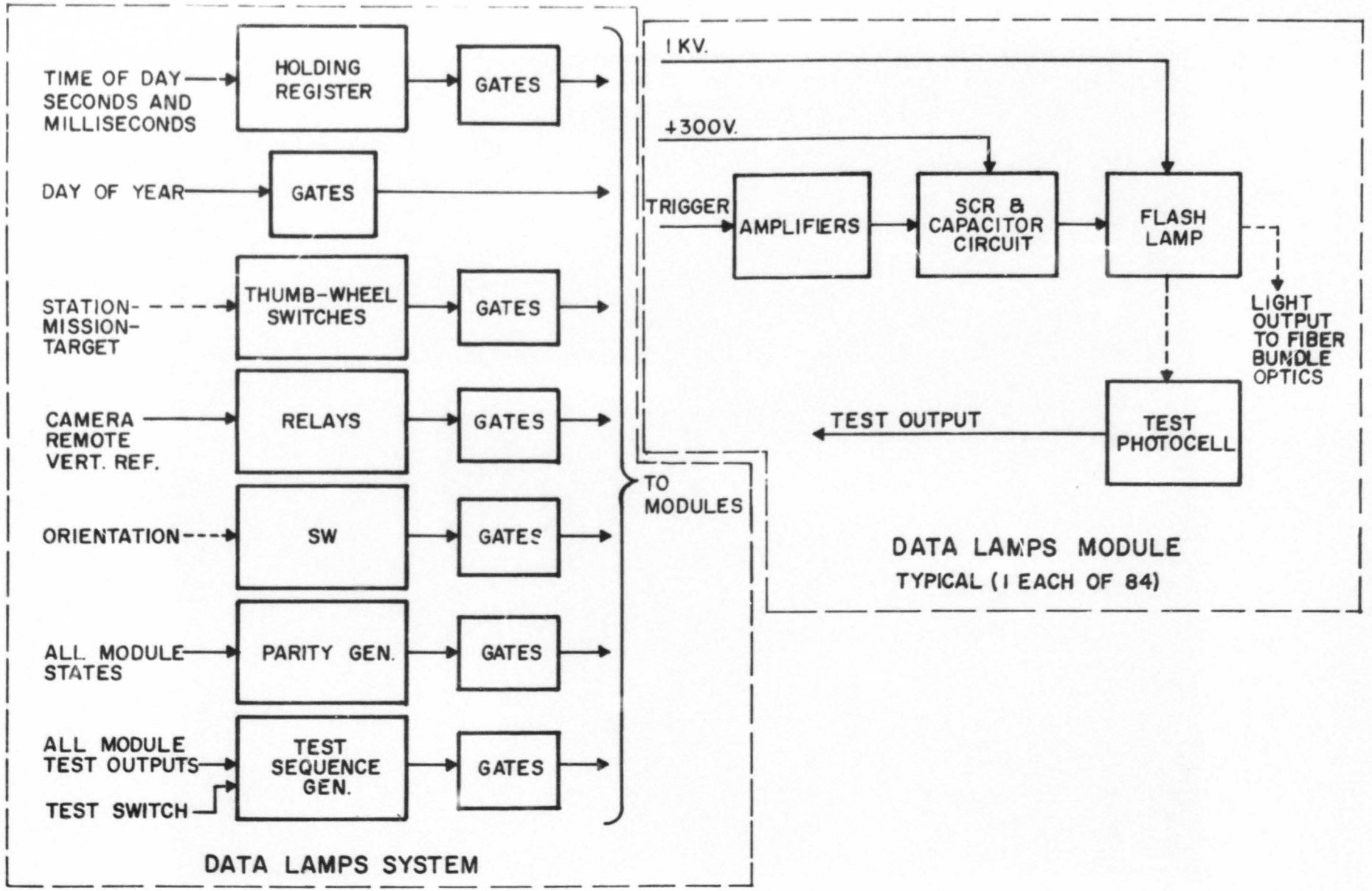

FIGURE 43 DATA LAMPS SYSTEM

TEST RESULTS

The complete matrix was tested upon acceptance of the cinetheodolite. An open circuit was traced to the thumbwheel switches and corrected. Day-of-year information is not available from the Modular IRIG Timing Terminal (MITT) and no other provisions had been made for insertion of this information. Therefore, this portion of the matrix was not used during the cinetheodolite testing period except during the built-in sequential tests. No failures occurred during the entire pointing accuracy test period. However, on several of the test plates taken, the entire matrix appeared to be appreciably out of focus. Since it was always the entire matrix, this could not have been caused by the data lamp system itself. It could have been caused by motion between the fiber optic bundle termination mask and the remaining optics in the cinetheodolite or by motion of any of these remaining optical elements. This includes the plate camera. The exact cause was not pinpointed because the optical elements inside the cinetheodolite are accessible only by major disassembly of the cinetheodolite and because a different data matrix recording system was procured for use in production cinetheodolites.

DEFICIENCIES

The data lamp system has been the most reliable portion of the entire cinetheodolite electronics. None of the FX-31 flashlamps have failed, nor has any other component of the system failed. However, the mass and volume of the assembly is excessive. Therefore, a new data recorder assembly was procured under Contract DAAD07 [illegible]7-C-0265 from Adtrol Electronics, Inc. This assembly consists of a recording head small enough for installation in the camera between the shutter and the film plane, and a recorder that weighs 30 pounds and requires only seven inches of panel space in a standard 19-inch cabinet.

Since procurement of a new camera was cancelled because of planned redesign of the cinetheodolite data train, the new data recorder assembly was acceptance tested but not installed in a WSMR Cinetheodolite camera. Day-of-year switches must be provided in the production system unless the MITT is modified to furnish this information.

MODULAR IRIG TIMING TERMINAL

BACKGROUND

Cinetheodolite data requirements include the highly accurate time tagging of each data sample with the time of day. The types of timing error that can contribute significantly to WSMR Cinetheodolite error are (1) the dial flash error (E_1), which is the discrepancy between t_d, dial flash or command pulse time, and t_r, range time, (2) phasing or synchronization error (E_2) (if a synchronous camera system is employed), which is the difference between the time t_s, the time midpoint of the shutter exposure and t_d, the time of the command; (3) shutter progression error (E_3) equal to $t_x - t_s$, where t_x is the time of the target image exposure by a rotating disk type shutter; and (4) the error due to the finite travel time of light from the target to the cinetheodolite.

Consideration of timing terminal requirements for field operation of the WSMR Cinetheodolite system indicates the need for a high degree of accuracy for t_d. Limiting timing error contribution to that producing a pointing error of 0.5 arc-second for high-performance missiles would require the recording of t_r with an accuracy of $\pm$25 microseconds. (Thus, if multistation asynchronous photographic recording is adopted for the WSMR Cinetheodolite system, a least significant timing bit of 25 microseconds or less will be required.) A multistation synchronous system will require a camera control system capable of synchronizing all WSMR Cinetheodolite shutter midpoint openings to $\pm$80 microseconds or less with a timing resolution for the recorded t_d of only 20 milliseconds. The rationale for these tolerances is given in the section titled "Camera System."

Because the test and evaluation described in this report involved only one instrument, no attempt was made to meet the timing requirements for multistation operation. Dynamic pointing accuracy tests of the instrument required no time recording, and static or star test timing accuracy and resolution requirements did not exceed 1 millisecond. These requirements were met by the Modular IRIG Timing Terminal (MITT).

CONFIGURATION AND THEORY OF OPERATION

The MITT selected for use with the WSMR Cinetheodolite is a Model 6420-813 Time Code Translator/Generator produced by Astrodata. It occupies 14 inches of rack space in one of the test complex electronics cabinets and is illustrated in Figure 44.

The MITT may be operated as a time code generator from an internal frequency standard. The time of day may be preset and the generator may be synchronized to an external reference source. A display is provided to

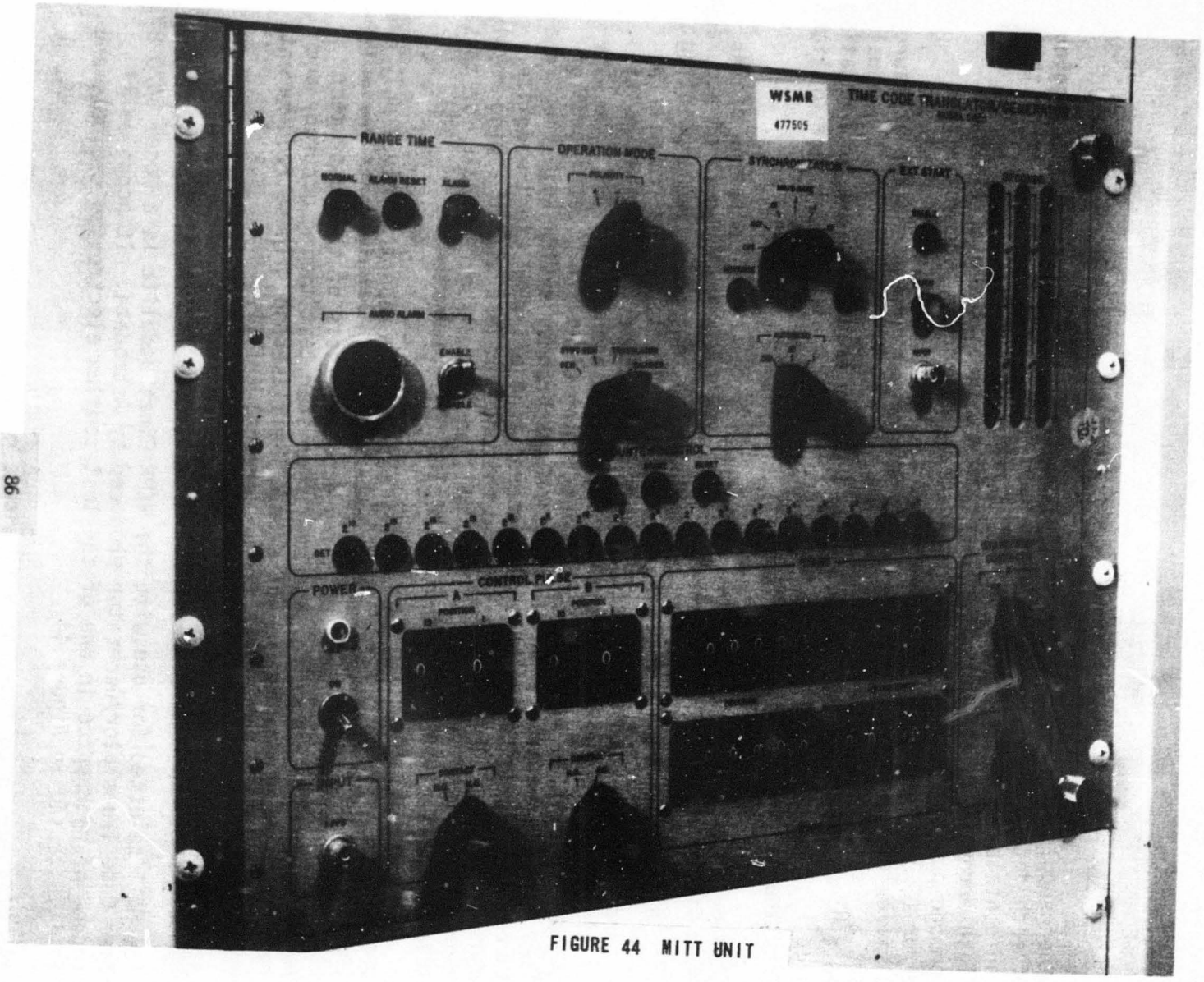

FIGURE 44 MITT UNIT

read out the generator time in seconds. The generator outputs are serial, parallel and serial-parallel time code; nine independent pulse trains; seven pulse rates; and two sets of control pulses.

The MITT will also accept modulated IRIG B range time code signals and automatically synchronize the time code generator with the input code. Should the input signal fail, the generator will continue to accrue time from the last value to which it was synchronized.

All output signals are simultaneously generated in precise synchronization with the input time code. An additional operating mode permits the translator to accrue time, using the carrier frequency of the input time code as a clock source (see Figure 45).

The MITT can perform either as a translator of received timing information or independently as a generator. Normally, the unit functions as a translator. However, when the input signal is lost or not available, the unit automatically changes its function to that of a generator.

As a translator, the unit extracts the straight binary time of day in seconds from the received IRIG B code, synchronizes an internal clock to the code signal and displays the time of day, thus derived, in straight binary. The following outputs are made available: a variety of pulse rates, outputs from 10-bit milliseconds and 17-bit seconds shift registers, and control pulses generated when a binary "1" exists at preselected index counts of the received code. The information is shifted into and out of the shift registers upon the reception of external commands.

Each IRIG code produces a position-identifier marker before each group of ten elements of its time code and at the beginning of a time frame. Only where two time frames join, do two position-identifier markers follow in succession. This condition constitutes a "reference marker" and is used to condition circuits for the synchronization of the internal clock with the received timing code during normal operation.

Once synchronization between the internal clock and the received timing code is achieved, the display and all outputs essentially represent the time of day generated by the internal clock. However, although the received timing information is supplementary at this time, this information continues to be jammed (side-loaded serially) into the counter that is used as the display. Simultaneously, the internal clock is being fed as a trigger to the same counter. Thus, this counter stores the accurate time of day as represented by the received timing code and the internal clock.

A visual and audio alarm is available to denote a loss of range timing input. This alarm prevents synchronization of the received timing information from occurring while the alarm condition exists. The counter that is used as the display continues to be updated by the internal clock during an alarm condition. Therefore, the unit is operating as a generator.

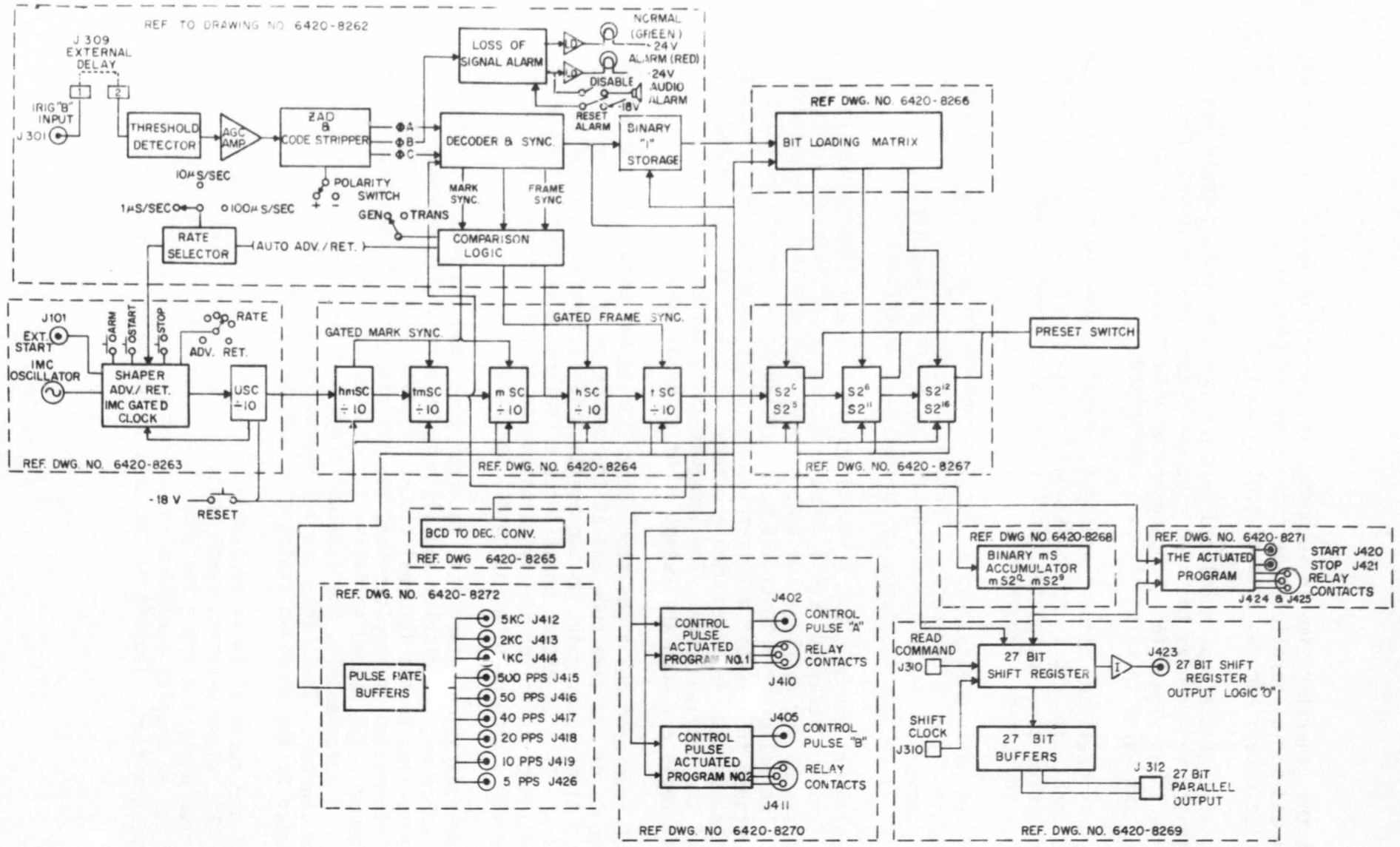

FIGURE 45. CODE TRANSLATOR SYSTEM

While received information is not present, the control pulse outputs are not available at the output connectors. Furthermore, the alarm condition must be manually reset before the received information can again be used to update the displayed time.

Should the received information not be re-established, the display can be manually reset to zero and the unit used as an elapsed time indicator. The display will then update from zero in one-second increments. Regardless the mode of operation, the outputs that are made available from the unit are derived from combinations of signals. These signals originate from the internal clock, the counter used as a display and decimal conversions of the count in the internal clock.

TEST RESULTS

The primary of the code input transformer on the AGC and Code Stripper card opened. The card was replaced and the replacement failed shortly thereafter. Since these failures occurred during a period of general thunderstorm activity at the range, it was believed to be caused by excess energy on the range timing lines. The practice of disconnecting the range timing input except during operation was adopted and no further trouble occurred.

The output of all clock pulsers is obtained from centertapped transformer secondaries which are referenced to the -18 volt supply instead of ground. This allows choice of output polarity. However, any ground of either conductor of the coaxial output produces a short circuit which results in component failure. The output signals must be coupled to interfacing equipment by means of input transformers with isolated primaries, or both conductors must be decoupled capacitively. Since the outer conductor of coaxial cables is normally grounded for shielding purposes, and since electronic equipment input circuits are usually ground referenced, this equipment contains a safety hazard for the operator and a reliability hazard to output electronics. These outputs should be ground referenced even if that requires separate connectors for each output polarity; or, at least, a warning should be printed on the equipment adjacent to such connectors as are not ground referenced. Several failures were caused by inadvertent grounding of some of these outputs during interface of the test complex with the cinetheodolite and during operational use of the equipment. No major problems were uncovered during the pointing accuracy tests but amplitude fluctuations of the range timing input signal occasionally required code stripper adjustments. The day of the year is not available and the time of day in microseconds is not an output of this MITT.

DEFICIENCIES

The following deficiencies exist.

1. Day of year is not available.

2. Time of day in microseconds is not available, but this would constitute a deficiency only if required for future WSMR Cinetheodolite production units operating in an asynchronous mode.

3. Some BNC coaxial connectors on the available outputs are ground referenced while others are returned to -18 volts, and no warning of this condition is given on the MITT or in the Operation and Maintenance Manual.

4. AGC of the timing code input signal is too limited for consistent reliable operation of the unit as a translator.

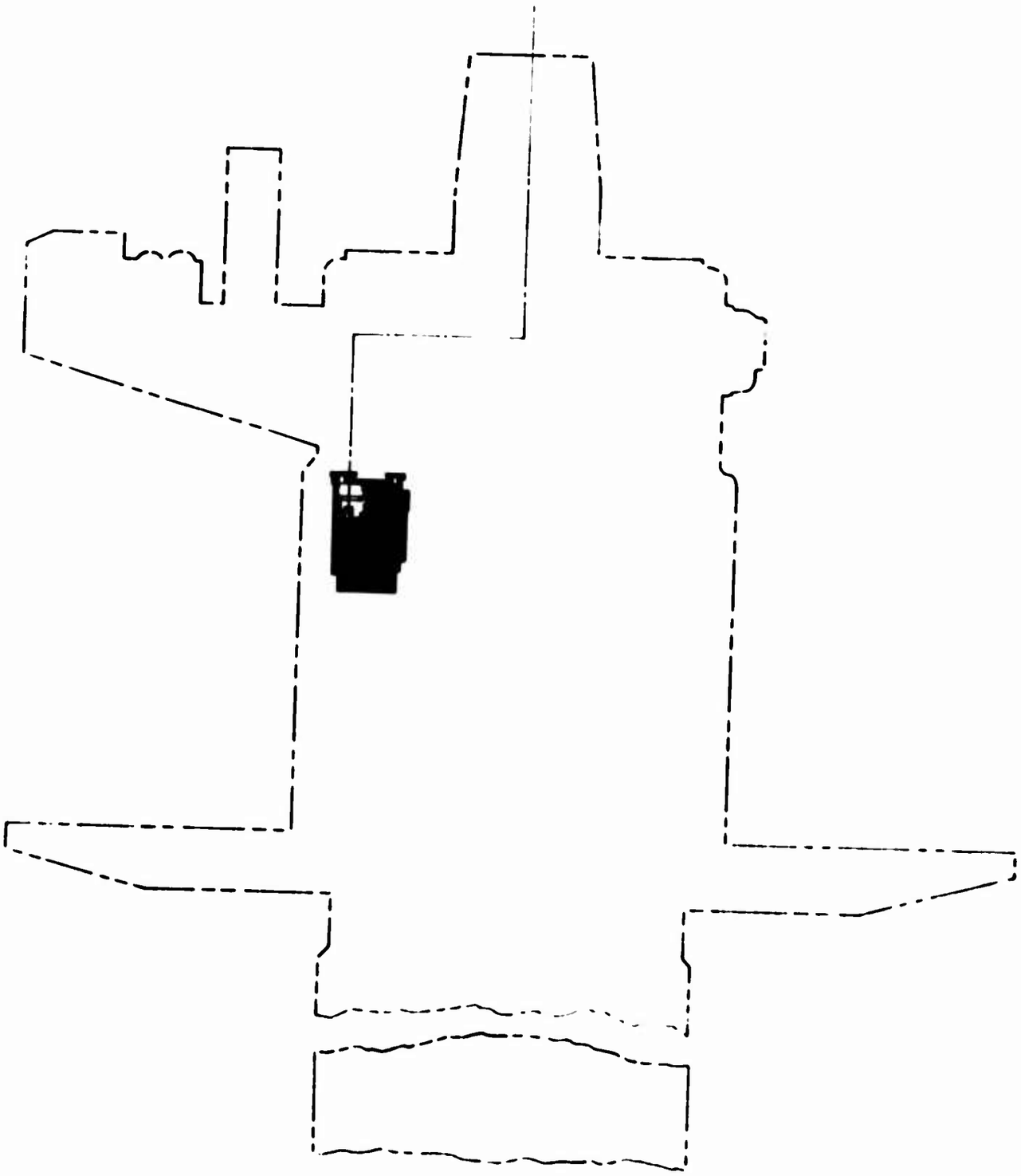

CAMERA
91

CAMERA SYSTEM

BACKGROUND

The camera developed for use in the WSMR Cinetheodolite employed a conventional pin-registered eight-hole, intermittent pull down, 35-mm film transport. Because the dial and fiducial images are divorced from mechanical errors by the optical compensation technique, pin registration would at first appear unnecessary. Pin registration was employed for two reasons: (1) to provide a positive stop of the film during the exposure period, and (2) to reduce the search area required in the automatic film reading process. Manual film reading techniques would not benefit substantially from registration of 35-mm film to better than ±0.002 inch. It is possible that other registration systems could also meet the registration requirements for automatic reading. Control of exposure, near the film plane, is provided by a conventional rotating-disc shutter assembly. Because simultaneous exposure of all dial and fiducial images is required, the minimum opening of any of the three 6.5-inch-diameter shutter discs is 45 degrees. This greatly limits the range of permissible exposures. For the lower frame rates, exposure time is excessive for most range applications; e.g., at five frames per second exposure time may be varied from 1/80 to 1/160 second, while, in many instances, 1/1000 second is desired and more than 1/250 second completely unacceptable. Conversely, lighting conditions at WSMR will often dictate an exposure of no less than 1/500 second; yet, the maximum permissible exposure at 50 frames per second is about 1/800 second. In the evaluation of the WSMR Cinetheodolite, little emphasis was placed on the camera testing because a cine camera was not used in the pointing accuracy tests. Instead, a special plate camera was developed for single frame exposures for use during the dynamic and static test program. It was also realized that the basic shutter design, limiting exposures for specific frame rates to small ranges, would be unacceptable for field use; consequently, little time was spent for testing or for the correction of other relatively minor camera deficiencies. It is quite clear that a different camera will be required in the production instrument However, some thought has been given to the design problems presented by the unique requirements of the WSMR Cinetheodolite: wide shutter aperture and short exposures at low frame rates. It may be that smaller, more efficient shutters can be located at other points in the optical data train and the main optical train. This would depend, of course, on the final configuration of the optical data train design. On the other hand, if the final data train design indicates a focal plane shutter, it may be that a pulsed shutter, combined with high and low speed capping shutters, will provide a wide range of exposures for each frame rate.

CONFIGURATION

The camera assembly consists of three basic parts: (1) a multidata camera, 35-mm, Model 208, Giannini Scientific, (2) a camera synchronization system, Model CS-52, Sequential Electronic Systems, and (3) a camera motor power supply. When in use, the camera is installed in the camera compartment of the cinetheodolite. The camera synchronization system and the camera motor power supply are installed in an electronics cabinet on the ground floor.

Camera

Figure 46 shows the camera complete with magazine and Figure 47 shows the camera film transport section. The camera consists of a main drive assembly, mounted in a case and driven by a dc motor. Attached to the case is a 1000-foot, double-reel magazine, with appropriate drive to insure proper film take-up and feed at all design speeds and conditions. The camera uses 35-mm film. Each frame, as referred to in this text, is a double frame, equal to two normal frames. The camera operates at film speeds of 5, 10, 20, and 50 double frames per second. A rotary switch on the operator's control panel controls the camera frame rate.

The camera shutter is seen in Figure 48. Two blades determine the shutter opening, which is variable from 45 to 90 degrees and is remotely controlled by a potentiometer on the control panel. A third shutter blade has a fixed 90-degree opening, and rotates at the rate of one revolution per frame, while the two variable blades rotate at four times per frame. This combination gives the exposure time listed in Table VI.

TABLE VI. EXPOSURE TIME VS. FRAME RATE

Frame Rate	Exposure Time
5 frames/sec	1/80 to 1/160 sec
10 frames/sec	1/160 to 1/320 sec
20 frames/sec	1/320 to 1/640 sec
50 frames/sec	1/800 to 1/1600 sec

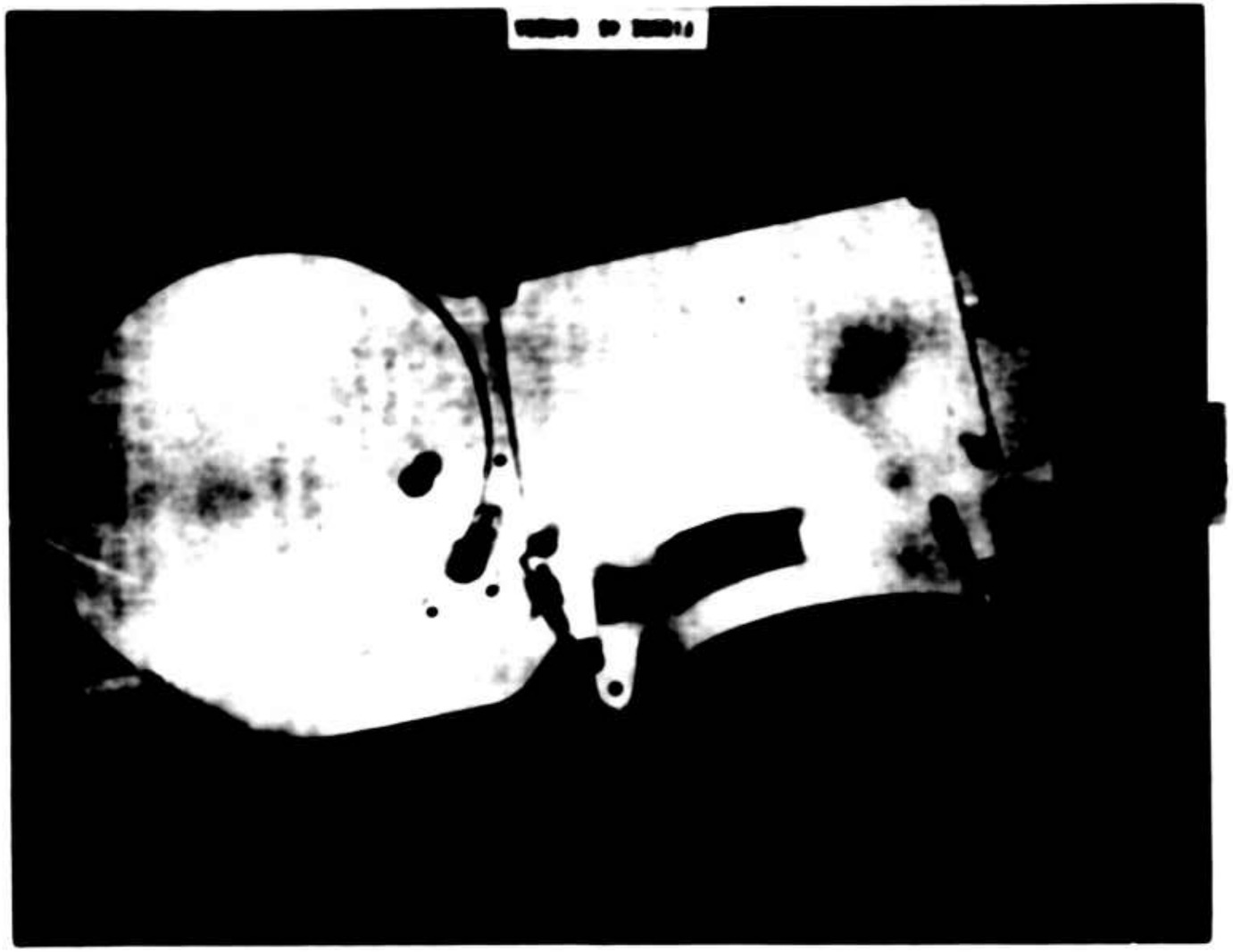

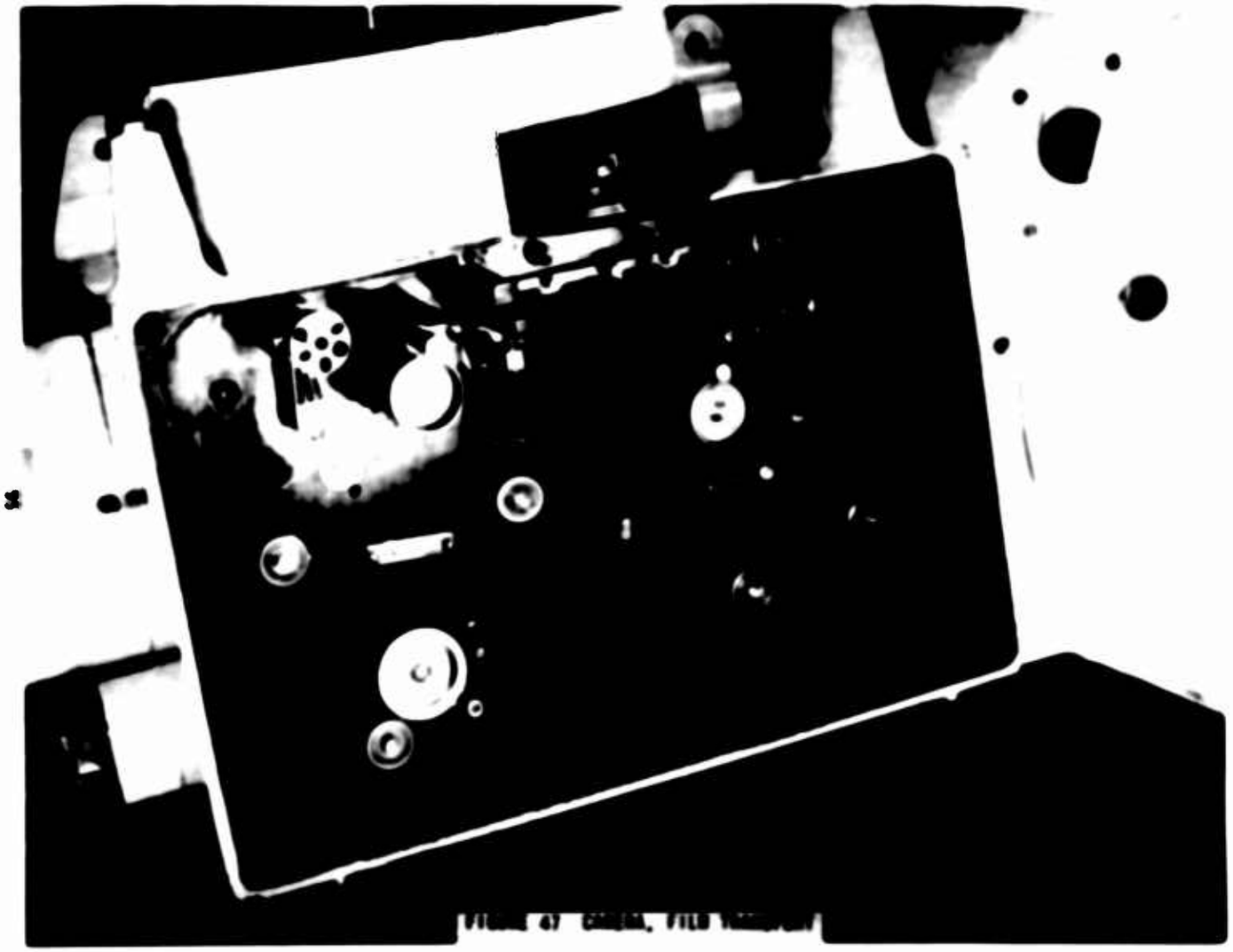

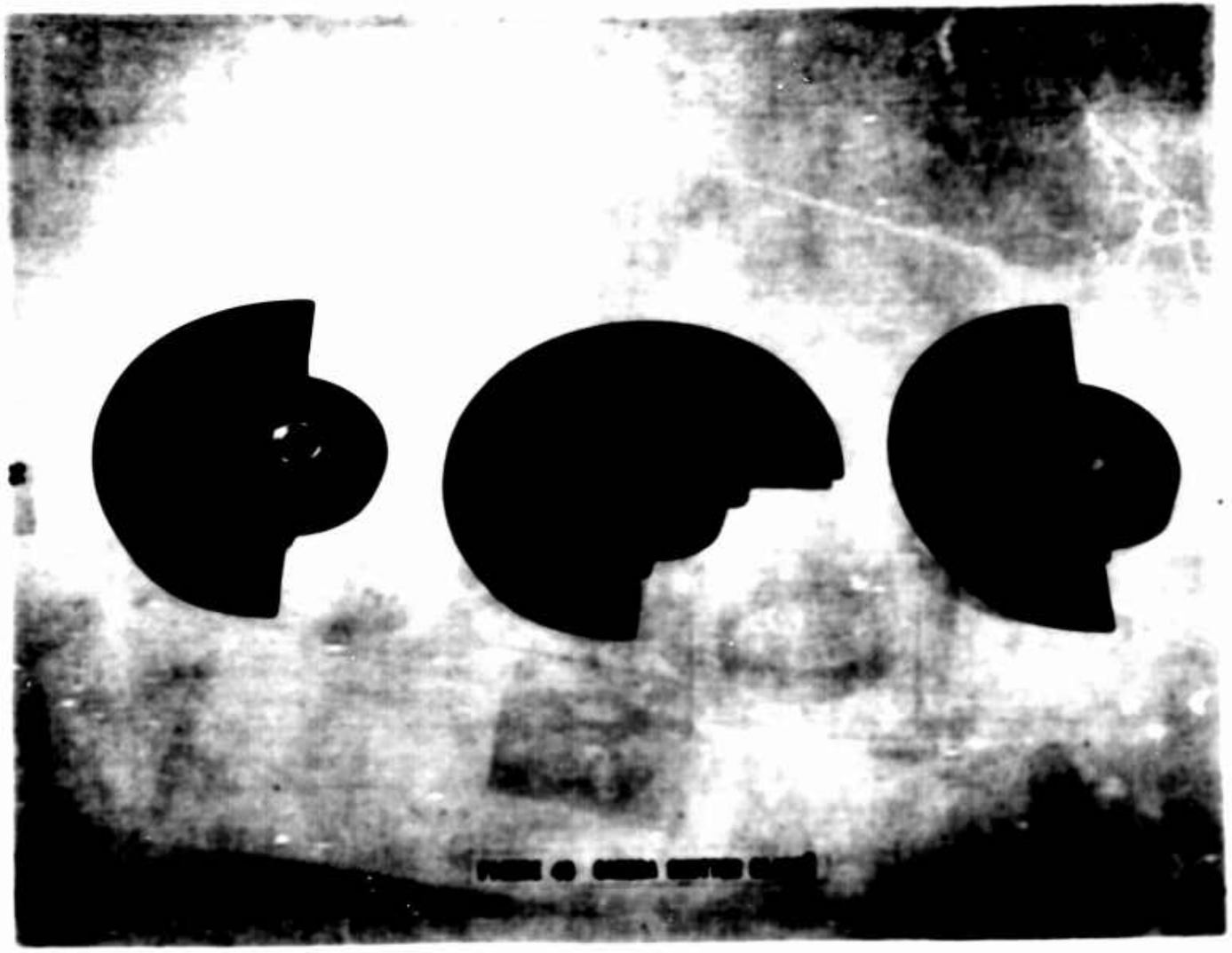

Camera Synchronization System

The camera synchronization system receives an external reference signal from the operator's main control unit. The reference signal is used by the synchronization system to achieve precise synchronization of the camera frame rate through exact speed and phase control of the motor drive mechanism. Other signal outputs from the camera synchronization system trigger the flashlamps and data lamps.

Camera Motor Power Supply

The camera motor power supply powers the film drive motor, the magazine motor (take-up), and the shutter motor. It is a solid-state, high-current, closely regulated, wide-range, variable-output supply. A particular feature of this supply is the use of silicon semiconductors for maximum stability, maximum protection against overloads and surges, and stable operation at elevated temperatures. An electronic current limiter with automatic recovery is included and excessive voltages are automatically removed from all semiconductors during abnormal operating conditions. The power supply output is isolated from the ac input, and dc outputs are ungrounded.

THEORY OF OPERATION

Camera

Interconnected with the film drive motor are two tone wheels. The first wheel has 100 teeth and the other wheel has one tooth, which produces an electrical output at the time midpoint of the shutter opening. The 100-teeth tone wheel is used to measure the velocity of the film drive motor, while the one-tooth tone wheel senses position. A film footage pulse is also interconnected with the camera drive motor. The tone wheels and the footage pulse outputs go to the camera synchronization system. The shutter aperture is controlled by a nulling relay and two potentiometers. The wiper of the first potentiometer, located on the shutter control panel of the main control units, is adjusted by the operator. The wiper of the second potentiometer is driven by the shutter motor. A 30-volt potential is across both potentiometers. When the operator makes a setting for the shutter aperture, the difference between the two wipers energizes the nulling relay, and supplies a driving voltage, of proper polarity, to the shutter motor. The shutter motor, while positioning the variable shutter blades for the proper opening, drives the wiper of the second potentiometer until the voltage picked off the two potentiometer wipers is equal. At this point, the relay opens and the shutter aperture is fixed.

Camera Synchronization System

The camera synchronization system, illustrated in Figure 49, consists of two subsystems: the reference indexing system, and the frequency/phase lock control system (FPL). The system achieves precise sychronization of camera frame rate with an external reference signal. The reference indexing system generates proper index reference signals for the FPL, and also adjusts the phase relationship between the reference signals and the camera feedback signals. Two magnetic pick-off tone wheels in the camera produce feedback outputs of 1 and of 100 pulses, respectively, per frame of film. This feedback contains the velocity and phase (position) information. The FPL provides ultra-precise speed and phase control of the motor drive mechanism.

TEST RESULTS

With the special plate camera the cinetheodolite camera assembly was not needed and has not been used since the original acceptance tests. During acceptance testing, the cinetheodolite camera could not be synchronized while accelerating to the chosen camera speed. In all cases synchronization was achieved only when decelerating to the chosen camera speed. Failure to synchronize when approached from the underspeed condition was evidently caused by time jitter in the tone wheel signals. Twist in the small diameter shutter shaft and backlash in the drive gearing, which includes two mechanical differentials, is believed to be responsible. The camera could not be driven above 50 frames per second when the test-run switch was in test position (not attempting to synchronize the camera). The film take-up motor could not handle a full reel of film at 50 frames per second unless the magazine film-tension adjustment was reduced excessively. An SCR in the film take-up motor control circuit failed during tests. It was replaced and no further failures occurred.

DEFICIENCIES

Multidata Camera

The following deficiencies exist: (1) film-drive torque is insufficient, (2) film take-up motor torque is insufficient, (3) shaft wind-up and gear backlash make synchronization difficult, and (4) exposure time is excessive at low frame rates.

Camera Synchronization System

Based upon its ability to synchronize the present camera with its deficiencies, it was concluded that the camera synchronization system was satisfactory. Detailed tests could not be conducted without considerable modification of the camera. As a result, the degree of synchronization permitted by the camera synchronization system was not determined. Regardless of whether or not a camera synchronization system is specified for

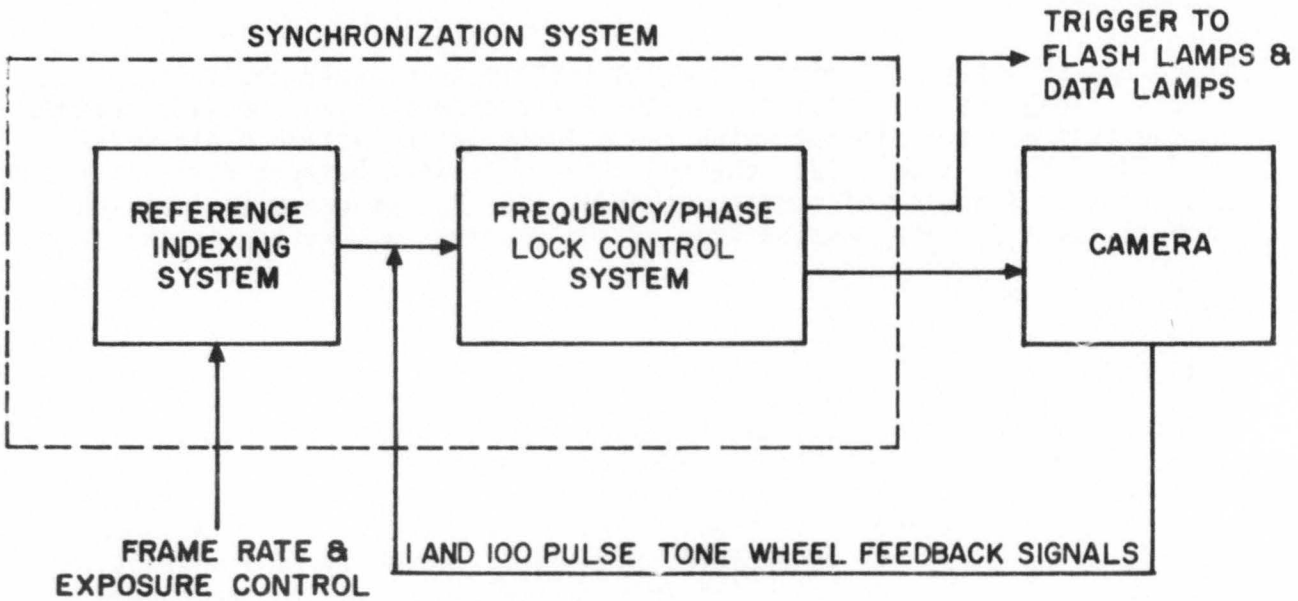

FIGURE 49 CAMERA CONTROL SYSTEM

the production model cinetheodolite, all sources of timing errors capable of producing a computer position error equivalent to a 0.5 arc-second pointing error will be considered.

DISCUSSION OF SHUTTER INDUCED ERRORS

The following discussion includes major sources of error, especially if the shutter system is a focal plane rotating disc type.

Timing Errors

Three types of system timing errors contribute to missile positional errors. They are (1) dial flash--the difference between the time recorded on the film and the time at which the azimuth and elevation dials were read (dial flash time), (2) phasing--the difference between dial flash time and the time midpoint of shutter opening, and (3) progression time--the time it takes for the leading edge of the shutter to move across the frame.

Position Errors

Dial Flash

Angular position error, E_1, caused by dial flash timing error, t_{err}, is directly proportional to missile angular velocity, V_m, at the camera station. That is, $E_1 = V_m \times t_{err}$, and $t_{err} = t_r - t_d$, where t_r is range time (exact time), and t_d is time of dial flash, i.e., time of azimuth and elevation data. As an example, the angular velocity of a missile at a range of 100,000 feet traveling in a course tangential to the camera at 10,000 feet per second is 5.7°/second (0.0205 arc-seconds/microsecond). If we assume this angular velocity and a permissible dial flash angular error of $\pm$0.5 arc-second, the maximum permissible dial flash timing error becomes

$$\frac{0.5}{0.0205} \approx 25 \text{ microseconds}.$$

Phasing

Angular position error, E_2, caused by phasing error, t_{err}, is a function of the rate of change of tracking corrections, dx/dt. That is, $E_2 = dx/dt \times t_{err}$ and $t_{err} = t_d - t_s$, where t_d is time of dial flash and t_s is shutter midpoint opening time. For example, from a study conducted by STEWS-DR-T, it was determined that the maximum dx/dt for Askania and Contraves cameras was 1.75°/sec (0.0063 arc-seconds/microsecond). If we assume this dx/dt and a permissible positional phasing error of 0.5 arc-seconds, the maximum permissible phasing error becomes

$$\frac{0.5}{0.0063} \approx 80 \text{ microseconds}.$$

Shutter Progression

Angular position error, E_3, caused by progression time of the shutter, t_{err}, is also a function of dx/dt. Shutter progression time can be obtained from the combination of shutter velocity and image location relative to frame center (midpoint of shutter opening time). It may be positive, negative or zero. $E_3 = dx/dt \times t_{err}$ and $t_{err} = t_x - t_s = (X_i - X_s)/(X_e - X_s) \times t_{exp}/2$, where t_x is time when shutter is at image position, t_s is time when shutter is at midpoint of frame exposure, X_i is image location on frame, X_s is frame center, X_e is frame edge, and t_{exp} is exposure time. If we assume this dx/dt, an exposure time of 1000 microseconds, and an image positioned at the edge of the frame, the amount of positional error due to shutter progression time becomes

$$\frac{0.0063 \text{ arc sec}}{\text{microsecond}} \times 500 \text{ microsecond} = 3.15 \text{ arc sec.}$$

CONCLUSIONS

If the exposure time were increased to 10 milliseconds, the maximum positional error due to progression time would be 31.5 arc-seconds. It can be seen from this that when rotating disc shutters are used with highly accurate cinetheodolites, progression errors must be removed or greatly reduced by suitable data reduction techniques. Increased accuracy requirements can be met by (1) modifying the MITT or its available outputs to obtain smaller increments of time than the presently available milliseconds, and utilization of spare data matrix positions to record these time increments or, (2) modifying the camera system to insure that synchronization occurs only at MITT millisecond time or within 80 microseconds thereafter. Modification of the MITT or its available outputs is preferred because it can be accomplished more economically and such modification would obviate the need for a precise camera synchronization system.

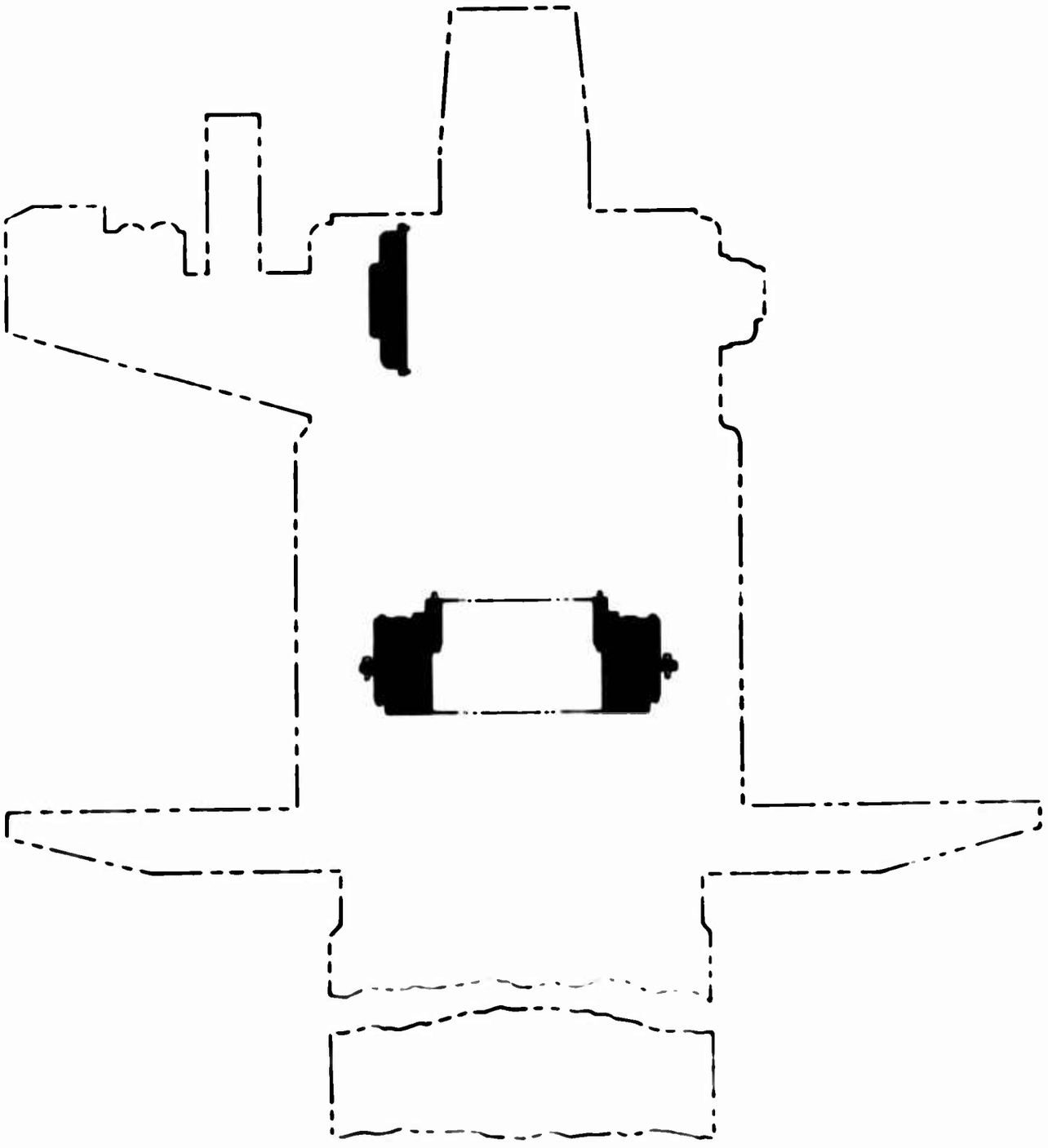

INSTRUMENT DRIVE SERVO

SERVO DRIVE SYSTEMS

CONFIGURATION

The elevation and the azimuth servo drive systems include the components listed in Table VII, and the annular platform servo drive system includes the components listed in Table VIII.

The preamplifiers, power amplifiers and power supplies are located in the K&E electronics cabinets at the ground level. The Inland motor generator for the annular platform is located outside the facility and the torque motors, tachometers and synchro transmitters are located in the equipment.

THEORY OF OPERATION

The azimuth and the elevation servo drive systems operate in either of two basic modes (reference Figures 50 and 51). They are velocity servos in LOCAL, operating from signals furnished by the manually controlled stiff stick; they are positional servos in REMOTE, operating from signals furnished by the analog comparator. The comparator output is proportional to the difference between the position commanded by the test complex electronics and the cinetheodolite position as determined by the servo repeater.

The annular platform drive system is a positional servo at all times. Its command input is the azimuth tachometer output. It obtains rate feedback from its own tachometers and positional feedback from the mechanically actuated follower potentiometer in the synchronizer assembly.

In LOCAL control the operator sits at the main control unit on the annular platform. While observing the target in motion through the tracking telescope, he controls the stiff stick to keep the target centered in the field of view. Since the main telescope and the tracking telescope are on the same axis, they move together in azimuth and elevation, and the operator thereby keeps the target in the field of view of the main telescope. The stiff stick signals feed the elevation and azimuth servo loops, each consisting of two preamplifiers, a power amplifier and a servomotor tachometer. The tachometers send rate feedback to the first preamplifiers. The limit potentiometers feed the second preamplifiers to provide rotational limits in elevation and azimuth. The azimuth tachometer output is also used as the command signal to the annular platform servo loop. This loop consists of a single preamplifier, a medium power amplifier, a motor-generator, and the two servo motor-tachometers which drive the annular platform. The tachometers furnish rate feedback to the preamplifier. An electro-mechanical assembly called the synchronizer maintains synchronized rotation of the annular platform and azimuth sections. A lag or overshoot of the annular platform causes the mechanically actuated follower

TABLE VII. AZIMUTH AND ELEVATION SERVO COMPONENTS

Function	Elevation	Azimuth
Preamplifiers	Analog 203 (2 ea)	Analog 203 (2 ea)
Power Amplifiers	Westamp A499-1 (500 W)	Westamp A499-1 (1000 W)
Power Supply	Technipower R40.0-25.0	Technipower R80.0-25.0
Torque Motor	Inland T10050A (35 lb-ft)	Inland TT24001 (500 lb-ft)
Synchro Transmitters	1X, 16X, 36X (1 ea)	1X, 16X, 36X (1 ea)

TABLE VIII. ANNULAR PLATFORM SERVO COMPONENTS

Preamplifiers	Reeves
Power Amplifier	Dynatron 1833-AN-060R1 (100 W)
Motor-Generator	Inland MG 5114A
Servo Motors	Diehl FD 84-31-1 0.6 hp max (2 ea)
Tachometers	Diehl FDE 41-35-1 (2 ea)
Field Power Supply	Reeves 100 V 2 A

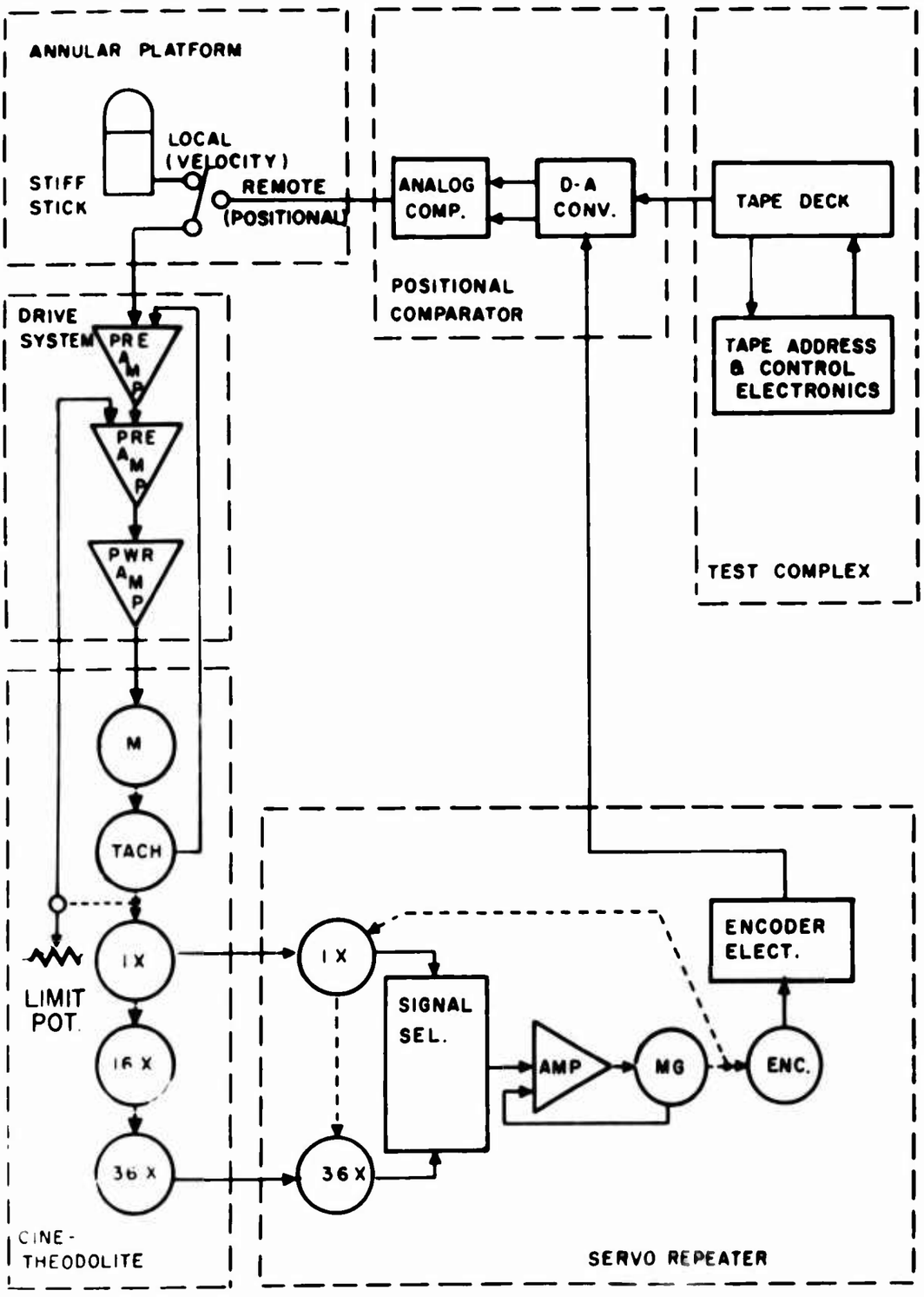

FIG. 50 ELEVATION SERVO SYSTEM

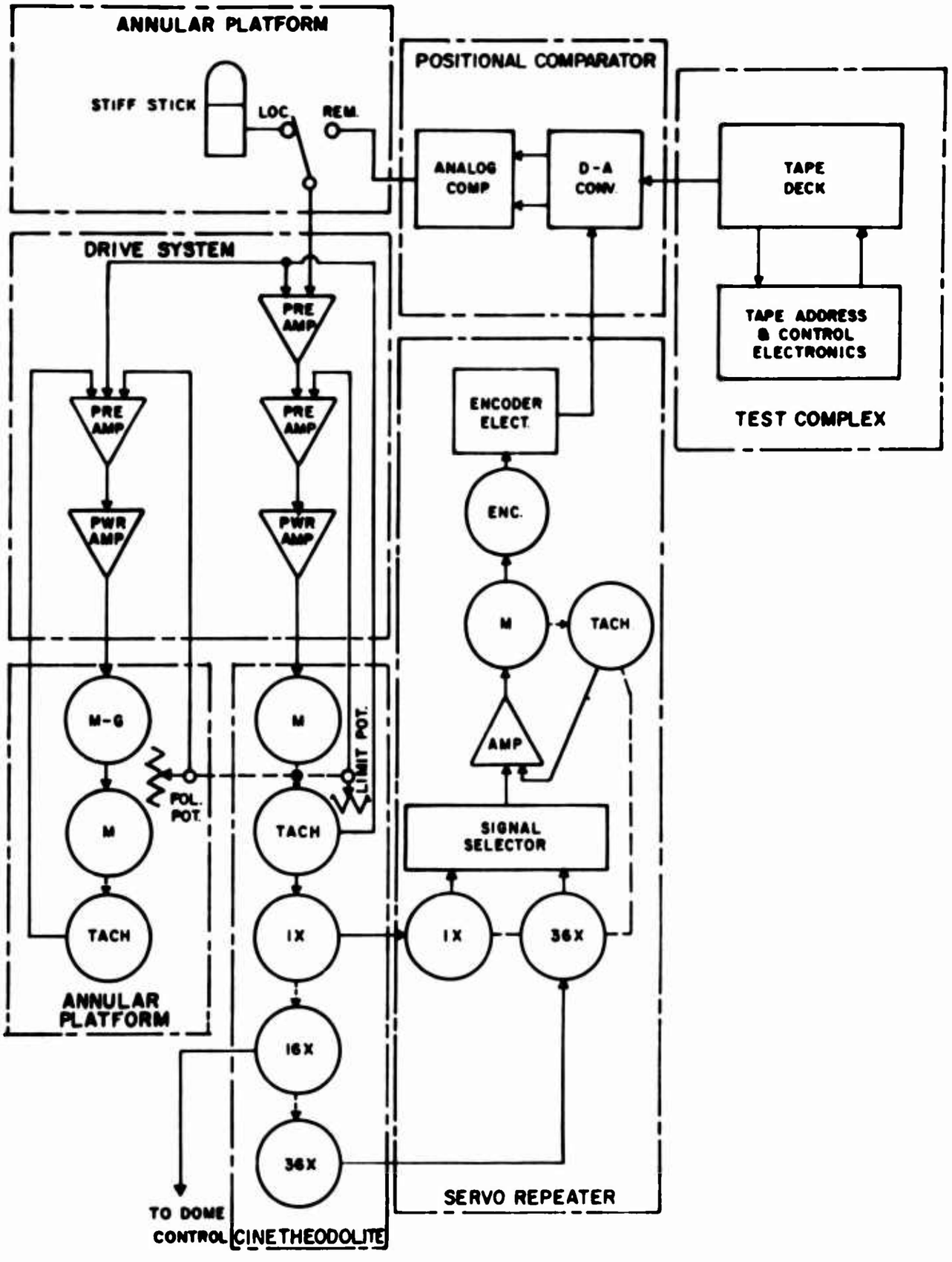

FIGURE 51 AZIMUTH/ANNULAR PLATFORM SERVO SYSTEMS

potentiometer to send a correction signal to the preamplifier of the annular platform servo loop. The amplitude and polarity of this signal is controlled by the magnitude and direction of the follower error. A tongue-and-groove bracket, the tongue portion mounted on the cinetheodolite and the bracket portion on the annular platform, actuates the potentiometer and should drag the annular platform with the azimuth section if the platform drive signal fails.

In addition to the limit potentiometers, there are mechanically actuated end-point limit switches which remove power amplifier inputs when actuated. As a final safety device to protect the main telescope, the elevation section has two hydraulic pistons, one at each end-point.

TEST RESULTS

Preliminary Tests of Annular Platform

Preliminary tests of the annular platform servo drive were conducted in January 1966[5]. Weights were placed on the platform to simulate operational conditions and open-loop tests were conducted. Results were as follows:

Maximum Velocity = 46° per second.

Acceleration from 0° to 30°/sec in less than 1/5 second.

The acceleration was more than double the requirements and the velocity exceeded the requirements by approximately 15%. It was not known how much change would be caused by the closed loop condition. Since the cinetheodolite was not scheduled for delivery until the spring of 1967, a follower pot simulator was designed and fabricated to facilitate closed loop tests before delivery. Closed loop tests were then conducted with the following results[6].

Angular acceleration for the first half-second from rest = 66°/sec .

Tracking error 0.42° maximum.

Pointing Accuracy Tests

The original dynamic pointing accuracy test plan utilized a special magnetic tape containing the required horizontal and vertical positions, velocities and accelerations. This plan was changed because of inherent time delay in the servo repeater and several drive system deficiencies.

The drive system was modified to meet the minimum requirements of the new dynamic test plan[7]. Several factors contributed to the need for modification of the servo drive systems:

1. Servo system compensation was inadequate.

2. Preamplifiers drifted excessively.

3. Three preamplifiers failed.

4. Three Westamp power amplifiers failed.

5. Power supplies for azimuth and elevation power amplifiers failed.

6. Power supply for annular platform servo motor fields failed.

7. Annular platform 100-watt amplifier drifted excessively and failed for lack of protection from inductive load transients.

Drive system rework included the following.

1. Replacement of failed preamplfiers and minimum redesign of entire preamplifier assembly.

2. Minimum recompensation of all three servo loops to meet test requirements.

3. Replacement of the failed Westamp power amplifiers with same type.

4. Replacement of the azimuth and elevation power supplies.

5. Replacement of the annular ring motor field power supply.

6. Repair and modification of the annular platform 100-watt amplifier.

Velocity servo tests were conducted on both the azimuth and elevation servo systems with the instrument as configured. Velocity servo tests of the annular platform were conducted by nulling the positional feedback signal from the follower potentiometer and mechanically disconnecting the potentiometer wiper. In addition, the rubber bumpers on the synchronizer assembly were removed during the tests to allow more platform motion relative to the cinetheodolite azimuth axis. Figure 52 shows an appreciable deadband in all three servo loops, with the annular platform deadband excessive.

Figure 53 shows gain and phase angle versus frequency for all three loops. It was plotted from data recorded during these tests. The cinetheodolite azimuth and elevation servo loop response was down less than 3 dB at 60 radians/sec with a phase angle lag of less than 40°. The response of the annular platform servo loop follows in Table IX.

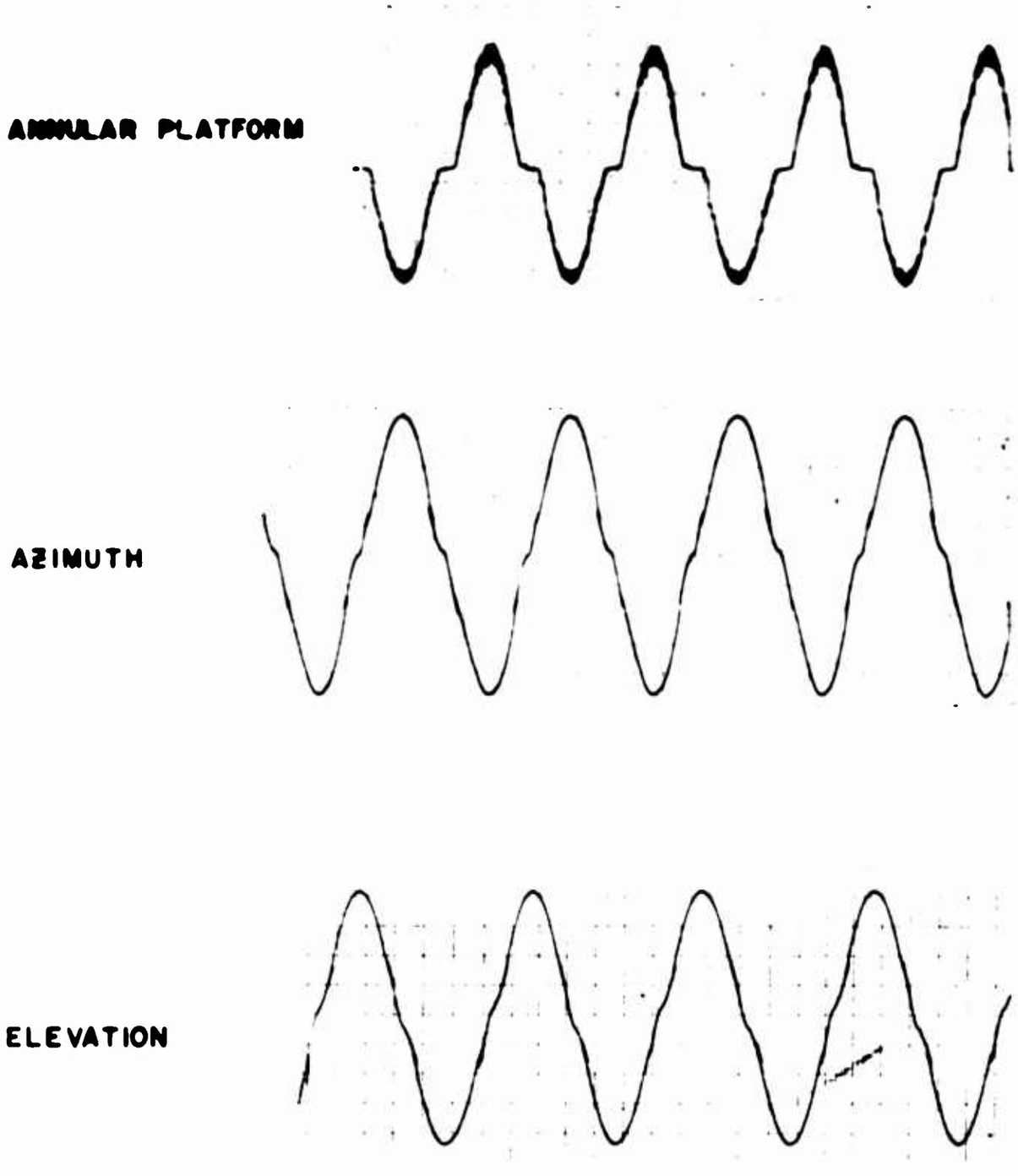

FIG. 52 SERVO LOOP DEADBANDS

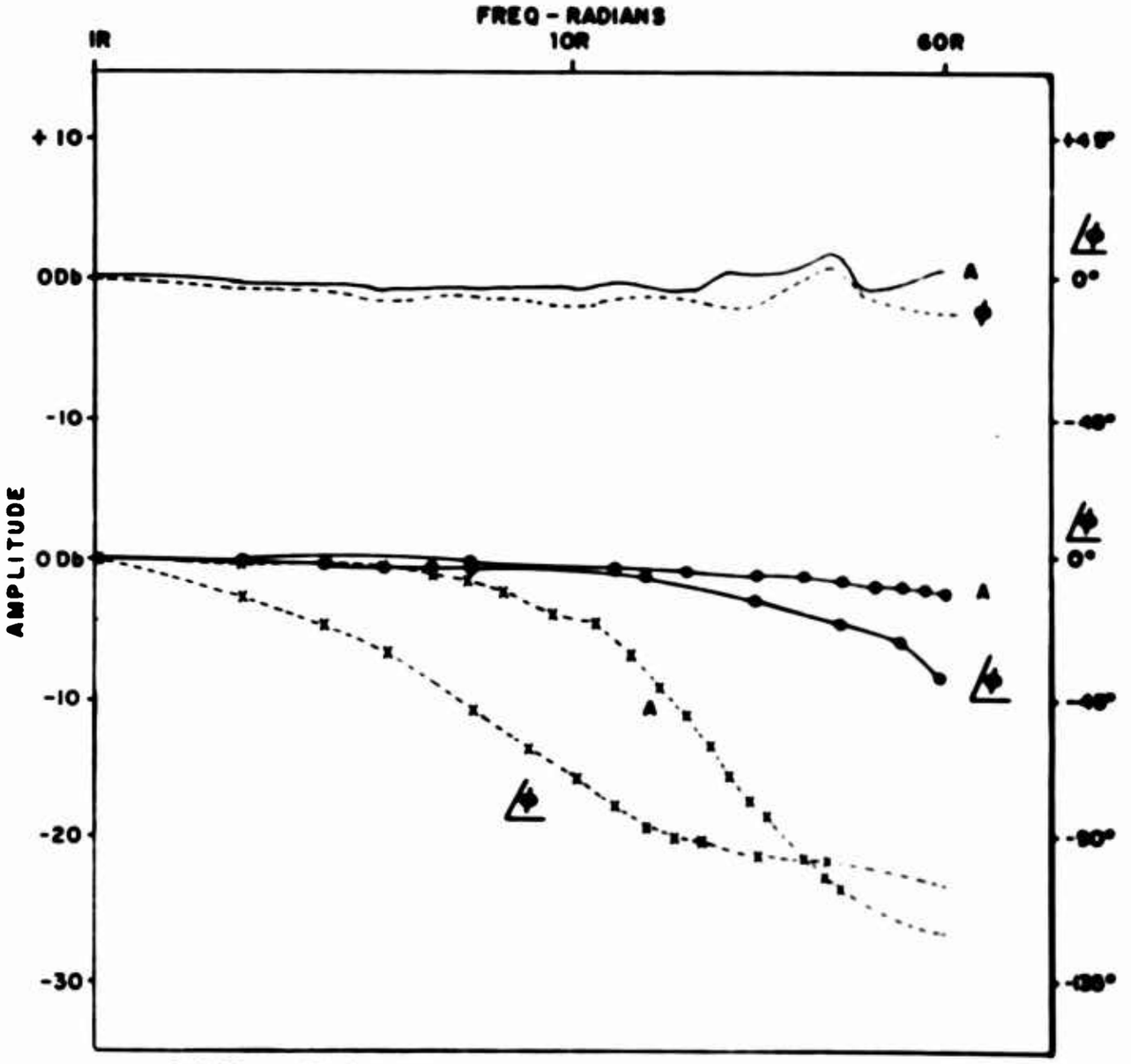

FIGURE 53 SERVO SYSTEMS RESPONSE

TABLE II. ANNULAR PLATFORM LOOP RESPONSE

Frequency	Amplitude	Phase Angle
8 radians/sec	-3 dB	-60°
12 radians/sec	-6 dB	-80°
18 radians/sec	-12 dB	-90°

The extreme response difference between the cinetheodolite azimuth servo and the annular platform servo precludes proper tracking of these two loops over any but a limited range of acceleration and velocity.

Since no attempts were made to optimize system tracking capabilities, only limited tracking tests were conducted. These tests indicate that with proper compensation the azimuth and elevation drive systems are capable of velocities as low as sidereal rate and as high as 40°/sec in azimuth and 50°/sec in elevation, and of accelerations of 30°/sec^2 in azimuth and 50°/sec^2 in elevation. The annular platform servo is unsatisfactory.

DEFICIENCIES

Manual tracking control must be very smooth because of the small field of view of the main telescope. Since the operator's chair is mounted on the platform, even small sudden motions between the platform and the cinetheodolite cannot be tolerated. This need for the platform to follow the cinetheodolite without any sudden lag or overshoot, at all cinetheodolite azimuth accelerations and velocities, imposes severe requirements upon the annular platform servo system. The inertia of the platform and the torque requirements of the platform servo greatly exceed those of the cinetheodolite. The control signal sent to the azimuth loop should also be sent to the annular platform loop, since both are to respond equally and at the same time. At present, the system with greatest inertia is informed last, yet expected to follow with minimum lag.

The following deficiencies still exist.

1. Elevation loop drifts.

2. Azimuth loop drifts.

3. Compensation is inadequate (all loops).

4. Crossfeed signal path exists from annular platform loop to the azimuth servo loop input.

5. Annular platform does not smoothly follow cinetheodolite at all accelerations and velocities.

6. Azimuth and elevation servo performance is limited by power rating of power amplifiers.

7. Three speed synchro and servo repeater combination is slow. It should be replaced by 15-bit shaft angle encoder systems. Several other deficiencies were corrected by replacements as detailed in "Test Results."

POSITIONAL SERVO REQUIREMENTS

Whenever the cinetheodolite servo drive systems operate in REMOTE, they are positional servos. At the time of the original WSMR Cinetheodolite contract, digital positional systems had not yet attained widespread use. As a result, the prototype cinetheodolite design utilized a multi-speed synchro system. This decision contributed several deficiencies which prevented comprehensive tracking rate tests on the instrument.

The synchro positional data must be converted to a more usable form. The purpose of the servo repeater is to convert synchro azimuth and elevation data to digital data.

A positional servo uses the difference between the commanded and present positions as its input signal. This comparison may be made while both sets of data are still digital or after they have been converted to analog voltages. Digital comparators require much more equipment, so an analog comparator was fabricated and used with the WSMR Cinetheodolite.

Digital commanded and present position azimuth and elevation signals are converted to analog signals by the four-channel D-to-A converter. The differences between the commanded and present position are then obtained from the analog comparator. The amplitude and polarity of the comparator outputs are proportional to the magnitude and direction of the positional difference. These voltages are the inputs to the azimuth and elevation servo systems. The servos drive to null these signals, thus positioning the cinetheodolite to the commanded azimuth and elevation.

SERVO REPEATER

Configuration

The servo repeater (SR) consists of a two-channel synchro-to-digital converter. One channel converts cinetheodolite azimuth attitude from two-speed synchro data into a 15-bit binary word. The other channel converts the elevation data. Each channel consists of 1X and 36X synchro receivers, a precision gearbox, an ac servo motor, a 15-bit encoder, servo electronics and encoder logic. The components are contained in a single rack-mounted chassis, seen in Figure 54, which is installed in a cabinet adjacent to the test complex electronics. A block diagram of the SR is shown in Figure 55.

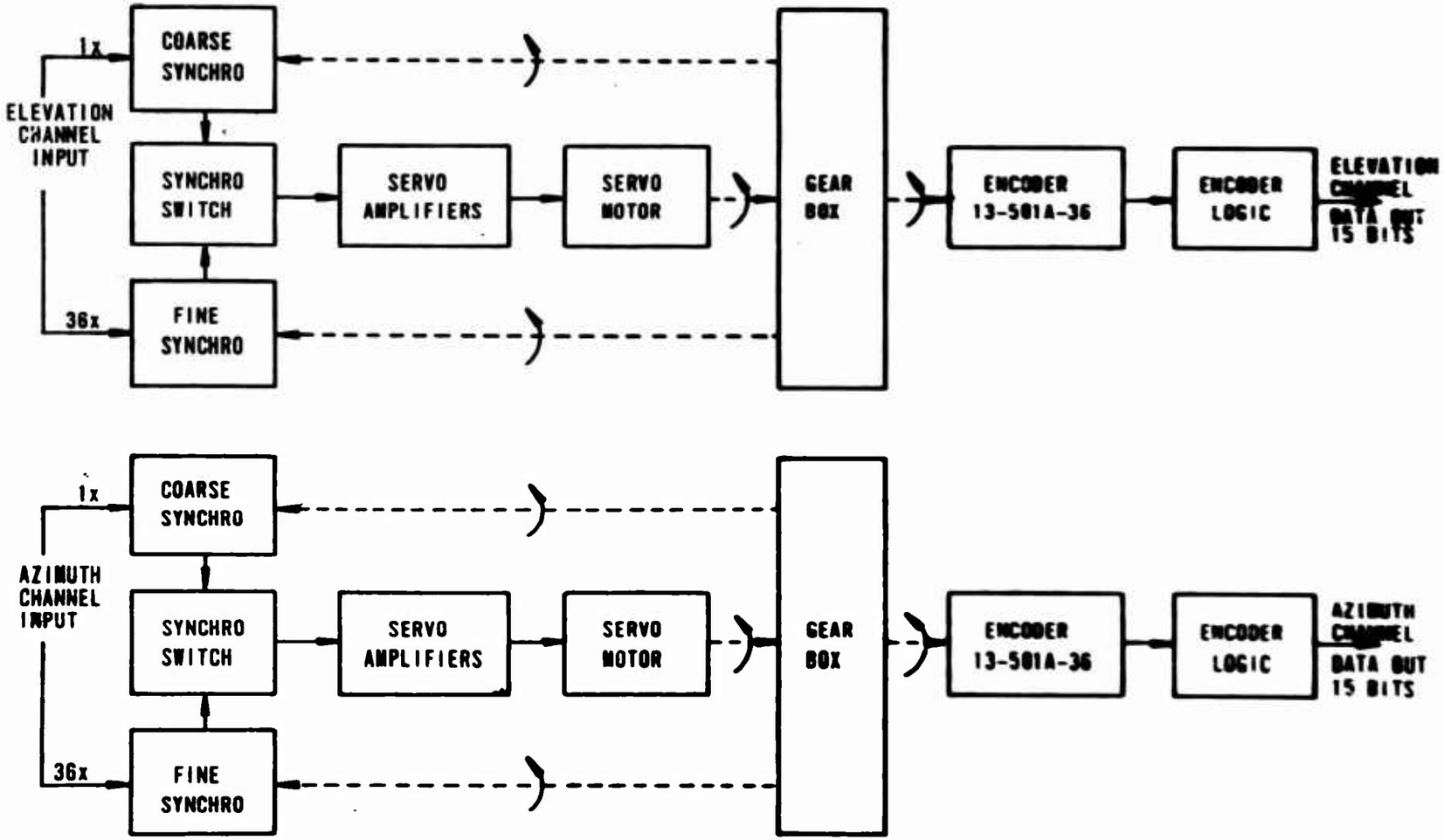

FIGURE 55 SERVO REPEATER, BLOCK DIAGRAM

The SR was subcontracted to Datex by K&E, the prime contractor, with the following specifications:

Output	15-bit pure binary, each axis
Accuracy	Static ±1 bit Dynamic ±8 bits at 30° per second

Theory of Operation

Each of the SR channels receives coarse (1X) and fine (36X) synchro signals that are applied to synchro receivers. The error signals, resulting from differences in the angular shaft positions between the rotors of the synchro receivers located in the servo repeater and the remote synchro transmitters located in the cinetheodolite, are applied to a switching circuit. The switching circuit determines whether coarse or fine error signals are applied to the amplifiers. In addition, a compensating (stick-off) voltage is added to the coarse error signal prior to the switching circuit.

The amplified error signal drives the servo motor. The servo motor drives a gear train which repositions the rotors of the synchro receivers to null the error signals. A Datex shaft position encoder is also coupled to the servo gear train in each channel, and generates output data in the form of voltage levels. Each encoder thus converts the angular shaft position of the input function to digital information. The digital data is processed by encoder logic circuits in each channel and is provided at the output of each channel of the SR as a 15-bit binary word.

Test Results

During static pointing accuracy tests on the cinetheodolite, the brush-type encoders caused erratic operation and were returned to the manufacturer for alignment and cleaning. No further failures occurred. While preparing the test complex for dynamic pointing accuracy tests, it was determined that the dynamic accuracy of the SR was much lower than required. The output lagged the cinetheodolite by more than twenty arc-minutes at 10 degrees per second velocity. This greatly exceeds the permissible lag. Since the cinetheodolite field of view is only 20 arc-minutes, the instrument could not be used as positional servo during the dynamic pointing accuracy tests.

No attempts were made at WSMR to determine the cause of this poor SR performance, and the SR was not returned to the manufacturer for several reasons.

1. Time schedules were tight.

2. The production cinetheodolites will probably contain shaft angle encoders instead of synchro transmitters, thus removing the need for a servo repeater.

3. An alternate method was devised to test the dynamic pointing accuracy of the cinetheodolite and this method required use of the SR for static position information.

The following deficiencies of the SR were discovered.

1. Dynamic accuracy is insufficient.

2. Brush encoders are undesirable because of maintenance problems.

DIGITAL-TO-ANALOG CONVERTER

Configuration

The digital-to-analog (D-to-A) converter system, seen in Figure 56, is essentially a 12-bit system which has been upgraded to a nominal 15-bit system. The three least significant bits were obtained by modifying off-the-shelf digital modules. The remaining 12 bits are converted to analog by a Model 854B2A-03B-2 D-to-A converter purchased from Texas Instruments. This unit was purchased as a two-channel device and a factory conversion to four channels was made later.

Theory of Operation

A conventional "switch and ladder network" D-to-A conversion method is used. Since this method is fully explained in technical literature, it will not be detailed here. The system converts the following four channels of digital data to analog form:

1. Cinetheodolite azimuth.

2. Cinetheodolite elevation.

3. Commanded azimuth.

4. Commanded elevation.

The input to each channel is angular data in 15-bit binary form. The output of each channel is a dc signal whose amplitude and polarity correspond to the angular magnitude and direction of the input.

Test Results

Consistent 14-bit accuracy was achieved in the overall system even though the converter system relies upon the stability and accuracy of the 12-bit D-to-A converter.

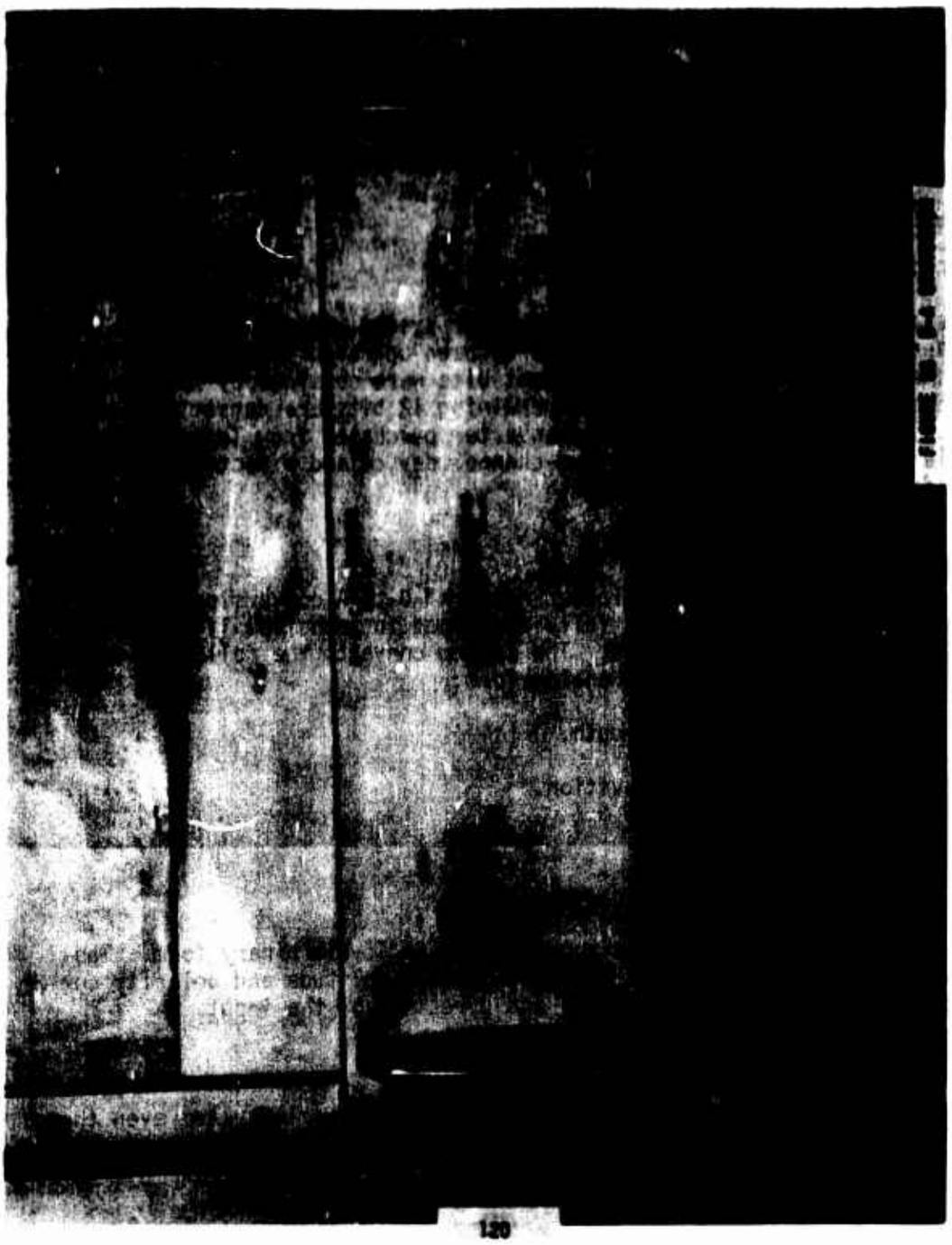

Several component failures occurred during interfacing and debugging of the test complex. Since no failures occurred during the entire pointing accuracy test period, it was assumed that the previous failures had been caused by improper interface conditions that were subsequently rectified.

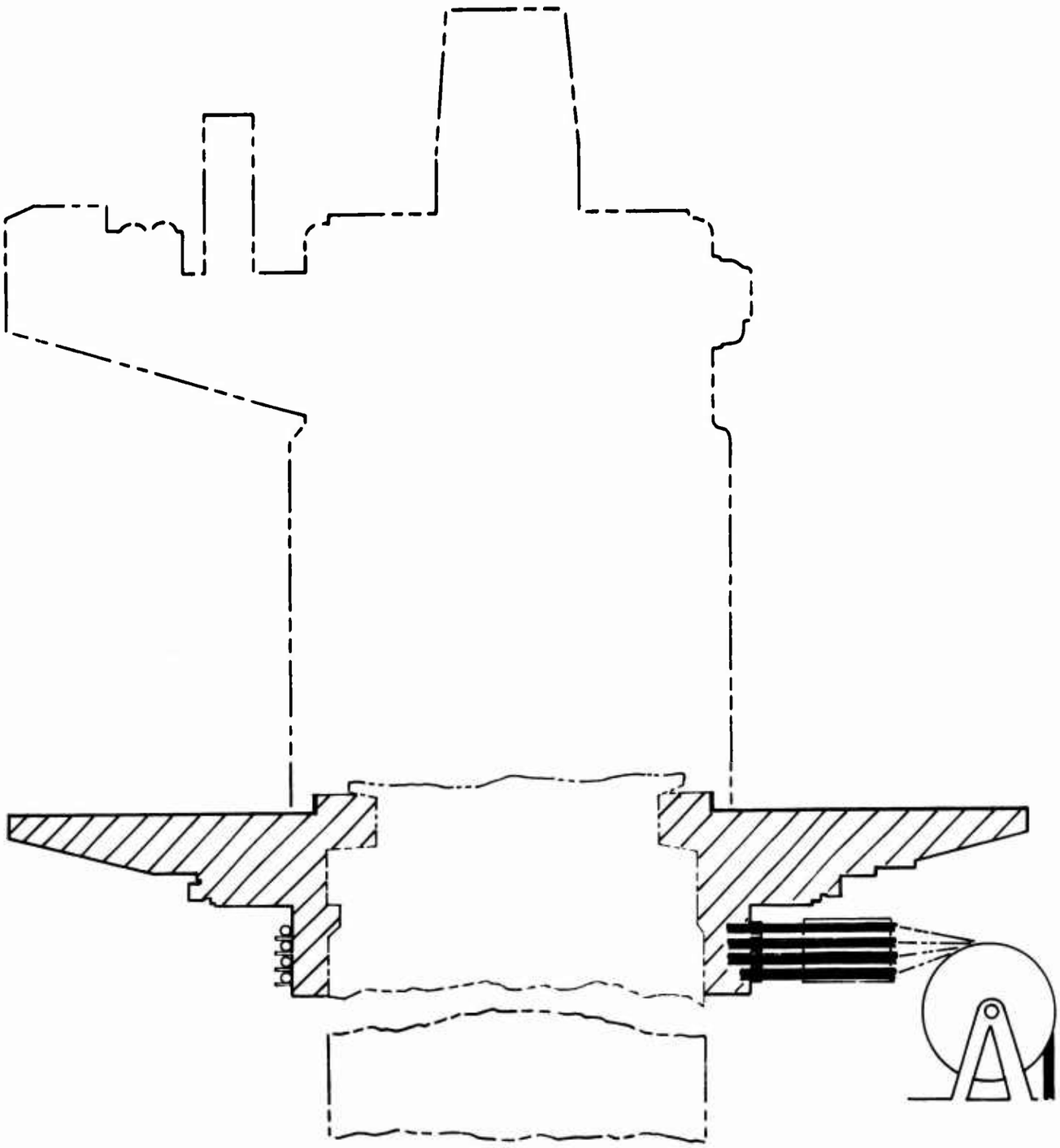

ANNULAR PLATFORM

 Preceding page blank

ANNULAR PLATFORM

GENERAL

Even though the WSMR Cinetheodolite accuracy is independent of moderate mechanical deformations that produce pointing errors in a conventional theodolite, the design philosophy of the breadboard instrument was to minimize mechanical errors and include in the mechanical design those features which would, even without optical compensation, permit "state-of-the-art" cinetheodolite performance. The philosophy was justified by the possibility that, should the optical compensation design prove inadequate or undesirable for some other reason, the development would provide the government with a good, well-designed American-made cinetheodolite and end the 25-year-old U. S. dependence upon foreign imports in this technological area. (There is a possibility that the future production versions of this instrument will include an annular platform so that compensated and uncompensated units can be assembled from the same castings. Potential demand for the less expensive, less accurate uncompensated unit by other U. S. agencies would have to be determined before this course could be justified. It is also possible that in future production units, maximum use of the optical compensation technique may render unnecessary some of the "good design features," including the annular platform, currently used in conventional theodolites. The resulting cost reduction could offset some of the cost increases required by the optical data train and other sophisticated components necessary to a 2 to 5 arc-second system.) Future value engineering analysis will determine the most cost-effective configuration for the WSMR Cinetheodolite and whether or not it will include an annular platform.

The annular platform illustrated in Figure 57 encircles the theodolite mount and rotates with it, but does not physically touch it at any point. The supporting columns of the annular platform are isolated from the cinetheodolite mounting pedestal and its supporting structure. The platform serves to isolate the operator and the forces created by his motions from the theodolite and to minimize deformation of the cinetheodolite structure and the coupling of disruptive forces to the gravity reference system.

The annular platform was designed by Reeves under subcontract from K&E. It was fabricated by Keystone Engineering under WSMR Contract DA-29-040-ORD-2704. After shipment to WSMR, it was assembled and tested by Lockheed Electronics Company, the service contractor.

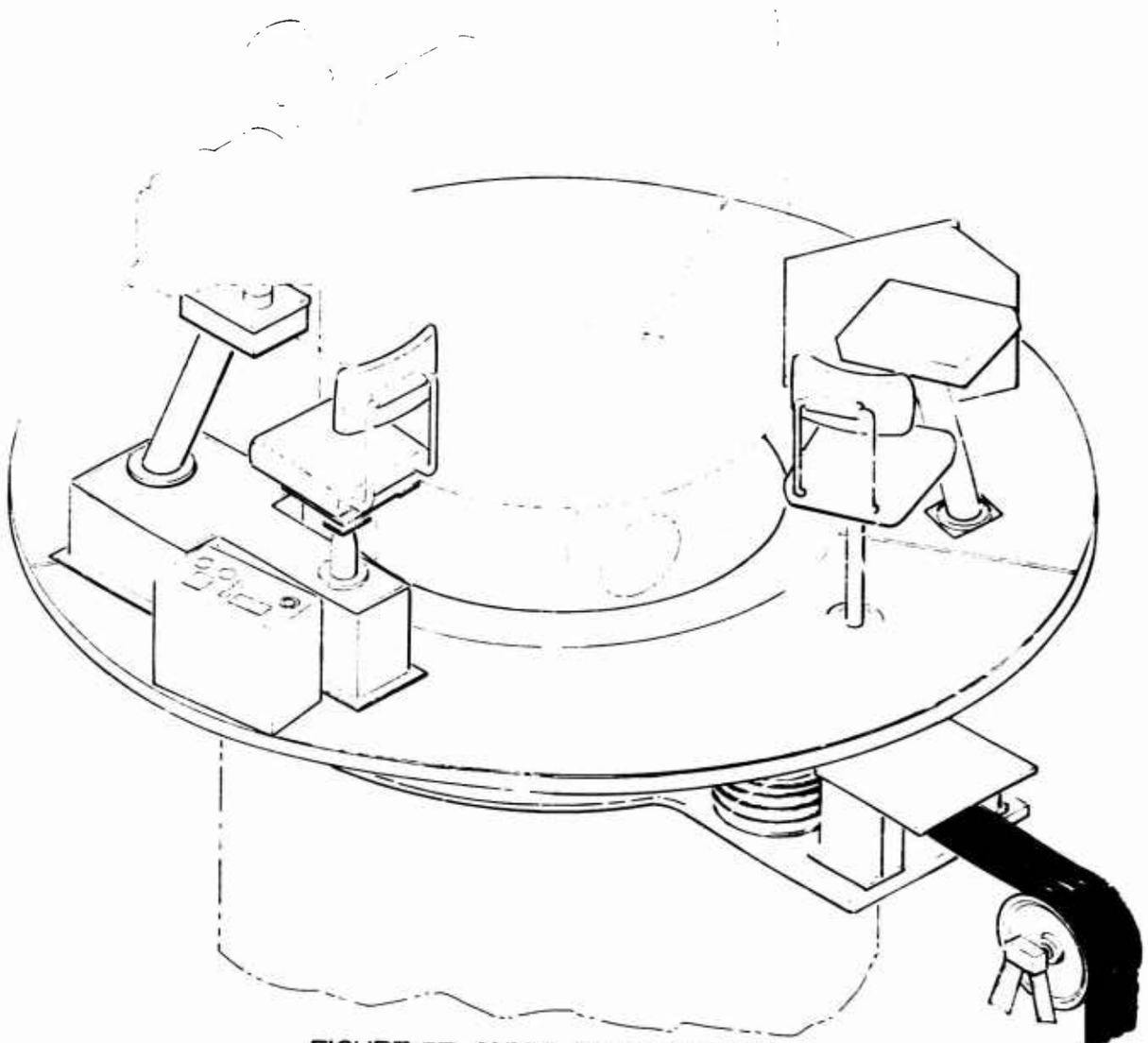

FIGURE 57 ANNULAR PLATFORM

CONFIGURATION

Platform

The rotating part of the platform consists of a weldment with an outside diameter of 108 inches and an inner diameter of 55.5 inches. It includes a top ring and a bottom ring joined by a circular section of 59.5 inches inside diameter and 5.5 inches deep. Stiffening is provided by 12 equally spaced radial ribs. The top is covered with removable sectors of 1/4 inch thick diamond tread aluminum plate. The weldment is bolted to the rotating inner race of a four-point contact ball bearing. The three-sector cable windup weldment is fastened to the lower side of this inner race by means of 24 bolts. It is made in three sectors so that it may be removed without disturbing the theodolite. The structure of the platform is such that a 300-pound vertical load applied to any two-square-inch area of the top plate results in a deflection of less than 0.125 inch. Weights and moments of inertia about the platform axis of rotation are shown in Table X.

Platform Drive

The annular platform is driven by two 0.6-HP Diehl dc servo motors through a spur gear speed-reduction unit. The speed reduction from motors to platform is 600. The nominal speed of this motor is 4000 rpm and the platform speed is therefore 40 degrees per second. The full-load torque of each motor is 9.45 lb-inches. Therefore, the torque on the platform at an estimated 85 percent drive efficiency is 9,650 lb-inches.

To drive the platform against the cable weights, an estimated torque of 1,920 lb-inches is required. This means that 7,730 lb-inches is available for acceleration of the platform at full speed, but acceleration of 50 degrees/sec^2 is not required at maximum speed. At a speed of 20 degrees per second, the torque available for acceleration is 19,300 minus 1,920 or 17,380 lb-inches.

The maximum acceleration is 1.04 rad/sec^2, the mass moment of inertia is 8,733 lb-inch-sec^2, and the product is the required torque T, which is 9,070 lb-inches.

Gearbox

The gears are housed in one aluminum casting. The two motor pinions, of 24 pitch and 29 teeth, drive an intermediate cluster gear with 145 teeth on the gear and 29 teeth, 16 pitch, on the pinion. This pinion drives

TABLE X. WEIGHTS AND MOMENTS OF INERTIA

	Weight lbs	Moment of Inertia lb-inch-sec^2
Platform weldment	622	2505
Cable windup weldment	477	927
Bearing inner race	176	475
Top cover	195	844
Gearbox	100	340
Bumper and linear pot. support	10	23
Chair with base	30	132
Hardware, etc.	50	135
Man	175	800
Platform drive motors		1750
Gears		550
Cable pulleys and weights		192
TOTAL	1835	8733

a gear with 145 teeth, and to its axis is keyed the final drive pinion with 29 teeth, 10 pitch. This pinion drives the bull gear with 696 teeth. Using standard gear formulas, the stress on the final drive pinion is calculated to be 11,400 lbs/sq in.

Every gear in the gearbox is made of S.A.E. 4,340 steel, heat-treated to 32-36 on the Rockwell C scale. It can be seen that the stresses are very conservative for the alloy chosen.

The gear mesh at the motor pinions can be adjusted by moving the motors. The final gear mesh is adjustable by moving the gearbox.

Platform Limit Stop

The stop mechanism consists of a V-shaped actuator pivoted at the apex and mounted on a platform that is fastened to the stationary base. The actuator is operated by a pin on the moving platform, and in turn it actuates a hydraulic buffer (dashpot). This mechanism allows for platform travel of 360 degrees in either direction. The V actuator also carries a cam that operates electrical limit switches, opening the drive motor circuits before the buffer is actuated.

The buffer must be able to absorb the kinetic energy of the platform and alidade rotating at a velocity of 40 degrees/sec (0.7 radians/sec). The Houdaille buffer No. 308410 can adequately absorb this energy should the theodolite-ring synchronization system fail.

Drop Cable Assembly

Necessary electrical connections from the control equipment through the annular platform are made through special low-fatigue drop cables fabricated by the High Temp Cable Company. The number and size of conductors required to supply power and control signals to the theodolite are illustrated in Table XI. The cable wrap is clockwise or counterclockwise, depending upon annular platform position. Cable length is approximately 60 feet, which is sufficient to allow one complete turn clockwise and one complete turn counterclockwise. Thus, total platform rotation is limited to approximately 720 degrees. The unwrapped portions of the cables extend into a cable well and are suitably guided and weighted to prevent fouling, as illustrated in Figure 58. Rotational limit switches remove platform electrical power as limits are approached and mechanical stops provide a safety backup in the event of limit switch failure.

The operator's control panel and chair are installed on the platform near the guide scope; the camera control panel and the removable camera operator's chair are installed on the platform near the camera compartment; and the power supply, for the azimuth and elevation flash heads, is mounted on the opposite side of the platform.

TABLE XI. DROP CABLES

Cable Number	Conductor Size	Number	
	22	3	Shielded
W 2001	22	5	
	20	2	Shielded
	20	6	
	18		
W 2002	20	6	
	24	96	
W 2003	22	22	
	20	13	
	18	8	
W 2004	20	2	Shielded
	20	8	
	16	2	
	12	6	
	10	1	
	TOTAL	256	

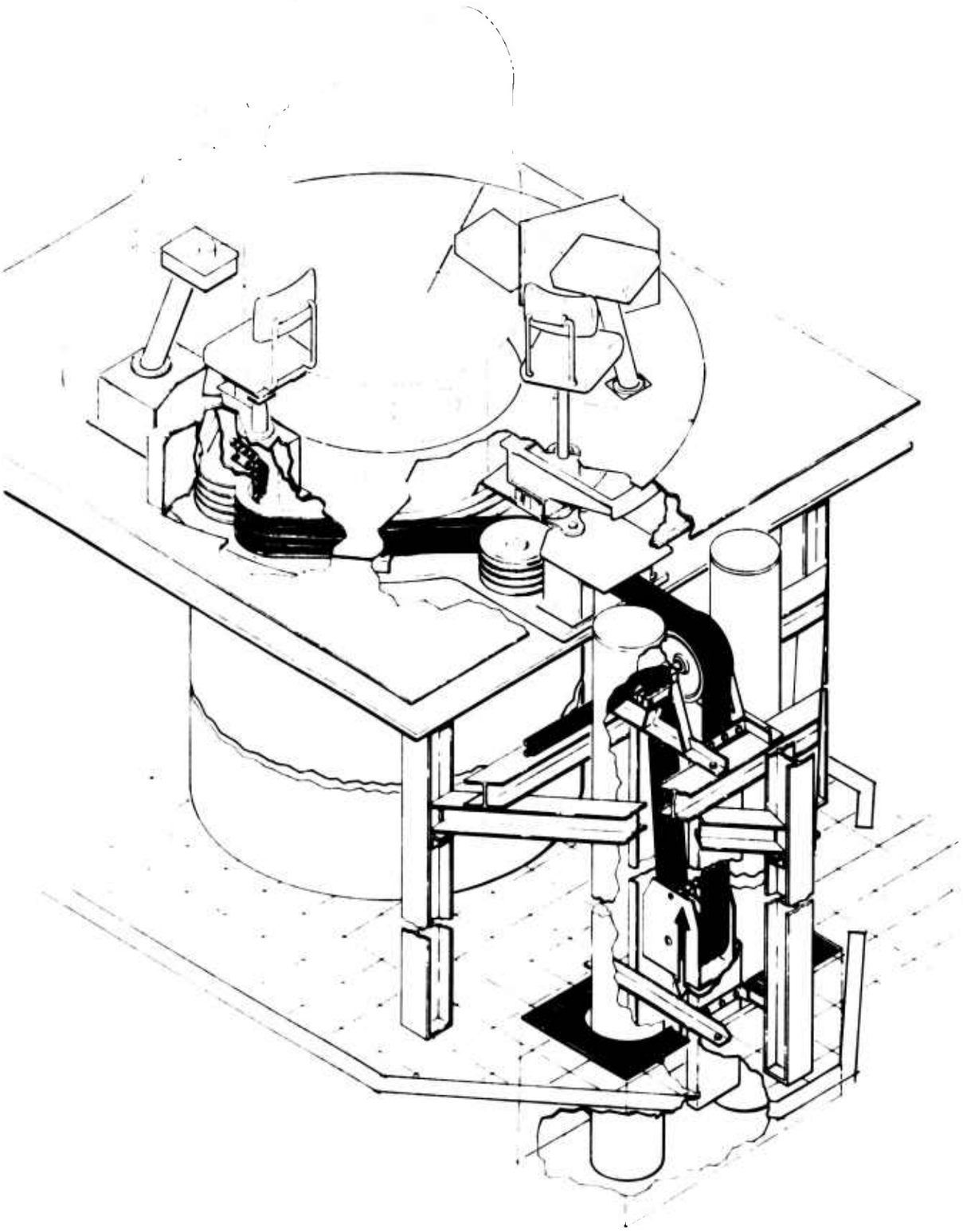

FIGURE 58. CABLE DROP ASSEMBLY

TEST RESULTS

Isolation

As reported in the section titled "The Gravity Reference Mirror System," some undesired coupling still exists between the annular platform or the cinetheodolite azimuth axis, and the GRM. The GRM was monitored during azimuth accelerations of the instrument, and recordings of the monitor output are shown in Figures 59 and 60. These figures clearly show that some coupling of translatory forces from the platform to the GRM and the theodolite still exists. Whether such forces were coupled from the cinetheodolite, the annular platform, or some combination of the two was not determined, since they rotate in unison.

Tracking Smoothness

Since the guide scope is mounted on the cinetheodolite and the operator is seated on the platform-mounted chair, the major requirement of the annular platform drive system is that there be no large, sudden relative motion between the platform and the cinetheodolite. The platform may be allowed to lead or lag the instrument by as much as one degree, as long as this requirement is met. During the testing period, the system failed to meet this requirement throughout the range of azimuth accelerations of the cinetheodolite. As reported in the section titled "Servo Drive Systems," compensation of all drive servo loops was inadequate. There are very large differences in inertia and torque loads of these drive systems. The varying load placed upon the annular platform servo by the drop cable added to the problem. The forces contributed by the drop cables and their counterweights were sufficient to overcome the frictional drag of the platform and to rotate it to the neutral (weights-down) position, even after the counterweights were reduced to the minimum acceptable value of ten pounds each. Calculations indicate that cable drag changes the available torque by $\pm$10 percent. This 20 percent total variation appreciably increases servo compensation problems. It is doubtful that the smooth tracking requirements can be met unless slip rings are used in place of the drop cables. This is unfortunate, since reliability of the drop cables is high as illustrated by the performance history given in Table XII. This performance was achieved without a single failure for any of the 256 cable conductors. It is estimated that this is equivalent to approximately two years of continuous field operation, which indicates a highly reliable cable system. To provide added conductors for the test complex, a small supplemental cable was added to the cable drop assembly. During the star tests, several of these added circuits opened, but the original cable itself did not fail.

CHART SPEED: 1mm / SECOND OF TIME
CHART SCALE FACTOR: — 0.25 ARC - SECONDS / MILLIMETER

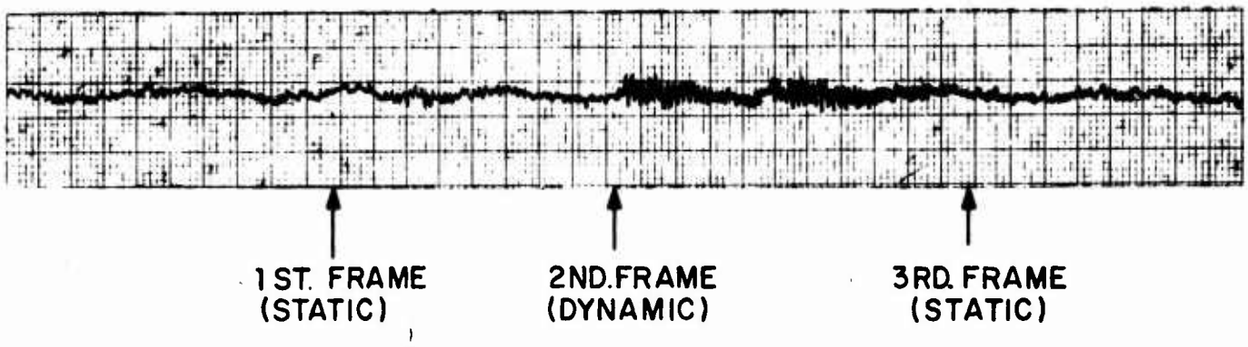

FIGURE 59. GRM RECORDING - PLATE 014
5 NOV. 1968

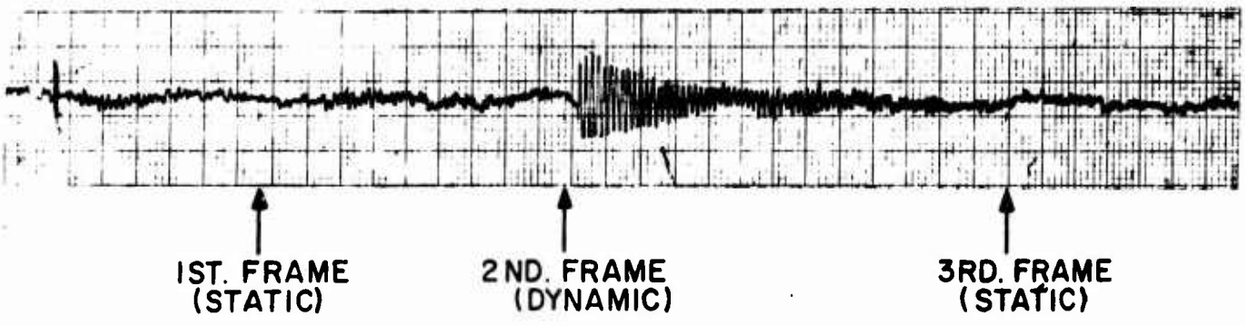

CHART SPEED: 1 mm / SECOND OF TIME
CHART SCALE FACTOR: — 0.25 ARC - SECONDS / MILLIMETER

FIGURE 60. GRM RECORDING - PLATE 016
5 NOV. 1968

TABLE XII. CABLE HISTORY

Test Period	Average Range of Motion	Time Duration	Estimated Rotation Degrees x 10^4
Dynamic Tests	<90°	8 months	5
Star Tests	<180°	12 months	36
Checkout	<360°	5 months	2
Maintenance Period		2 months	2

Deficiencies

The following deficiencies exist:

1. The platform cannot currently meet the basic smooth tracking requirement because of load variations due to drop cables.

2. Excessive volume and mass contribute to GRM shock excitation and increase the smooth tracking problems.

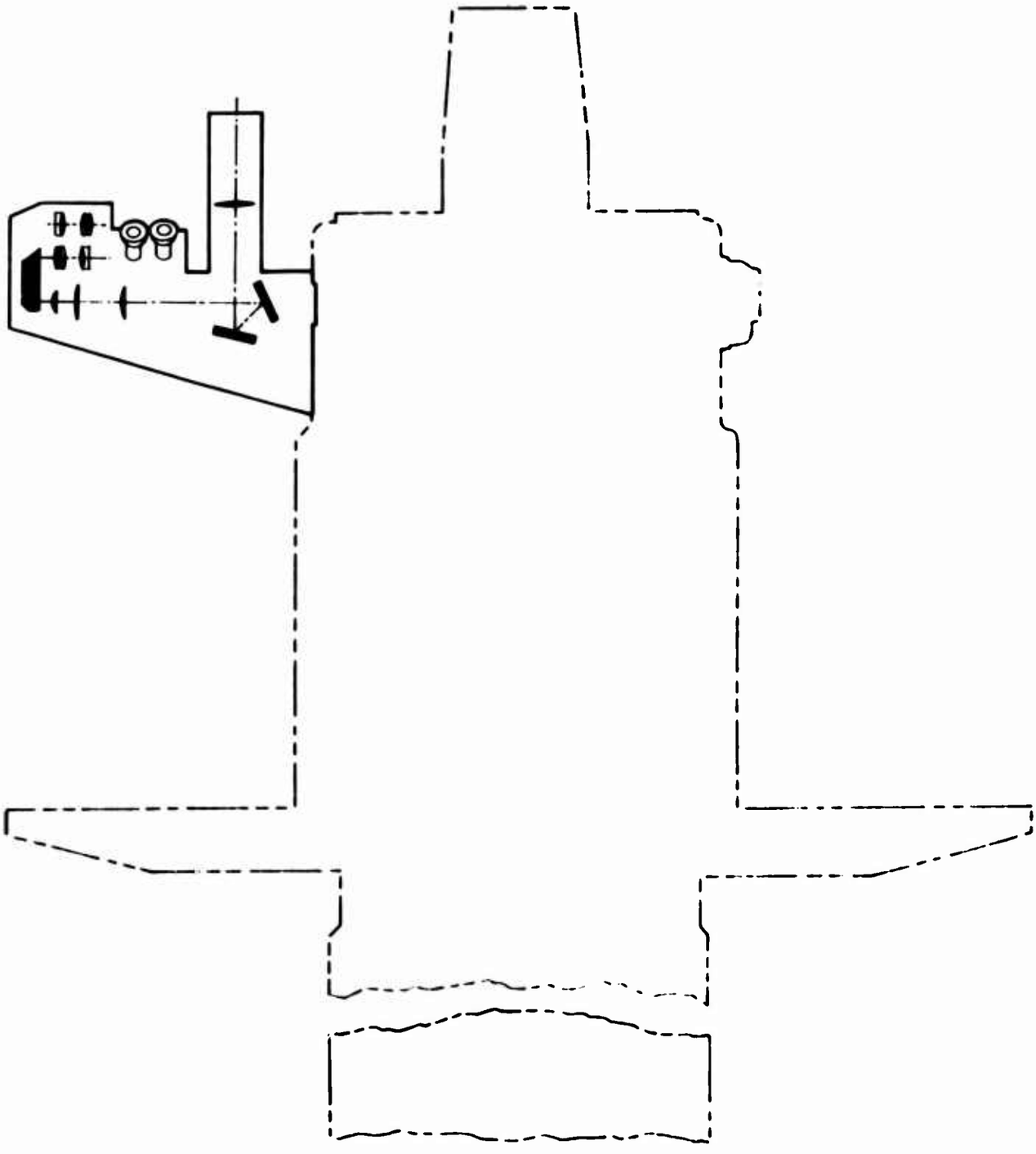

GUIDE SCOPE

Preceding page blank

GUIDE TELESCOPE

BACKGROUND

There are many optional variables to choose from when designing a guide telescope system for a tracking instrument. Choice of optical characteristics involves magnificiation, field size, eye relief, resolution, contrast, transmittance, and objective size. Then there are the human engineering features that are much more complex. For example, there are these choices.

1. Objective End:

   Mono-objective

   Bi-objective

   Scanning mirror (or prism)

2. Ocular End:

   Monocular

   Binocular

   In-line viewing

   90° elbow viewing

   Tracking ocular

   Fixed position ocular (tracking objective)

   Adjustable position ocular

3. Any combination of the above.

4. A combination of a guide tele-objective and closed-circuit TV.

A committee of range instrumentation personnel studied these combinations and their recommendations resulted in a choice of design characteristics for the present guide telescope on the WSMR Cinetheodolite.

DESCRIPTION

The guide telescope used on the WSMR Cinetheodolite as illustrated in Figures 61 and 62 is a mono-objective, binocular, variable power telescope. The operator looks forward into an inclined binocular eyepiece and with the turn of a knob may select a magnification of 10, 20, or 40 power. A filter wheel is also available to enhance image contrast.

The objective has a 100-mm diameter and a focal length of 801-mm. The ocular is a 50-degree eyepiece of 30-mm effective focal length. Imaging is done by the use of a lens pair rather than prisms. A Pechan prism is used for image derotation and a Galilean system is inserted in the optical path for a power changer.

The nominal visual optical properties are as given in Table XIII.

No true stereoscopic vision is required in most missile tracking; therefore, a single objective of sufficient aperture to give needed resolution, exit pupil, and illumination was chosen. There are two important reasons for selection of the more complex binocular eyepiece: (1) binocular vision provides less eye strain, (2) fewer targets are lost due to eye blinking. Both of these properties are important when tracking small or low-contrast objects.

TABLE XIII. GUIDE SCOPE OPTICAL PROPERTIES

	10 Power	20 Power	40 Power
Field of view	5°	2-1/2°	1-1/4°
Exit pupil	3.8-mm	4.9-mm	1.6-mm
Eye relief	21-1/2-mm	21-1/2-mm	21-1/2-mm
Objective diameter used	38-mm	98-mm	64-mm
Relative illumination	14.4	24	2.3
Percent transmission (with the most efficient coatings)	14%	15.2%	14%

Using a monocular telescope for object search and identification, objects are lost by the observer because of two characteristics of the eye: the blinking of the eyes and floating "motes" which will blank out small objects. Investigations of the benefits of various types of search telescopes have

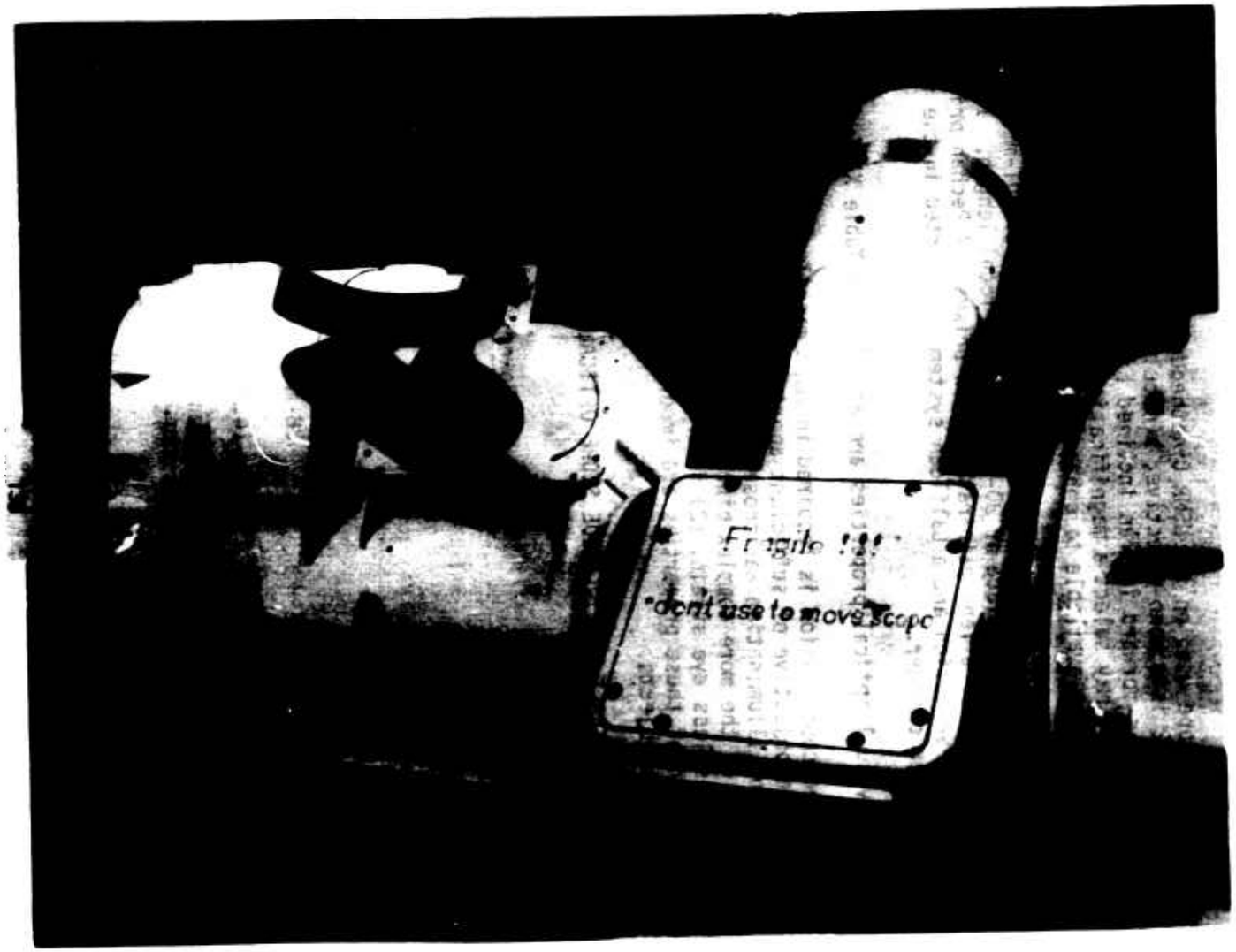
Fragile !!!
"dont use to move scope"

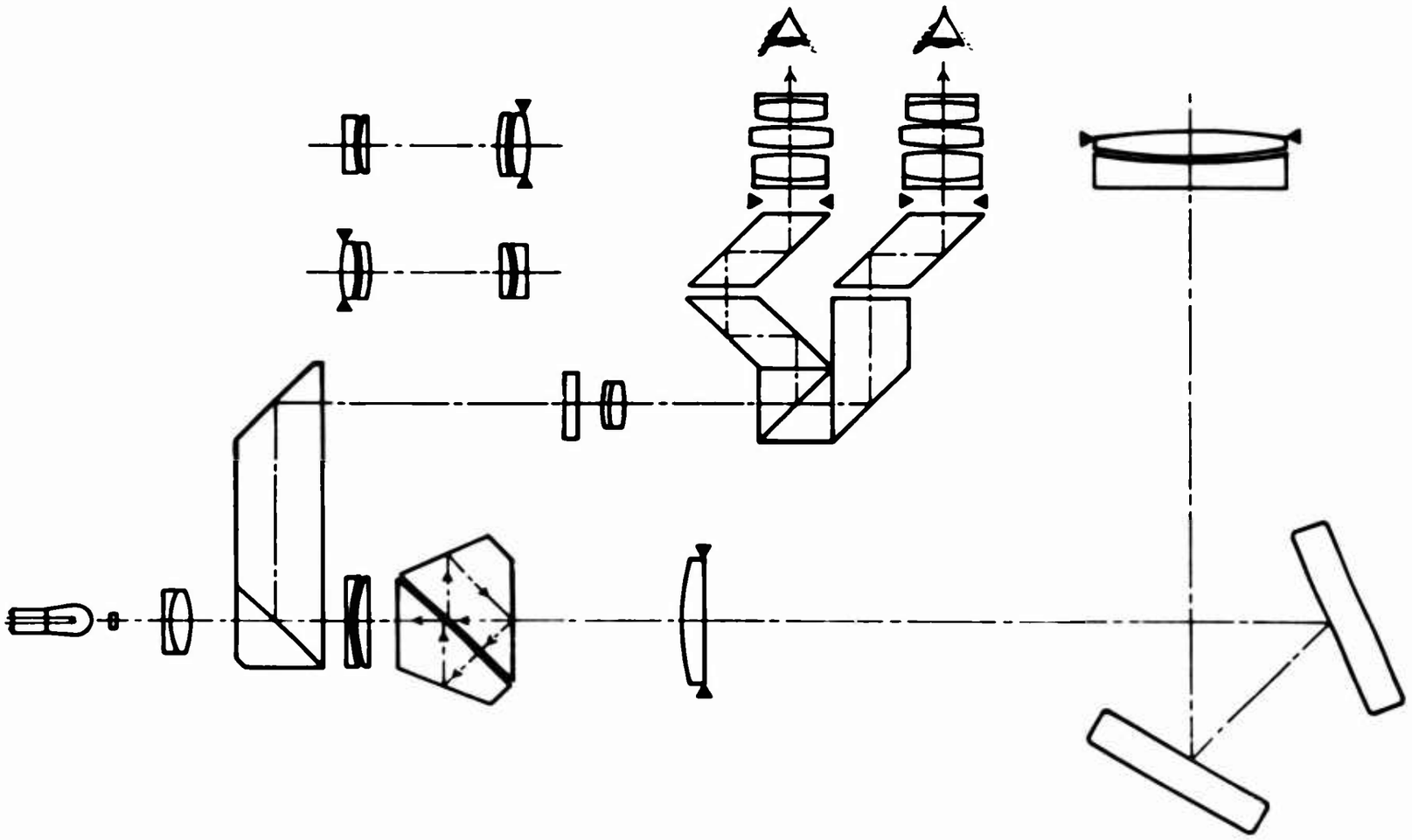

FIGURE 62 GUIDE SCOPE OPTICS

been conducted and it has been found that it is extremely rare for both eyes to blink simultaneously or to have vision blocked by motes in the same area of both eyes. Therefore, binocular vision has an advantage even though stereo vision is not involved.

The choice of a binocular eyepiece system added difficulties to the problem of optical design for which many compromises were made. For example, the use of prisms for derotation and to provide binocular vision restricted the field size. The multiple power feature added many lenses with the consequent aberrations, air/glass surfaces and loss of light transmission. All of the added lenses and prisms also contribute to the loss of resolution and contrast.

DEFICIENCIES

1. Field Stops - The proper field and aperture stops have not been used. There are ghost images at the field edge caused by the lack of prism face stops.

2. Power Changers - The use of Galilean power changers coupled with a small exit pupil allows one to "look around" the entrance pupil image. This is distracting to the operator.

3. Twenty Power Magnification - Magnification at the 20 power position is actually close to 25 power and should be reduced to take advantage of a larger field and exit pupil.

4. Frequent Loss of Collimation - The coupling used between the main optical system and the tracking telescope is the bellows type. This type of coupling was used to permit a small amount of misalignment between the two systems without degrading the performance of the system. However, lack of torsional rigidity of this particular bellows resulted in the loss of collimation between the two optical systems. Stress introduced by operator contact or high tracking rates will misalign the guide scope.

RECOMMENDATIONS

It is recommended that a brief study be made to re-evaluate the guide telescope requirements in view of the long period since breadboard choices were made. For example, WSMR should reconsider requirements, such as target size, target range (both minimum and maximum), and target contrast. This would determine the geometric properties. Associated with a basic philosophy of the position and duties of the tracker personnel, the following questions should be answered: Should the operator ride the instrument or an insulated platform? Should the operator face in the direction of target or at a right angle to the theodolite optical axis? Is the eyepiece to be fixed or should operator's head track? Could closed circuit TV be used to advantage?

ACCURACY EVALUATION

ORIGINAL TEST PLAN AND ITS DIFFICULTIES

The unique and primary performance characteristic attributed to the WSMR Cinetheodolite is the ability to compensate for or nullify the large mechanical error contributions induced by accelerations associated with high tracking rates. It was the development goal that tests of the WSMR Cinetheodolite would establish a ratio of static to dynamic pointing accuracy near the 1:1.2 theoretical limit and design goal of the system. To make a meaningful estimate of the ratio would require the estimate of the pointing errors to be accurate to ±0.25 arc-seconds. In 1965, when the tests were planned, it was realized that measurements accurate to ±0.25 arc-seconds would be extremely difficult to achieve. The goal was defended on the basis that state of the art photogrammetric techniques could, at that time, read ballistic camera and astronomical star plates to an accuracy of 1 to 2 microns In 1965 the achievable dial and fiducial image quality of the WSMR Cinetheodolite could not be accurately predicted, but there were no apparent reasons to assume that the position of the image centroids could not be read to ±6 microns. After installation and checkout of the instrument at Bill Site all attempts to read the first photographic plates to better than 10 to 20 microns failed. Of course, poor image quality produced by the deficient data train was the principal reason that six micron accuracy could not be achieved. However, the large number of mensuration stage readings per plate (225) was a burden on the reader personnel and had a considerable effect upon reading accuracy. Problems of excessive dial and fiducial reading error, therefore, made it impractical to conduct the instrument evaluation completely as originally planned in 1965.

In addition to the original astronomical star tests outlined in "Accuracy Evaluation Plan WSMR Cinetheodolite," Optics Division Technical Memorandum 64-2, a second independent method for static accuracy determination was planned. The method employed optical alignment equipment and was related (to some extent) to conventional methods used for surveying theodolite accuracy assessment. The test used a dual beam collimator mounted on a pivoted track (great circle) supported on a massive horizontal track shown in Figure 63. One beam of the dual beam collimator emerged at a slightly different but fixed angle from the other. The great circle track and mount were designed so that the collimator could be moved to any position in the hemisphere. The test procedure would be to first measure the angular direction of the one beam of light from the collimator with the cinetheodolite. The cinetheodolite would then be rotated to be in line with the other beam of light from the collimator and a measurement taken of this direction with the cinetheodolite. The dual beam collimator would then be moved along the circular track so that the first beam was realigned with the cinetheodolite and the procedure repeated until the circle was "closed." Using this method, a very close check could be made on the

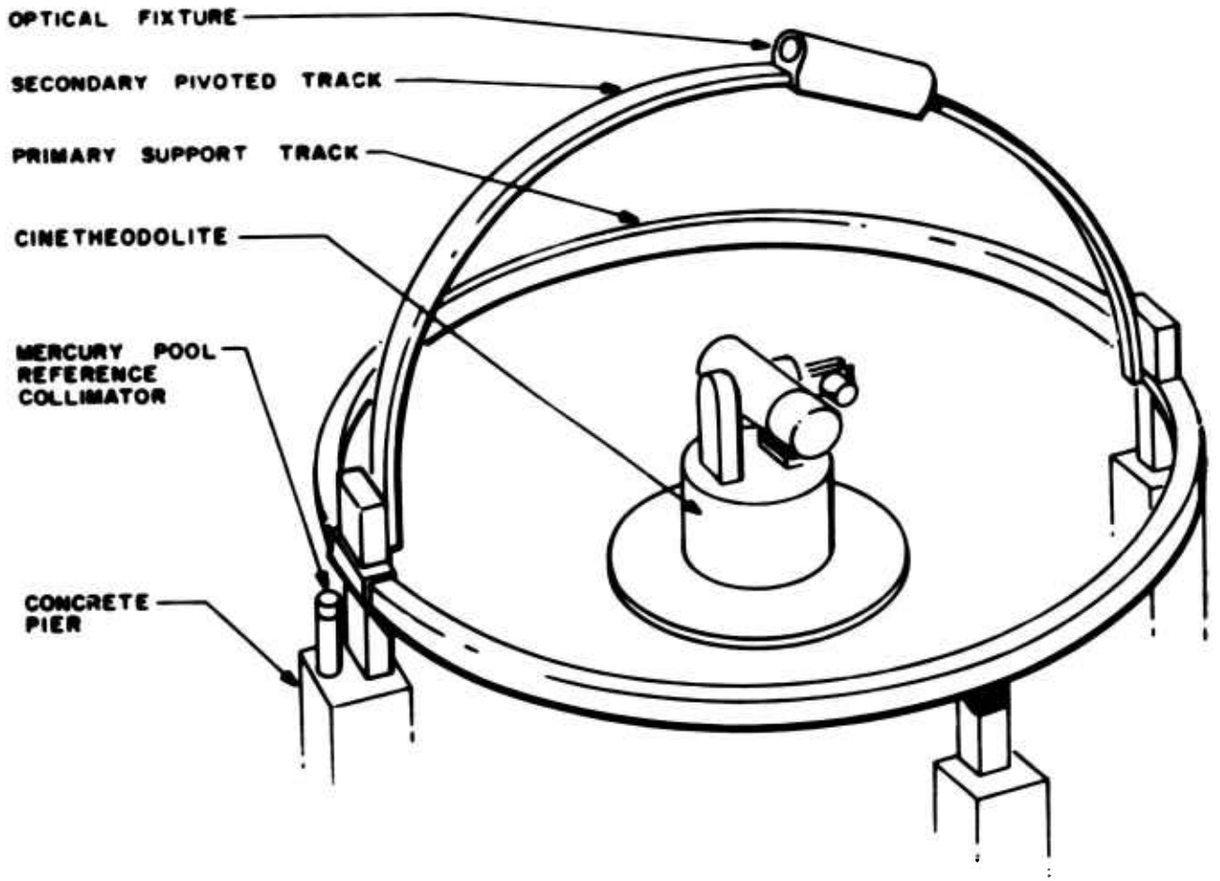

FIGURE 63. PROPOSED TEST STRUCTURE

azimuth and elevation graduated circles. This method of static testing also had the advantage of being free from the influence of atmospheric error. The method was also to have been a powerful tool for diagnosis of obscure difficulties anticipated in the first phase of the evaluation process.

Although the optical alignment equipment was fabricated and installed, attempts to close the circle were unsuccessful. Lack of stability in the dual beam collimator support fixtures caused by unanticipated geo-seismic motion of the supporting piers introduced excessive error. To leave the impression that these were the only major problems experienced in the attempted implementation of this method would be oversimplification. No single component of the Optical Alignment complex was without design problems. Each major component of the massive structure required a wide range of accurate positional alignment and a mechanical stability to 0.5 arc-seconds. To maintain this stability without highly sophisticated compensation and stabilization techniques was a very difficult, if not impossible, task and was certainly underestimated in the planning stage of the test program. The source of much difficulty was the inadequacy of of basic optical test instrumentation to monitor dynamic conditions experienced outside the laboratory. Massive structures, formerly considered as stable or static references in an environment of 15 to 20 arc-second theodolites, were required to account for their dynamic position when used to measure the pointing direction of a 2 arc-second theodolite. An example of this is illustrated in the dynamic tests of the section titled "The Gravity Reference Mirror System."

Other tests, considered feasible as proposed in the original test plan, had to be either modified or abandoned entirely. For instance, the original dynamic test plan proposed a technique to simultaneously subject the elevation and azimuth axes to forces of acceleration. This method had to be abandoned because the response of the digital encoder was not sufficient to enable accurate and rapid programming of the theodolite optical axis through the artificial star coordinates. As an alternative, azimuth and elevation dynamics had to be tested separately using independent procedures. This requires twice as many measurements as the original plan would have required. Time schedules of the WSMR Cinetheodolite exploration development did not permit the rebuilding of a test complex that would be adequate to implement the original test plan. For other reasons, this proved to be no real handicap to the ultimate test and evaluation program of the breadboard, e.g., the dual beam collimator technique for critical testing of the azimuth and elevation circles would have had to be abandoned anyway because the ultra-precise incremental measurements, essential to the original plan, would have been masked by the dial and fiducial reading errors, resulting from the data train design deficiencies in the breadboard instrument. This in no way implies that task team efforts to develop very critical and highly advanced theodolite testing techniques were wasted. The technical knowledge resulting from the exercise will be of value in developing the diagnostic and acceptance test procedures for the future cinetheodolite system of advanced design.

The alternate test methods that ultimately evolved proved completely adequate for the validation of the WSMR Cinetheodolite design concept. The tests determined the instrumental static pointing accuracy and established with high level of confidence the improbability of any significant dynamic error contribution, even with the instrument structure under severe accelerative forces. The following paragraphs describe the test requirements and the alternate test plan that was implemented.

ALTERNATE TEST PLAN

Static Test Plan

The astronomical method, based upon the use of known angular positions of fixed stars at specified sidereal times, was selected as the method to determine static pointing accuracy of the cinetheodolite. The angular positions of stars could be known to an accuracy limited by star catalogue errors and by refraction error uncertainty which is normally very small at high elevation angles. A series of well distributed fourth and fifth magnitude stars with elevation angles exceeding 25° was selected. Photographs of the stars were to be made as each trailed across the field of view with the cinetheodolite in a fixed position. Each star trail was to be interrupted by a shutter for timing purposes. The sequence of exposures originally selected was open 8 seconds, close 2 seconds, open 4 seconds, close 2 seconds, open 1 second, close 2 seconds, open 1/2 second, close 2 seconds, open 1/4 second, close 2 seconds, open 1/8 second, close. This would give a series of seven star images, one of which (for star magnitudes within the proper range) would be round, punctiform, of small diameter and otherwise suitable for precise measurement. At the midpoint of the 2 second exposure, the angle data, fiducial data, and timing data was to be recorded on the same photograph as the star trail image.

Dynamic Test Plan

To determine the cinetheodolite pointing error contributed by the instrument dynamics, a direct difference method was selected. For each dynamic test the cinetheodolite was to first statically photograph a fixed (stationary) artificial star with motionless elevation and azimuth axes. Immediately thereafter a second photograph was to be taken of the fixed artificial star with the cinetheodolite rapidly slewing through the artificial star coordinates. The difference in the target bearings as reduced from the two sets of photogrammetric measurements would be the theodolite error contributed by that particular dynamic condition. For the static and dynamic tests the alternate test plan provided continuous monitoring of environmental conditions, such as ambient temperature, barometric pressure, wind velocities, etc.

Test Equipment Development

To implement the pointing accuracy tests, a test complex was designed, built, and installed at Bill Site. Figure 64 is a block diagram of the electronic control systems used in performing the static and dynamic tests.

Plate Camera

In order to minimize thermal shrinkage, Estar base 35-mm instrumentation type film was used. This film is prestretched and then stress relieved in the manufacturing process. Estimates of pointing measurement error due to differential thermal shrinkage were less than 0.5 arc-seconds with proper film development; however, there was still some question as to whether or not negligible shrinkage could be achieved with the hot spray film development process used at WSMR. In order to eliminate this variable from the tests, it was decided that photographic glass plates would be used for all of the WSMR Cinetheodolite pointing accuracy tests. A special plate camera assembly consisting of a camera sequencing unit, a camera control unit, and a plate camera was designed and fabricated.

The plate camera assembly enabled the star data to be recorded photographically with great accuracy using any desired shutter sequencing. The original shutter sequence produced a spaced series of exposures of 8 seconds, 4 seconds, 2 seconds (with data strobe at time midpoint), 1 second, 1/2 second, 1/4 second, and 1/8 second. As the earth's angular rate of rotation is only 15 arc seconds per second of time, an in-house developed pulse shutter synchronized to ± 1 millisecond with IRIG time contributed negligible errors into the difference determinations of known and observed star positions.

Position Programmer

To minimize the effects of disturbances in local environment and limit the range of thermal stresses within the instrument to short term (<8 hours) variations, it was deemed necessary to photograph a complete set (± 50) of preselected fourth and fifth magnitude stars during a single night. This would have been a formidable task to an experienced astronomer even if the theodolite had been equipped with an equatorial mount But, to accurately position an alta-azimuth mount for each of the 50 star photographs, the theodolite operator (equipped only with predetermined azimuth-elevation-time data and a plate camera) would find the task impossible in an eight hour period unless some automated aiding process was provided In order to collect a sufficient amount of data in a relatively short period of time, it was necessary to design and fabricate a mount position programmer. The position programming assembly (consisting of an address register, address comparator, and an 8-channel tape recorder) was fabricated and interfaced with the cinetheodolite system. This equipment provided a means of rapidly positioning the cinetheodolite to any position (± 1 arc min) stored on the magnetic tape. The information stored on the tape was produced by a

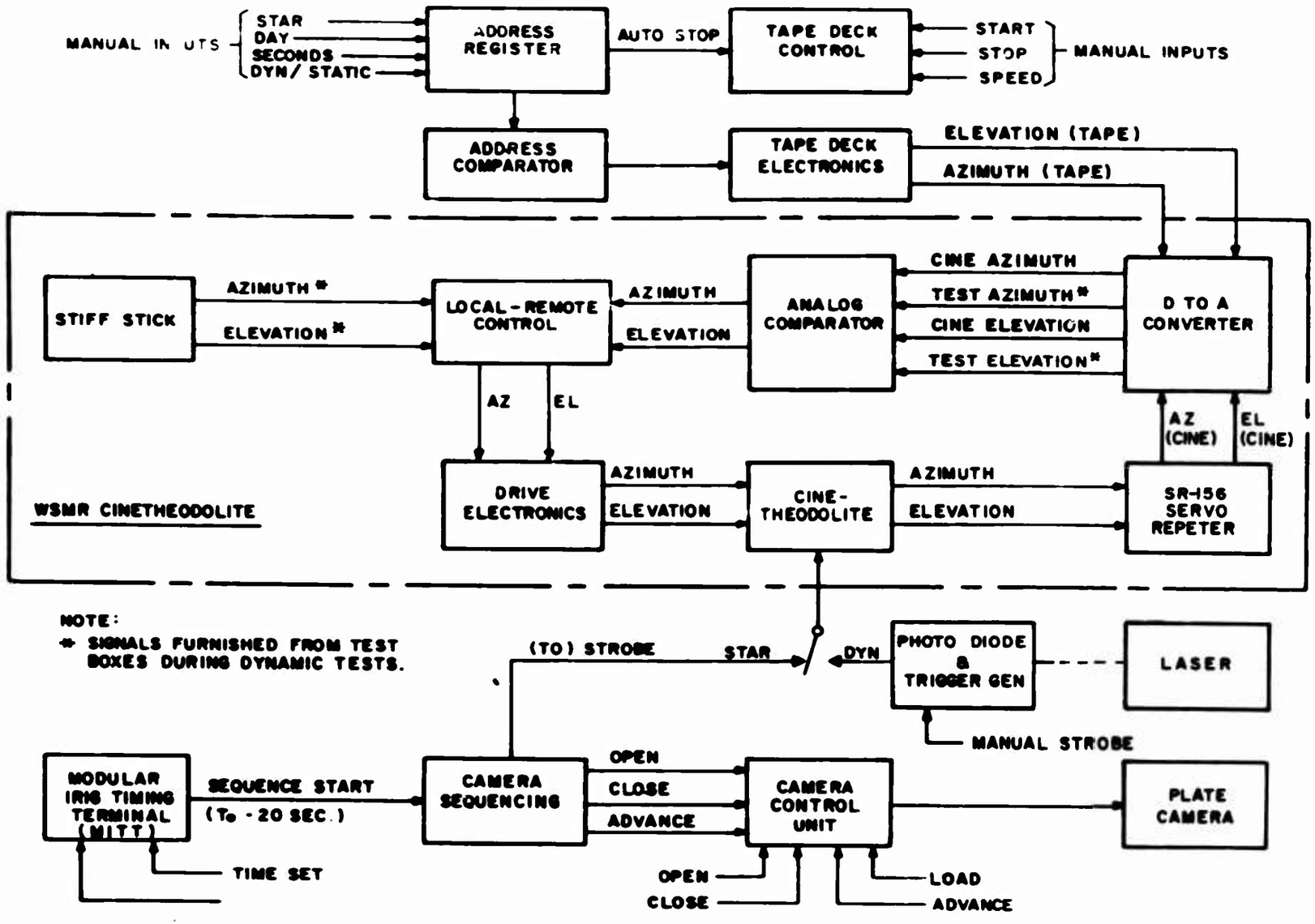

FIGURE 64. TEST COMPLEX CONTROL SYSTEM

computer program written by Data Reduction personnel at WSMR. The computations used are given in Appendix A. To obtain optimum exposures with the Tri-X photographic emulsion used on the test plates, stars of fourth and fifth magnitude were selected. This program converted the right ascension and declination of each star to the proper cinetheodolite azimuth and elevation angles for each desired time.

Dynamic Test Equipment

The dynamic tests utilized much of the test complex developed for star tests. In addition, the following major elements were developed: (1) great circle fixture, (2) target collimator, and (3) position laser and photodiode.

The great circle fixture, as shown in Figure 65, is a heavy steel structure that serves to support the target collimator. The same figure also shows the concrete piers on which the great circle fixture is placed. These piers are isolated from the rest of the test facility to minimize any motion that could be induced by the cinetheodolite or by test personnel.

The target collimator, Figure 66, is used to simulate a point light source at infinity, or artificial star. Its major components are an FX-31 flashtube, a Barlow lens, and a 48-inch f8 catadioptric lens.

The target collimator may be positioned to any point on the surface of the hemisphere that is on the locus of the great circle fixture. This is done by rotating the great circle fixture in azimuth and raising or lowering the collimator along the arc of the great circle.

A small one-milliwatt laser is mounted alongside the collimator. The laser beam is directed at a photodiode, mounted on the side of the cinetheodolite telescope tube. The signal generated, when the laser beam strikes the photodiode, is used to trigger the strobe circuits. In this way, the strobe may be synchronized with the passage of the artificial star through the field of view of the cinetheodolite. Since the artificial star is produced by a 10 microseconds flash of light, it appears on the plate as a point. This flash is strobed by the same trigger that strobes the graduated circle and fiducial flashlamps.

The main drive system was used to accelerate the cinetheodolite to simulate tracking missions for the dynamic tests. The drive control system used in the static pointing accuracy tests was modified for direct static and dynamic inputs.

TEST PROGRAM

Static Tests

The breadboard WSMR Cinetheodolite instrument was installed by K&E at Bill Site, White Sands Missile Range, in May of 1967 and was checked out and accepted by the Government in June 1967. Interface of the instrument

FIGURE 85 GREAT CIRCLE FIXTURE

with the in-house developed test complex was completed in September 1967 and the static test program started the following month and continued until July 1968. The program produced several hundred star photographs. Many of the photographs were unacceptable because of missing fiducial image components and poor fiducial or star image quality. Many of the tests were aborted because of cloud cover, poor atmospheric conditions, or failure of test complex components. Missing fiducial ball and dial data images resulted from either instrument flashlamp failure or the dial aperture deficiency discussed in the section titled "Optical Data Train." After preliminary tests were completed the following test procedure was adopted.

Static Test Procedure

Power is turned on to the cinetheodolite and test complex, and the cinetheodolite operator loads the camera. About three minutes before the desired time of the first plate exposure, the test operator in the test equipment room loads the address register with the day of year, the desired star number, and the desired exposure time. He then starts the automatic tape search for this message. When the chosen message is found, the tape deck stops and the cinetheodolite is automatically positioned to the proper coordinates. These are the coordinates of the star at the midpoint of the first one-quarter-second exposure. The cinetheodolite operator verifies the presence of a star in the field of view. The test operator then arms the camera sequencing unit, which starts automatically at the preset time as indicated by the MITT. The sequencing unit controls the camera to produce the chosen sequence of exposures and to strobe the data lamps at the proper time.

At the completion of the shutter sequence, the photographic plate is automatically advanced to the next frame, the test operator changes the address register to a new star number and time, and the sequence is repeated. Each plate holds three frames of data. The cinetheodolite operator changes plates as required. This procedure permitted star photography to proceed at a pace sufficiently rapid to photograph a complete series of fourth and fifth magnitude stars in a 3 to 4 hour period which minimized the variation in the refraction error and the local instrumental environment effects during the test period.

Dynamic Tests

The original test plan permitted static and dynamic testing to proceed in parallel, i.e., the night operation for the static or star photography and the daylight hours were reserved for dynamic testing. This plan was not followed because the preliminary results of static photographs of the artificial star collimator cast serious doubt on even the short term (30 seconds) stability of this device.

As in-house testing of the GRM had also confirmed the presence of geoseismic noise at higher levels than had been anticipated, attempts were made to determine the frequency and amplitude of vibrations prevalent at the test

site. The WSMR Calibration Laboratory conducted preliminary test at Bill Site that indicated vertical accelerations of the great circle test fixture columns of approximately 270 micro-g's at 0.3 to 7.25 cycles per second, and radial accelerations in the same range of frequencies, but at slightly reduced magnitude. Vertical accelerations appeared fairly constant in amplitude, but radial accelerations exhibited relatively quiet periods, during which such disturbances were only one-third as great as during worst-case conditions. No apparent correlation was observed between wind conditions and such accelerations. The actual great circle fixture displacements were not accurately determined because of the unknown radius of motion and the wide frequency range of the disturbances.

A Hilger-Watts autocollimator was placed on the west pedestal (supporting column) of the great circle fixture and a mirror placed on the north pedestal. The autocollimator was vertically oriented and the cinetheodolite was accelerated in azimuth. A recording of the autocollimator output, reproduced in Figure 67, clearly shows that such azimuth accelerations of the instrument cause motion of the great circle pedestals.

Next, another autocollimator was installed on top of the cinetheodolite tube and another mirror was mounted on the barrel of the artificial star collimator, which was positioned to 45 degrees elevation on the great circle fixture. A recording was made of the output of both autocollimators and is reproduced in Figure 68. This recording shows an apparent correlation between the signals of the two autocollimators whenever either the west or the north pedestal was stepped on. These displacements were approximately equal, and indicate that some undesirable relative motion can exist between the cinetheodolite and the artificial star during dynamic testing, even though such motion is almost lost in geoseismic noise.

Air turbulence in the dome causes refraction errors of undetermined magnitude. Figures 69 and 70 illustrate the effect of body heat on collimator light. During dynamic testing, care was taken to avoid contributing to the air turbulence any more than necessary.

Because the geoseismic and turbulence distribution density functions closely approximate the so-called "normal" distribution or bell curve, it was felt that errors contributed by such noise would be greatly reduced by statistical methods of data analysis.

Although alternate techniques were considered, each was limited by atmospheric error, probably to a degree equivalent to that produced by fixture motion.

Also, at this time, it had become obvious that dynamic measurements, regardless of the technique employed, would be limited by the poor fiducial and dial image quality and the consequent large reading error. Therefore, after several remedial modifications to reduce the great circle fixture motion, a decision was made to conduct the dynamic pointing accuracy tests by utilizing the artificial star collimator and the following procedure was adopted.

AUTOCOLLIMATOR ON WEST PEDESTAL
MIRROR ON NORTH PEDESTAL

CHART SPEED: 1mm / SECOND OF TIME
CHART SCALE FACTOR = −3 1/2 mm / ARC SECOND

FIGURE 67. EFFECTS OF CINETHEODOLITE AZIMUTH ACCELERATIONS UPON GREAT CIRCLE PEDESTALS.

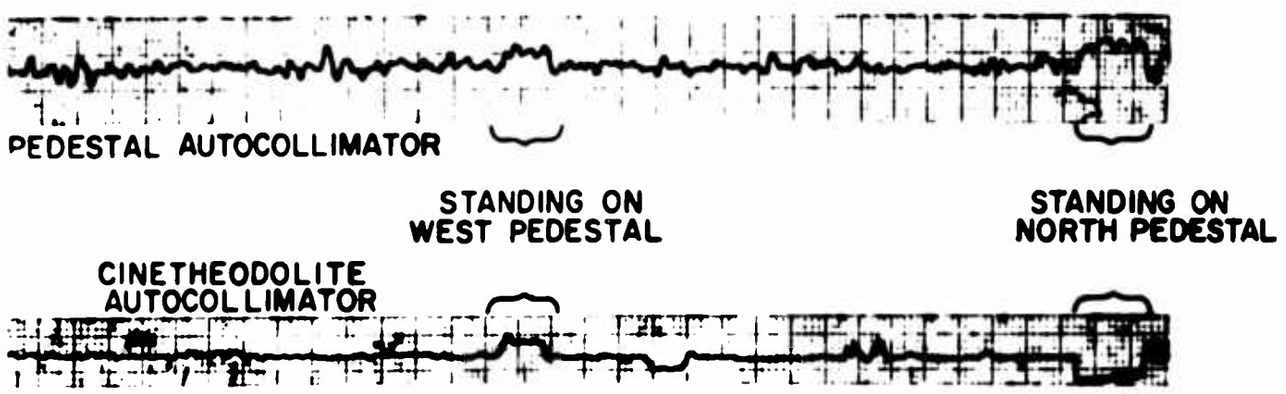

FIGURE 68. RECORDING OF CINETHEODOLITE AND PEDESTAL AUTOCOLLIMATORS, SHOWING MOTION CORRELATION.

CHART SPEED: 1 mm / SECOND
SCALE FACTOR: ≃ 0.4 ARC - SEC / mm

FIGURE 69. AUTOCOLLIMATOR RECORDING SHOWING NORMAL TURBULENCE.

CHART SPEED: 1 mm / SECOND
SCALE FACTOR: ≃ 0.4 ARC - SEC / mm

FIGURE 70. AUTOCOLLIMATOR RECORDING SHOWING INCREASED TURBULENCE.

Dynamic Test Procedure

In preparing to photograph the target (artificial star), the operator insures that it is in the field of view of the cinetheodolite optical system. To do this, a microscope is mounted in the camera to allow the operator to view the image plane. The cinetheodolite is very slowly rotated on its axes until the operator can see the target through the microscope. This is a time-consuming process, and consequently, the azimuth and elevation shaft angle encoder readings are carefully noted for future reference. The direction of the laser beam is now adjusted so that it strikes the small surface area of the photodiode which is mounted on the cinetheodolite telescope tube. This aligns the system so that the target is in the field of view of the cinetheodolite when the laser beam strikes the photodiode.

The first photograph for the dynamic pointing accuracy test is taken with the cinetheodolite at rest and pointed at the target collimator. Any necessary repositioning is accomplished by slowly moving the cinetheodolite in azimuth and elevation until the encoder readings agree with those previously recorded. A photographic plate is loaded into the camera, the camera shutter is opened, and a control signal is sent to the strobe circuits to trigger the dial, fiducial, data matrix and target flashlamps. The camera operator closes the shutter and advances the photographic plate to the next frame. The operator then locks the cinetheodolite in position in one axis and rotates the cinetheodolite a few degrees in the other axis. The laser is turned on and a signal is sent to the drive control system to move the cinetheodolite at the desired angular velocity or acceleration. As the target rapidly enters the field of view of the cinetheodolite, the laser beam strikes the surface of the photodiode, thus triggering the flashlamps. This is the dynamic exposure, and appears as the second frame on the plate. The mount is then returned to the original position and another static photograph is taken of the target. The dynamic test data consists of many photographic plates taken in the manner described above, each having a static, a dynamic, and a second static exposure. The parameters that are varied from test plate to test plate are the target position and angular acceleration or velocity of the cinetheodolite.

Temperature Tests

In order to determine the effects of temperature differentials upon elements critical to pointing accuracy, i.e., the 0° deviator and the penta prism assemblies thermocouples were installed at key points along the optical data train during the assembly of the instrument. Because of the sheltered nature of the optical elements and their close proximity only slight (<1°F) differentials were indicated in preliminary tests.

It was, therefore, decided to determine only the overall effect of changes in ambient temperature on the optical orientation of the theodolite and reserve the thermocouple measurements for diagnostic testing if needed.

The effects of temperature change were noted by determining the position of the azimuth and elevation index marks, and the major centroid of the four fiducial marks, with respect to one of the data matrix marks as shown in Figure 71. A comparison was then made of the positions of the marks on one photograph to the positions of the same marks on subsequent photographs. A data matrix mark was selected because this mark was completely independent of any effects of the optical orientation system.

A series of eight photographs, showing the location of the marks, was taken with the dome closed and the temperature at a constant 78° F. The dome was then opened and the sun was allowed to shine directly on the instrument. Fifteen minutes after the dome was opened, and when the temperature within the dome had begun to rise, another series of photographs was taken. The first set was taken in one-minute intervals; the second, in two-minute intervals; and the third, in three-minute intervals. The photographs were taken over a period of about 70 minutes and a temperature range that varied from 78° F to 95° F.

DATA ANALYSIS

Target Position Computation

The basic pointing and boresight error information for the WSMR Cinetheodolite is recorded on the film in the format shown in Figure 72. This data is made up of the elevation and azimuth numerical dial readings, the elevation index mark E, the azimuth index mark A, and the four fiducial marks F, G, H, and J. The information that allows the determination of the angular position of the cinetheodolite telescope tube is made up of the azimuth and elevation dial numerals and the position of the azimuth and elevation dial bars and index marks. The four fiducial marks further refine this information and allow the determination of the angular position of the actual photographic pointing axis. The distinction between the angular position of the telescope tube and the angular position of the photographic pointing axis is explained in the following paragraphs.

The numerical azimuth and elevation dial data is registered on the film in ten-arc-minute intervals. This data is displayed in Arabic numerals and can be read without any measurement. The lengths M_e and M_a, shown in Figure 72, represent ten-arc-minute segments of the instrument azimuth and elevation dials. In order to measure the length M_e or M_a, the vertical centerline of each of the dial bars must be determined. The centroid of the set of dial bars on the left side and the centroid of the set of dial bars on the right side of the numerical dial recording are determined. Having located these centroids, the lengths M_e and M_a can be determined by measuring the distance between them. A line through the centroids of the index marks intercepts the lines M_e and M_a at the lengths N_e and N_a from the centroid of the left-hand set of dial bars. This line is the V-axis of the film format. The quotients N_e/M_e and N_a/M_a represent the fractions

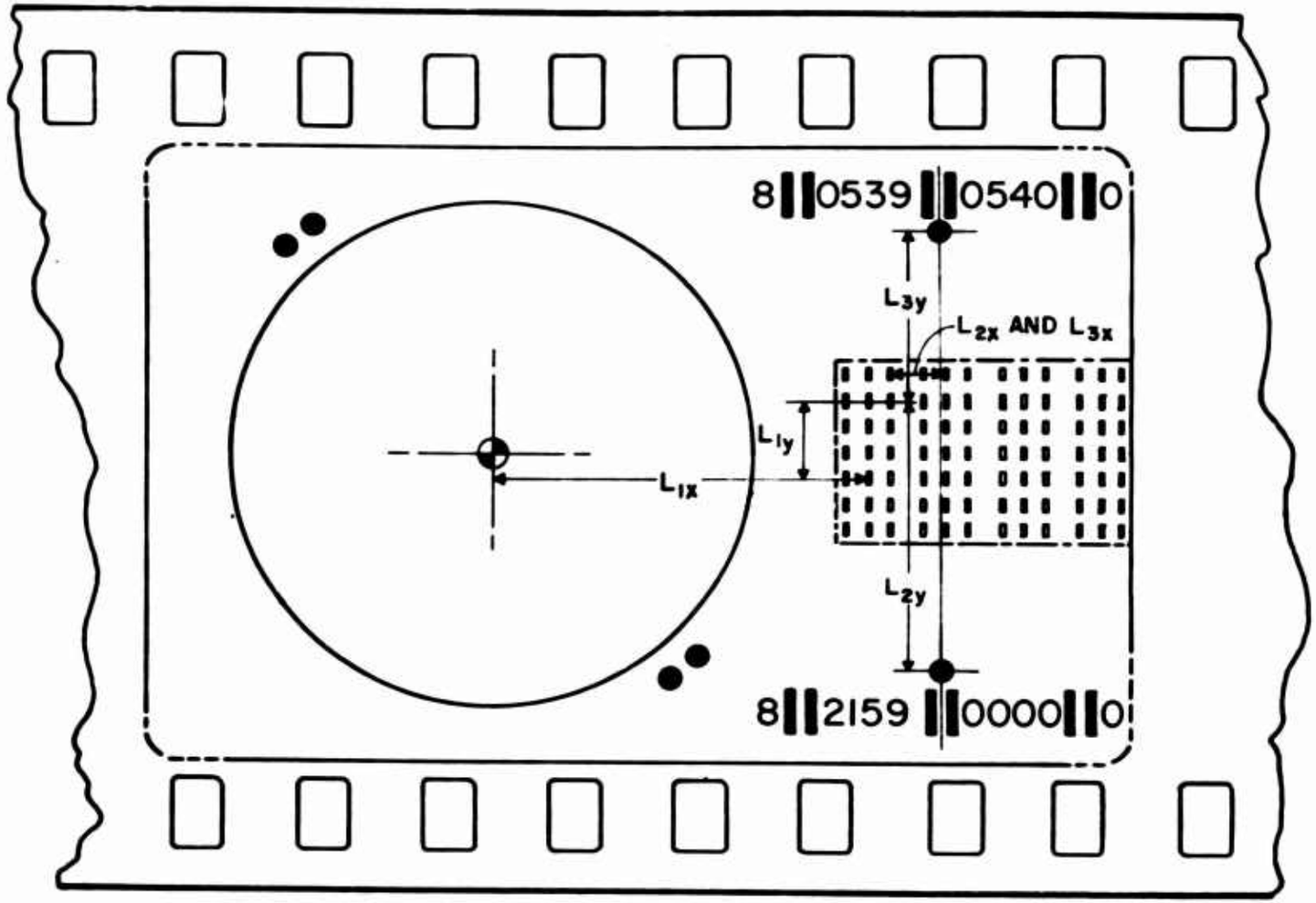

FIGURE 71. WSMR CINETHEODOLITE DATA FORMAT (TEMPERATURE TEST)

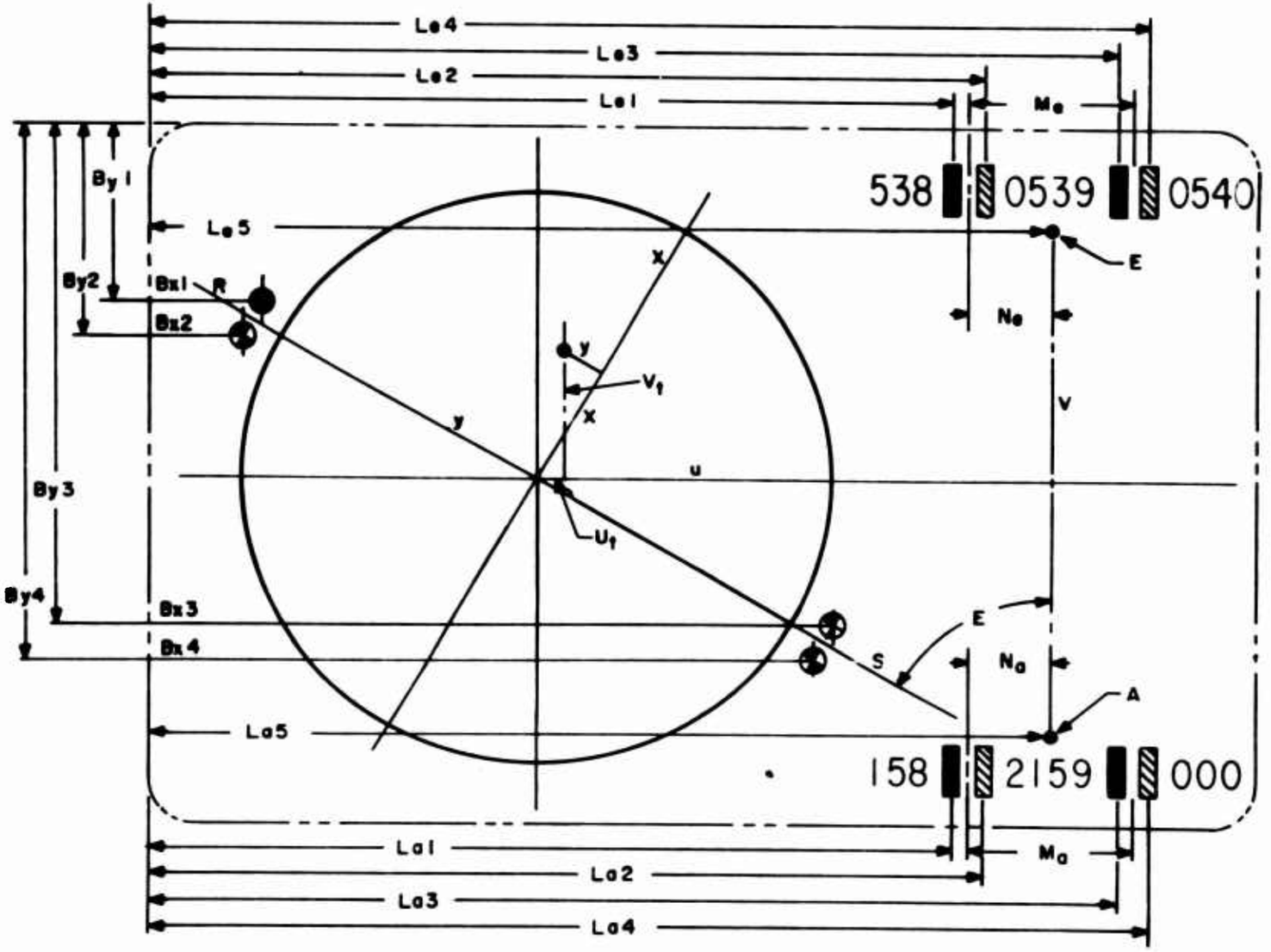

FIGURE 72. DATA FORMAT

of ten arc-minutes that must be added to the numerical dial readings. These angular measurements give the orientation of the cinetheodolite telescope tube with respect to an arbitrary coordinate system that must be ultimately referenced to WSMR range coordinates.

Location of the four fiducial marks F, G, H, and J enables a determination of the intersection of the photographic pointing axis with the film format. First, the centroid of each fiducial mark is located with respect to the U- and V-axis of the film format as shown in Figure 72. By locating the centroid of each fiducial mark, the centroid of the four fiducial mark system is located and a line R-S, through it at an angle E with the V-axis, indicates a true vertical or the Y-direction in the film plane. Angle E is the elevation angle determined earlier from the elevation dial and elevation index. Data measurement of the boresight error in X and Y, as shown in Figure 72, can now be performed. The mathematical details of the calculations referred to above are given in Appendix B. The total azimuth and elevation angles define the position of the target with respect to the instrument.

The data presented on each frame of the test plates is the same for the static and the dynamic tests, except that in the first case, the target photographed is a star, and in the other the target is collimated light from a flashlamp.

The data plates were read on a Mann Comparator by personnel of the Physical Science Laboratory of New Mexico State University. Each data point was read five times and the average of these was used in the computation described in Appendix B.

Some problems arose in reducing the data when it was noted that the field of view for the dial images was not large enough for three sets of bars, as was shown in Figure 34. Quite frequently during the star tests, only one full set of bars appeared in the format, and a considerable number of plates turned out to be useless. This condition did not occur during the dynamic tests because the operator could preselect the position of the mount. Accurate reading of the data points was difficult because the images were not very sharply defined. Further discussion of the reading error problem is given below.

Reading Error

As stated before, one of the principal original objectives of the WSMR Cinetheodolite test and evaluation program was to determine the precise magnitude of the static and dynamic pointing errors. It was desired to derive these magnitudes to an accuracy of half an arc-second. A simple test showed, however, that this objective was unrealistic, with the poor image quality of the points being read. The test consisted of reading a

complete set of plates computing the pointing errors, then rereading the plates and recomputing the pointing errors independently. Table XIV shows these errors and computations on the differences between Reading 1 and Reading 2. The overall average difference between the two sets of pointing errors was 1.43 arc-seconds vertically and 1.94 arc-seconds horizontally. Figure 73 shows the spread of the differences in the form of a histogram.

It was later decided that the plate reading accuracy might be increased by changing the order of reading the various points on each plate. Fifteen different points (illustrated in Figure 74) were to be measured on each frame, using the Mann Comparator. Previously, each point was read five times in succession before proceeding to the next point. It was suggested that with this method (Method 1) the operator unconsciously tended to remember where and how the reticle of the comparator crossed the photographic image, and that this fact influenced the readings and effectively eliminated the statistical advantage of multiple readings.

In the proposed method of delayed repetition (Method 2), a single measurement was to be taken on each of the 15 points in sequence. This procedure was to be repeated four more times so that each of the 15 points was measured a total of five times. The strength of this alternate procedure was supposed to lie in presenting the operator with a relatively unfamiliar photographic image each time he made a measurement. With a series of readings to be made before any repetition, it was considered unlikely that the operator would remember any particular reticle/image pattern that would tend to bias him on succeeding measurements.

Four plates were used in the test to compare the two methods. Three, considered to be of medium quality (#07, #10, #11), were selected from the regular test plates, and the fourth was an "ideal" plate made by photographing a precise drawing. This drawing was scaled from the existing data format. The sizes of the fiducial images and the dial bars were made precisely to scale. Therefore, the only difference between a regular plate and the "ideal" plate was the image quality.

Each of the three regular test plates was read by a different person, all of whom were experienced in reading photographic plates on the Mann Comparator. The following general procedure was used.

1. The operator read the first frame of his plate using Repetition Method 1.

2. He then removed the plate and put it back on the comparator stage so as to give it a new arbitrary orientation on the instrument.

3. He repeated steps 1 and 2 until the frame had been read three times. This resulted in data for three complete frames, which was later reduced by the regular computer program for dynamic plates. However, since

TABLE XIV. READING ERROR COMPUTATION

	Horizontal Arc Sec			
N	Reading 1 Horiz	Reading 2 Horiz	ΔH (1-2)	ΔH^2
1	0.87	1.93	-1.06	1.12
2	11.21	11.35	-0.14	0.02
3	-9.19	-6.35	-2.84	8.07
4	-4.80	-2.45	-2.35	5.52
5	-6.22	-6.99	0.77	0.59
6	-5.72	-5.42	-0.30	0.09
7	4.07	3.34	0.73	0.53
8	-0.68	0.65	-1.33	1.77
9	0.01	0.77	-0.76	0.58
10	-0.05	-0.79	0.74	0.55
11	4.11	0.89	3.22	10.37
12	-0.24	-0.30	0.06	0.00
13	-4.29	-1.19	-3.10	9.61
14	0.49	2.10	-1.61	2.59
15	-2.44	-0.75	-1.69	2.86
16	-1.73	-0.71	-1.02	1.04
17	-0.88	-0.01	-0.87	0.76
18	-1.82	-1.87	0.05	0.00
19	-0.37	0.51	-0.88	0.77
20	-0.67	-2.78	2.11	4.45
21	0.66	-0.24	0.90	0.81
22	2.41	1.04	1.37	1.88
23	2.48	2.22	0.26	0.07
24	-6.21	-5.23	-0.98	0.96
25	-2.78	-2.58	-0.20	0.04
26	0.16	0.27	-0.11	0.01
27	-0.19	-0.58	0.39	0.15
28	-1.71	-2.55	0.84	0.71
29	-1.01	0.02	-1.03	1.06
30	-0.81	-1.31	0.50	0.25
31	-1.61	-1.06	-0.55	0.30
32	1.31	1.21	0.10	0.01
33	-3.81	-3.85	0.04	0.00
34	-0.88	-0.12	-0.76	0.58
35	-0.42	1.10	-1.52	2.31
36	-1.27	-1.57	0.30	0.09
37	14.94	15.16	-0.22	0.05

TABLE XIV. READING ERROR COMPUTATION (Cont'd)

	Horizontal Arc Sec			
N	Reading 1 Horiz	Reading 2 Horiz	ΔH (1-2)	ΔH^2
38	11.24	13.32	-2.08	4.33
39	-6.21	-4.29	-1.92	3.69
40	-2.07	-2.46	0.39	0.15
41	-3.91	-4.98	1.07	1.14
42	-5.95	-3.80	-2.15	4.62
43	2.20	1.85	0.35	0.12
44	-3.01	-2.78	-0.23	0.05
45	0.48	1.83	-1.35	1.82
46	1.11	-0.50	1.61	2.59
47	0.31	-1.32	1.63	2.66
48	-1.18	-2.44	1.26	1.59
49	-4.13	0.35	-4.48	20.07
50	-5.66	-3.46	-2.20	4.84
51	-2.92	-0.84	-2.08	4.33
52	-3.69	-4.30	0.61	0.37
53	0.40	0.11	0.29	0.08
54	-3.74	-3.18	-0.56	0.31
55	0.85	1.41	-0.56	0.31
56	-1.22	-0.31	-0.91	0.83
57	-0.12	-0.07	-0.05	0.00
58	-2.11	-3.37	1.26	1.59
59	2.12	0.85	1.27	1.61
60	-4.63	-3.78	-0.85	0.72
61	1.73	0.34	1.39	1.93
62	2.51	2.20	0.31	0.10
63	0.46	0.97	-0.51	0.26
64	-0.58	-1.81	1.23	1.51
65	-1.93	-0.97	-0.96	0.92
66	1.34	1.22	0.12	0.01
67	-3.59	0.55	-4.14	17.14
68	1.90	2.58	-0.68	0.46
69	-1.75	-1.18	-0.57	0.32
70	1.35	2.87	-1.52	2.31
71	-1.31	0.61	-1.92	3.69
72	-0.67	-0.91	0.24	0.06

TABLE XIV. READING ERROR COMPUTATION (Cont'd)

	Vertical Arc Sec			
N	Reading 1 Vert	Reading 2 Vert	ΔH (1-2)	ΔH^2
1	-2.26	-2.40	0.14	0.02
2	1.49	1.49	0.00	0.00
3	4.64	0.29	4.35	18.92
4	-0.49	1.16	-1.65	2.72
5	4.11	-0.18	4.29	18.40
6	0.64	1.78	-1.14	1.30
7	4.06	1.21	2.85	8.12
8	4.32	2.46	1.86	3.46
9	-1.02	-1.24	0.22	0.05
10	-0.87	0.29	-1.16	1.35
11	4.87	2.59	2.28	5.20
12	-2.63	0.21	-2.84	8.07
13	0.29	-1.76	2.05	4.20
14	3.81	2.45	1.36	1.85
15	4.01	4.99	-0.98	0.96
16	2.48	1.31	1.17	1.37
17	2.46	0.21	2.25	5.06
18	0.82	3.41	-2.59	6.71
19	3.34	3.19	0.15	0.02
20	0.12	0.59	-0.47	0.22
21	4.03	0.24	3.79	14.36
22	-0.39	-1.67	1.28	1.64
23	1.86	3.64	-1.78	3.17
24	-7.15	-2.40	-4.75	22.56
25	-1.47	-3.82	2.35	5.52
26	-1.05	-0.38	-0.67	0.45
27	-1.33	-1.95	0.62	0.38
28	1.83	2.93	-1.10	1.21
29	-3.80	-4.31	0.51	0.26
30	4.01	1.61	2.40	5.76
31	-2.70	-0.84	-1.86	3.46
32	-3.13	-5.35	2.22	4.93
33	0.50	0.20	0.30	0.09
34	-5.06	-3.16	-1.90	3.61
35	-4.14	-3.41	-0.73	0.53
36	1.36	0.98	0.38	0.14
37	-2.90	-3.43	0.53	0.28
38	0.16	2.72	-2.56	6.55

TABLE XIV. READING ERROR COMPUTATION (Cont'd)

	Vertical Arc Sec			
N	Reading 1 Vert	Reading 2 Vert	ΔH (1-2)	ΔH^2
39	4.86	2.06	2.80	7.84
40	5.40	2.20	3.20	10.24
41	1.71	-1.31	3.02	9.12
42	0.49	0.03	0.46	0.21
43	0.06	-1.47	1.53	2.34
44	2.28	1.40	0.88	0.77
45	1.01	0.36	0.65	0.42
46	-0.62	-1.39	0.77	0.59
47	-1.12	1.69	-2.81	7.90
48	-3.03	0.35	-3.38	11.42
49	2.56	1.89	0.67	0.45
50	-1.17	0.18	-1.35	1.82
51	3.66	2.70	0.96	0.92
52	-0.30	-0.78	0.48	0.23
53	1.83	-1.07	2.90	8.41
54	-0.04	-0.64	0.60	0.36
55	1.40	3.27	-1.87	3.50
56	0.27	1.88	-1.61	2.59
57	2.06	1.38	0.68	0.46
58	-0.60	-1.90	1.30	1.69
59	0.89	1.91	-1.02	1.04
60	-9.35	-6.05	-3.30	10.89
61	0.10	-2.26	2.36	5.57
62	-2.04	-0.68	-1.36	1.85
63	-3.82	-3.27	-0.55	0.30
64	-0.20	-1.08	0.88	0.77
65	-2.27	-2.45	0.18	0.03
66	4.60	3.38	1.22	1.49
67	1.36	-0.24	1.60	2.56
68	-3.30	-4.08	0.78	0.61
69	-0.18	1.64	-1.82	3.31
70	-0.60	-0.61	0.01	0.00
71	-1.90	0.62	-2.52	6.35
72	3.20	2.36	0.84	0.71

$$\sigma_H = \sqrt{\frac{\Sigma \Delta H^2}{N}} = 1.42951 \qquad \sigma_V = \sqrt{\frac{\Sigma \Delta V^2}{N}} = 1.93543$$

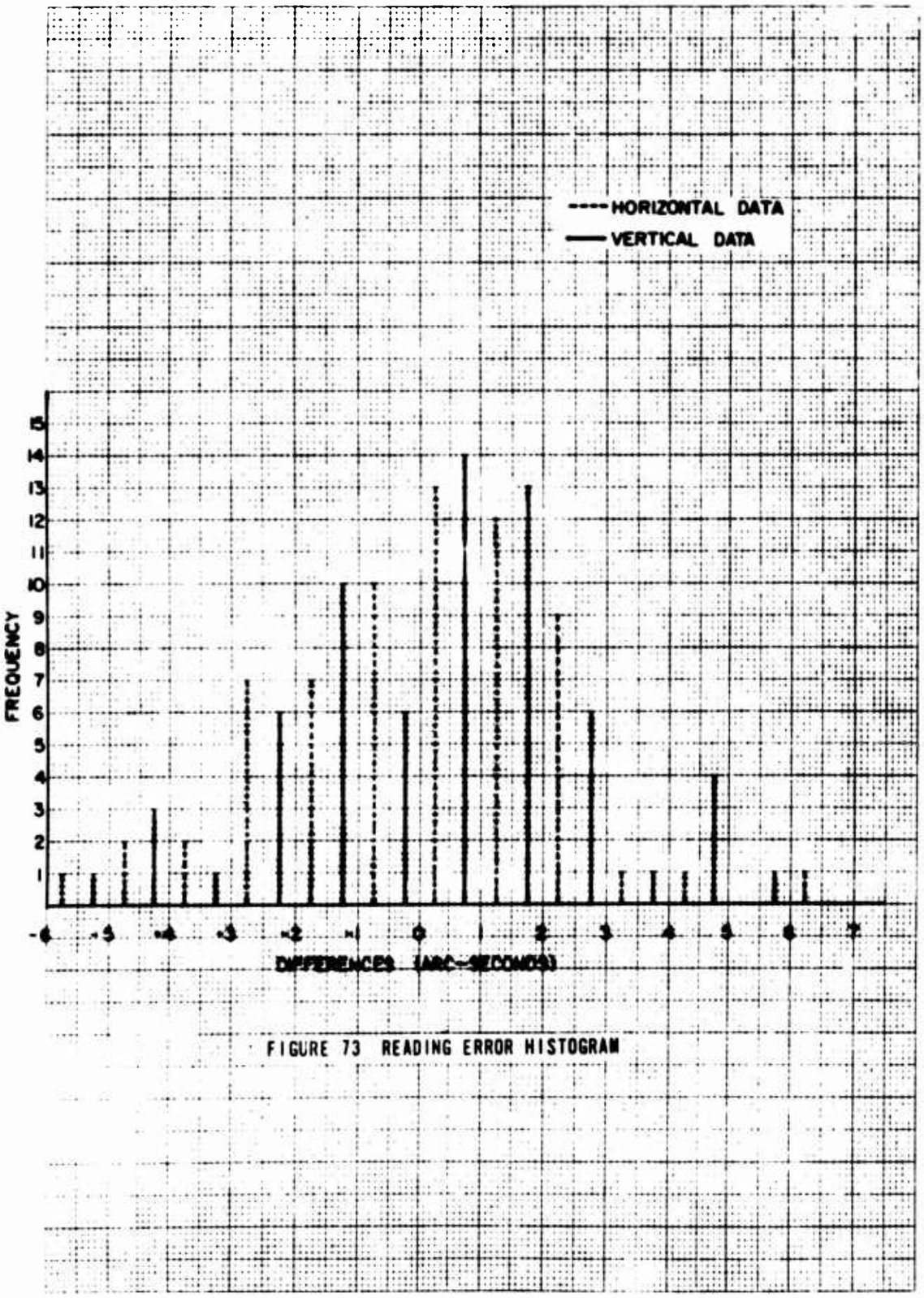

FIGURE 73 READING ERROR HISTOGRAM

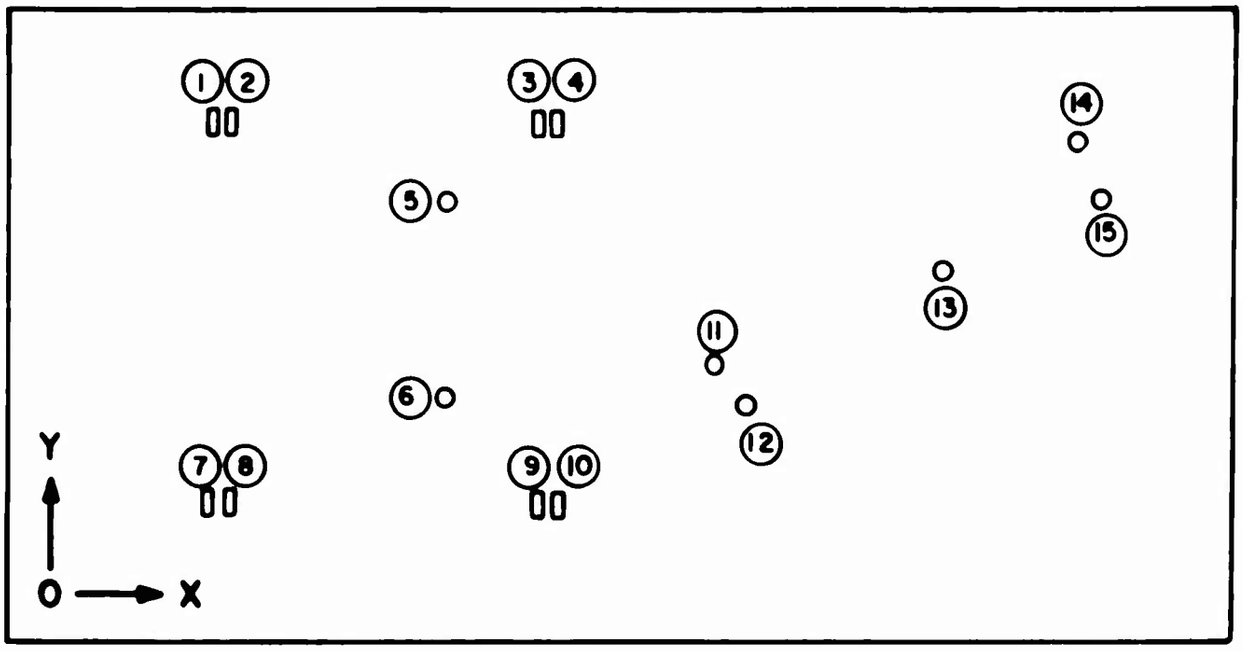

FIGURE 74 MEASUREMENT POINTS ON EACH FRAME

the same frame was read, all true static and dynamic errors would be zero, and the reduced data would represent only the reading error component of the data derived from a typical dynamic plate. The plate reading procedure continued as follows.

4. The operator repeated steps 1, 2, and 3 on Frame 2 of his plate, and then on Frame 3.

5. He then switched from Method 1 to Method 2 and went through steps 1 through 4 again on the same plate.

6. Finally, he read the ideal plate, going through steps 1, 2, and 3, but omitting step 4, since the ideal plate contained only one frame of data. Two of the operators used both methods of repetition on the ideal plate, but Operator 1, for unknown reasons, used only Method 2.

Table XV and Figure 75 give the reduced data in seconds of arc and indicate that Method 2 resulted in a lower error for only one plate, while Method 1 was the best for the other two plates. It can be seen that the reading error for these plates was still in the neighborhood of two arc-seconds. For the ideal plate, it was found that the errors were somewhat lower. The reduced data is given in Table XVI and plotted in Figure 76.

Throughout the WSMR Cinetheodolite development program, it has been realized that automatic film reading would be a requirement for an operational cinetheodolite system because of the large number of points in the dial and fiducial film format that must be accurately read. That the excessive reading error previously discussed could have been greatly reduced by employment of an automatic film reader is, of course, speculation. The readability of dynamic test plate No. 0012, Frame 3, by an automatic reader may be assessed by examination of the microdensitometer trace shown in Figure 77. It is certain that the number of readings per point could, with automatic reading, have been increased with a consequent increase in the quality of the statistical data.

Dynamic Test Results

As described in the dynamic test procedure, each photographic plate contains three photographs of the same fixed target. The first frame is a static exposure, the second a dynamic, and the third is another static exposure. After developing, the plates are read to obtain the X and Y positions of all data points on each frame. A sample of the raw data from these readings is presented in Table XVII. This raw data is then used to compute (1) the target position in all three frames, (2) the target positional difference between the first and second frame, and (3) the target positional difference between the first and third frame.

TABLE XV. DIFFERENCES AMONG THREE READINGS OF SAME FRAME

Method	Operator	Plate	Frame	D.H.	D.V.	S.H.	S.V.	AVG.
1	1	07	1	1.60	3.98	-0.90	3.69	
1	1	07	2	-1.48	2.83	-1.17	2.60	2.16
1	1	07	3	-1.42	4.09	0.17	2.05	
2	1	07	1	2.89	1.03	0.71	0.30	
2	1	07	2	0.78	1.96	0.59	-1.94	1.81
2	1	07	3	2.44	8.29	0.41	0.43	
1	2	10	1	0.91	0.66	-1.53	-0.79	
1	2	10	2	0.04	0.44	1.69	2.59	1.15
1	2	10	3	-1.07	1.79	0.56	1.70	
2	2	10	1	2.03	2.95	1.85	1.78	
2	2	10	2	3.29	2.23	2.19	0.23	1.99
2	2	10	3	2.33	2.28	0.47	2.22	
1	3	11	1	-0.90	3.02	-0.09	2.19	
1	3	11	2	-1.86	2.20	-0.25	-1.49	1.23
1	3	11	3	-0.16	2.12	0.09	-0.39	
2	3	11	1	-0.59	4.97	-0.09	1.88	
2	3	11	2	-0.36	4.39	1.10	3.12	2.27
2	3	11	3	-4.39	2.26	-2.37	-1.77	

DH = Second reading minus first reading of a frame (horizontal component).

DV = Second reading minus first reading of a frame (vertical component).

SH = Third reading minus first reading of a frame (horizontal component).

SV = Third reading minus first reading of a frame (vertical component).

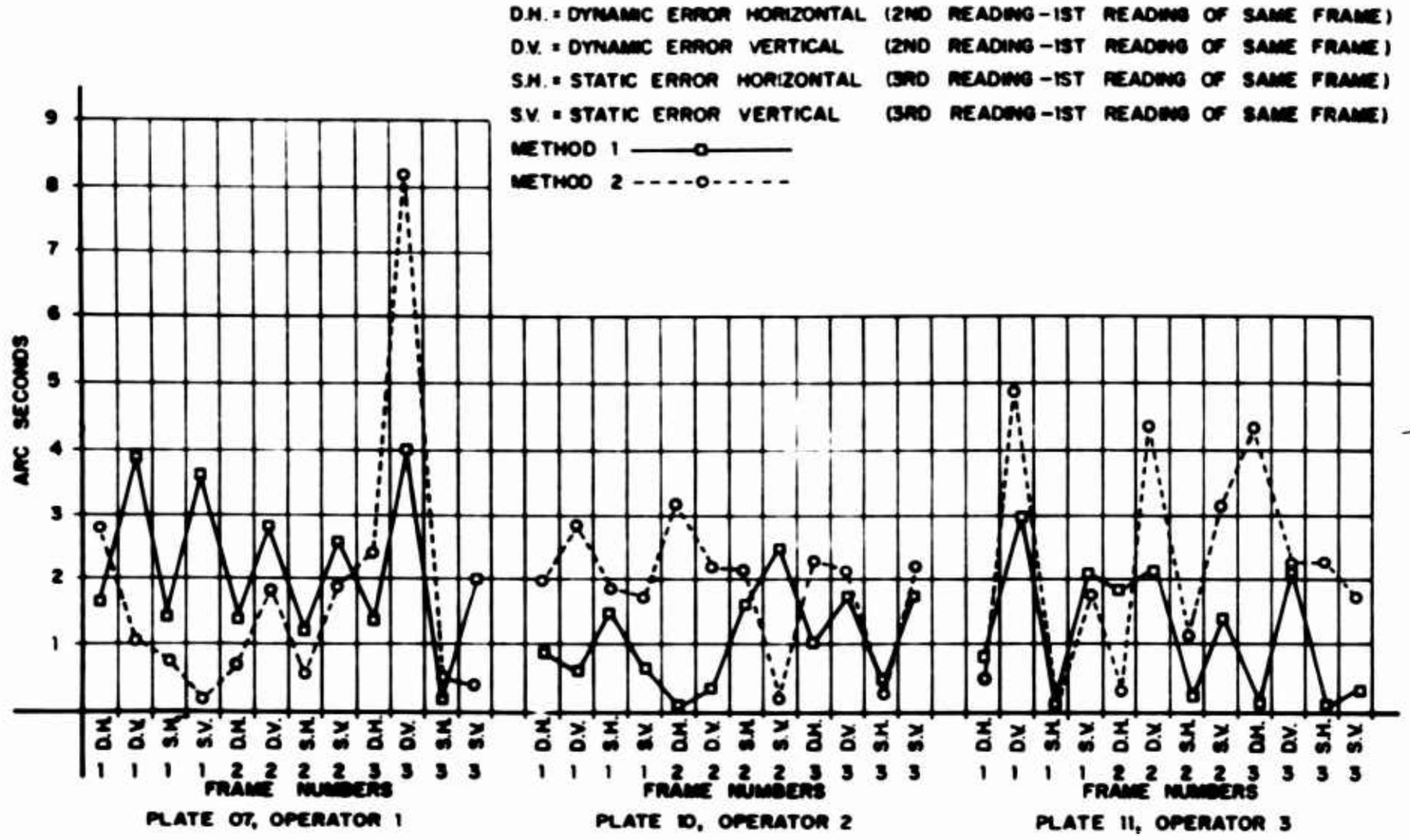

FIGURE 75. NUMERICAL DIFFERENCE BETWEEN READINGS OF THE SAME FRAME

TABLE XVI. ERRORS OF THREE READINGS FROM FRAME 1 OF THE IDEAL PLATE

Method	Operator	Plate	D.H.	D.V.	S.H.	S.V.
2	1	00	-1.16	0.23	-0.67	0.65
1	2	00	1.14	-0.61	2.03	-0.70
2	2	00	-0.19	1.35	1.13	0.75
1	3	00	0.30	-1.20	0.32	1.27
2	3	00	0.09	-0.59	-0.10	-0.28

DH = Second reading of frame 1 minus first reading of frame 1.

DV = Second reading of frame 1 minus first reading of frame 1.

SH = Third reading of frame 1 minus first reading of frame 1.

SV = Third reading of frame 1 minus first reading of frame 1.

THE IDEAL FRAME IS A PHOTOGRAPH OF A DRAWING

D.H. = DYNAMIC ERROR HORIZONTAL (2ND READING – 1ST READING OF THE ONE FRAME)

D.V. = DYNAMIC ERROR VERTICAL (2ND READING – 1ST READING OF THE ONE FRAME)

S.H. = STATIC ERROR HORIZONTAL (3RD READING – 1ST READING OF THE ONE FRAME)

S.V. = STATIC ERROR VERTICAL (3RD READING – 1ST READING OF THE ONE FRAME)

METHOD 1 ——o——

METHOD 2 - - - -o- - - -

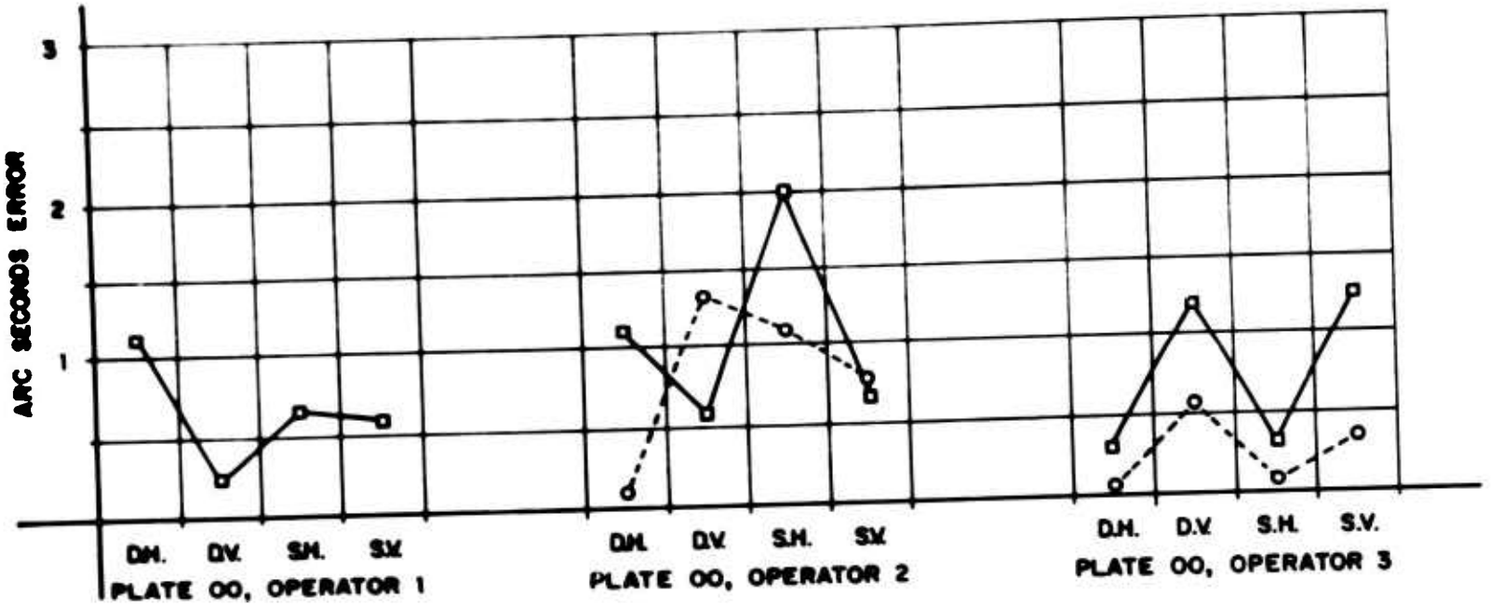

FIGURE 76. NUMERICAL DIFFERENCE BETWEEN READINGS FOR THE IDEAL FRAME

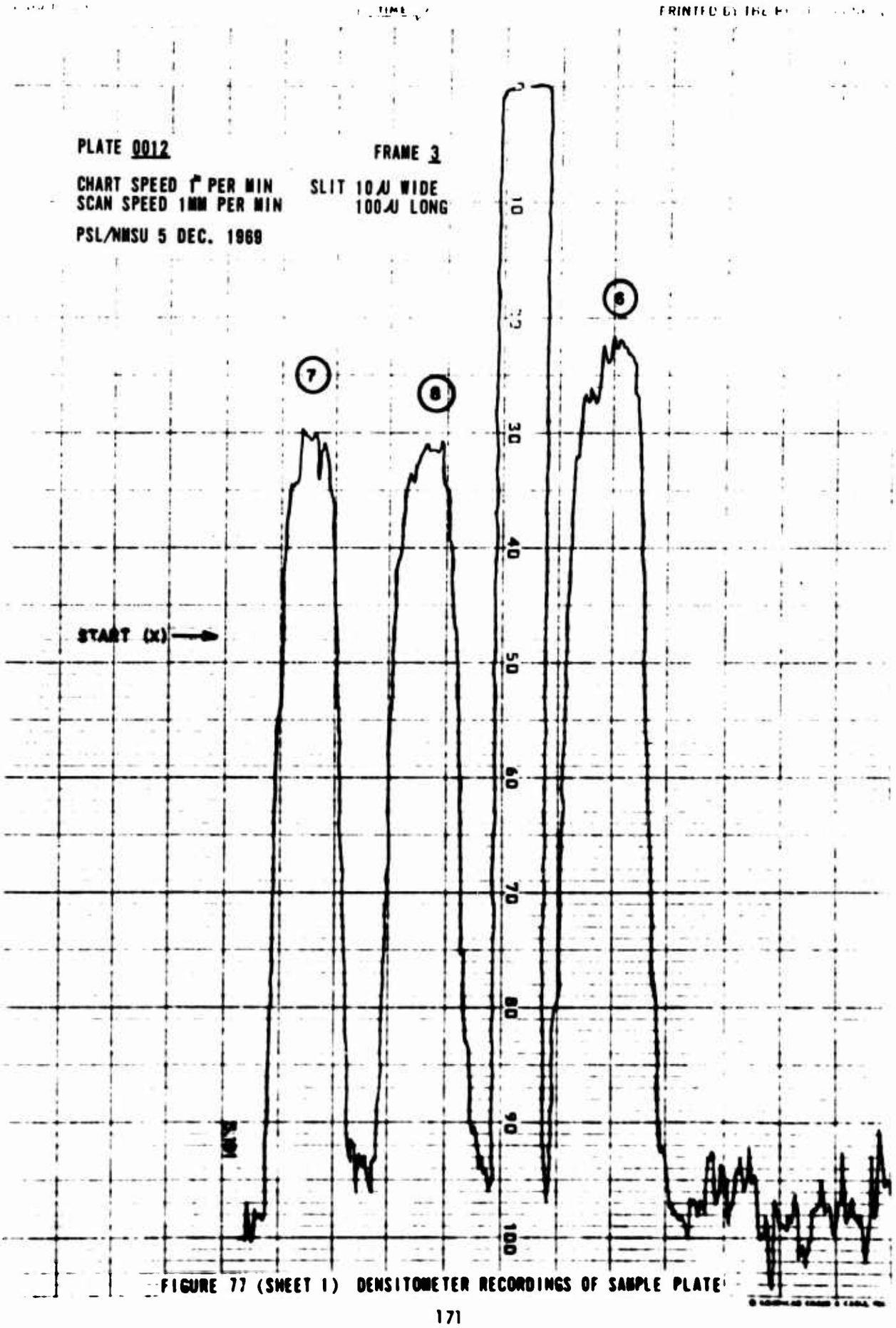

FIGURE 77 (SHEET 1) DENSITOMETER RECORDINGS OF SAMPLE PLATE

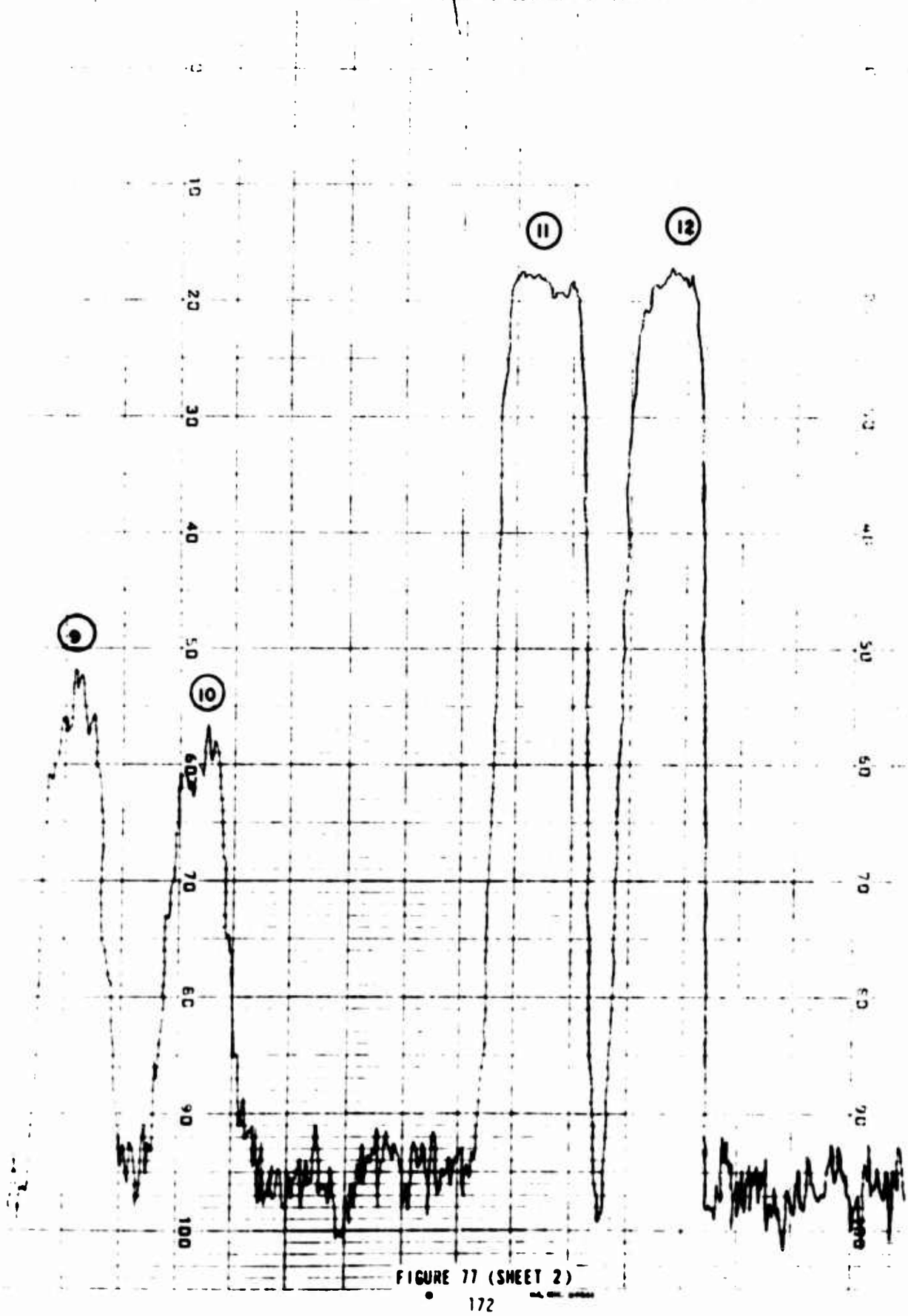

FIGURE 77 (SHEET 2)

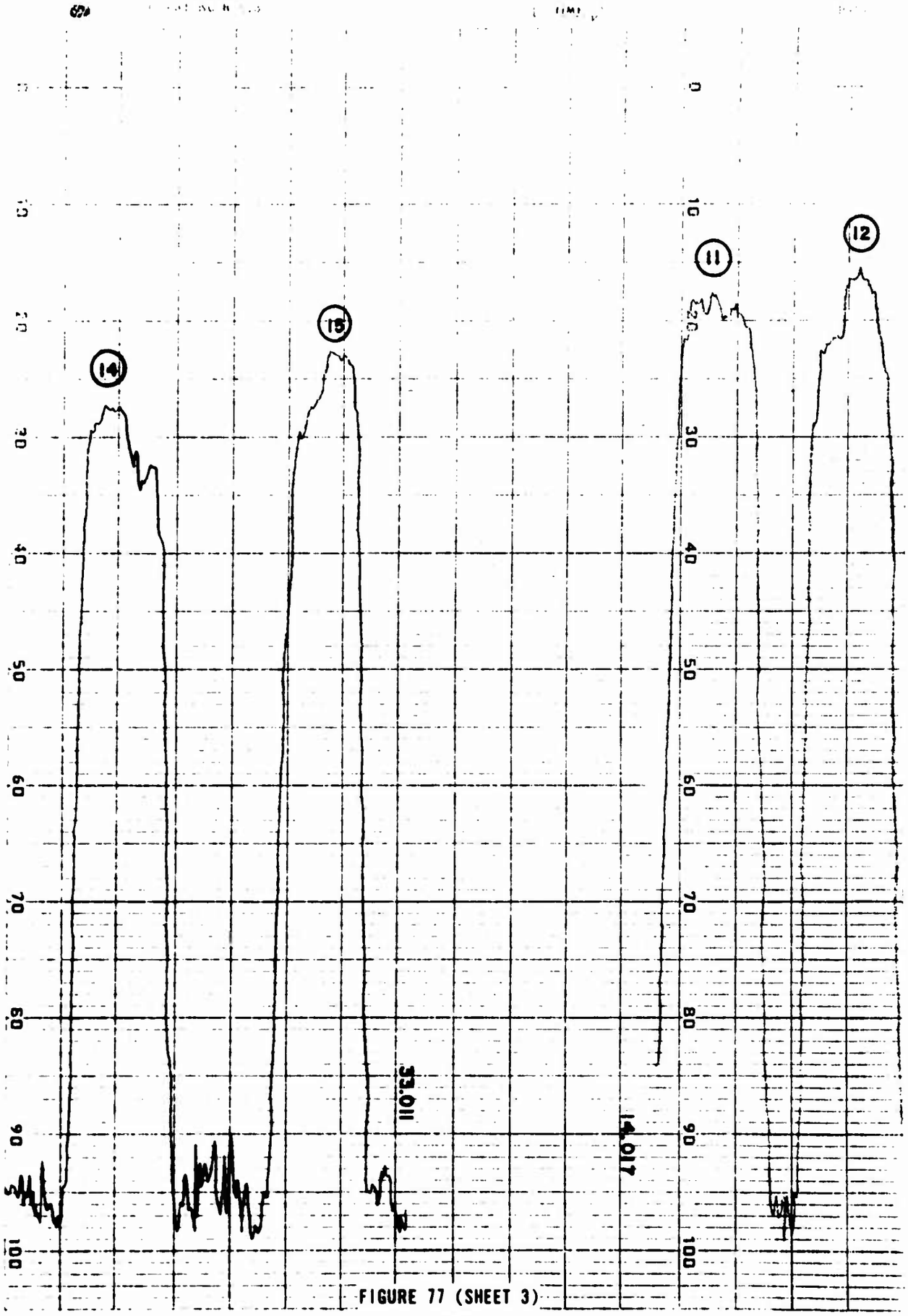

FIGURE 77 (SHEET 3)

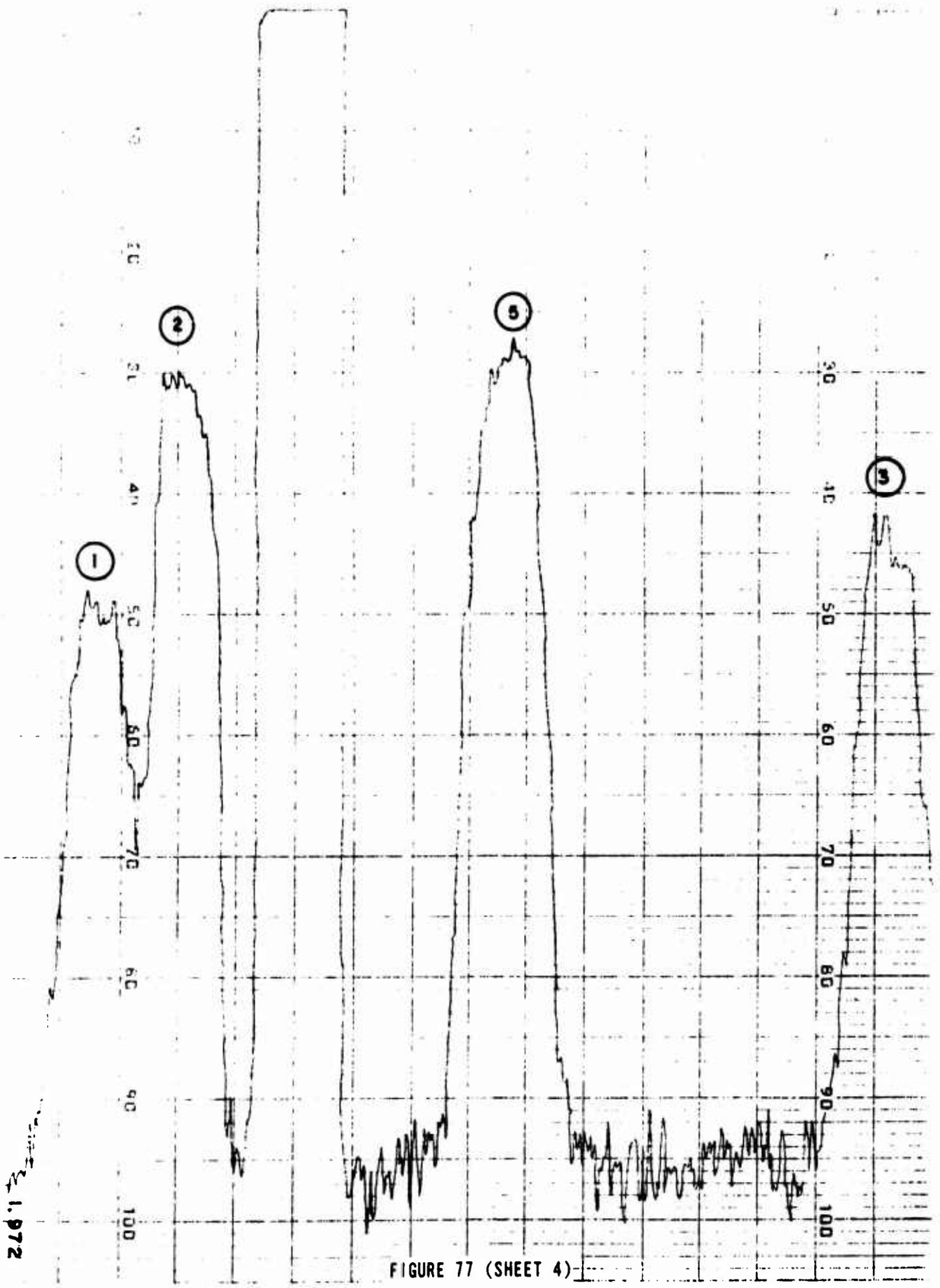

FIGURE 77 (SHEET 4)

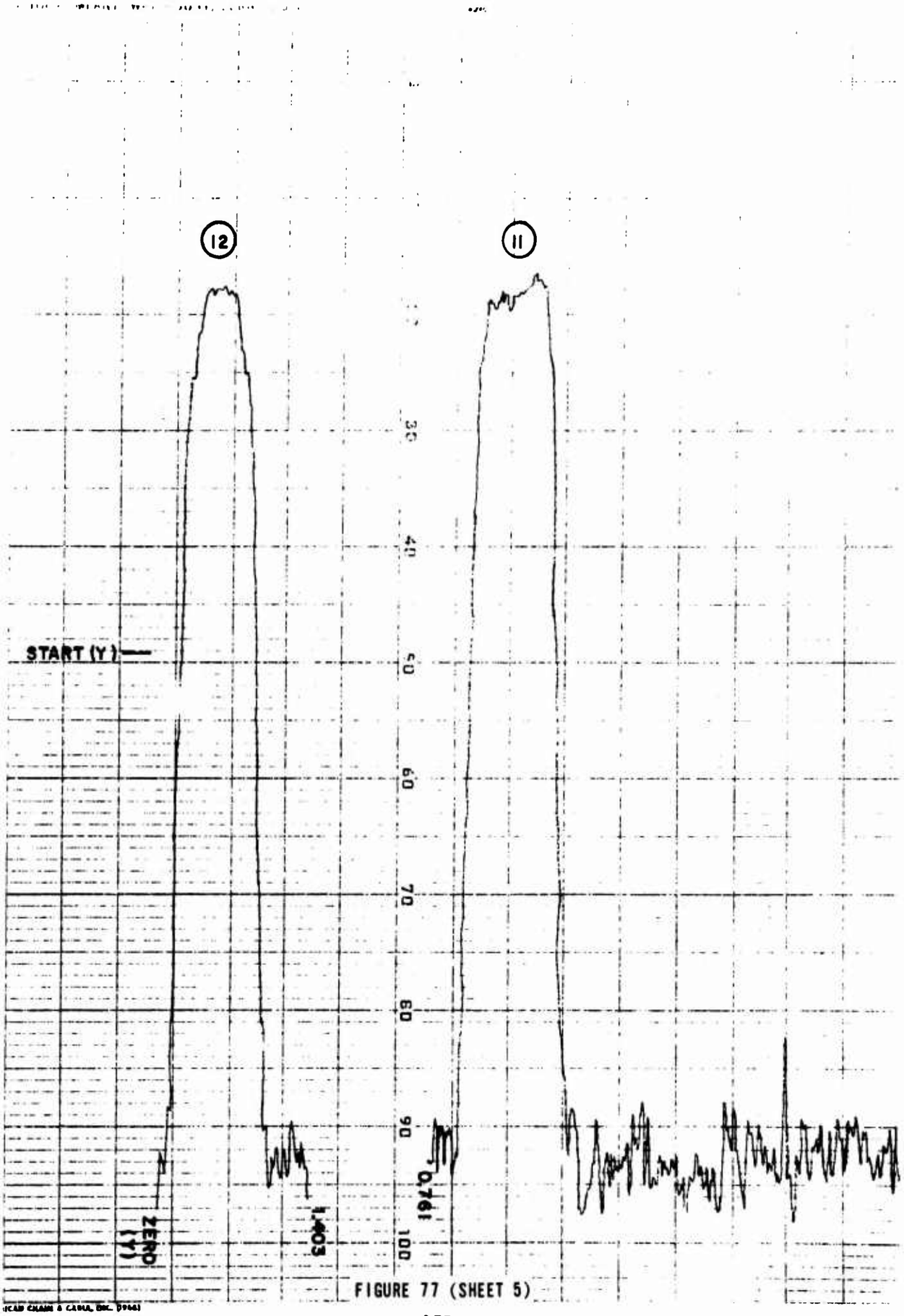

FIGURE 77 (SHEET 5)

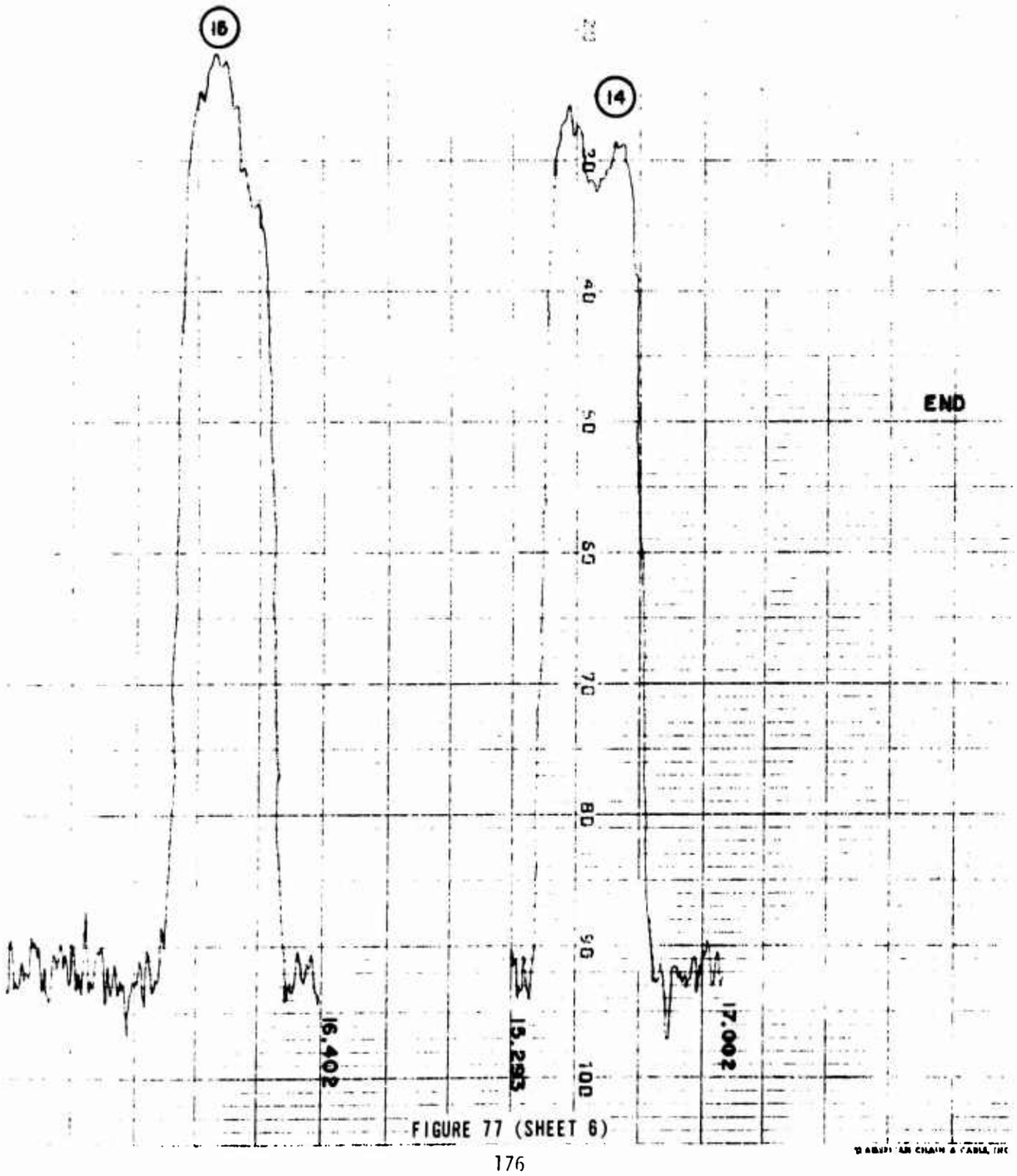

FIGURE 77 (SHEET 6)

TABLE XVII. DYNAMIC PLATE READINGS

PLATE LE0002 FRAME 1 STATIC, FRAME 2 5DEG/SEC, FRAME 3 STATIC

PLATE SHOT ON 04 NOV 68 TIME = 0 SECONDS Z FOR FRAME NUMBER 1

815.

14.08700	14.85800	20.90900	21.68700	18.10500	133.25200	
14.09400	14.86800	20.91500	21.69600	18.09600	133.25000	
14.09800	14.87300	20.91600	21.69000	18.09500	133.25500	
14.08100	14.86800	20.92200	21.68500	18.09800	133.26100	
14.07900	14.85900	20.94300	21.67300	18.10700	133.25800	LAST

104.

16.18600	17.24600	23.06700	24.20800	18.13200	150.45500	
16.17900	17.25500	23.09500	24.22000	18.13900	150.46000	
16.18800	17.24600	23.11900	24.20200	18.12600	150.45800	
16.18600	17.25300	23.11200	24.19600	18.11500	150.45200	
16.16400	17.24300	23.117000	24.18100	18.12000	150.45300	LAST
26.47600	27.61200	42.30400	44.18300	33.35900	-0.	
26.46200	27.61200	42.30500	44.18100	33.37500	-0.	
26.45700	27.62100	42.30700	44.18000	33.36800	-0.	
26.45600	27.63200	42.30800	44.18100	33.36400	-0.	
26.45200	27.61900	42.30600	44.19000	33.36500	-0.	LAST
148.74100	149.74900	134.4400	134.66400	142.02500	-0.	
148.74000	149.74600	134.44200	134.68000	142.02300	-0.	
148.74100	149.75100	134.44100	134.68700	142.02000	-0.	
148.74900	149.74300	134.43900	134.68200	142.02000	-0.	
148.75300	149.74200	134.43600	134.68100	142.02100	-0.	LAST
129.06500	129.06500	129.06500	129.06500	-0.	-0.	
129.06500	129.06500	129.06500	129.06500	-0.	-0.	
129.06500	129.06500	129.06500	129.06500	-0.	-0.	
129.06500	129.06500	129.06500	129.06500	-0.	-0.	
129.06500	129.06500	129.06500	129.06500	-0.	-0.	LAST
151.33900	151.33900	151.33900	151.33900	-0.	-0.	
151.33900	151.33900	151.33900	151.33900	-0.	-0.	
151.33900	151.33900	151.33900	151.33900	-0.	-0.	
151.33900	151.33900	151.33900	151.33900	-0.	-0.	
151.33900	151.33900	151.33900	151.33900	-0.	-0.	LAST

Ideally, the difference between the first and second frame would be a measurement of dynamic error, but it includes reading errors and target positional errors due to fixture motion. Therefore, the difference between the first and third frames is used as a measure of random contributions to the dynamic error.

A series of tests was conducted at a fixed elevation angle of 45°. The data from tests with different dynamic conditions were analyzed separately. The four dynamic conditions were (1) elevation axis moving upward, (2) elevation axis moving downward, (3) azimuth axis moving clockwise, and (4) azimuth axis moving counterclockwise. Nearly all of the data presented are for dynamic conditions with the greatest angular acceleration that the mount servos were capable of producing.

The data were analyzed by two statistical techniques: (1) t-tests for differences between means and (2) one-way analysis of variance for fixed effects (also differences between means). All of the information available about the possible effects of instrument dynamics on pointing is contained in the differences between pointing angles computed from the second and first frames. These differences are labeled D_i. A parallel piece of information, which comes, however, from only static observations, is the difference in pointing angles computed from the third and first frames. These differences are labeled S_i. The other symbols to be used in the discussion are defined as follows:

m - sample mean (may be subscripted S or D for static, dynamic, respectively.

s^2 - sample variance (may be similarly subscripted).

N - number of observations within a sample.

F - F-statistic.

t - t-statistic.

To test the hypothesis that the means of two normal distributions are equal, assuming that the standard deviations are equal, but unknown, the appropriate statistic is

$$t = \sqrt{N}\,\frac{m_D - m_S}{\sqrt{s_D^2 + s_S^2}}$$

(see Reference 8). To test the hypothesis that the standard deviations of two normal distributions are equal, the appropriate statistic is

$$F = \frac{s_D^2}{s_S^2}$$

The one-way analysis of variance procedure is described in Reference 8. The quantities which are computed are listed below.

SS_3^* - mean square value of the "between treatment" means, i.e., mean square value of the dynamic and static mean values.

SS_2^* - mean square value "within treatments."

SS* - total mean square.

The statistic to be considered is

$$F = \frac{SS_3^*}{SS_2^*}$$

For a "fixed-effects" model, if F is large there is a large probability that there is a significant difference between the dynamic and static mean values.

Tables XVIII through XXIII and Figures 78 through 81 give all of the raw data, i.e., the differences between Frames 2 and 1 and Frames 3 and 1. The tables also give all of the statistical quantities described above. All of the dimensioned data in the tables is in units of arc-seconds or arc-seconds squared. The tables also contain tabulated values of the t- and F-statistics with the appropriate number of degrees of freedom and at significance levels which result in numbers for these statistics which are close to the values computed for the data. The tabulated statistics given are:

1. For $F = s_D^2/s_S^2$: $F_{\alpha,N-1,N-1}$

2. For $F = SS_3^*/SS_2^*$: $F_{\alpha,2,2(N-1)}$

3. For t: $t_{\alpha/2,N-1}$,

where α is the level of significance of the test. A narrative summary of the information in these tables is given in the following paragraphs.

For the October 3rd data the analysis of variance data gives no reason for concluding that the static and dynamic means are different. For the horizontal data the t-test shows that more than 80% of samples of this size would have a value of t larger than that for this set, by chance alone. For the vertical data the value of t would be larger than it actually is between

TABLE XVIII. DYNAMIC CONDITIONS: ELEVATION AXIS MOVING UPWARD
DATE: 3RD OCTOBER

	HORIZONTAL		VERTICAL	
	DYNAMIC	STATIC	DYNAMIC	STATIC
RAW DATA	-0.64	2.63	-1.73	-0.22
	1.09	3.34	-2.01	0.76
	3.60	0.49	-0.59	1.64
	6.81	4.98	0.10	-0.09
	2.68	2.86	0.81	-1.00
	2.50	3.11	3.19	1.30
	3.56	4.10	-1.74	0.47
	1.55	2.22	0.86	0.01
	2.01	-2.37	-0.36	-0.90
	0.36	2.11	-1.47	-1.23
N	10	10	10	10
m	2.35	2.36	-.29	.07
s	2.06	2.05	1.61	.97
$F = s_D^2/s_S^2$	1.01	$F_{.5,9,9} = 1.00$ $F_{.3,9,9} = 1.43$	2.76	$F_{.1,9,9} = 2.44$ $F_{.05,9,9} = 3.18$
$t = \sqrt{N}\,\frac{(m_D - m_S)}{\sqrt{s_D^2 + s_S^2}}$	.005	$t_{.4,9} = .261$	.610	$t_{.3,9} = .543$ $t_{.2,9} = .883$
SS^*_3	0		.68	
SS^*_2	4.22		1.77	
SS^*	4.00		1.72	
$F = SS^*_3/SS^*_2$	<1		<1	

TABLE XIX. DYNAMIC CONDITIONS: AZIMUTH AXIS MOVING COUNTERCLOCKWISE
DATE: 4TH NOVEMBER

	HORIZONTAL		VERTICAL	
	DYNAMIC	STATIC	DYNAMIC	STATIC
R/W DATA	2.06	0.18	1.26	1.58
	1.54	1.91	2.22	3.39
	0.17	0.12	-0.13	1.34
	1.47	2.98	2.98	3.13
	1.59	1.61	2.39	-3.47
	3.07	0.28	-1.49	-1.18
	0.89	0.16	1.55	1.38
	-0.98	-0.21	1.17	1.17
	2.21	0.68	-1.46	1.01
	2.45	1.08	2.76	1.61
N	10	10	10	10
m	1.45	.88	1.13	1.00
s	1.18	1.01	1.64	2.00
$F = s_D^2/s_S^2$	1.35 $F_{.3,9,9} = 1.43$		<1	
$t = \sqrt{N}\,\frac{(m_D - m_S)}{\sqrt{s_D^2 + s_S^2}}$	1.16 $t_{.2,9} = .883$ $t_{.1,9} = 1.383$		.158 $t_{.4,9} = .261$	
SS^*_3	1.61		.08	
SS^*_2	1.20		3.34	
SS^*	1.22		3.17	
$F = SS^*_3/SS^*_2$	1.34 $F_{.3,1,18} = 1.14$ $F_{.1,1,18} = 3.01$		<1	

TABLE XX. DYNAMIC CONDITIONS: ELEVATION AXIS MOVING UPWARD
DATE: 6TH FEBRUARY

	HORIZONTAL		VERTICAL	
	DYNAMIC	STATIC	DYNAMIC	STATIC
RAW DATA	-3.31	-5.40	1.26	-0.64
	1.66	2.01	-0.16	-1.59
	-1.31	2.19	-3.46	-0.77
	1.95	-1.78	0.91	0.66
	0.11	-0.37	5.54	2.64
	-0.30	1.29	-5.43	1.05
	0.27	3.97	-2.58	3.29
	-3.17	2.28	0.40	5.13
	-0.98	-0.66	1.71	5.52
	-3.54	-2.06	0.28	-2.17
	1.09	1.69	1.68	5.87
	-0.45	2.45	1.01	2.68
	0.85	0.79	-1.01	-1.10
	2.28	4.81	-0.92	0.40
	-1.77	-0.14	-0.71	2.18
N	15	15	15	15
m	-.44	.74	-.10	1.54
s	1.90	2.58	2.54	2.62
$F = s_D^2/s_S^2$	<1		<1	
$t = \sqrt{n} \frac{(m_D - m_S)}{\sqrt{s_D^2 + s_S^2}}$	1.44 $t_{.1,14} = 1.345$ $t_{.05,14} = 1.761$		1.74 $t_{.05,14} = 1.761$ $t_{.05,14} = 1.761$	
SS_3^*	10.43		20.22	
SS_2^*	5.12		6.67	
SS^*	5.31		7.14	
$F = SS_3^*/SS_2^*$	2.04 $F_{.13,1,28} = 1.11$ $F_{.1,1,28} = 2.89$		3.03 $F_{.05,1,28} = 4.20$ $F_{.05,1,28} = 4.20$	

TABLE XXI. DYNAMIC CONDITIONS: ELEVATION AXIS MOVING DOWNWARD
DATE: 3RD MARCH

	HORIZONTAL		VERTICAL	
	DYNAMIC	STATIC	DYNAMIC	STATIC
RAW DATA	1.17	-0.35	3.55	-0.20
	3.51	0.96	0.18	1.87
	1.41	1.93	0.	-2.61
	2.08	-2.38	-2.98	1.05
	4.46	2.62	3.59	2.91
	0.06	3.08	-0.10	-0.90
	-0.84	-2.32	5.77	-0.01
	3.33	-0.05	-2.53	-0.51
	2.71	-2.78	10.86	-4.07
	6.10	5.05	2.55	-0.03
	2.98	-1.30	0.21	0.54
	4.37	-1.33	0.60	1.85
	1.68	-4.39	-5.53	-2.39
	1.19	-2.61	-5.53	-2.39
	5.77	-1.88	5.59	3.00
	5.46	1.80	1.16	0.11
	3.41	2.69	-2.14	3.21
N	17	17	17	17
m	2.87	-.07	1.01	.25
s	1.98	2.61	4.05	2.02
$F = s_D^2/s_S^2$	<1		4.02 $F_{.005,16,16} = 3.87$	
$t = \sqrt{N}\,\frac{(m_D - m_S)}{\sqrt{s_D^2 + s_S^2}}$	3.72 $t_{.001,16} = 3.686$		.69 $t_{.3,16} = .535$ $t_{.2,16} = .865$	
SS_3^*	73.85		2.29	
SS_2^*	5.37		10.76	
SS^*	7.44		10.50	
$F = SS_3^*/SS_2^*$	13.75 $F_{.001,1,30} = 13.3$		<1	

TABLE XXII. DYNAMIC CONDITIONS: AZIMUTH AXIS MOVING CLOCKWISE
DATE: 4TH MARCH

	HORIZONTAL		VERTICAL	
	DYNAMIC	STATIC	DYNAMIC	STATIC
RAW DATA	0.96	4.92	0.86	2.98
	1.30	2.02	2.58	3.42
	-3.22	-0.72	-0.10	-1.44
	0.18	-1.35	-1.39	-0.35
	-1.28	0.79	2.29	3.00
	2.92	0.49	2.81	3.70
	-2.05	1.56	-4.01	-1.58
	0.58	0.66	-0.05	-0.72
	-0.68	0.38	1.02	0.47
	2.67	1.30	5.81	2.30
	1.37	0.82	-0.58	-2.47
	3.23	2.84	-6.66	-5.56
	3.91	2.93	2.39	-0.62
	-1.69	-1.94	-0.36	-1.55
	0.82	0.38	2.82	-1.29
	0.57	0.25	-0.64	1.89
	0.28	0.65	2.80	0.60
	1.57	-0.11	0.91	-0.11
	1.41	0.52	-1.57	-1.60
N	19	19	19	19
m	.68	.86	.47	.06
s	1.86	1.56	2.78	2.38
$F = s_D^2/s_S^2$	1.42	$F_{.3,18,20} = 1.28$ $F_{.1,18,20} = 1.86$	1.37	
$t = \sqrt{N}\,\frac{(m_D - m_S)}{\sqrt{s_D^2 + s_S^2}}$	.335	$t_{.4,18} = .257$ $t_{.3,18} = .534$	.494	
SS_3^*	.33		1.63	
SS_2^*	2.96		6.70	
SS^*	2.89		6.56	
$F = SS_3^*/SS_2^*$	<1		<1	

TABLE XXIII. DYNAMIC CONDITIONS: AZIMUTH AXIS MOVING CLOCKWISE
DATE: 5TH MARCH

	HORIZONTAL		VERTICAL	
	DYNAMIC	STATIC	DYNAMIC	STATIC
RAW DATA	-6.97	-3.40	0.27	2.06
	-3.52	-2.95	1.11	2.16
	-6.96	-4.72	-9.20	-1.31
	-5.30	-3.69	1.77	0.02
	1.89	1.67	1.19	-1.47
	-0.09	-2.32	2.44	1.37
	0.64	2.27	-1.23	0.37
	-1.35	-0.25	0.27	-1.40
	0.70	-0.41	2.61	1.70
	-0.90	-3.03	0.21	0.31
	-1.25	1.22	-1.74	1.92
	0.62	-3.94	2.41	0.17
	-2.37	-1.56	4.96	2.69
	-1.07	-3.25	1.29	-0.76
	-1.11	-0.30	0.21	-1.07
	-2.06	-1.79	3.38	-0.63
	-1.39	-0.06	3.14	3.24
	-3.81	-0.17	0.53	1.84
	-1.35	-0.83	0.23	1.36
	0.64	-2.17	-1.68	-1.95
	0.59	0.33	3.59	1.89
	-2.95	-2.94	-2.40	-6.03
	0.46	1.25	-3.76	-2.44
	1.63	1.78	-0.37	-0.75
	-0.19	0.47	-1.93	-3.26
	-1.86	-1.86	2.93	-1.07
	1.18	0.11	-4.28	-2.45
	-0.72	0.72	1.61	3.37
	-0.18	0.96	-0.82	-0.23
	2.09	2.58	-5.34	-4.08
	-2.37	-1.35	0.23	1.63
	1.98	3.97	-3.13	-0.59
	2.00	0.10	-3.38	0.63
	-0.97	-1.24	1.00	2.34
N	34	34	34	34
m	-1.01	-.73	.15	-.01
s	2.33	2.09	2.44	2.16

TABLE XXIII. DYNAMIC CONDITIONS: AZIMUTH AXIS MOVING CLOCKWISE (Cont'd)
DATE: 5TH MARCH

	HORIZONTAL		VERTICAL	
	DYNAMIC	STATIC	DYNAMIC	STATIC
RAW DATA				
$F = s_D^2/s_S^2$	1.24 $F_{.3,30,30} = 1.21$		1.29	
$t = \sqrt{N}\,\frac{(m_D - m_S)}{\sqrt{s_D^2 + s_S^2}}$	.522 $t_{.3,30} = .530$		.292 $t_{.4,30} = .255$	
SS_3^*	1.34		.45	
SS_2^*	4.89		5.31	
SS^*	4.84		5.23	
$F = SS_3^*/SS_2^*$	<1		<1	

FIGURE 78 ELEVATION UPWARD

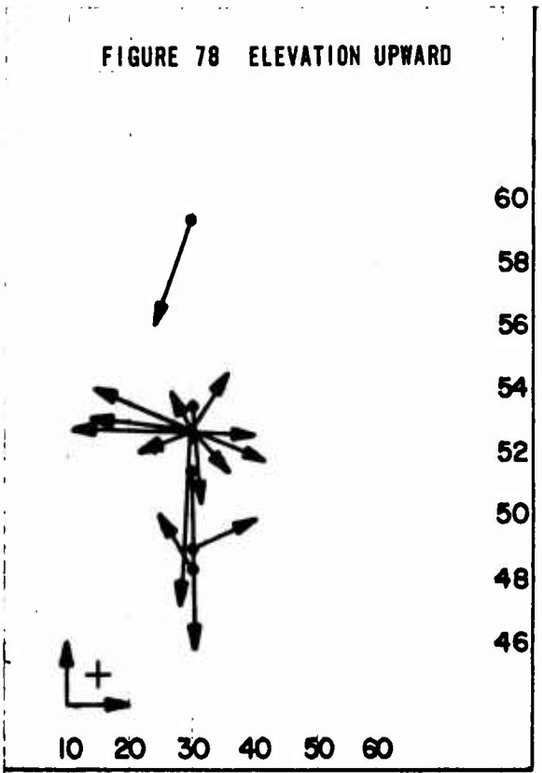

FIGURE 79 ELEVATION DOWNWARD

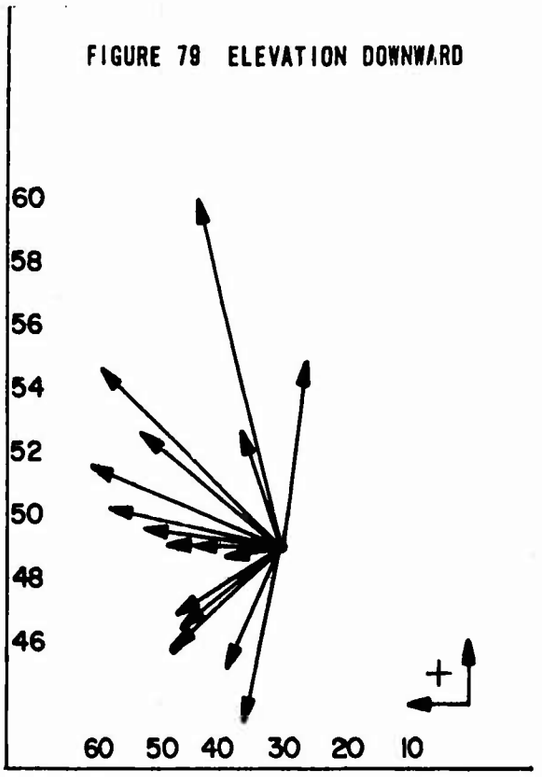

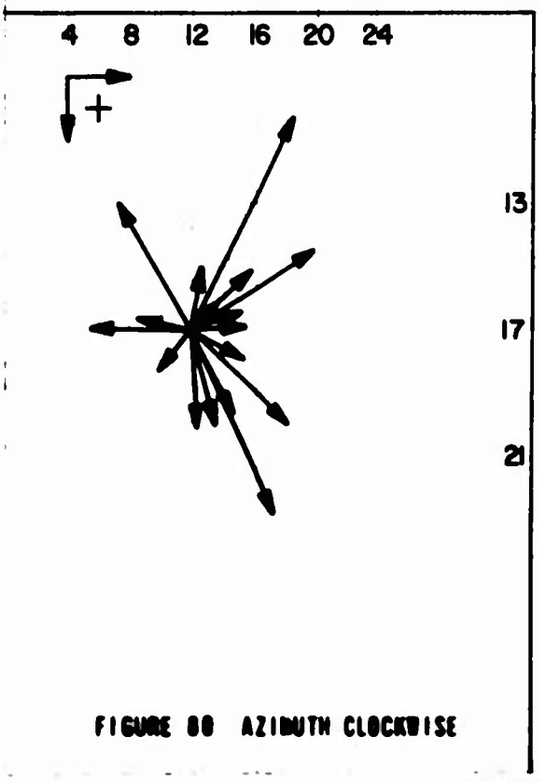

FIGURE 80 AZIMUTH CLOCKWISE

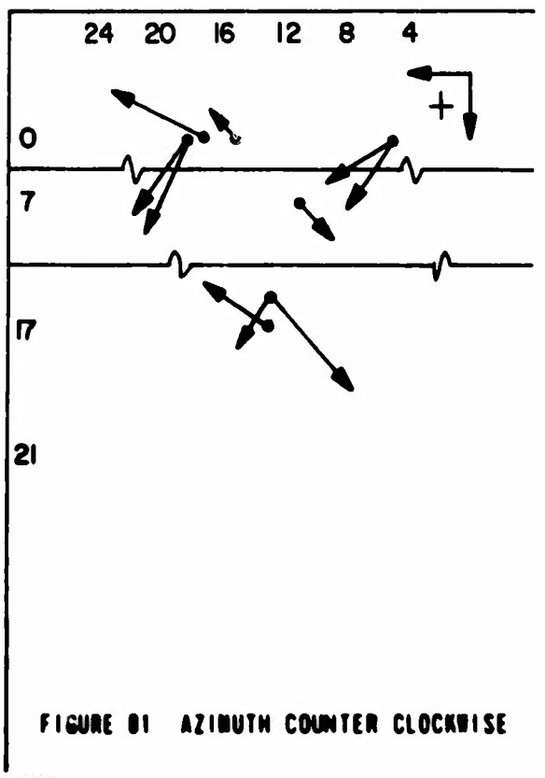

FIGURE 81 AZIMUTH COUNTER CLOCKWISE

DYNAMIC ERRORS
1 [illegible] .2 ARC SEC

40% and 60% of the time just due to chance. Regarding the differences in variances, for the horizontal data the value of F could be this large nearly 50% of the time. For the vertical data, the value of F could be this large by chance for nearly 10% of samples of this size.

For the November 4th data all of the vertical data clearly indicate that there is no increase in the means and variances due to dynamics. For the horizontal data the value of F from the analysis of variance could have been as large as it is nearly 30% of the time by chance. The t-test value could have been as large as it is between 20% and 40% of the time due to normal variation between samples. The value of F comparing the sample variances could have been as large as it is for more than 30% of random samples of the size used.

For the February 6th data, there is clearly no increase in the sample variances due to dynamics for both the horizontal and vertical data. For the horizontal data, the analysis of variance data shows that the observed difference between means could result from chance about 20% of the time and the t-test shows that this difference would have been observed nearly 20% of the time. For the vertical data both tests show that the observed difference would have occurred nearly 10% of the time due to chance variation.

For the March 3rd data, in the vertical case, the analysis of variance and the t-test indicate that there is not a significant difference between the means. The value of F for the comparison between the variances indicates that the size of the dynamic variance would be this much greater than the static variance only 5 times in 1000 by chance. For the horizontal data, there is no indication of a signficant dynamic increase in variance. There does appear, however, to be a difference between the means, as shown by t-test and analysis of variance which would occur only once or twice in 1000 samples by chance.

For the March 4th and March 5th data, all of the tests indicate either no increase in error due to dynamics or differences which could have easily occurred by chance.

Static Test Results

The static test results are based on photographs of fourth and fifth magnitude stars whose positions are known accurately to 0.5 arc-seconds or less. The technique used in computing the angular position of the star on the photographic plates is identical to that used in computing the position of the target in the dynamic tests. Therefore, part of the same computer program is used. These star positions are compared to the star positions that are based on time of exposure and the location of the WSMR Cinetheodolite. Star position elevation angle corrections for refraction

are made, based on the computations given in Appendix A. Standard values of barometric pressure and temperature were used in making the star tapes; the measured values are used in the computations of actual star position.

The static accuracy figures quoted in this report come from a set of observations of 72 stars. This set consists of four subsets corresponding to four different nights on which the observations were made. The dates for the observations were June 13, June 26, June 27, and July 11.

The observations, extending over this entire month, were treated as one homogenous set. That is, the data reduction procedures used were applied to the whole set, not to each separate night's results. Stated differently, the data reduction was carried out with the assumption that all aspects of the instrument that affect the net pointing angle remain stable for one month. No mathematical adjustment to the data and no physical adjustment to the instrument was carried out over a time period of less than one month.

The following corrections to the cinetheodolite pointing angle were carried out for the static error evaluation. Because the instrument is gravity-based, the local gravity deflection error was subtracted from the elevation angle. The gravity deflection at Bill Site can be represented by

$$8.9 \cos(A - 121°) \text{ arc-seconds},$$

where A is the cinetheodolite azimuth angle. This data was obtained from a special survey made by U. S. A. Topographic Command personnel stationed at WSMR. Because of an erroneous assumption made in the design of the azimuth graduated circle optics and the optics for the associated index mark, the azimuth angle, as normally read, will be in error by an amount which depends on the forward mislevel of the instrument. This design error is amenable to computational correction because the forward mislevel of the instrument can be completely determined by the relative positions of the four fiducial images. Each sample of data was therefore corrected in azimuth by an amount proportional (actually one-half) to the forward mislevel for that particular sample. This software procedure, necessary because of a hardware error, is entirely in keeping with the spirit of the WSMR Cinetheodolite design concept. A third data adjustment consisted in choosing the scale factor which yielded the smallest rms value for the residuals. This is a parameter which should be chosen in this way. The actual value used was about 1% different from the design value. Finally, the adjustments due to the instrumental error model were carried out by a least squares procedure. The error model is represented by the following equations.

$$R_u = b_1 \cos E + b_2 \sin E + b_3$$

$$R_v = b_4$$

R_u and R_v are "angular" plate-coordinate residuals. E is the elevation angle. b_1 results from errors of the rhomboidal deviation assembly zero-degree angle error and fixed penta prism 45-degree angle error and the azimuth zero-degree reference error. b_2 results from the other errors of the fixed 90-degree deviation assembly. b_3 results from the 45-degree angle errors of the rotating 90-degree deviation assembly. b_4 results from the other errors of the rotating 90-degree deviation assemblies and the elevation zero-degree reference error.

The results of the star tests are given in Table XXIV and Figures 82 through 85. These results are summarized by the horizontal and vertical standard errors of a single observation which are as follows:

horizontal	2.78 arc-seconds
vertical	2.79 arc-seconds

Examination of the residuals given in Table XXIV suggests a couple of things. First, there seems to be a rough grouping of the horizontal residuals according to the four sets which correspond to different night's observations. This could be due to the need for an azimuth zero reference which is different for each night because of random motions of the instrument pedestal (the azimuth graduated circle is closely coupled to the pedestal, only the large spherical leveling system is a movable element between pedestal and circle). A rerun of the least squares adjustment was made allowing the b_1 term to be separately determined for each of the four sets of raw data. When this was done the overall standard deviations for a single observation were as follow:

horizontal	2.51 arc-seconds
vertical	2.79 arc-seconds

The variation of the b_1 coefficient from the average for each of the four nights was as follows:

1st set -3.02 arc-seconds

2nd set -0.21 arc-seconds

3rd set +2.19 arc-seconds

4th set +1.03 arc-seconds

It is most likely that such variation comes from the pedestal and earth motion. The figures cited support the need for a high precision azimuth orientation system. A second qualitative conclusion formed from scanning

TABLE XXIV. STAR RESIDUALS ARC-SEC

DATE	STAR NO.	STAR POSITION (DEG.) AZIMUTH	STAR POSITION (DEG.) ELEVATION	RESIDUALS (ARC-SEC) AZIMUTH	RESIDUALS (ARC-SEC) ELEVATION
13 Jun 68	3	346	27	4.1445	0.8066
	3	346	27	5.9924	1.1928
	3	346	27	3.2544	1.0546
	6	4	44	4.4606	-1.7735
	12	38	39	0.9780	3.6287
	12	38	39	2.5139	1.9636
	15	339	53	0.6640	-1.6568
	17	326	25	0.4844	-2.9357
	40	333	74	0.4114	-3.0507
	102	271	32	0.7402	-1.5924
	103	265	38	3.2726	-0.7693
	103	266	37	1.0429	0.8460
	103	266	37	3.4909	-0.0294
	104	261	45	-2.3398	-1.5366
26 Jun 68	35	301	46	4.4716	1.1070
	35	301	45	2.8676	2.3738
	36	307	60	4.3843	-4.0549
	42	57	48	1.9447	-1.0285
	43	56	33	-2.0105	5.2389
	47	76	32	0.5500	4.6071
	104	251	56	-1.4806	-5.8385
	105	224	67	-5.7353	-4.7673
	105	225	66	-2.3639	-6.2539
	110	118	59	-1.3170	-0.8242
	112	100	41	-2.3519	-0.1238
	113	90	34	-2.8734	-0.3504
	120	107	34	-1.8837	-1.7478
	121	141	52	-1.0099	1.9395
	122	172	56	0.8643	-3.1880
	124	219	50	-1.0084	-0.5547
	165	230	27	2.8481	-4.0858
	165	230	26	5.2896	-0.6363
	166	222	36	2.8036	-0.8843
	167	208	40	0.6836	0.7774
	167	209	40	1.6242	-1.7563
	170	187	42	1.3013	-0.5530
	200	185	28	-0.0559	6.0645
	200	185	28	-1.1810	3.0510
	37	309	29	-2.0725	1.5121
	37	309	29	0.8076	6.3864
	65	100	40	-0.3886	0.7568
	115	121	34	-3.5286	0.1062
	171	210	36	-2.4708	-2.0671

TABLE XXIV. STAR RESIDUALS ARC-SEC (Cont'd)

DATE	STAR NO.	STAR POSITION (DEG.) AZIMUTH	ELEVATION	RESIDUALS (ARC-SEC) AZIMUTH	ELEVATION
27 Jun 68	51	97	74	2.9569	-2.3400
	44	51	30	-4.1908	3.4630
	43	58	43	0.5348	1.8400
	201	188	29	2.2099	3.6699
	201	188	29	3.1113	1.5584
	171	160	40	-2.1397	2.8631
	171	161	40	-4.2761	1.1138
	37	307	33	-2.8444	2.3189
	52	285	40	-1.3129	1.2306
	64	74	27	-6.3332	0.2238
	66	89	27	-5.5960	0.3044
11 Jul 68	37	309	63	-0.4111	-1.4474
	42	56	58	0.8382	-2.5202
	43	58	43	-0.5720	-1.8971
	44	52	31	-5.6802	2.0108
	47	83	45	-1.3609	1.8125
	47	83	45	-1.1142	-2.5014
	50	86	62	1.1864	-5.9157
	53	271	57	-2.7143	-3.2773
	112	109	50	1.4788	-0.0329
	112	110	51	2.3021	-2.3297
	113	97	43	1.8773	-1.7186
	121	159	57	1.7862	-3.9021
	123	210	55	-1.0163	-0.0020
	123	211	55	-2.1939	2.1232
	124	229	45	-0.6512	1.1018
	124	229	45	-0.3379	1.7283
	172	152	35	-0.7321	3.5343
	173	136	31	-2.6237	5.6337

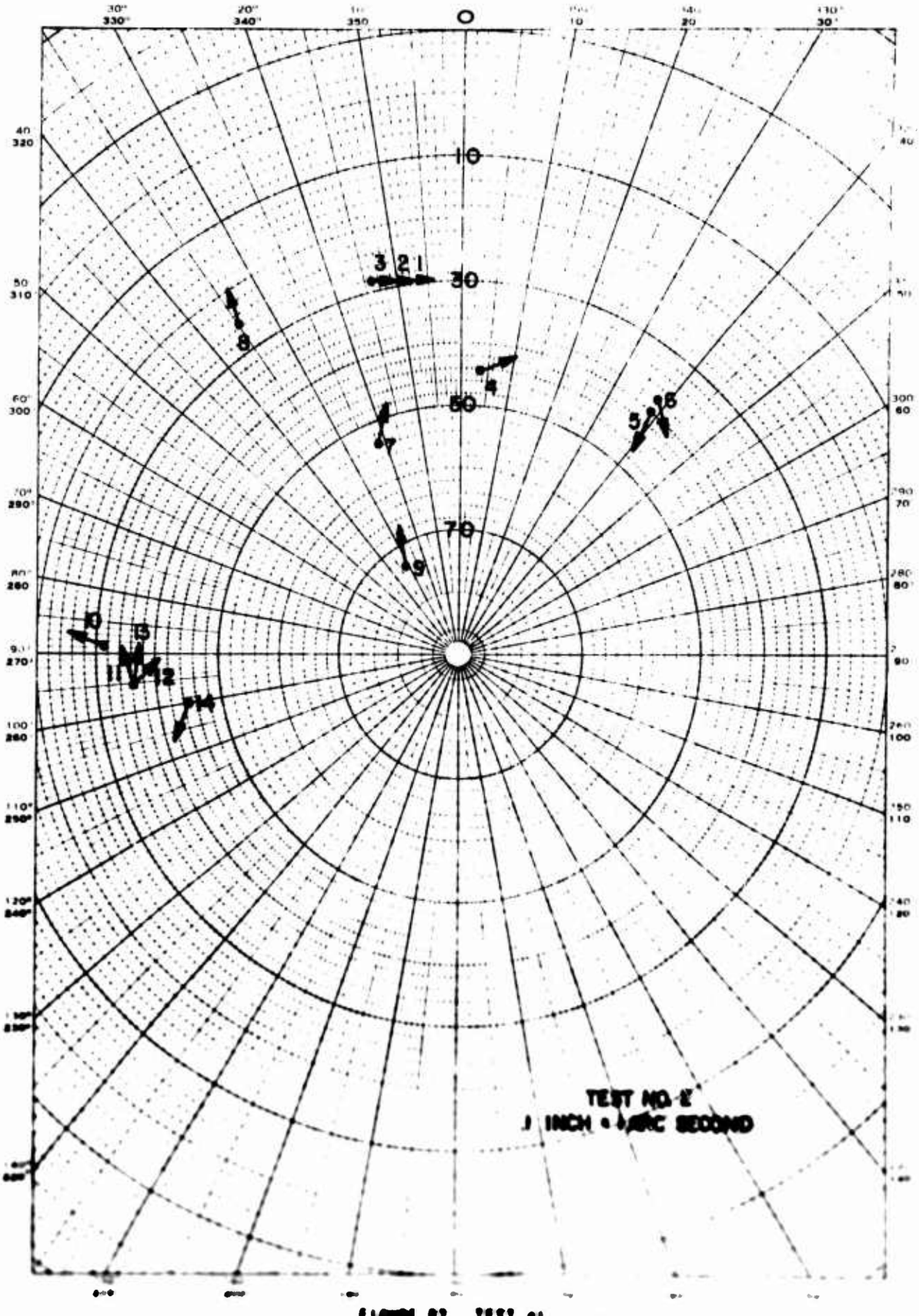

EUGENE DIETZGEN CO.
MADE IN U. S. A.

NO 340-P DIETZGEN GRAPH PAPER
POLAR CO-ORDINATE

FIGURE 82 TEST 01 193

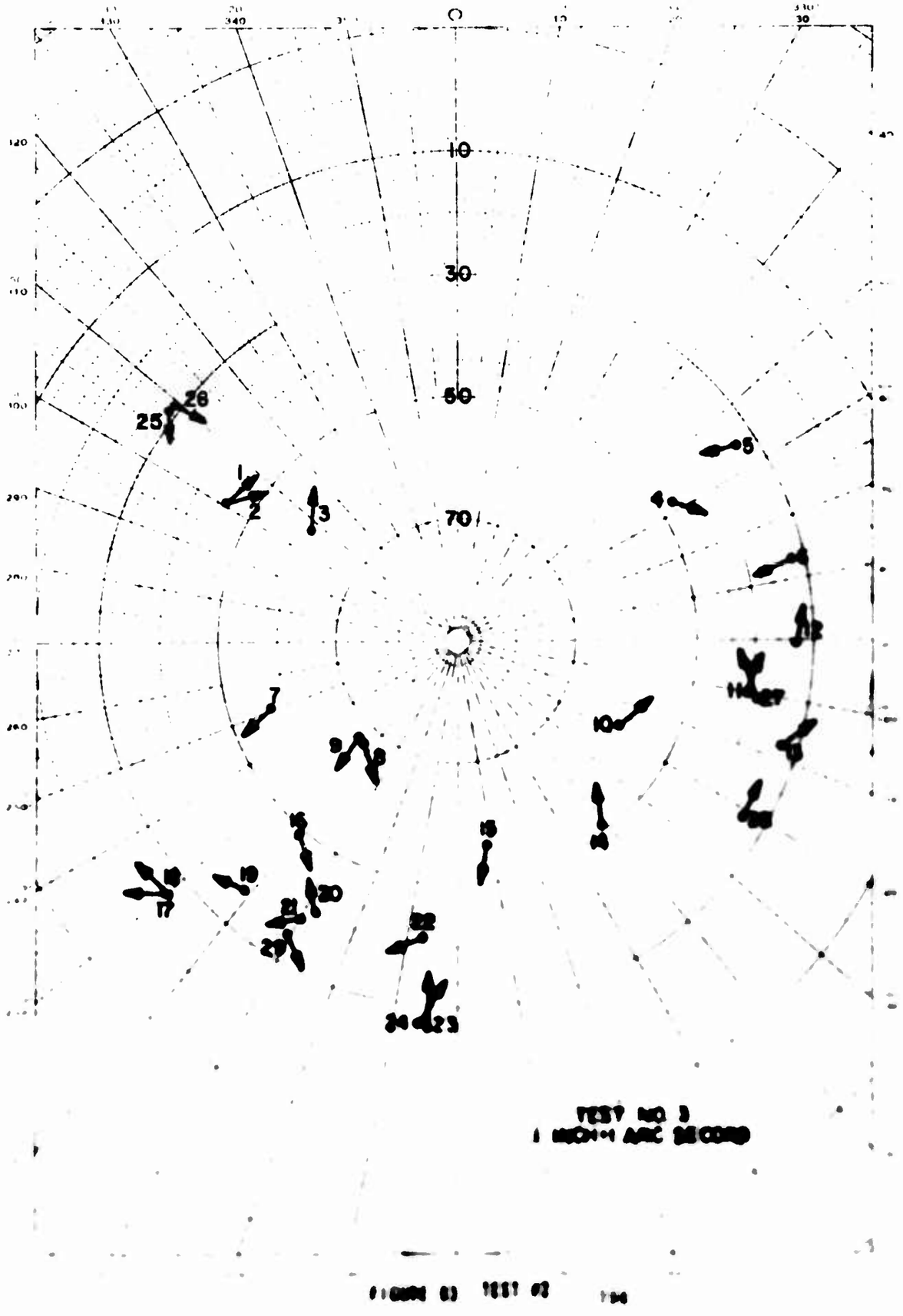
10
30
50
70
25
26
1
2
3
5
4
7
8
9
10
11
12
13
14
15
16
17
18
19
20
21
22
23
24

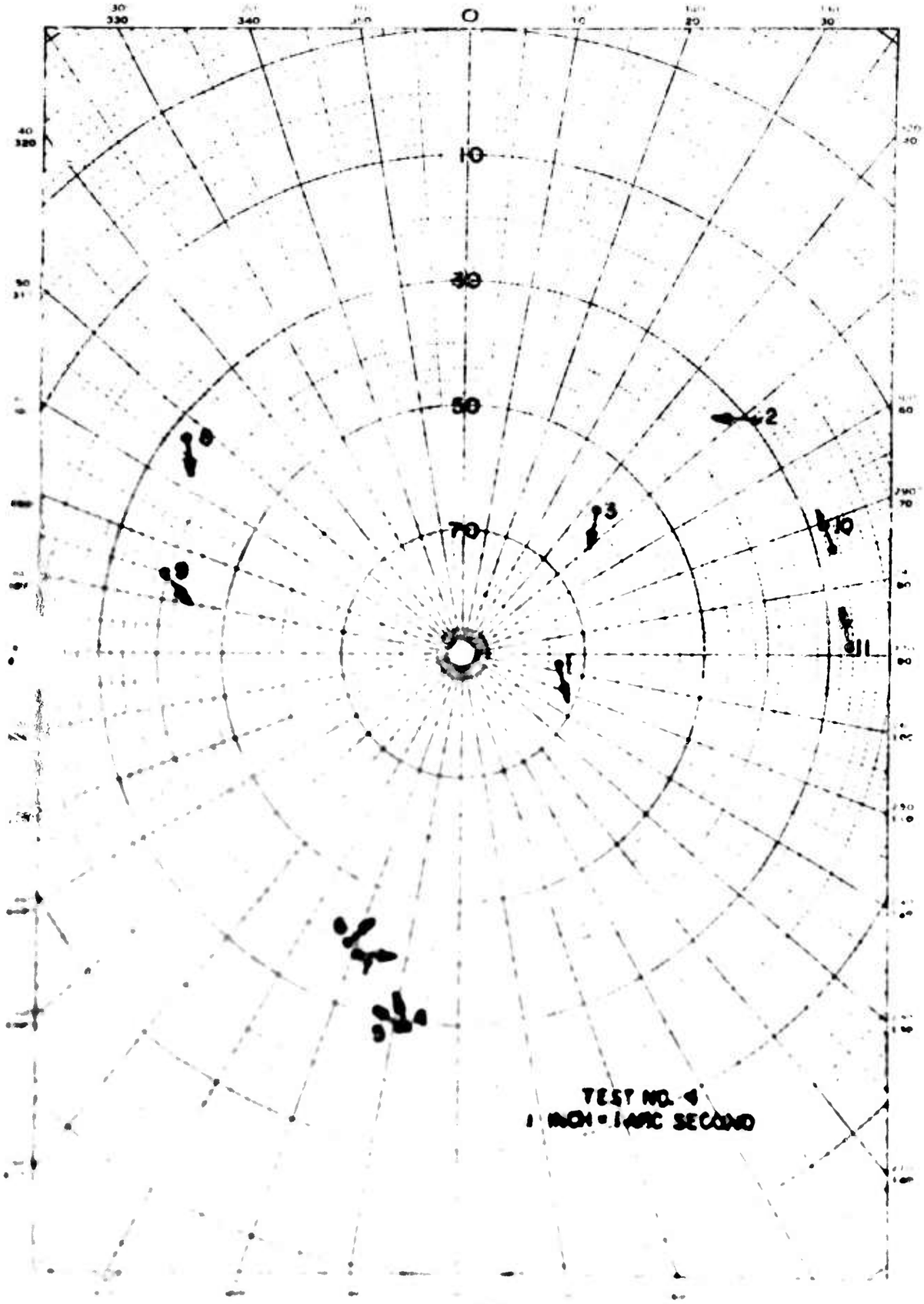
0
10
20
30
40
50
60
70
80
90
TEST NO. 4
1 INCH = 1 MPC SECOND

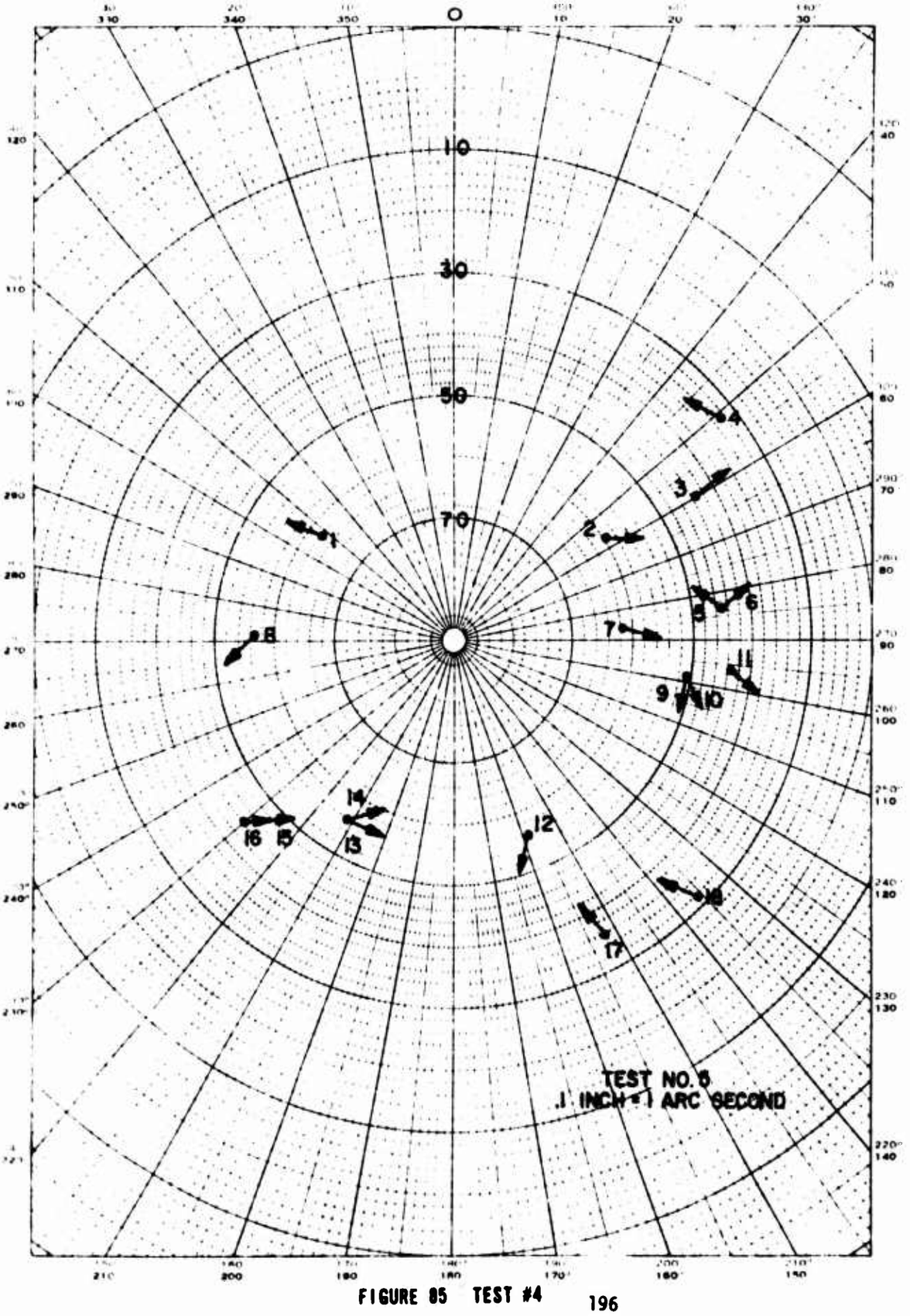

FIGURE 85 TEST #4

the residuals is that there is a trend in the elevation residuals which is a function of the elevation angle. Large positive residuals are frequently associated with small elevation angles and large negative residuals with higher elevation angles. No firm explanation is offered for this apparent effect, however, it could be associated with some systematic refraction error anomaly. For instance, a layer of warmer air right above the cinetheodolite site could cause the observed trend. Such problems could be systematically explored with the WSMR Cinetheodolite, especially if the plate reading error could be reduced so that nonrandom effects show up more clearly. A final observation about the residuals can be made which is not obvious from the listed results. This is that the least square adjustment for instrumental errors has a relatively small effect on the rms value of the residuals. The values of the standard error of a single observation without adjustment for systematic instrument effects are as follow:

horizontal	2.86 arc-seconds
vertical	2.79 arc-seconds

Temperature Test Results

The computer program used to reduce the star position from the static test data was slightly altered and was used to compute the position of selected data matrix marks.

Noting Figures 86 and 87, it appears that for the first 35 minutes the positions of the marks are somewhat stable. Any variations in the positions of the marks, during this time period, may be attributed to reading error. However, after about 35 minutes, there appears to be a definite change, especially in the case of the azimuth and elevation index marks in the Y-direction. There seems to be less change in the location of the major centroid of the four fiducial marks. This may be due to the greater number of readings it takes to define the major centroid as compared to the number of readings required to define the position of the azimuth and elevation index marks.

The conditions under which the test was run represent an extreme case, compared to conditions present during a normal tracking mission. Changes in ambient conditions can be held to a minimum by controlling the conditions within the astrodome during a tracking mission or by opening the dome a few minutes before a tracking mission.

Conclusions

Static Pointing Accuracy

The WSMR Cinetheodolite static pointing accuracy, as reduced from the star test data, is represented by a standard deviation of 2.8 arc-seconds.

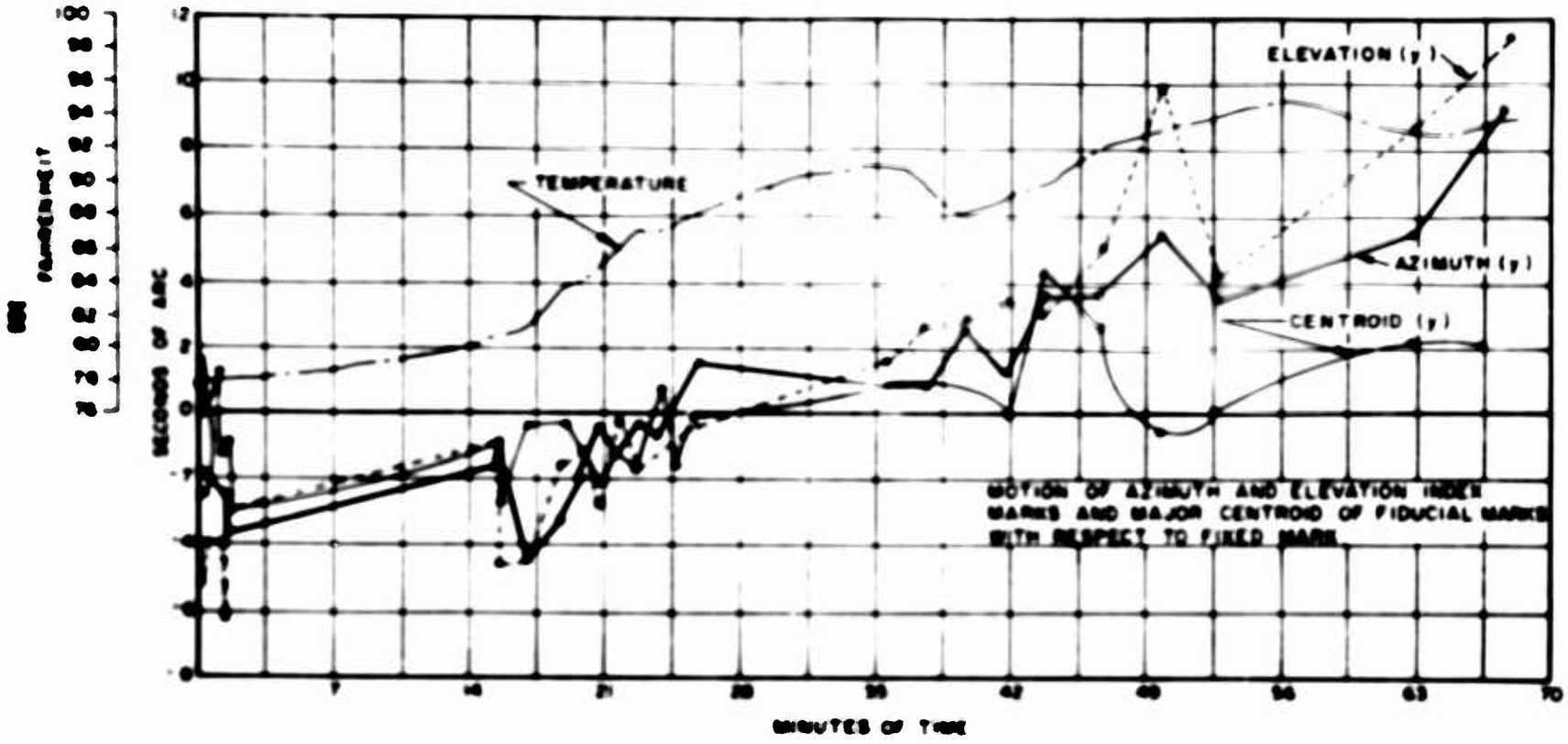

FIGURE 66 TEMPERATURE TEST GRAPH

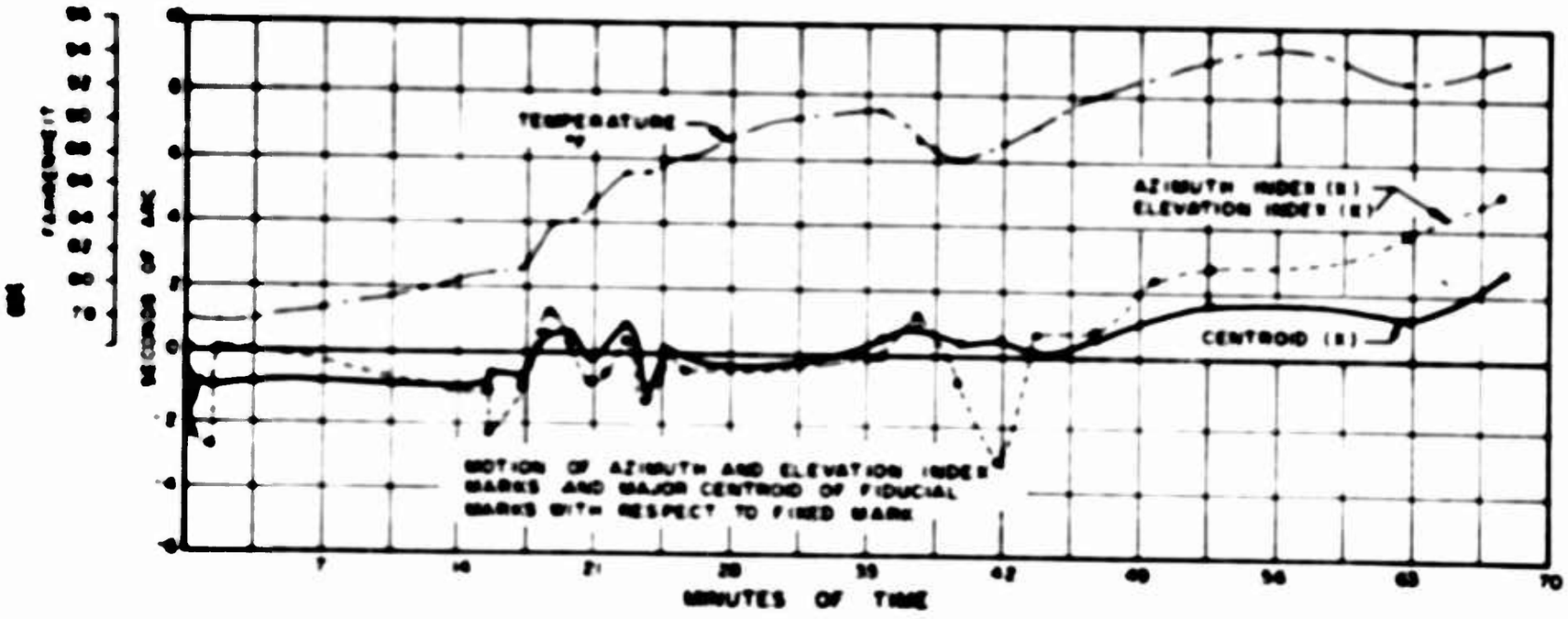

FIGURE 87 TEMPERATURE TEST GRAPHS

Optical system errors, circle engraving errors, GRM errors, error in atmospheric refraction correction, star catalogue errors, and plate reading errors are present in the star test data. The following optical system errors and limitations contribute to measurement errors.

Optical system resolution, as measured by analyses of target patterns, varied from 1.3 to 2.6 seconds. "Barrel" distortion tests indicated a minor fall-off of magnification with increasing distance from the geometric center of the field. This distortion varied from 0.18 arc-second at the top to 0.79 arc-second on the left side. (Reference section titled "Main Optics.")

Circle dial errors could not be determined by system test since the dual beam collimator, which was to be used to "close the circle," was deficient. Based upon manufacturer's drawings, the circles were to be divided to a tolerance of 0.5 arc-second. GRM errors, based upon GRM initial balance tolerance and random variations induced by geoseismic noise, are approximately 0.3 arc-second maximum. A random error due to atmospheric turbulence called "image dancing" may be as large as one or two arc-seconds, with an error of two seconds being rather improbable. The atmospheric refraction correction for actual star position is believed to have fixed the star position to within 0.5 arc-second or less. The star catalogue errors may be as large as 0.5 arc-second. The plate reading error propagates into the solution with a standard deviation of approximately 2 arc-seconds.

All of these errors are random in nature. Since statistical methods were used in reducing the star data to obtain the WSMR Cinetheodolite static pointing accuracy, the derived figures are believed to be accurate within a small tolerance.

Dynamic Accuracy

Reduction of the dynamic test plate data resulted in a dynamic error ranging from -1.0 arc-second to 2.9 arc-seconds in azimuth and from -0.3 arc-second to 1.0 arc-second in elevation.

However, data from the same test plates, based upon the first and third frame static exposure comparisons, indicates a static discrepancy variance ranging from -0.7 arc-second to 2.4 arc-seconds in azimuth and from 0 arc-second to 1.5 arc-seconds in elevation.

These static discrepancies result from GRM errors and plate reading errors as explained above. It is apparent that these same error sources are present during the dynamic test plate exposures. In addition to these error sources, common to both the static pointing accuracy star plate exposures and the dynamic test plate exposures, motions of the great circle test fixture and of the artificial star collimator enter into all of the

dynamic test plate data. Air turbulence in the dome also contributes an unknown amount of refraction error. In general, the sums of these error contributions did not exceed 0.3 arc-second peak-to-peak when the cine-theodolite was not in motion.

As a result, it is impossible to establish the precise WSMR Cinetheodolite dynamic pointing accuracy and, likewise, to determine the exact static-to-dynamic pointing accuracy ratio.

In order to determine how well the cinetheodolite compensates for dynamic mechanical errors, the statistical analysis discussed in "Dynamic Test Results" had to be performed. The statistical data, except for one case, indicate that there is no significant bias (no difference between the means) between static and dynamic data; and, also except for one case, that there is no significant increase in the variance of dynamic observations relative to static observations. The apparent bias in the horizontal data for the March 3rd test is considered to be spurious. This conclusion is based upon two considerations. First, the dynamics of this test were in the elevation axis. There is no reason to expect that acceleration about the elevation axis alone could produce horizontal errors. Second, the other elevation axis dynamic tests reveal no such effect. The large variance for the dynamic vertical case on March 3rd is not confirmed by any other test. There is no reason why elevation axis moving downward dynamics should cause any significant increase in variance. It is probable that March 3rd was a day with poor observing conditions, i.e., relatively large fixture motion.

Considering the result of the star tests and the fact that plate measurement error contributed about 2 arc-seconds to the net error, it seems possible to assert with good confidence that the static pointing error of the bread-board instrument does not exceed 2 arc-seconds (one sigma). This is better than the design goal. Further, the testing has clearly indicated that there is, at a high confidence level, no difference between the static and dynamic pointing error, so that we can also conclude that a second major design goal has been achieved.

CONCLUSIONS AND RECOMMENDATIONS

The primary design goal of the exploratory development, a cinetheodolite with a dynamic instrumental pointing accuracy of 2 arc-seconds, was achieved. This represents a significant breakthrough in the field of theodolite technology; however, secondary design goals, such as good tracking performance, high-quality dial and fiducial images, and a 50-per-second sample rate, were not realized.

Each subsystem has serious design deficiencies that would be unacceptable in an operating field instrument, but, as this report has indicated, each of the deficiencies can be corrected with well-established design practices. At the time of this report, correction of the fiducial illumination system deficiencies seems assured by the apparently successful results being achieved by the optical redesign contract. As correction of the camera deficiencies is regarded mainly as engineering and relatively minor development, it is concluded that the exploratory development phase of the WSMR Cinetheodolite task has been successfully completed.

Therefore, immediate start of the production phase of the development (operational system development) is recommended. It is also recommended that the test complex be modified or updated in order to test the production prototype instrument and follow-on production units in a more timely and efficient manner than that employed in the test of the breadboard instrument.

It is further recommended that a parallel effort be directed toward development of an effective fieldworthy orientation system and an improved design for the WSMR Cinetheodolite field station facilities.

APPENDIX A

STAR POSITION COMPUTATIONS

The computer program converts right ascension and declination of each star to azimuth and elevation angles from the cinetheodolite to star at each desired time. A table of constants containing the following information for each star is found in the Boss Catalog.

R_o, δ_o = right ascension and declination, respectively, of the star referenced to the mean equator and equinox at the beginning of 1950.

ID = star identification.

$\frac{dR_o}{dt}, \frac{d\delta_o}{dt}$ = annual variation in the right ascension and declination, respectively. The annual variation includes precession and proper motion.

S_R, S_δ = secular variation in right ascension and declination, respectively.

Constants for the year of observation are found in the American Ephemeris and Nautical Almanac.

M = precession in right ascension.

N = precession in declination.

E = mean obliquity.

Input data will be

t = time in whole years measured from 1950 to the year of observation.

U.T. = universal time of the observations desired.

A, B, C, D = Besselian day numbers (tabulated in the American Ephemeris and Nautical Almanac for each day of the year).

STG = sidereal time at Greenwich for 0^h U.T., i.e., the hour angle of the first point of Aires. Sidereal time is listed in the American Ephemeris and Nautical Almanac.

Δh = number of hours that have elapsed from 0^h U.T. to the time of observation.

λ = longitude of the station. (Positive in the Western Hemisphere.)

ϕ = latitude of the station.

COMPUTATIONAL PROCEDURE:

(1) Compute the mean coordinates of each star using the following formulas:

$$R_1 = R_o + t\left(\frac{dR_o}{dt} + \frac{.01S_R t}{2}\right) \qquad (1)$$

$$\delta_1 = \delta_o + t\left(\frac{dR_o}{dt} + \frac{.01S_\delta t}{2}\right) \qquad (2)$$

(2) Compute the apparent coordinates of each star for the date of observation using the following equations:

$$R = R_1 + Aa + Bb + Cc + Dd \qquad (3)$$

$$\delta = \delta_1 - Aa' + Bb' + Cc' + Dd' \qquad (4)$$

where

$$a = \frac{m}{n} + \sin R_1 \tan \delta_1$$

$$b = \cos R_1 \tan \delta_1$$

$$c = \cos R_1 \sec \delta_1$$

$$d = \sin R_1 \sec \delta_1$$

and

$$a' = \cos R_1$$

$$b' = \sin R_1$$

$$c' = \tan \epsilon \cos \phi_1 - \sin R_1 \sin \phi_1$$

$$d' = \cos R_1 \sin \phi_1$$

(3) Compute, for each desired time of each star, the hour angle of the star:

$$H = STG + C - \alpha - R + U.T. \qquad (5)$$

where

C = 9.8565 seconds x Δh.

(4) Compute the direction cosines of the line from the camera to the apparent position of the star by

$$\cos A \cos E = \cos \phi \sin \delta - \sin \phi \cos H \cos \delta \qquad (6)$$

$$\sin A \cos E = -\sin H \cos \delta \qquad (7)$$

$$\sin E = \sin \phi \sin \delta + \cos \phi \cos H \cos \delta \qquad (8)$$

where

A = azimuth angle.

E = elevation angle (actual).

(5) Compute the azimuth and elevation angles from the camera to the apparent position of the star:

$$A = \tan^{-1}\left[\frac{\quad}{\cos} \; \frac{-\sin H \cos \delta}{\sin \delta - \sin \phi \cos H \cos \delta}\right] \qquad (9)$$

$$E = \sin^{-1}[\sin \phi \sin \delta + \cos \phi \cos H \cos \delta] \; . \qquad (10)$$

(6) Correct the elevation angle for refraction. A brief derivation of the refraction correction will be given here.

In the following figure, let Z be the zenith angle at which the star is observed from the ground, and let ζ be the zenith angle of the light beam before it enters the atmosphere

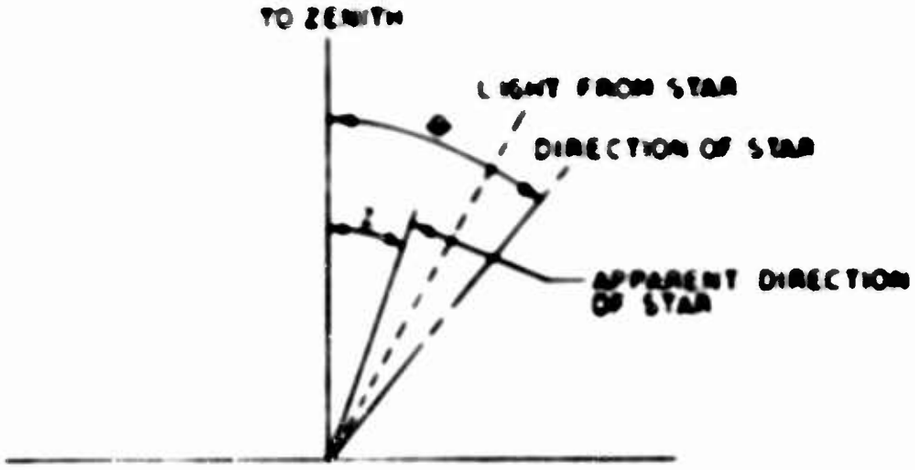

By use of Snell's law, the following equation may be written

$$\sin \zeta = n_0 \sin Z \tag{11}$$

where n_0 is the index of refraction of the air at the point of observation O. Let $\zeta = Z + r$, the angle of refraction. In terms of r, Equation (11) becomes

$$\sin (Z + r) = n_0 \sin Z$$

or

$$\sin Z \cos r + \cos Z \sin r = n_0 \sin Z. \tag{12}$$

Since r is a small angle we can write $\cos r = 1$ and $\sin r = r$ and Equation (12) becomes

$$\sin Z + r \cos Z = n_0 \sin Z$$

and

$$r = (n_0 - 1) \tan Z \ . \tag{13}$$

$(n_D - 1)$ is given as an inverse function of pressure and temperature.

$$(n_D - 1) = \frac{aP}{T} \tag{14}$$

where

P is in millibars, T is in degrees Kelvin, r is in arc seconds, and a = 16.1.

If temperature is given in degrees centigrade, then Equation (14) becomes

$$(n_D - 1) = \frac{aP}{273.16 + T°C} \tag{15}$$

Substituting Equation (15) in Equation (13) yields

$$r = \left(\frac{aP}{273.16 + T°C}\right) \tan Z \tag{16}$$

where

$$Z = (90° - E - r) .$$

Again since r is very small angle

$$\tan Z = \tan (90° - E - r) = \tan (90° - E) .$$

If a pressure and temperature are not supplied then a standard pressure and temperature of

P = 1013.10 mb

T = 10° C.

will be used. The apparent elevation angle then becomes

$$E = E + r . \tag{17}$$

APPENDIX B

DETAILS OF TARGET POSITION COMPUTATION

The angular position of the WSMR Cinetheodolite is determined from the dial data as follows:

$$E = D + Ne$$

where

E = elevation dial angle,

D = numerical elevation dial reading in minutes, and

Ne = angular segment to be added to dial reading.

$$Ne = \left[\frac{Le_4 + Le_3}{2}\right] - Le_5 = \left[\frac{Le_4 + Le_3 - 2Le_5}{2}\right]$$

$$Me = \left[\frac{Le_4 + Le_3}{2}\right] - \left[\frac{Le_1 + Le_2}{2}\right] = \left[\frac{Le_4 + Le_3 - Le_1 - Le_2}{2}\right]$$

where Me = ten-arc-minute segment. Therefore,

$$Ne = Me \left[\frac{Le_4 + Le_3 - 2Le_5}{Le_4 + Le_5 - Le_1 - Le_2}\right] .$$

Since Me represents a ten-arc-minute segment, we have

$$Ne = 10 \left[\frac{Le_4 + Le_3 - 2Le_5}{Le_4 + Le_5 - Le_1 - Le_2}\right]$$

where Ne is in minutes.

$$E = D + 10\left[\frac{Le_4 + Le_3 - 2Le_5}{Le_4 + Le_5 - Le_1 - Le_2}\right] .$$

For the azimuth dial angle A, we have

$$A = D + 10\left[\frac{La_4 + La_3 - 2La_5}{La_4 + La_5 - La_1 - La_2}\right] .$$

The pointing direction of the instrument is defined by the centroid of the four fiducial marks, i.e.,

$$\overline{X} = \frac{Bx_1 + Bx_2 + Bx_3 + Bx_4}{4}$$

$$\overline{Y} = \frac{By_1 + By_2 + By_3 + By_4}{4}$$

To calculate the tracking error X_T and Y_T, one must first rotate the axes about the angle E which is the elevation dial angle calculated above. This rotation gives us a coordinate system where the Y-axis represents the elevation direction and the X-axis represents the azimuth direction with respect to the instrument. The azimuth correction then becomes

$$X_T = \cos E\ (U_T + V_T \tan E)$$

$$= U_T \cos E + V_T \sin E$$

where

X_T = target distance from centroid on X-axis,

U_T = target distance from centroid on U-axis, and

V_T = target distance from centroid on V-axis.

In azimuth, we must use the proper scale factor $\propto$ and a secant correction using the angle E to convert this linear measurement to an angular measurement. We obtain the actual angle X as follows:

$$X = \propto \sec E \, X_T$$

$$= \propto \sec E \, (U_T \cos E + V_T \sin E) \, .$$

For elevation the secant correction is not required and we have

$$Y_T = \cos E \, (V_T - U_T \tan E)$$

$$= V_T \cos E - U_T \sin E$$

and

$$Y = \propto Y_T$$

$$= \propto (V_T \cos E - U_T \sin E) \, .$$

These target corrections are added algebraically to the angles computed from the azimuth and elevation dial data.

LITERATURE CITED

1. Hoge, J. C. H., "A Method for the Determination of the Transfer Function of a Linear Second Order Servomechanism from Its Step Function," Optics Division Engineering Memorandum 65-4, WSMR, New Mexico, 1965.

2. Taylor, E. Wilford, Theodolite Design and Construction, Cooke, Throughton, and Sims, 1955.

3. Lee, R. P., "Cinetheodolite Calibration and Orientation," Final Report on WSMR Task 1-2-3, April 1957.

4. Merritt, E. J., "Testing of Cinetheodolite by Stars," NPG Report No. 1461, May 1956.

5. "Preliminary Test of Annular Ring for WSMR Cinetheodolite," Optics Division Engineering Memorandum 66-3, WSMR, New Mexico, February 1966.

6. "WSMR Cinetheodolite Annular Ring Test Report," Lockeed Electronics Company Engineering Memorandum 66-13, September 1966.

7. "Accuracy Evaluation Tests of WSMR Cinetheodolite," Optics Division Technical Memorandum 69-4, WSMR, New Mexico, June 1969.

8. Bowker, Albert H., and Lieberman, Gerald J., Engineering Statistics, Prentice-Hall, Inc., 1959.

Unclassified
Security Classification

DOCUMENT CONTROL DATA - R & D

(Security classification of title, body of abstract and indexing annotation must be entered when the overall report is classified)

1. ORIGINATING ACTIVITY (Corporate author)	2a. REPORT SECURITY CLASSIFICATION
Deputy for National Range Engineering Instrumentation Development Directorate White Sands Missile Range, New Mexico	Unclassified
	2b. GROUP

3. REPORT TITLE

EXPLORATORY DEVELOPMENT OF THE WSMR CINETHEODOLITE

4. DESCRIPTIVE NOTES (Type of report and inclusive dates)

Final Report

5. AUTHOR(S) (First name, middle initial, last name)

Lowell D. Yates

6. REPORT DATE	7a. TOTAL NO. OF PAGES	7b. NO. OF REFS
June 1970	215	8

8a. CONTRACT OR GRANT NO.	9a. ORIGINATOR'S REPORT NUMBER(S)
b. PROJECT NO. 1S265302D240 04 02	STEWS-RE-I-70-2
c.	9b. OTHER REPORT NO(S) (Any other numbers that may be assigned this report)
d.	

10. DISTRIBUTION STATEMENT

This document has been approved for public release and sale; its distribution is unlimited.

11. SUPPLEMENTARY NOTES	12. SPONSORING MILITARY ACTIVITY

13. ABSTRACT

A breadboard instrument was developed for the purpose of establishing the feasibility of a novel and unique type of theodolite with far greater dynamic pointing accuracy than is possible with conventional theodolites. This report documents the results of the test and evaluation and the measurement techniques employed. The report discusses design deficiencies of the breadboard instrument along with recommended improvements for future development of an operational instrument.

DD FORM 1 NOV 65 1473 REPLACES DD FORM 1473, 1 JAN 64, WHICH IS OBSOLETE FOR ARMY USE.

Unclassified
Security Classification

14. KEY WORDS	LINK A		LINK B		LINK C	
	ROLE	WT	ROLE	WT	ROLE	WT
Cinetheodolite Cinetheodolite, High Dynamic Accuracy Cinetheodolite, Test and Evaluation Optics Instrumentation, Range, Optical						